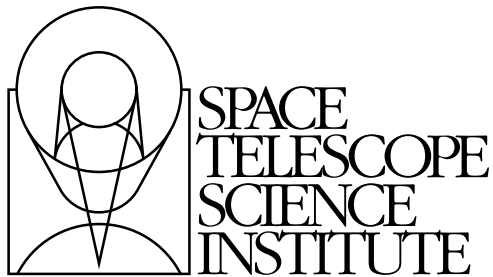


---

Version 5.0  
March, 2006

# ACS Data Handbook



Space Telescope Science Institute  
3700 San Martin Drive  
Baltimore, Maryland 21218  
[help@stsci.edu](mailto:help@stsci.edu)

## User Support

For prompt answers to any question, please contact the STScI Help Desk.

- **E-mail:** [help@stsci.edu](mailto:help@stsci.edu)
- **Phone:** (410) 338-1082 or 1-800-544-8125

## World Wide Web

Information and other resources are available on the ACS World Wide Web page:

- URL: <http://www.stsci.edu/hst/acs/>

## ACS Revision History

Version	Date	Editor
5.0	March 2006	Cheryl Pavlovsky, Anton Koekemoer & Jennifer Mack
4.0	January 2005	Cheryl Pavlovsky et al.
3.0	July 2004	Cheryl Pavlovsky et al.
2.0	November 2003	Jennifer Mack et al.
1.0	January 2002	Jennifer Mack et al.

## Authorship

### Authorship

This document is written and maintained by the ACS Team in the Imaging Branch of the Instruments Division of STScI which consists of the following individuals: Biretta, J., Bohlin, R., Chiaberge, M., Cox, C., Dressel, L., Fruchter, A., Giavalisco, M., Gilliland, R., Gonzaga, S., Koekemoer, A., Lucas, R., Mack, J., Maiz-Apellaniz, J., Mutchler, M., Pavlovsky, C., Platais, V., Proffitt, C., Riess, A., Sahu, K., Sembach, K., Sirianni, M., van der Marel, R., and Walborn, N.

In publications, refer to this document as:

Pavlovsky, C., et al. 2006, "ACS Data Handbook", Version 5.0, (Baltimore: STScI).

Send comments or corrections to:  
Space Telescope Science Institute  
3700 San Martin Drive  
Baltimore, Maryland 21218  
E-mail:[help@stsci.edu](mailto:help@stsci.edu)

# Table of Contents

<b>Preface</b> .....	ix
<i>How to Use this Handbook</i> .....	ix
<b>Acknowledgments</b> .....	xi
<b>Chapter 1: ACS Overview</b> .....	1-1
1.1 Instrument Design and Capabilities.....	1-1
1.1.1 Detectors .....	1-2
1.1.2 ACS Optical Design.....	1-4
1.1.3 ACS Geometric Distortion.....	1-4
1.2 Basic Instrument Operations.....	1-7
1.2.1 Target Acquisitions .....	1-7
1.2.2 Typical ACS Observing Sequence .....	1-7
1.2.3 Data Storage and Transfer .....	1-8
1.2.4 Parallel Operations .....	1-8
<b>Chapter 2: ACS Data Structure</b> .....	2-1
2.1 Types of ACS Files .....	2-2
2.1.1 Data Files and Suffixes.....	2-2
2.1.2 Association Tables .....	2-2
2.1.3 Trailer Files.....	2-4
2.2 ACS File Structure .....	2-5
2.3 Data Storage Requirements.....	2-7
2.4 Headers and Keywords .....	2-9
<b>Chapter 3: ACS Calibration Pipeline</b> .....	3-1
3.1 On The Fly Reprocessing (OTFR).....	3-2

3.2 Pipeline Overview .....	3-3
3.2.1 CALACS: Image Calibration .....	3-3
3.2.2 MultiDrizzle and PyDrizzle: Distortion Correction and Dither Combination .....	3-5
3.2.3 When is OTFR <b>not</b> Appropriate? .....	3-5
3.3 Structure of CALACS .....	3-6
3.4 CALACS Processing Steps .....	3-10
3.4.1 ACSCCD .....	3-11
3.4.2 ACSREJ .....	3-16
3.4.3 ACS2D .....	3-20
3.4.4 ACSSUM .....	3-25
3.5 Manual Recalibration of ACS Data .....	3-25
3.5.1 Requirements for Manual Recalibration .....	3-25
3.5.2 CALACS Examples .....	3-28

## **Chapter 4: Distortion Correction and Drizzling of ACS Images** .....

4.1 ACS Geometric Distortions .....	4-2
4.1.1 Distortion Model .....	4-2
4.1.2 On-orbit Calibration Programs .....	4-5
4.1.3 Results .....	4-5
4.1.4 Distortion Reference Files (IDCTAB & DGEOFILE) .....	4-11
4.2 Combination of Dithered Data .....	4-13
4.2.1 Introduction to Dithering .....	4-13
4.2.2 Introduction to Drizzle .....	4-14
4.2.3 Overview of Drizzle-Related Software Tools .....	4-15
4.2.4 Association Table Usage .....	4-16
4.3 PyDrizzle .....	4-17
4.4 MultiDrizzle .....	4-17
4.4.1 Steps Performed by MultiDrizzle .....	4-18
4.4.2 Multidrizzle in the ACS Pipeline .....	4-18
4.4.3 Data Quality Flags for Bad Pixels: The 'Bits' Parameter .....	4-19
4.4.4 MultiDrizzle Data Products .....	4-20

4.5 Post-Pipeline Reprocessing .....	4-21
4.5.1 Example 1: Running PyDrizzle on a Single Exposure .....	4-24
4.5.2 Example 2: Running PyDrizzle on an Association file .....	4-24
4.5.3 Example 3: Running MultiDrizzle with Different Output Image Options .....	4-25
4.5.4 Example 4: Re-Running MultiDrizzle to Improve Sky Subtraction .....	4-27
4.6 Refining the Shifts: Manually and with Tweakshifts .....	4-30
4.6.1 Delta Shifts .....	4-31
4.6.2 Absolute Shifts .....	4-31
4.6.3 Constructing the 'shiftfile' .....	4-32
4.6.4 Example 5: Improving the Image Registration for Different Visits .....	4-35
4.6.5 Tweakshifts .....	4-38
4.7 MultiDrizzle Details: Example Application to the Tadpole Galaxy .....	4-40
4.8 Creating Custom Association Tables .....	4-58
<b>Chapter 5: ACS Error Sources .....</b>	<b>5-1</b>
5.1 Readout Noise and A-to-D Conversion .....	5-1
5.1.1 Readout Noise .....	5-1
5.1.2 A-to-D Conversion .....	5-2
5.2 Bias Subtraction .....	5-2
5.2.1 Bias Calibration Issues .....	5-2
5.2.2 Bias Jump .....	5-5
5.2.3 Bias Subarrays for the WFC and HRC .....	5-6
5.3 Dark Current, Hot Pixels, and Cosmic Rays .....	5-6
5.3.1 Dark Current .....	5-6
5.3.2 Hot Pixels .....	5-9
5.3.3 Cosmic Rays .....	5-13
5.4 Flat Fields .....	5-16
5.4.1 Ground Flats (P-flats) .....	5-16
5.4.2 L-flats .....	5-17
5.4.3 Pipeline Flats .....	5-22
5.4.4 Earth Flat Verification .....	5-27
5.4.5 Sky Flats .....	5-28

5.5 Image Anomalies .....	5-28
5.5.1 Dust Motes.....	5-28
5.5.2 Optical Ghosts and Scattered Light .....	5-29
5.5.3 Cross Talk.....	5-32
5.5.4 Scattered Earth Light.....	5-37
5.6 Generic Detector and Camera Properties.....	5-38
5.6.1 Gain Calibration.....	5-38
5.6.2 Full Well Depth .....	5-40
5.6.3 Linearity at Low to Moderate Intensity .....	5-40
5.6.4 Linearity Beyond Saturation .....	5-43
5.6.5 Shutter Stability.....	5-45
<b>Chapter 6: ACS Data Analysis .....</b>	<b>6-1</b>
6.1 Photometry .....	6-1
6.1.1 Photometric Systems, Units, and Zeropoints .....	6-1
6.1.2 Aperture and Color Corrections.....	6-3
6.1.3 Pixel Area Maps.....	6-5
6.1.4 PSF.....	6-11
6.1.5 CTE.....	6-14
6.1.6 Red Leak .....	6-21
6.1.7 UV Contamination .....	6-22
6.2 Astrometry.....	6-24
6.2.1 Coordinate Transformations .....	6-24
6.2.2 Absolute and Relative Astrometry .....	6-26
6.2.3 Impact of Guide Star Failure.....	6-26
6.3 Polarimetry.....	6-28
6.3.1 Absolute Calibration .....	6-28
6.3.2 Instrumental Issues.....	6-28
6.3.3 Flats.....	6-32
6.3.4 Polarization Calibration.....	6-32
6.4 Coronagraphy .....	6-34
6.4.1 Flat Fielding .....	6-35
6.4.2 PSF Subtraction.....	6-35
6.4.3 Photometry .....	6-36
6.4.4 Ghosting .....	6-36
6.5 Ramp Filters .....	6-37
6.5.1 Introduction.....	6-37
6.5.2 Existing Ground Calibrations .....	6-37
6.5.3 Future In-flight Calibrations .....	6-38

6.6 Spectroscopy with the ACS Grisms  
and Prisms..... 6-39

6.6.1 What to Expect from ACS Slitless  
Spectroscopy Data..... 6-40

6.6.2 Pipeline Calibration..... 6-42

6.6.3 Slitless Spectroscopy Data and Dithering ..... 6-44

6.6.4 Extracting and Calibrating Slitless Spectra..... 6-45

6.6.5 Accuracy of Slitless Spectra Wavelength  
and Flux Calibration ..... 6-50

**Index** .....Index-1





# Preface

---

## How to Use this Handbook

This handbook is designed to help users manipulate, process and analyze data from the Advanced Camera for Surveys (ACS) which was installed on-board the Hubble Space Telescope (HST) during the 2002 servicing mission (SM3B). It is presented as an independent and self-contained document and is designed for users familiar with HST data but new to ACS. Users who wish to find more general information including instructions for retrieving data from the HST archive, a description of HST file formats, and a discussion of IRAF/STSDAS software for displaying and processing these data, are referred to a companion volume, the Introduction to the *HST Data Handbook* at:

[http://www.stsci.edu/hst/HST\\_overview/documents/datahandbook](http://www.stsci.edu/hst/HST_overview/documents/datahandbook)

While the purpose of this handbook is to provide comprehensive information for the treatment of ACS data and present the in-flight data calibration program results, a brief discussion of the ACS capabilities, design and basic instrument operations (Chapter 1) is also included. For a detailed discussion please refer to the ACS Instrument Handbook. One important concern for users is the large volume of ACS data compared to other HST instruments, addressed in Chapter 2, with a discussion of the ACS file structure. Chapter 3 describes the ACS calibration pipeline software **CALACS**, the ACS reference files, and instructions for manually recalibrating data. Given the large ACS field of view, and hence the importance of geometric distortion, Chapter 4 is devoted to a thorough discussion of the ACS distortion. We discuss the **MultiDrizzle** software which corrects for distortion in ACS images, performs cosmic ray rejection, and combines multiple dithered images using drizzle. We also describe ways to modify its parameters for users who wish to improve or fine-tune the drizzling process for specific scientific goals. Chapter 5 describes the sources of uncertainty in ACS data and Chapter 6 describes the data reduction issues relevant for work with ACS data.

Since many of the instrument characteristics may be revised over a short time frame, readers are advised to consult the ACS web pages (<http://www.stsci.edu/hst/acs/>) for the latest information regarding ACS performance and calibration.

■ Cheryl Pavlovsky, Anton Koekemoer & Jennifer Mack (Editors, ACS Data Handbook)

# Acknowledgments

The technical and operational information contained in this Handbook is the summary of the experience gained by members of the STScI ACS Team, the ACS group at ST-ECF, and by the ACS IDT. Members of the STScI ACS Team are Ken Sembach (lead), John Biretta, Ralph Bohlin, Marco Chiaberge (ESA), Colin Cox, Linda Dressel, Andrew Fruchter, Mauro Giavalisco, Ron Gilliland, Shireen Gonzaga, Inge Heyer, Anton Koekemoer, Ray Lucas, Jennifer Mack, Jesus Maiz-Apellaniz (ESA), Max Mutchler, Cheryl Pavlovsky, Vera Platais, Charles Profitt, Adam Riess, Kailash Sahu, Marco Sirianni (ESA), Roeland van der Marel, and Nolan Walborn.

The ST-ECF ACS group is Richard Hook, Martin Kuemmel, Soeren Larsen, and Jeremy Walsh.

The ACS IDT is Holland Ford (PI), Garth Illingworth (Deputy PI), George Hartig, Mark Rafal, Frank Bartko, Tom Broadhurst, Bob Brown, Chris Burrows, Ed Cheng, Mark Clampin, Jim Crocker, Paul Feldman, Marijn Franx, David Golimowski, Randy Kimble, John Krist, Tom La Jeunesse, Mike Lesser, Doug Leviton, George Miley, Marc Postman, Piero Rosati, Bill Sparks, Pam Sullivan, Zlatan Tsvetanov, Paul Volmer, Rick White, Bob Woodruff, David Ardila, Narciso Benitez, John Blakeslee, Rychard Bouwens, Larry Bradley, Nicholas J.G. Cross, Ricardo Demarco, Tomotsugu Goto, Caryl Gronwall, Brad Holden, Nicole Homeier, Andre´ Martel, Simona Mei, Felipe Menanteau, Gerhardt Meurer, Veronica Motta, Marco Sirianni, and Hien Tran.

The contributions of Warren Hack, Alan Welty, Tom Wheeler, and Susan Rose are greatly appreciated.



# ACS Overview

In this chapter. . .

1.1 Instrument Design and Capabilities / 1-1

1.2 Basic Instrument Operations / 1-7

This chapter provides an overview of the capabilities and design of the Advanced Camera for Surveys (ACS) and describes the basic instrument operations. For more information we refer you to the *ACS Instrument Handbook* which gives a technical description of the instrument's properties, expected performance, operations, and calibration.

---

## 1.1 Instrument Design and Capabilities

The ACS camera is designed to provide HST with a deep, wide-field survey capability from the visible to near-IR, high resolution imaging from the near-UV to the near-IR, and solar blind far-UV imaging. The primary design goal of the ACS Wide-Field Channel is to achieve a factor of 10 improvement in discovery efficiency compared to WFPC2, where discovery efficiency is defined as the product of imaging field of view (FOV) and instrument throughput.

ACS comprises three channels, each optimized for a specific goal:

- Wide field channel (WFC):  $\sim 202 \times 202$  arcsecond field of view from 3700–11,000 Å, and peak efficiency of 48% (including the Optical Telescope Assembly). The plate scale of  $\sim 0.049$  arcsec/pixel provides critical sampling at 11,600 Å.

- High resolution channel (HRC):  $29 \times 25$  arcsecond field of view from 2000–11,000 Å, and peak efficiency of 29%. The plate scale of  $\sim 0.027$  arcsec/pixel provides critical sampling at 6300 Å.
- Solar Blind Channel (SBC):  $35 \times 31$  arcsecond field of view from 1150–1700 Å, and peak efficiency of 7.5%. The plate scale of  $\sim 0.032$  arcsec/pixel provides a good compromise between resolution and field of view.

In addition to these three prime capabilities, ACS also provides:

- Grism spectroscopy: Low resolution ( $R \sim 100$ ) wide field spectroscopy from 5500–11,000 Å available in both the WFC and the HRC.
- Objective prism spectroscopy: Low resolution ( $R \sim 100$  @ 2000 Å) near-UV spectroscopy from 2000–4000 Å available in the HRC.
- Objective prism spectroscopy: Low resolution ( $R \sim 100$  @ 1216 Å) far-UV spectroscopy from 1150–1700 Å available in the SBC.
- Coronagraphy: Aberrated beam coronagraphy in the HRC from 2000–11,000 Å with 1.8 arcsecond and 3.0 arcsecond diameter occulting spots.
- Imaging Polarimetry: Polarimetric imaging in the HRC and WFC with relative polarization angles of  $0^\circ$ ,  $60^\circ$  and  $120^\circ$ .

ACS is a versatile instrument that can be applied to a broad range of scientific programs. For example, the high sensitivity and wide field of the WFC in the visible and near-infrared will make it the instrument of choice for deep imaging programs in this wavelength region. The HRC, with its excellent spatial resolution, provides full sampling of the HST PSF at  $\lambda > 6000$  Å and can be used for high precision photometry in stellar population programs. The HRC coronagraph can be used for the detection of circumstellar disks and QSO host galaxies.

### 1.1.1 Detectors

ACS uses one or more large-format detectors in each channel:

- The WFC detector, called ACS/WFC, employs a mosaic of two  $2048 \times 4096$  Scientific Imaging Technologies (SITe) CCDs, with  $\sim 0.049$  arcsecond pixels, covering a nominal  $\sim 202 \times 202$  arcsecond field of view, and a spectral response from  $\sim 3700$  to 11,000 Å.
- The HRC detector, called ACS/HRC, is a  $1024 \times 1024$  SITe CCD, with  $\sim 0.028 \times 0.025$  arcsecond pixels, covering a nominal  $29 \times 25$  arcsecond field of view, and spectral response from  $\sim 2000$  to 11,000 Å.

- The SBC detector, called the ACS/SBC, is a solar-blind CsI Multi-Anode Microchannel Array (MAMA), with  $1024 \times 1024$   $\sim 0.034 \times 0.030$  arcsecond pixels, and a nominal  $35 \times 31$  arcsecond field of view, with far-UV spectral response from  $\sim 1150$  to  $1700 \text{ \AA}$ .

### The WFC & HRC CCDs

The ACS CCDs are thinned, backside-illuminated devices cooled by thermo-electric cooler (TEC) stacks and housed in sealed, evacuated dewars with fused silica windows. The spectral response of the WFC CCDs is optimized for imaging at visible to near-IR wavelengths. The HRC CCD covers wavelengths similar to the WFC but the spectral response has been additionally optimized for the near-UV. Both CCD cameras produce a time-integrated image in the ACCUM data-taking mode. The HRC can also be operated in target acquisition (ACQ) mode for coronagraphic observations. As with all CCD detectors, there is noise (*readout noise*) and time (*read time*) associated with reading out the detector following an exposure. The minimum exposure time is  $0.1 \text{ sec}$  for HRC, and  $0.5 \text{ sec}$  for WFC, and the minimum time between successive identical exposures is  $45 \text{ sec}$  (HRC) or  $\sim 135 \text{ sec}$  (WFC) for full-frame and can be reduced to  $\sim 36 \text{ sec}$  for subarray readouts. The dynamic range for a single exposure is ultimately limited by the depth of the CCD full well ( $\sim 85,000 e^-$  for the WFC and  $155,000 e^-$  for the HRC), which determines the total amount of charge that can accumulate in any one pixel during an exposure without saturation. Cosmic rays will affect all CCD exposures: CCD observations should be broken into multiple exposures whenever possible, to allow removal of cosmic rays in post-observation data processing.

### The SBC MAMA

The SBC MAMA is a *photon-counting* detector which provides a two-dimensional ultraviolet capability, optimized for the far-UV. It can only be operated in ACCUM mode. The ACS MAMA detector is subject to both *scientific* and *absolute* brightness limits. At high local ( $\geq 50 \text{ counts sec}^{-1} \text{ pixel}^{-1}$ ) and global ( $> 285,000 \text{ counts sec}^{-1}$ ) illumination rates, counting becomes nonlinear in a way that is not correctable. At only slightly higher illumination rates, the MAMA detectors are subject to damage. We have therefore defined absolute local and global count-rate limits, which translate to a set of configuration-dependent bright-object screening limits. Sources which violate the absolute count rate limits in a given configuration *cannot be observed in those configurations*.

### 1.1.2 ACS Optical Design

The ACS design incorporates two main optical channels: one for the WFC and one which is shared by the HRC and SBC. These channels are illustrated in figures 3.1 and 3.2 of the *ACS Instrument Handbook*. Each channel has independent corrective optics to compensate for HST's spherical aberration. The WFC has three optical elements, coated with silver, to optimize instrument throughput in the visible. The silver coatings cut off at wavelengths shortward of 3700 Å. The WFC has two filter wheels which it shares with the HRC, offering the possibility of internal WFC/HRC parallel observing for some filter combinations. The HRC/SBC optical chain comprises three aluminized mirrors, overcoated with MgF<sub>2</sub>. The HRC or SBC channels are selected by means of a plane fold mirror. The HRC is selected by inserting the fold mirror into the optical chain so that the beam is imaged onto the HRC detector through the WFC/HRC filter wheels. The SBC channel is selected by moving the fold mirror out of the beam to yield a two mirror optical chain which images through the SBC filter wheel onto the SBC detector. The aberrated beam coronagraph is accessed by inserting a mechanism into the HRC optical chain. This mechanism positions a substrate with two occulting spots at the aberrated telescope focal plane and an apodizer at the re-imaged exit pupil.

While there is no mechanical reason why the coronagraph could not be used with the SBC, for health and safety reasons (due to brightness limits of the MAMA detector) **use of the coronagraph is forbidden with the SBC.**

### 1.1.3 ACS Geometric Distortion

The ACS detectors exhibit significantly more distortion than previous HST instruments. All ACS observations must be corrected for distortion before any photometry or astrometry is derived. For a thorough discussion of ACS Geometric Distortion, we refer the reader to Chapter 4.

The principal cause of the ACS distortion is that the optics have been designed with a minimum number of components, consistent with correcting for the spherical aberration induced by the Optical Telescope Assembly (OTA), without introducing coma. The result is a high throughput, but focal surfaces far from normal to the principal rays. The WFC detector is tilted at 22 degrees giving an elongation of 8% along the diagonal. The HRC and SBC detectors have a 25 degree tilt giving an elongation of 12%. In each case, the scale in arcseconds per pixel is smaller along the radial direction of the OTA field of view than along the tangential direction. When projected on the sky, this causes each detector to appear "rhombus-shaped" rather than square. The angle on the sky between the x and y axes is 84.9 degrees for the WFC1, 86.1 for the WFC2 and 84.2 degrees for the HRC.

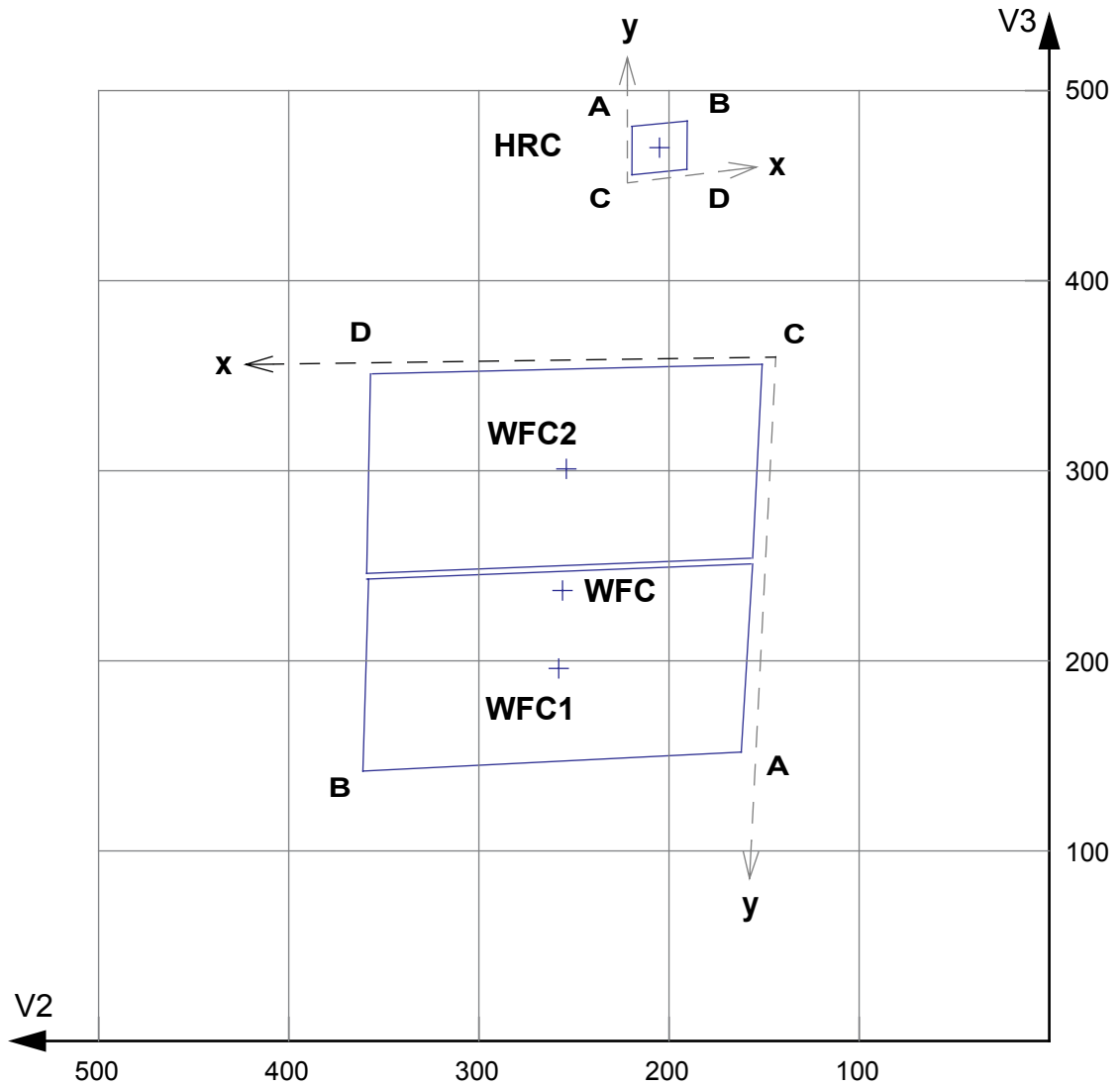


The orientations of the ACS detector edges are approximately in line with the V2 and V3 coordinate axes of the telescope. Consequently, the eigenaxes of the scale transformation are along the diagonals for WFC and the apertures and pixels appear non-rectangular in the sky projection. For the HRC and SBC the situation is even more irregular because the aperture diagonals do not lie along a radius of the HST field of view. Figure 1.1 shows the ACS apertures in the telescope's V2/V3 reference frame and illustrates the "rhombus" shape of each detector. A telescope roll angle of zero degrees would correspond to an on-sky view with the V3 axis aligned with North and the V2 with East. The readout amplifiers are also indicated for each detector.

If these were the only distortions present, their impact on photometry and mosaicing/dithering could be simply computed. A more problematic effect is the variation of scale and pixel area across each detector. For the WFC this amounts to a change of  $\sim 10\%$  in scale from corner to corner. For the HRC and SBC this variation is only about  $1\%$ , since these detectors cover much smaller fields of view. The area on the sky covered by a WFC pixel varies by  $\sim 18\%$  from corner to corner, allowance for which *must* be made in photometry.

Dithering and mosaicing are complicated by the fact that an integral pixel shift near the center of the detector will translate into a non-integral displacement for pixels near the edges. This is not a fundamental limitation, but will imply some computational complexity in registering images and will depend on an accurate measurement of distortions.

Figure 1.1: ACS apertures compared with the V2/V3 reference frame. The read-out amplifiers (A,B,C,D) are indicated on the figure. When ACS data are processed through MultiDrizzle in the HST pipeline, the resulting drizzled images are oriented with their x,y axes corresponding approximately to the x,y axes shown here. Thus, the WFC data products are oriented so that WFC1 (chip 1, which uses amps A,B) is on top (see also Figure 2.2), and the HRC data products are also oriented such that amps A,B are on top.



---

## 1.2 Basic Instrument Operations

### 1.2.1 Target Acquisitions

For the majority of ACS observations target acquisition is simply a matter of defining the appropriate aperture for the observation. Once the telescope acquires its guide stars, the target will be within  $\sim 1\text{--}2$  arcseconds of the specified pointing. For observations with the ramp filters, one must specify the desired central wavelength for the observation. For the special case of coronagraphic observations, an onboard target acquisition will need to be specified. The nominal accuracy of the combined target acquisition and slew procedure is  $\sim 0.03$  arcseconds, comparable to that achieved by STIS.

### 1.2.2 Typical ACS Observing Sequence

An important issue for observers to consider is the “packaging” of their observations, i.e. how observations are CR–SPLIT to mitigate the impact of cosmic rays, whether sub-stepping or “dithering” of images is required, and how, if necessary, to construct a mosaic pattern to map the target. For an online library of pointing patterns, refer to the ACS dither web page:

<http://www.stsci.edu/hst/acs/proposing/dither>

HRC observations and narrowband observations with the WFC are more likely to be read-noise limited, requiring consideration of the optimum CR–SPLIT times. Observations with the MAMA detectors do not suffer from cosmic rays or read noise, but long integration times are often needed to obtain sufficient signal-to-noise in the photon-starved ultraviolet.

A typical ACS observing sequence consists of a series of CR–SPLIT and dithered  $\sim 10\text{--}20$  minute exposures for each program filter. Coronagraphic observations require an initial target acquisition observation to permit centering of the target under the occulting mask. Observers generally need not take their own calibration exposures.

### 1.2.3 Data Storage and Transfer

At the conclusion of each exposure, the science data are read out from the detector and placed in ACS's internal buffer memory, where they are stored until it can be transferred to the HST solid state data recorder (and thereafter to the ground). The internal buffer memory is large enough to hold one WFC image, or sixteen HRC or SBC images, and so the buffer will typically need to be dumped during the following WFC exposure, assuming it is longer than 340 seconds. For shorter exposures an extra overhead of this length is imposed.

ACS's internal buffer stores the data in a 16 bit-per-pixel format. This structure imposes a maximum of 65,535 counts per pixel. For the MAMA detectors this maximum is equivalent to a limit on the total number of detected photons per pixel which can be accumulated in a single exposure. For the WFC and HRC, the full well (and not the 16 bit buffer format) limits the photons per pixel which can be accumulated without saturating in a single exposure when  $GAIN > 1$  and  $GAIN > 2$ , respectively, are selected.

### 1.2.4 Parallel Operations

Parallel observations with the WFC and HRC are possible with ACS for certain filter combinations. ACS can be used in parallel with any of the other science instruments on HST within restrictions described in detail in the *ACS Instrument Handbook*. There are significant constraints on the use of the MAMA detectors in parallel. The policy for applying for parallel observing time is described in the *HST Call for Proposals*.



CHAPTER 2:

# ACS Data Structure

**In this chapter. . .**

2.1 Types of ACS Files / 2-2

2.2 ACS File Structure / 2-5

2.3 Data Storage Requirements / 2-7

2.4 Headers and Keywords / 2-9

This chapter describes the ACS data products, including a discussion of file suffixes, association tables, and trailer files. It describes the FITS file structure and data storage requirements for ACS images. Finally, a description of the FITS header keywords is provided for both primary and extension headers.

## 2.1 Types of ACS Files

### 2.1.1 Data Files and Suffixes

The file suffixes given to ACS data products are described in Table 2.1 and closely mimic the suffixes used by STIS. The initial input files to the calibration pipeline are the raw (RAW) files from Generic Conversion and the association (ASN) table, if applicable, for the complete observation set.

For CCD images, a temporary file, with the suffix BLV\_TMP, is created once bias levels are subtracted and the overscan regions are trimmed. This file is renamed with the FLT extension after the standard calibrations (flat fielding, dark subtraction, etc.) are complete. The FLT files will serve as input for cosmic ray rejection (if required). For CR-SPLIT exposures, a temporary ‘*cr-combined image*’ (CRJ\_TMP) is created and then renamed with the CRJ extension once basic calibrations are complete. Single MAMA images are given the FLT suffix once calibrations are complete. By definition, these images do not have an overscan region and are not affected by cosmic rays. The calibrated products of a REPEAT-OBS association will be several individually calibrated FLT exposures and a summed flat-fielded (but not cosmic-ray cleaned) SFL image.

Table 2.1: ACS File Suffixes:

File Suffix	Description	Units
_RAW	Raw data	<i>DN</i>
_ASN	Association file for observation set	
_SPT	Telemetry and engineering data	
_TRL	Trailer File with processing comments	
_BLV_TMP	Overscan-trimmed individual exposure (renamed to _FLT)	<i>DN</i>
_CRJ_TMP	Uncalibrated, CR-rejected Combined image (renamed to _CRJ)	<i>DN</i>
_FLT	Calibrated, Flat fielded individual exposure	<i>electrons</i>
_CRJ	Calibrated, CR-rejected, Combined image	<i>electrons</i>
_SFL	Calibrated, Repeat-Obs, Combined image	<i>electrons</i>
_DRZ	Calibrated, Geometrically Corrected, Dither-Combined image	<i>electrons/sec</i>

### 2.1.2 Association Tables

Association tables are useful for keeping track of the complex set of relationships that can exist between exposures taken with ACS, especially with REPEAT-OBS, CR-SPLIT, and dithered exposures. Images taken at a given dither position may be additionally CR-SPLIT into multiple

exposures. In these cases, associations are built to describe how each exposure relates to the desired final product. As a result, ACS associations will create one or more science products from the input exposures, unlike NICMOS or STIS associations. The relationships defined in the association table determine how far through the calibration pipeline the exposures are processed and when the calibrated exposures are combined into sub-products for further calibration.

ACS data files are given the following definitions:

- An *exposure* is a single image, the “atomic unit” of HST data.
- A *dataset* is a collection of files having a common root name (first 9 characters).
- A *sub-product* is a dataset created by combining a subset of the exposures in an association.
- A *product* is a dataset created by combining sub-products of an association.

ACS association tables were designed to closely resemble the NICMOS association format, with three primary columns: MEMNAME, MEMTYPE, and MEMPRSNT. The column MEMNAME gives the name of each exposure making up the association and output product name(s). The column MEMTYPE specifies the role the file has in the association. A unique set of MEMTYPES specific to ACS were adopted to provide the support for multiple products. These types are summarized in Table 2.2.

Table 2.2: Exposure types in ACS associations. The suffix “n” is appended to the MEMTYPE when multiple sets are present within a single association.

MEMTYPE	Description
EXP-CRJ	Input CR-SPLIT exposure (single set)
EXP-CR $n$	Input CR-SPLIT exposure for CR-combined image $n$ (multiple sets)
PROD-CRJ	CR-combined output product (single set)
PROD-CR $n$	CR-combined output product $n$ (multiple sets)
EXP-RPT	Input REPEAT-OBS exposure (single set)
EXP-RP $n$	Input REPEAT-OBS exposure for repeated image $n$ (multiple sets)
PROD-RPT	REPEAT-OBS combined output product (single set)
PROD-RP $n$	REPEAT-OBS combined output product $n$ (multiple sets)
EXP-DTH	Input dither exposure
PROD-DTH	Dither-combined output product

A sample association table for a two-position dithered observation with `CR-SPLIT=2` is presented in Table 2.3. This example shows how both `MEMNAME` and `MEMTYPE` are used to associate input and output products. The `MEMTYPE` for each component of the first `CR-SPLIT` exposure, `JxxxxxECM` and `JxxxxxEGM`, are given the type `EXP-CR1`. The sub-product `Jxxxxx011` is designated in the table with a `MEMTYPE` of `PROD-CR1`. The last digit of the product filename corresponds to the output product number in the `MEMTYPE`. A designation of zero for the last digit in the filename is reserved for the dither-combined product.

The column `MEMPRSNT` indicates whether a given file already exists. For example, if cosmic ray rejection has not yet been performed by `CALACS`, the `PROD-CRn` files will have a `MEMPRSNT` value of “no”. The sample association table in Table 2.3 shows the values of `MEMPRSNT` prior to `CALACS` processing.

Table 2.3: Sample Association Table `Jxxxxx010_ASN`

<code>MEMNAME</code>	<code>MEMTYPE</code>	<code>MEMPRSNT</code>
<code>JxxxxxECM</code>	<code>EXP-CR1</code>	yes
<code>JxxxxxEGM</code>	<code>EXP-CR1</code>	yes
<code>Jxxxxx011</code>	<code>PROD-CR1</code>	no
<code>JxxxxxEMM</code>	<code>EXP-CR2</code>	yes
<code>JxxxxxEOM</code>	<code>EXP-CR2</code>	yes
<code>Jxxxxx012</code>	<code>PROD-CR2</code>	no
<code>Jxxxxx010</code>	<code>PROD-DTH</code>	no

### 2.1.3 Trailer Files

Each task in the `CALACS` package creates messages during processing which describe the progress of the calibration and which are sent to `STDOUT`. In the pipeline processing for other HST instruments, trailer files were created by simply redirecting the `STDOUT` to a file. Because multiple output files can be processed in a single run of `CALACS`, creating trailer files presents a unique challenge. Each task within the `CALACS` package must decide which trailer file should be appended with comments and automatically open, populate, and close each trailer file.

`CALACS` will *always overwrite* information in trailer files from previous runs of `CALACS` while preserving any comments generated by Generic Conversion. This ensures that the trailer files accurately reflect the most recent processing performed. The string `CALACSBEG` will mark the first comment added to the trailer file. If a trailer file already exists, `CALACS` will search for this string to determine where to append



processing comments. If it is not found, the string will be written to the end of the file and all comments will follow. Thus any comments from previous processing are overwritten and only the most current calibrations are recorded.

As each image is processed, an accompanying trailer file with the `.trl` ending will be created. Further processing will concatenate all trailer files associated with the output product into a single file. Additional messages will then be appended to this concatenated file. Thus, some information is duplicated across multiple trailer files, but for any product processed within the pipeline, the trailer file is ensured to contain processing comments from each input file.

Linking trailer files together can result in multiple occurrences of the *CALACSBEG* string. Only the first, however, determines where **CALACS** will begin overwriting comments if an observation is reprocessed.

---

## 2.2 ACS File Structure

The ACS calibration pipeline assembles data received from HST into datasets, applies the standard calibrations, and stores the uncalibrated datasets in the HST Data Archive. The structure of these data products is based on the STIS and NICMOS file format and consists of multi-extension FITS files which store science (SCI), data quality (DQ) and error (ERR) arrays, as shown in Figure 2.1.

ACS WFC data come from two CCD chips and are treated as separate observations, with a SCI, DQ and ERR array for each chip, and with both chips being stored in the same FITS file. The result is a FITS file with 6 data extensions plus a global header for a single WFC exposure. The WFC apertures are plotted with respect to the V2/V3 reference frame in Figure 2.2 and are oriented such that the x-axis is approximately to the right and the y-axis is approximately straight up. For pipeline data products, chip 2 is below chip 1 in y-pixel coordinates and was therefore defined as extension 1. Thus, the chip/extension notation is counterintuitive. To display the science image for chip 1, the user must specify the extension `'file.fits[sci,2]'`. Similarly, the data quality and error array for chip 1 are specified as `[dq,2]` and `[err,2]`.

A single HRC or SBC exposure comes from a single chip and has only 3 data extensions plus a global header. While the raw and calibrated WFC images contain 6 data extensions, the drizzled product will always contain 3 data extensions, no matter which detector was used. When WFC data is drizzled, both chips are included in a single FITS extension.

Figure 2.1 illustrates the basic format for storing ACS images. An uncalibrated (RAW) exposure contains a primary header plus, for each chip, a SCI extension (in 16-bit integer format), an empty ERR extension, and an empty DQ array. The calibrated product from **CALACS** contains a

primary header plus, for each chip, a SCI extension (in 32-bit float format), an ERR extension (32-bit float), and a DQ extension (16-bit integer).

**MultiDrizzle** removes the effects of the geometric distortion and produces a drizzled (DRZ) product which has the multi-extension FITS file shown in Figure 2.1. The SCI extension contains the distortion-corrected data (32-bit float), the WHT extension contains the weight mask (32-bit float), and the CTX extension contains the context image (32-bit integer). For more information on these DRZ product extensions, refer to “Data Products” in Section 4.4.

Figure 2.1: Data format for calibrated and drizzled ACS modes. Note that for calibrated science data, WFC1 (chip 1) corresponds to extension [sci,2].

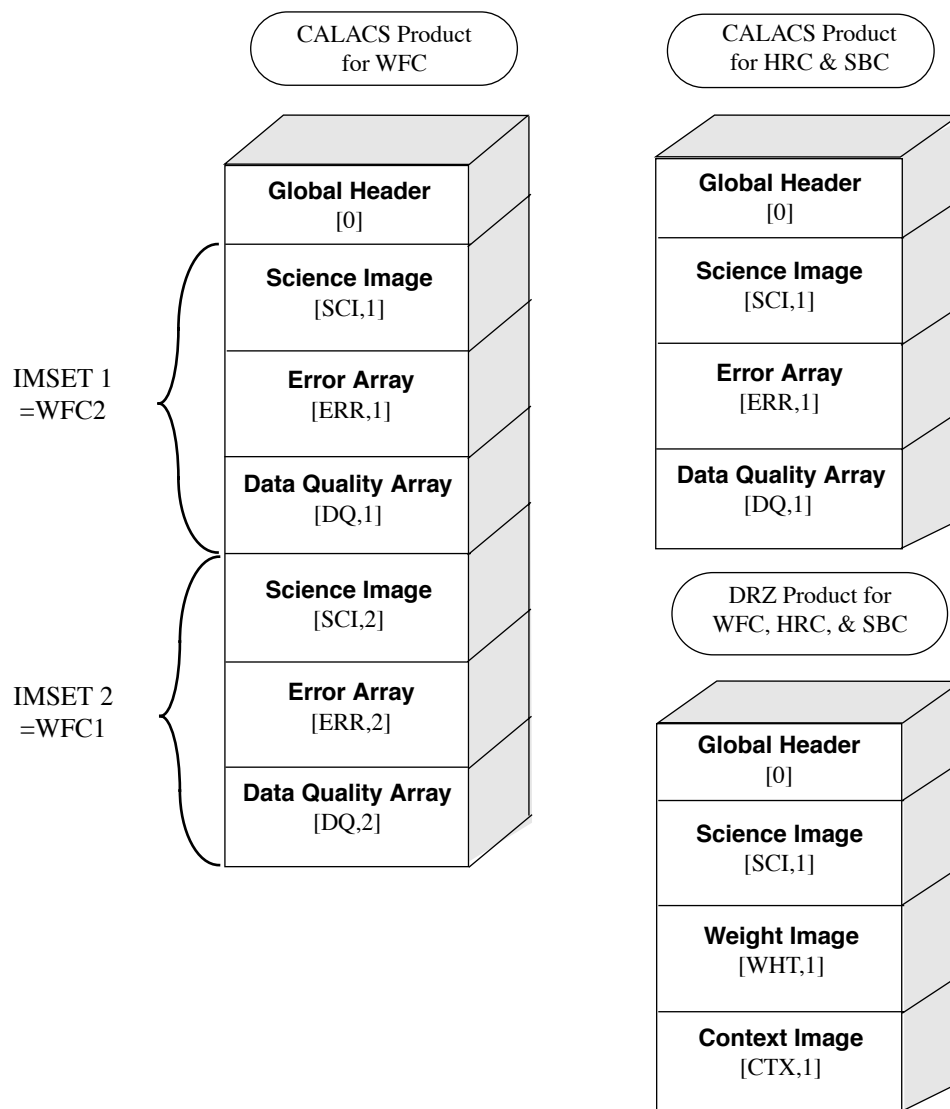
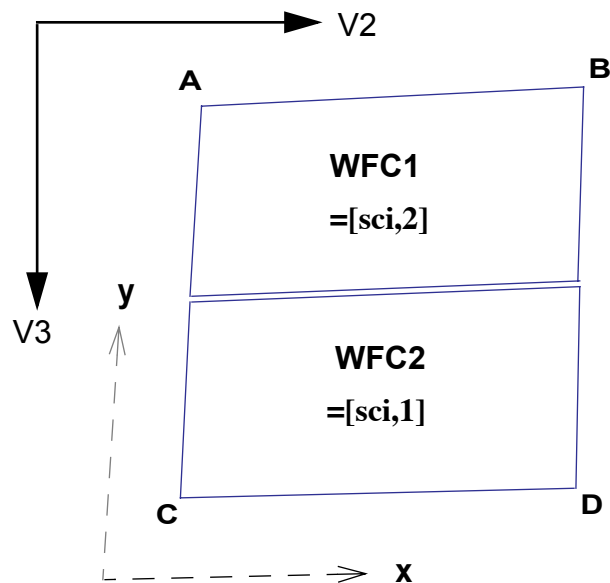


Figure 2.2: WFC apertures compared with the V2/V3 reference frame. The read-out amplifiers (A,B,C,D) are indicated on the figure. In detector pixel coordinates, WFC1 (chip 1, which uses amps A,B) is on top. The science image for chip 1 is therefore specified as [sci,2].



## 2.3 Data Storage Requirements

Users are reminded to consider the large size of WFC exposures when allocating disk space for storing and reprocessing ACS data. Raw images serve as input to the calibration pipeline and have the file sizes (in MB) given in Table 2.4. The WFC image includes two SCI arrays, while the HRC and SBC detectors have a single array. The raw image sizes presume that both the SCI and DQ arrays are populated with short integer values, but that the ERR arrays are NULL (all pixels have a value of zero).

During **CALACS** processing, the SCI arrays are converted from integer to floating point values. The null ERR array is populated with floating point values, and the null DQ array is populated with integer values. As a result, the size of calibrated images (in MB) is much larger. The image size in pixels is given in Table 2.5. Calibrated images taken with the WFC and HRC detectors are smaller than raw images because the overscan regions have been trimmed during processing.

After calibration, **MultiDrizzle** combines the science, data quality, and error arrays for each detector into a single science, weight, and context extension. Once the distortion is corrected, the size of the drizzled images will be larger (in pixels and also in MB) than the calibrated images due to the fact that their projection on the sky is rhombus-shaped, rather than square. The specific dimensions of the drizzled image depend on the image

orientation and on which distortion model is currently in use in the pipeline and will vary slightly (~1-2 pixels) due to the effects of velocity aberration.

Table 2.4: Size (in MB) of raw, calibrated, and drizzled ACS images for each detector. The drizzled image sizes are distortion-corrected only and assume no additional rotation, dither offset or scale change.

Detector	Size of FITS file ( $S_{raw}$ )	Size of FITS file ( $S_{cal}$ )	Size of FITS file ( $S_{drz}$ )
WFC (2 Chips)	68.7 MB	168 MB	215 MB
HRC (1 Chip)	4.4 MB	10.5 MB	16 MB
SBC (1 Chip)	4.2 MB	10.5 MB	16 MB

Table 2.5: Size (in pixels) for raw, calibrated, and drizzled ACS images for each detector. The drizzled image sizes are distortion-corrected only and assume no additional rotation, dither offset or scale change. The size of drizzled images will vary slightly due to velocity aberration effects.

Detector	$X_{raw}$	$Y_{raw}$	$X_{cal}$	$Y_{cal}$	$X_{drz}$	$Y_{drz}$
WFC (2 Chips)	4144	2068	4096	2048	4213	4240
HRC (1 Chip)	1062	1044	1024	1024	1164	1138
SBC (1 Chip)	1024	1024	1024	1024	1397	1341

While the size of calibrated, drizzled HRC and SBC images is comparable to that of STIS or WFPC2, the ACS WFC images are over 16 times as large. The following equation can be used to estimate the minimum amount of free storage required for processing associated ACS data:

$$D_{min} = n \cdot S_{raw} + (1 + n) \cdot S_{cal} + (2.1 + p^2) \cdot S_{drz}$$

where:

- $D_{min}$  is the minimum free disk space required for processing,
- $n$  is the number of exposures in each CR-SPLIT set or REPEAT-OBS set,
- $S_{raw}$  is the size of the raw exposure (from Table 2.4),
- $S_{cal}$  is the size of the calibrated exposure (from Table 2.4),
- $S_{drz}$  is the size of the distortion-corrected exposure (from Table 2.4),
- $p$  is the percentage shift (in pixels) across all dither positions

## 2.4 Headers and Keywords

While the ACS image headers for the WFC, HRC, HRC-ACQ, and SBC observations have very similar formats, two main differences are apparent. The MAMA (SBC) headers require a slightly modified structure from the CCD (WFC, HRC) headers, and the HRC-ACQ headers require several unique keywords.

In Table 2.6 and Table 2.7, we describe the ACS header keywords, with a note indicating to which detector those keywords refer. The primary header keywords (FITS extension 0) are given in Table 2.6, and the extension header keywords (FITS extensions > 0) are given in Table 2.7. For more information about primary and extension FITS headers, refer to Section 2.1.1 of the HST Data Handbook Introduction.

Table 2.6: ACS Primary Header Keywords (FITS extension 0)

KEYWORD	DESCRIPTION
SIMPLE	data conform to FITS standard (T/F)
BITPIX	bits per data value
NAXIS	number of data axes
EXTEND	file may contain standard extensions (T/F)
NEXTEND	number of standard extensions
GROUPS	image is in group format? (T/F)
DATE	date this file was written (yyyy-mm-dd)
FILENAME	name of file
FILETYPE	type of data found in data file
TELESCOP	telescope used to acquire data
INSTRUME	identifier for instrument used to acquire data
EQUINOX	equinox of celestial coordinate system
<b>DATA DESCRIPTION KEYWORDS (All Detectors)</b>	
ROOTNAME	rootname of the observation set
IMAGETYP	type of exposure identifier
PRIMESI	instrument designated as prime
<b>TARGET INFORMATION (All Detectors)</b>	
TARGNAME	proposer's target name
RA_TARG	right ascension of the target (deg) (J2000)
DEC_TARG	declination of the target (deg) (J2000)
<b>PROPOSAL INFORMATION (All Detectors)</b>	
PROPOSID	PEP proposal identifier
LINENUM	proposal log line number
PR_INV_L	last name of principal investigator
PR_INV_F	first name of principal investigator
PR_INV_M	middle name / initial of principal investigator

<b>EXPOSURE INFORMATION (All Detectors)</b>	
SUNANGLE	angle between sun and V1 axis
MOONANGL	angle between moon and V1 axis
SUN_ALT	altitude of the sun above Earth's limb
FGSLOCK	commanded FGS lock (fine, coarse, gyros, unknown)
TWOGYRO	observation scheduled with only two gyros? (Y/N)
DATE-OBS	UT date of start of observation (yyyy-mm-dd)
TIME-OBS	UT time of start of observation (hh:mm:ss)
EXPSTART	exposure start time (modified Julian date)
EXPEND	exposure end time (modified Julian date)
EXPTIME	exposure duration (seconds)--calculated
EXPFLAG	exposure interruption indicator
<b>POINTING INFORMATION (All Detectors)</b>	
PA_V3	position angle of V3-axis of HST (deg)
<b>TARGET OFFSETS (POSTARGS) (All Detectors)</b>	
POSTARG1	POSTARG in axis 1 direction
POSTARG2	POSTARG in axis 2 direction
<b>DIAGNOSTIC KEYWORDS (All Detectors)</b>	
OPUS_VER	OPUS software system version number
CAL_VER	CALACS code version
PROCTIME	pipeline processing time (MJD)
<b>SCIENCE INSTRUMENT CONFIGURATION (All Detectors)</b>	
OBSTYPE	observation type (imaging, spectroscopic, coronagraphic)
OBSMODE	operating mode
CTEIMAGE	type of charge transfer image, if applicable
SCLAMP	lamp status: NONE or name of lamp which is on
NRPTXP	number of repeat exposures in set (default=1)
SUBARRAY	data from a subarray (T) or full frame (F)
DETECTOR	detector in use: WFC, HRC or SBC
FILTER1	element selected from filter wheel 1
FILTER2	element selected from filter wheel 2
FWOFFSET	computed filter wheel offset (0, +1, -1)
FWERROR	filter wheel position error flag (T, F)
LRFWAVE	proposed linear ramp filter wavelength
APERTURE	aperture name
PROPAPER	proposed aperture name
DIRIMAGE	direct image for grism or prism exposure
CTEDIR	CTE measurement direction: serial or parallel
CRSPLIT	number of cosmic ray split exposures
<b>MAMA OFFSETS (SBC Only)</b>	
MOFFSET1	axis 1 MAMA offset
MOFFSET2	axis 2 MAMA offset

<b>LOCAL RATE CHECK IMAGE (SBC Only)</b>	
LRC_XSTS	local rate check image exists (T/F)
LRC_FAIL	local rate check failed (T/F)
<b>CALIBRATION SWITCHES: PERFORM, OMIT (All Detectors)</b>	
STATFLAG	calculate statistics? (T/F)
WRERR	write out error array extension? (T/F)
DQICORR	data quality initialization?
ATODCORR	correct for A to D conversion errors?
BLEVCORR	subtract bias level computed from overscan image?
BIASCORR	subtract bias image?
FLSHCORR	subtract post flash image?
CRCORR	combine observations to reject cosmic-rays?
EXPSCORR	process individual observations after cr-reject?
SHADCORR	apply shutter shading correction?
GLINCORR	correct for global detector non-linearities? (SBC only)
LFLGCORR	flag pixels for local and global nonlinearities? (SBC only)
DARKCORR	subtract dark image?
FLATCORR	apply flat field correction?
PHOTCORR	populate photometric header keywords?
RPTCORR	add individual repeat observations?
DRIZCORR	drizzle-combine dithered images?
<b>CALIBRATION REFERENCE FILES (All Detectors)</b>	
BPIXTAB	bad pixel table
CCDTAB	CCD calibration parameter table
ATODTAB	analog-to-digital correction file
OSCNTAB	CCD overscan table
BIASFILE	bias image file name
FLSHFILE	post flash image file name
CRREJTAB	cosmic-ray rejection parameter table
SHADFILE	shutter shading correction file
MLINTAB	MAMA linearity correction table (SBC only)
DARKFILE	dark image file name
PFLTFILE	pixel-to-pixel flat field file name
DFLTFILE	delta-flat field file name
LFLTFILE	low order flat
CFLTFILE	Coronagraphic Spot Flat
SPOTTAB	Table with Coronagraphic Spot Position versus Date
PHOTTAB	photometric throughput table (not used)
GRAPHTAB	HST graph table
COMPTAB	HST components table
IDCTAB	image distortion correction table
DGEOFILE	distortion correction image
MDRIZTAB	MultiDrizzle parameter table

<b>COSMIC RAY REJECTION ALGORITHM PARAMETERS (WFC, HRC, HRC ACQ)</b>	
MEANEXP	reference exposure time
SCALENSE	multiplicative scale factor applied to noise
INITGUES	initial guess method (min, med)
SKYSUB	sky value subtracted (mode, none)
SKYSUM	sky level from the sum of all constituent images
CRSIGMAS	statistical rejection criteria
CRRADIUS	rejection propagation radius (pixels)
CRTHRESH	rejection propagation threshold
BADINPDQ	data quality flag used for rejection
REJ_RATE	rate at which pixels are affected by cosmic rays
CRMASK	flag CR-rejected pixels in input files? (T/F)
MDRIZSKY	sky value computed by MultiDrizzle
<b>PATTERN KEYWORDS (WFC, HRC, SBC)</b>	
PATTERN1	primary pattern type
P1_SHAPE	primary pattern shape
P1_PURPS	primary pattern purpose
P1_NPTS	number of points in primary pattern
P1_PSPAC	point spacing for primary pattern (arcsec)
P1_LSPAC	line spacing for primary pattern (arcsec)
P1_ANGLE	angle between sides of parallelogram patt (deg)
P1_FRAME	coordinate frame of primary pattern
P1_ORINT	orientation of pattern to coordinate frame (deg)
P1_CENTR	center pattern relative to pointing (yes/no)
PATTSTEP	position number of this point in the pattern
<b>POST FLASH PARAMETERS (WFC, HRC, HRC ACQ)</b>	
FLASHDUR	exposure time in seconds: 0.1 to 409.5
FLASHCUR	post-flash current (off, low, med, high)
FLASHSTA	status (successful, aborted, not performed)
SHUTRPOS	shutter position (A or B)
<b>ENGINEERING PARAMETERS (WFC, HRC, HRC ACQ)</b>	
CCDAMP	CCD amplifier read out configuration
CCDGAIN	commanded gain of CCD (electrons/DN)
CCDOFSTA	commanded CCD bias offset for amplifier A (electrons)
CCDOFSTB	commanded CCD bias offset for amplifier B (electrons)
CCDOFSTC	commanded CCD bias offset for amplifier C (electrons)
CCDOFSTD	commanded CCD bias offset for amplifier D (electrons)



<b>CALIBRATED ENGINEERING PARAMETERS (WFC, HRC, HRC ACQ)</b>	
ATODGNA	calibrated gain for CCD amplifier A (electrons/DN)
ATODGNB	calibrated gain for CCD amplifier B (electrons/DN)
ATODGNC	calibrated gain for CCD amplifier C (electrons/DN)
ATODGND	calibrated gain for CCD amplifier D (electrons/DN)
READNSEA	calibrated read noise for amplifier A (electrons)
READNSEB	calibrated read noise for amplifier B (electrons)
READNSEC	calibrated read noise for amplifier C (electrons)
READNSED	calibrated read noise for amplifier D (electrons)
BIASLEVA	bias level for amplifier A (electrons)
BIASLEVB	bias level for amplifier B (electrons)
BIASLEVC	bias level for amplifier C (electrons)
BIASLEVD	bias level for amplifier D (electrons)
<b>TARGET ACQUISITION PARAMETERS (HRC only)</b>	
ACQTYPE	type of acquisition
ACQNAME	rootname of acquisition exposure
<b>TARGET ACQUISITION PARAMETERS (HRC ACQ only)</b>	
ACQTYPE	type of acquisition
CENTMETH	target acquisition centering method
CRELIM	perform cosmic ray rejection in acquisition
CCDBIASS	CCD bias subtracted from target acq image? (y/n)
BIASLEV	CCD bias level used to process acquisition exp.
CHECKBOX	size of checkbox for finding algorithms
TARGAREA	area of target (detector pixels)
<b>ASSOCIATION KEYWORDS (All Detectors)</b>	
ASN_ID	unique identifier assigned to association
ASN_TAB	name of association table
ASN_MTYP	role of exposure in association

Table 2.7: ACS Extension Header Keywords (FITS extensions &gt; 0)

KEYWORD	DESCRIPTION
XTENSION	extension type
BITPIX	bits per data value
NAXIS	number of data axes
NAXIS1	length of first data axis
NAXIS2	length of second data axis
PCOUNT	number of group parameters
GCOUNT	number of groups
INHERIT	inherit the primary header
EXTNAME	extension name
EXTVER	extension version number
ROOTNAME	rootname of the observation set
EXPNAME	9 character exposure identifier
DATAMIN	minimum data value (electrons)
DATAMAX	maximum data value (electrons)
BUNIT	brightness units (counts, electrons, electrons/sec)
BSCALE	scale factor for array value to physical value
BZERO	physical value for an array value of zero
<b>WORLD COORDINATE SYSTEM AND RELATED PARAMETERS (All Detectors)</b>	
WCSAXES	number of World Coordinate System axes
CRPIX1	x-coordinate of reference pixel
CRPIX2	y-coordinate of reference pixel
CRVAL1	first axis value at reference pixel
CRVAL2	second axis value at reference pixel
CTYPE1	the coordinate type for the first axis
CTYPE2	the coordinate type for the second axis
CD1_1	partial of first axis coordinate w.r.t. x
CD1_2	partial of first axis coordinate w.r.t. y
CD2_1	partial of second axis coordinate w.r.t. x
CD2_2	partial of second axis coordinate w.r.t. y
LTV1	offset in X to subsection start
LTV2	offset in Y to subsection start
LTM1_1	reciprocal of sampling rate in X
LTM2_2	reciprocal of sampling rate in Y
ORIENTAT	position angle of image y axis (degrees E of N)
RA_APER	RA of aperture reference position
DEC_APER	Dec of aperture reference position
PA_APER	position angle of aperture reference position (deg)
VAFCTOR	velocity aberration plate scale factor

<b>WFC CCD CHIP IDENTIFICATION (WFC only)</b>	
CCDCHIP	CCD chip (1 or 2)
<b>READOUT DEFINITION PARAMETERS (All Detectors)</b>	
CENTERA1	subarray axis1 center point in unbinned detector pixels
CENTERA2	subarray axis2 center point in unbinned detector pixels
SIZAXIS1	subarray axis1 size in unbinned detector pixels
SIZAXIS2	subarray axis2 size in unbinned detector pixels
BINAXIS1	axis1 data bin size in unbinned detector pixels
BINAXIS2	axis2 data bin size in unbinned detector pixels
<b>PHOTOMETRY KEYWORDS (All Detectors)</b>	
PHOTMODE	observation configuration for photometric calibration
PHOTFLAM	inverse sensitivity ( $\text{erg s}^{-1} \text{cm}^{-2} \text{A}^{-1}$ for 1 electron/sec)
PHOTZPT	ST magnitude zero point
PHOTPLAM	pivot wavelength
PHOTBW	rms bandwidth of filter plus detector
<b>REPEATED EXPOSURES INFO (WFC, HRC, HRC ACQ)</b>	
NCOMBINE	number of image sets combined during CR rejection
<b>DATA PACKET INFORMATION (All Detectors)</b>	
FILLCNT	number of segments containing fill
ERRCNT	number of segments containing errors
PODPSFF	podps fill present? (T/F)
STDCFFF	ST DDF fill present? (T/F)
STDCFFP	ST DDF fill pattern (hex)
<b>ON-BOARD COMPRESSION INFORMATION (WFC Only)</b>	
WFCMPRSD	was WFC data compressed? (T/F)
CBLKSIZ	size of compression block in bytes
LOSTPIX	number of pixels lost due to buffer overflow
COMPTYP	compression type performed? (partial/full)
<b>TARGET ACQUISITION PARAMETERS (HRC ACQ Only)</b>	
TARGA1	fsw located subarray axis1 coord. of target
TARGA2	fsw located subarray axis2 coord. of target
APERA1	fsw located subarray axis 1 coord. of aperture
APERA2	fsw located subarray axis 2 coord. of aperture
APERLKA1	axis 1 detector pixel of acq aperture center
APERLKA2	axis 2 detector pixel of acq aperture center
MAXCHCNT	counts in the brightest checkbox
BOPOFFA1	axis 1 offset (arcs) object moved off aperture
BOPOFFA2	axis 2 offset (arcs) object moved off aperture

<b>ENGINEERING PARAMETERS (SBC Only)</b>	
GLOBRATE	global count rate
GLOBLIM	was global linearity level exceeded?
<b>IMAGE STATISTICS AND DATA QUALITY FLAGS (All Detectors)</b>	
NGOODPIX	number of good pixels
SDQFLAGS	serious data quality flags considered 'bad' by CALACS
GOODMIN	minimum value of good pixels (electrons)
GOODMAX	maximum value of good pixels (electrons)
GOODMEAN	mean value of good pixels (electrons)
SOFTERRS	number of soft error pixels (DQF=1)
SNRMIN	minimum signal to noise of good pixels
SNRMAX	maximum signal to noise of good pixels
SNRMEAN	mean signal to noise of good pixels
MEANDARK	average of the dark values subtracted (electrons)
MEANBLEV	average of all bias levels subtracted (electrons)
MEANFLSH	Mean number of counts in post flash exposure (electrons)
<b>ORIGINAL (OLD) WORLD COORDINATE SYSTEM INFORMATION (All Detectors)</b>	
WCSCDATE	Time WCS keywords were copied
OCRPIX1	x-coordinate of reference pixel
OCRPIX2	y-coordinate of reference pixel
OCRVAL1	first axis value at reference pixel
OCRVAL2	second axis value at reference pixel
OCTYPE1	the coordinate type for the first axis
OCTYPE2	the coordinate type for the second axis
OCD1_1	partial of first axis coordinate w.r.t. x
OCD1_2	partial of first axis coordinate w.r.t. y
OCD2_1	partial of second axis coordinate w.r.t. x
OCD2_2	partial of second axis coordinate w.r.t. y
ONAXIS1	x-axis length
ONAXIS2	y-axis length
OORIENTA	position angle of image y axis (degrees E of N)

# ACS Calibration Pipeline

In this chapter. . .

3.1 On The Fly Reprocessing (OTFR) / 3-2
3.2 Pipeline Overview / 3-3
3.3 Structure of CALACS / 3-6
3.4 CALACS Processing Steps / 3-10
3.5 Manual Recalibration of ACS Data / 3-25

This chapter describes the ACS calibration pipeline and the On-the-Fly-Reprocessing (OTFR), which is standard for all HST data requested from the STScI archive. The pipeline software consists of two separate packages: **CALACS** and **MultiDrizzle**. **CALACS** primarily removes various instrumental signatures and updates header keyword values. **MultiDrizzle** corrects images for geometric distortion, performs cosmic ray rejection, and combines observations which were taken as part of a dither pattern.

The data products from OTFR are described, as well as considerations and requirements for manual recalibration. The remaining bulk of the chapter is devoted to a detailed description of **CALACS**. While **MultiDrizzle** is also used during pipeline processing, a detailed discussion of this software is deferred to Chapter 4.

---

## 3.1 On The Fly Reprocessing (OTFR)

OTFR is now the standard way of processing data which has been requested by the user from the STScI archive. It provides the best calibrated products by reprocessing the raw telemetry files “on-the-fly” for distribution each time data is requested. Each observation requires calibrations suited to the particular mode used for taking data. Calibration data specific to the various modes of ACS operation are prepared and archived in the Calibration Data Base System (CDBS).

The STScI calibration pipeline consists of two main software systems: the Operations Pipeline Unified System (OPUS) and the Data Archive and Distribution System (DADS). Raw spacecraft telemetry data from Goddard Spaceflight Center are transmitted to STScI in the form of POD files. When a user requests data from the HST Archive, OTFR uses the POD files as input to the OPUS step called Generic Conversion and generates the uncalibrated “raw” data. At the same time, Generic Conversion queries the CDBS to determine the most up-to-date reference files for the observation configuration. OPUS then runs **CALACS** to process the uncalibrated data, using specific ACS reference images and tables from the CDBS. With these data, DADS populates a database which is accessible to users via StarView. DADS then distributes any data (both calibrated and uncalibrated) requested for download to the user. (See Chapter 1 of the HST Introduction for more information.)

The most current ACS reference files are used by **CALACS** each time OTFR is run. The calibration reference files (e.g. flat fields, bad pixel tables) are also available from the HST Archive. Since reference files such as CCD biases and darks are frequently updated, OTFR may use different reference files depending on the date of reprocessing. Previously, the archived data from DADS had to be manually recalibrated by running the calibration software on the user’s home workstation with the updated reference files. OTFR replaces this step by automatically recalibrating with the most current reference data available. The user simply waits until the contemporaneous reference files are in place and requests the data via StarView or the HST web-based archive request form. The image header keywords are then updated with the names of the reference files used during that OTFR run. The PROCTIME keyword is updated to reflect the pipeline processing date and time in MJD.

OTFR allows the user to avoid downloading archived data which is outdated because of software changes made for bug fixes, improved algorithms, new capabilities, or header keyword changes. An archive request for calibrated data will result in OTFR reprocessing and distributing data which uses the latest software versions available.

Currently OTFR will distribute *all* files associated with an ACS observation, including both the uncalibrated and calibrated files. Future

versions could enable users to select only certain parts of the dataset, for example the final calibrated image. Future versions could also enable users to set calibration parameters for a particular OTFR run. Until then, OTFR will process with default values. Of course, the option of recalibrating aside from OTFR always exists. (See “Manual Recalibration of ACS Data” in Section 3.5.)

---

## 3.2 Pipeline Overview

Pipeline processing is carried out by 2 separate packages: **CALACS**, which corrects for instrumental effects and produces calibrated products, and **MultiDrizzle**, which corrects for distortion, performs cosmic ray rejection, and uses Drizzle/PyDrizzle to combine associated dithered data.

### 3.2.1 CALACS: Image Calibration

The **CALACS** software consists of a series of individual tasks that:

- Orchestrate the flow of data through the pipeline.
- Perform the initial tasks of basic two-dimensional image reduction (e.g., overscan subtraction, bias subtraction) for CCD data.
- Reject cosmic rays from CR-SPLIT CCD data.
- Perform the remaining tasks of basic two-dimensional image reduction (e.g., dark subtraction, flat fielding) for CCD and MAMA data.
- Sum any REPEAT-OBS exposures.

The calibrated products from the pipeline may still contain artifacts such as hot pixels and cosmic-rays. If hot pixels are to be detected and flagged by **CALACS**, dithered exposures are required. Similarly, cosmic ray rejection by the pipeline requires the specification of CR-SPLIT exposures in the observing program. Finally, the definition of associations has been expanded to include exposures that use REPEAT-OBS and POS TARG offsets, thereby allowing these data to be automatically corrected in the pipeline for cosmic-rays during subsequent processing with **MultiDrizzle**.

While intermediate steps in **CALACS** make use of sky subtraction, for example for identifying cosmic-rays, all data products created by the pipeline will *not* be sky subtracted. Fully calibrated data products (with suffixes FLT, CRJ, SFL) will be in units of *electrons*.

#### **CALACS and Single exposures**

A single raw ACS exposure is processed by **CALACS** following the steps outlined in Section 3.3. These steps include the standard detector

calibrations: bias subtraction, dark subtraction, flat fielding, etc. When **CALACS** processes a single raw exposure, the calibrated product is given the FLT suffix. The data in the calibrated SCI and ERR extensions are in units of *electrons*.

### **CALACS and Multiple exposures**

The same processing steps performed on single images are performed for multiple images which are part of an association. The result is a single calibrated product in units of *electrons*.

**CALACS** will recognize and correctly process CR-SPLIT or REPEAT-OBS exposures by interpreting the association table and determining which exposures should be combined during calibration. REPEAT-OBS exposures are individually run through all the calibration steps to create calibrated, flat-fielded (FLT) product for each input file. The FLT images are then summed to create the summed flat-fielded (SFL) product. No cosmic-ray rejection is performed for REPEAT-OBS images, until subsequent processing by **MultiDrizzle**.

Observations taken as part of a CR-SPLIT association, on the other hand, are combined during cosmic-ray rejection. First, the bias and dark subtraction is performed. Then, the images are combined while at the same time rejecting cosmic rays. The product is then flat fielded to create a single calibrated, cosmic-ray rejected, flat-fielded (CRJ) image.

### **CALACS and Dithered exposures**

Observations which use the dither patterns provided in the proposal instructions will be automatically associated for combining in the pipeline. As of Cycle 14, pointing patterns specified with POS-TARGs are also automatically combined in the pipeline. An effort is under way to retroactively create POS-TARG associations for pre-Cycle 14 datasets. Any pattern designed with POS-TARGs will not be associated. When processing observations which are part of a dither pattern, **CALACS** will produce a calibrated FLT, CRJ, or SFL file at each dither position. It will not, however, combine images from multiple positions. Further pipeline processing by **MultiDrizzle** will correct for geometric distortion and combine dithered images.

Table 3.1: The input and output image suffixes from **CALACS** and **MultiDrizzle** are given for various observing modes.

Image Type	CALACS Input	CALACS Output	MultiDrizzle Input	MultiDrizzle Output	Cosmic Ray Rejected?
Single	RAW	FLT	FLT	DRZ	No
RPT-OBS	ASN+RAW	FLT+SFL	ASN+FLT	DRZ	Yes
CR-SPLIT	ASN+RAW	FLT+CRJ	ASN+FLT	DRZ	Yes
DITH-PATTERN	ASN+RAW	FLT	ASN+FLT	DRZ	Yes



### 3.2.2 MultiDrizzle and PyDrizzle: Distortion Correction and Dither Combination

All ACS data will be automatically corrected for distortion during pipeline processing using the **MultiDrizzle** task which automatically performs image registration, cosmic ray rejection and final drizzle combination. This task relies on the IDCTAB reference file for a description of the distortion model. **MultiDrizzle** understands the ACS association tables which allow the pipeline to combine dithered observations. Observations which use the dither patterns provided in the proposal instructions, as well as exposures that rely on explicit POS-TARG offsets, are automatically associated for combining in the pipeline. **MultiDrizzle** will automatically produce images which are both astrometrically and photometrically accurate regardless of whether they were taken as a single exposure or a set of dithered exposures.

The flat-fielded, calibrated products from **CALACS** are listed in Table 3.1. The calibrated product of a single ACS exposure is an FLT file. The product of a CR-SPLIT or REPEAT-OBS association is a CRJ or SFL file, respectively. The product of a dither pattern is an FLT, CRJ or SFL file at *each* dither position. Using the FLT files as input, **MultiDrizzle** performs the geometric correction on *all* data (dithered or not), carries out cosmic ray rejection, and combines multiple dithered images into a single output image with the DRZ suffix. For WFC observations, both chips are combined into a single extension. **MultiDrizzle** also converts the data to units of count rate (*electrons/sec*).

It is important to recognize that **MultiDrizzle** is built around an earlier script, **PyDrizzle**, which was capable of aligning the images and correcting for the geometric distortion but did *not* remove cosmic-rays, instead relying on the CRJ products as input. The use of **MultiDrizzle** supersedes this, and uses the original FLT files directly as input to perform cosmic ray rejection and produce a final drizzled output image. This has significant advantages in cases where small numbers of CR-SPLIT images were obtained at a small number of different dither positions, as **MultiDrizzle** will use all the information from the FLT files to produce the best cosmic ray rejection. The resulting drizzled images should be generally useful for science as-is, although subsequent reprocessing off-line with **MultiDrizzle** may be desirable to optimize the data for some specific scientific applications. For information on obtaining this software, we refer the reader to Section 3.5.1.

### 3.2.3 When is OTFR *not* Appropriate?

The goal of the ACS pipeline is to provide data calibrated to a level suitable for initial evaluation and analysis for all users. Observers frequently require a detailed understanding of the calibrations applied to their data and the ability to repeat, often with improved products, the calibration process at their home institution. There are several occasions

when OTFR is not ideal and when off-line interactive processing by the user is required:

- when running **CALACS** with personal versions of reference files,
- when running **CALACS** with non-default calibration switch values,
- when images must be cleaned of artifacts such as new hot pixels or cosmic-rays.

While the final drizzled images from **MultiDrizzle** have been produced using parameters that are suitable for the widest range of scientific applications, there may remain some specific datasets that would benefit significantly from further processing off-line. For example, a different pixel scale or orientation may be desired, or cosmic ray rejection parameters might need to be slightly modified for some datasets. Therefore, the same version of **MultiDrizzle** script that is in the pipeline is also available to users in STSDAS for off-line processing of data that have been retrieved from the pipeline. **MultiDrizzle** provides a single-step interface to the complex suite of tasks in the STSDAS **dither** package. It is built around the **PyDrizzle** software and needs to be executed within the PyRAF environment. For more information, we refer the reader to Chapter 4.

---

## 3.3 Structure of CALACS

The **CALACS** package consists of four individual tasks listed in Table 3.2. These tasks are called automatically by **CALACS**, but each may be run separately should some variation in the normal processing be desired by the user.

Table 3.2: Tasks in the **CALACS** pipeline

<b>ACSCCD</b>	CCD specific calibrations
<b>ACSREJ</b>	Cosmic-ray rejection task
<b>ACS2D</b>	Basic MAMA and CCD calibrations
<b>ACSSUM</b>	Repeat-obs summing task

The flow of data through the ACS calibration pipeline and the decisions made while working with associated data are diagrammed in Figure 3.1. These calibration steps are also outlined below:

- Calculate a noise model for each pixel and record in the error array
- Flag known bad pixels and saturated pixels in the data quality array
- Subtract bias-level determined from overscan regions (CCD only)
- Subtract bias image (CCD only)

- Subtract post-flash image, if required (CCD only)
- Perform cosmic-ray rejection and combining of CR-SPLIT data (CCD only)
- Perform global linearity corrections (MAMA only)
- Scale and subtract dark image and calculate mean dark value
- Divide by flat field and multiply by gain
- Calculate photometry header keywords for flux conversion
- Calculate image statistics

Additional calibration steps are performed by **MultiDrizzle**, including:

- Compute offsets between dithered images (using **PyDrizzle**)
- Correct the geometric distortion of non-dithered images
- Perform cosmic ray rejection using the FLT files as input
- Convert the data units from electrons to electrons per second
- Combine calibrated dithered observations into a single product

As indicated in Figure 3.1, the calibration tasks have been split to handle CCD-specific calibrations (**ACSCCD**) separately from those steps which can be applied to any ACS data (**ACS2D**). For example, the MAMA data obtained with the SBC do not have the overscan regions found in CCD data.

The initial processing performed on CCD data alone is shown in Figure 3.2. The reference files appropriate for each processing step and the calibration switches controlling them are also given beside the name of the task they control. The output (overscan-trimmed image) from **ACSCCD** is then sent through **ACS2D** as shown in Figure 3.3. Raw MAMA data are processed from the start with **ACS2D**, which initializes the error and DQ arrays (already performed for CCD data) and which performs linearity corrections.

Figure 3.1: Flow Diagram for ACS data with CALACS task names in bold.

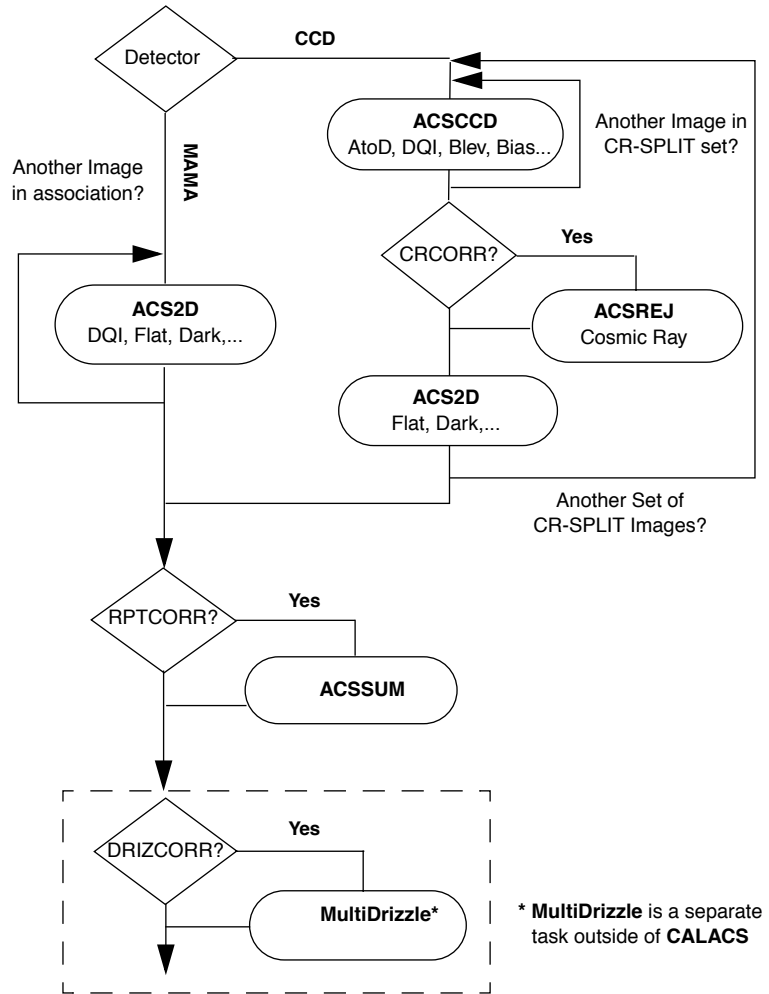


Figure 3.2: Flow diagram for CCD data using ACSCCD in CALACS.

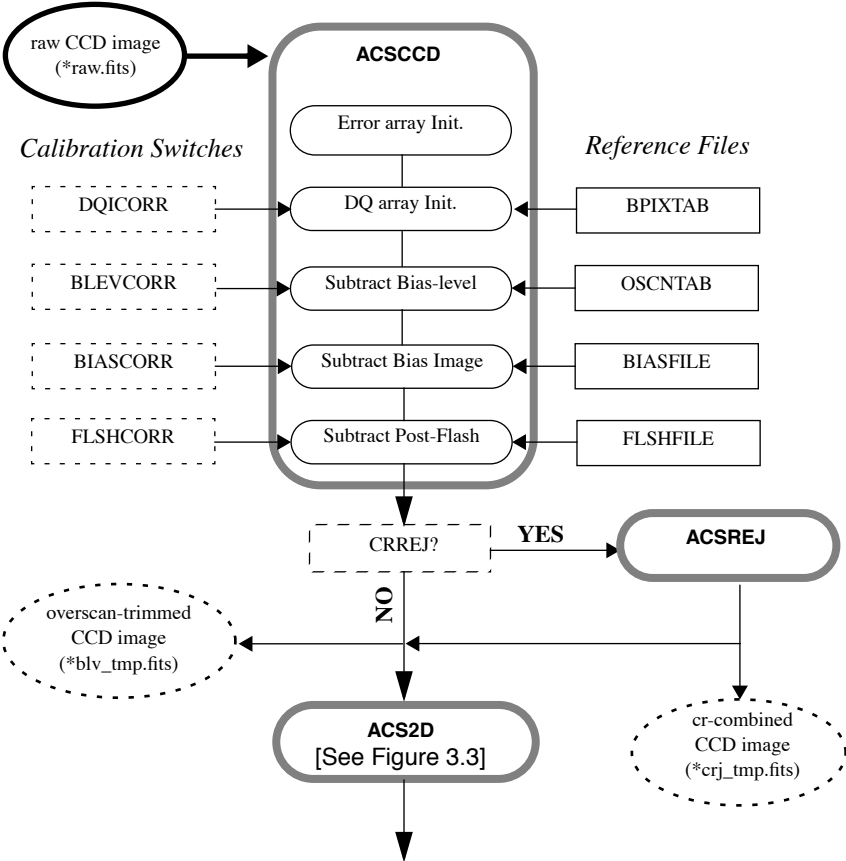
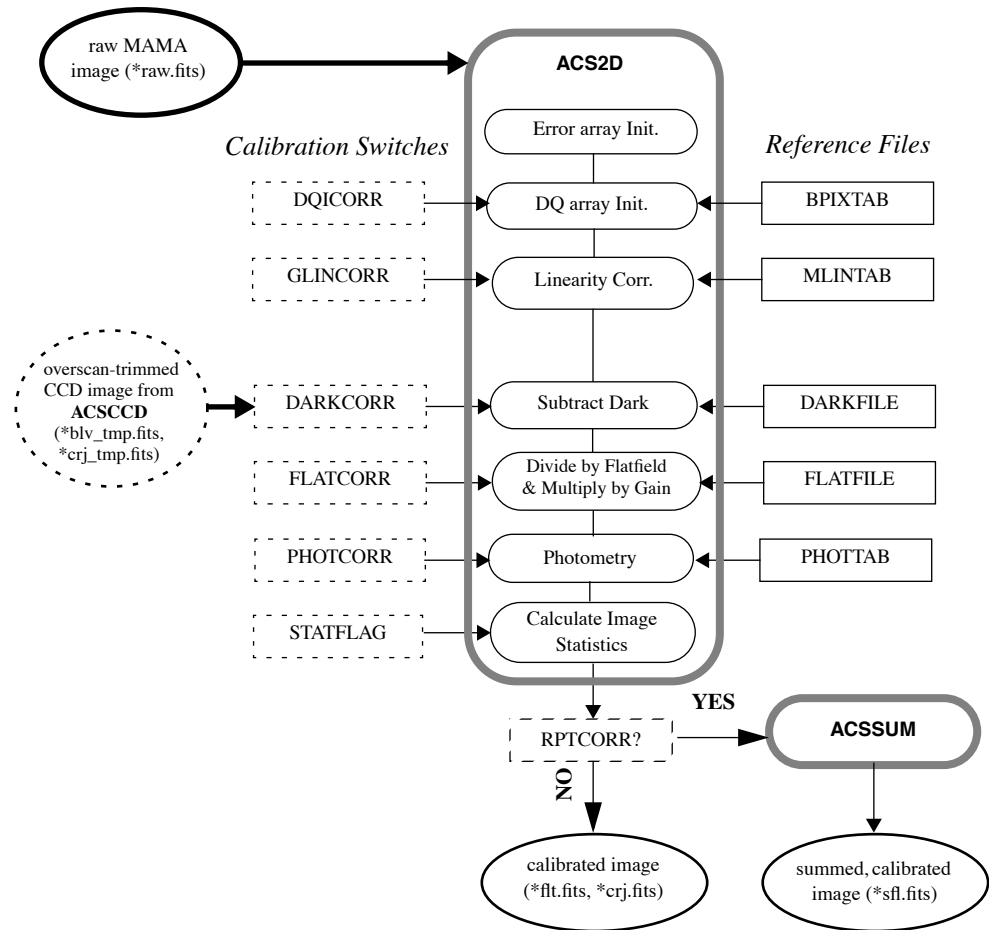


Figure 3.3: Flow diagram for MAMA and overscan-trimmed CCD data using ACS2D in CALACS.



## 3.4 CALACS Processing Steps

The **CALACS** pipeline consists of four individual calibration tasks: **ACSCCD**, **ACSREJ**, **ACS2D**, and **ACSSUM**. These tasks are listed in Table 3.2 and diagrammed in Figure 3.1. **CALACS** is responsible for controlling the processing rather than actually calibrating the data. The individual tasks apply the desired calibration steps to the data and create the output products, including the trailer files.

In the following four sections, we describe each **CALACS** task, give a detailed description of the calibrations steps performed within each task, and give a brief description of the reference files used for each step.

### 3.4.1 ACSCCD

This routine contains the initial processing tasks for all ACS CCD data. These tasks are listed in operational order in Table 3.3. The bulk of this routine was based on the code for **CALSTIS1**. **ACSCCD** processes each image in the input list one at a time, using the header keywords to determine which calibrations are performed. Upon completion of **ACSCCD**, the overscan regions will be trimmed from the image and an output image with the file extension ‘\_blv\_tmp.fits’ is created.

Table 3.3: ACSCCD processing tasks

<b>doNoise</b>	Initialize error array
<b>doDQI</b>	Initialize data quality array
<b>doAtoD</b>	Perform A to D correction (currently skipped)
<b>doBlev</b>	Subtract bias level from overscan region
<b>doBias</b>	Subtract bias image
<b>doFlash</b>	Subtract post-flash image (if required)
<b>Final Output</b>	Output overscan-trimmed or full image

#### doNoise - Error Array Initialization

- Header Switch: None
- Header Keywords Updated: None
- Reference File: CCDTAB (\*\_ccd.fits)

The first processing step is initializing the image error array. The **doNoise** function examines the ERR extension of the input data to determine the state of the array. Input ‘\_raw.fits’ images delivered by Generic Conversion will contain a NULL ERR array, defined by the keywords NPIX1, NPIX2 and PIXVALUE, where PIXVALUE=0. If the ERR array has already been expanded and contains values other than zero, then this function does nothing. Otherwise, **CALACS** will initialize the array and **doNoise** will assign a simple noise model.

The noise model reads the science array and for each pixel calculates the error value  $\sigma$  (in DN for the CCD, in counts for the MAMA):

$$\sigma_{\text{CCD}} = \sqrt{(DN - bias)/(gain) + (readnoise/gain)^2}$$

$$\sigma_{\text{MAMA}} = \max(1, \sqrt{\text{counts}})$$

Because MAMA data is not processed with **ACSCCD**, the **doNoise** function is later called as part of **ACS2D**.

The CCDTAB reference file, the CCD Characteristics Table, is used to initialize the ERR array by determining the bias, gain, and readnoise for each observation. The table contains one row for each amp configuration which can be used during readout. Each configuration is uniquely identified

by the list of amps possible (CCDAMP), the particular chip being read out (CCDCHIP), the commanded gain (CCDGAIN), the commanded bias level (CCDBIAS), and the pixel bin size (BINAXIS). CCDTAB uses these commanded values to determine each amp's physical read-out characteristics, including readnoise (READNSE), A-to-D gain (ATODGN), and bias level (CCDOFST). Note that by using the bias level from the CCDTAB, instead of from a full bias image, to create the ERR array, slight errors may be introduced which could be relevant for faint sources.

### **doDQI - Bad Pixel Determination**

- Header Switch: DQICORR
- Header Keywords Updated: None
- Reference File: BPIXTAB (\*\_bpx.fits), CCDTAB (\*\_ccd.fits)

The function **doDQI** initializes the data quality (DQ) array by combining it with a table of known bad pixels for the detector, stored in the Bad-Pixel reference table (BPIXTAB). The type of bad pixel flags are listed in Table 3.4.

The DQ array may have already been partially populated to reflect pixels which were affected by telemetry problems or compression buffer overflow. Other DQ flags will be added in further processing steps (such as cosmic-ray rejection). For CCD data, the values in the SCI extension are also checked for saturation by comparison with the value of the SATURATE column in the CCD parameters table CCDTAB.

The **doDQI** function combines the DQ flags from pre-processing, from the BPIXTAB, and from saturation tests into a single result for the particular observation. These values are combined using a “bitwise/logical OR operator” for each pixel. Thus, if a single pixel is affected by two DQ flags, those flag values will be added in the final DQ array. This array then serves as a mask so that **CALACS** can ignore bad pixels during processing.

The BPIXTAB reference file maintains a record of the (x,y) position and DQ value for all known bad pixels in each CCD. These pixels may change as some hot pixels are annealed and others appear over time, for example. Permanently bad pixels due to chip defects may be flagged during Generic Conversion, and it is the job of the BPIXTAB to maintain the list of bad pixels applicable for a given time period.



Table 3.4: Flags for the DQ array

Flag Value	Definition
0	good pixel
1	Reed-Solomon decoding error
2	data replaced by fill value
4	bad detector pixel or beyond aperture
8	masked by aperture feature
16	hot pixel (dark current >0.08 e/sec)
32	CTE tail of hot pixel
64	warm pixel (dark current 0.02 to 0.08 e/sec)
128	bias structure (mostly bad columns)
256	saturation (full well or a-to-d)
512	bad pixel in reference file
1024	weak trap
2048	a-to-d saturation
4096	cosmic ray rejected by MultiDrizzle (based on all FLT files)
8192	cosmic ray rejected by ACSREJ (only done for CR-SPLITS)
16384	<i>reserved</i>



*A more detailed description of the Data Quality flags used in ACS data products, and their history, can be found on the web page:*

*[http://www.stsci.edu/hst/acs/analysis/reference\\_files/data\\_quality\\_flags.html](http://www.stsci.edu/hst/acs/analysis/reference_files/data_quality_flags.html)*

### **doAtoD - A-to-D Correction (skipped)**

- Header Switch: ATODCORR
- Header Keywords Updated: None
- Reference File: ATODTAB (\*\_a2d.fits)

The **doAtoD** function converts pixel values in the raw input image from units of DN (16-bit integer) to counts (32-bit float). An analog-to-digital correction would be applied if the CCD electronic circuitry, which performs the analog-to-digital conversion, were biased toward the assignment of certain DN (data number) values. Ground test results show that this correction is not currently needed, so the ATODCORR switch will always be set to OMIT.

**doBlev - Bias-level Correction**

- Header Switch: BLEVCORR
- Header Keywords Updated: BIASLEV[A,B,C,D], MEANBLEV, CRPIX[1,2], LTV[1,2]
- Reference File: OSCNTAB (\*\_osc.fits)

The **doBlev** function fits the bias level from the overscan region and subtracts it from the image data. The definition of the overscan region is taken from the OSCNTAB reference file. With these regions defined, the overscan level for each row of the input image is measured and a straight line is fit as a function of image line number. The fit will then be evaluated for each row of the input image, and that value will be subtracted from each pixel of that row. If the measured overscan level for a given row is greater than 3 sigma times the mean of all rows, that row will be excluded from the linear fit. If the overscan level cannot be determined, or if the overscan region is not present in the input image, a default value (the CCDBIAS from the CCD parameters table) will be subtracted instead. In this case, an error message will be written to the image trailer file.

In **CALSTIS**, the overscan regions were removed from the image just after the bias-level subtraction, since no subsequent processing was required. **CALACS**, on the other hand, retains the output image in memory until the completion of all the processing steps in **ACSCCD**. The overscan regions will not be trimmed until the image is written to disk at the completion of **ACSCCD**.

The positional keywords CRPIX\* and LTV\* will be updated to reflect the offset due to removing the overscan. In addition, the mean value of all overscan levels will be computed and written to the SCI extension header as MEANBLEV. The individual bias level measured for each amplifier will be written to the SCI header as BIASLEV\*.

The OSCNTAB reference file (Overscan Region Table) describes the overscan regions to be used for measuring the bias level of the observation. Each row corresponds to a specific configuration, given by the CCD amp and chip used. The columns TRIMX\* give the number of columns to trim off the beginning and end of each line (the physical overscan region), while the TRIMY\* columns give the number of rows to trim off the top and bottom of each column (the virtual overscan region). The result of trimming (TRIMX1 + TRIMX2) columns and (TRIMY1 + TRIMY2) rows gives the final calibrated image sizes, 4096x2048 for a full WFC image and 1024x1024 for a full HRC image. The OSCNTAB columns BIASSECTA\* and BIASSECTB\* give the range of image columns to be used for determining the bias level in the leading and trailing regions, respectively, of the physical overscan region. The virtual overscan region is also defined in the OSCNTAB, where (VX1, VY1) indicates the beginning of the upper or lower overscan region, extending to the position (VX2, VY2).

To determine which overscan regions were actually used for determining the bias level, users are encouraged to check the OSCNTAB reference file. If desired for manual calibration, users may modify the bias

section and virtual overscan region definitions in the reference table, but the TRIMX\*, TRIMY\* columns must not be changed.

### **doBias - Bias Image Subtraction**

- Header Switch: BIASCORR
- Header Keywords Updated: None
- Reference File: BIASFILE (\*\_bia.fits)

Subtraction of the bias image is performed prior to cosmic-ray rejection using the function **doBias**. The appropriate reference image, BIASFILE, is selected using the DETECTOR, CCDAMP, and CCDGAIN keywords. The dimensions of the science image are used to distinguish observations which use the entire chip from sub-array images. Because the bias image has already been scaled by the gain and had the overscan values subtracted, the bias image may have a mean pixel value which is less than one.

Due to the way the bias reference image is created, part of the dark subtraction is also included in this step. Dark counts accumulate for an additional time beyond the exposure time, primarily the time required to read out the detector, and this portion of the dark current is subtracted along with the bias. This is described further in the section on Dark Image Subtraction.

The bias reference files are updated frequently (~weekly). The BIASFILE has the same dimensions as a full-size science image, 1062x1044 for HRC and 4144x2068 for WFC, allowing for simple image arithmetic on arrays of equal size. Only after the completion of **ACSCCD** are the images trimmed to 1024x1024 (HRC) and 4096x2048 (WFC). **CALACS** assumes that CCD data will not be read-out in binned mode, so any image which is not the full size is assumed to be a sub-array.

For sub-array images, **CALACS** uses the LTV[1,2] keywords to extract the appropriate region from the reference file and apply it to the sub-array input image. For users who take their own bias files, the BIASFILE keyword will need to be updated manually before recalibrating. This is described in detail in Section 3.5.2.

### **doFlash - Post-Flash Subtraction**

- Header Switch: FLSHCORR
- Header Keywords Updated: MEANFLSH
- Reference File: FLSHFILE (\*\_fls.fits)

ACS has a post-flash capability to provide the means of mitigating the effects of Charge Transfer Efficiency degradation. The proposer controls whether to use this capability via the FLASHEXP optional parameter in the Phase II proposal. FLSHCORR has a default value of OMIT for pipeline processing even if post-flash is used, thus allowing the excess sky background to remain in the calibrated products. The user may recalibrate with this changed as desired.

The function **doFlash** will subtract the Post-Flash reference file, FLSHFILE, from the science image. This file has the same dimensions as a full-size science image, 1062x1044 for HRC and 4144x2068 for WFC,

allowing for simple image arithmetic on arrays of equal size. The appropriate FLSHFILE is selected using the following keywords from the image header: DETECTOR, CCDAMP, CCDGAIN, FLASHCUR and SHUTRPOS.

First, the success of the Post-Flash exposure is verified by checking the keyword FLASHSTA. If any problems were encountered, a comment will be added to the history comments in the SCI extension header. The FLSHFILE is then normalized to one second for the appropriate post-flash current level (LOW, MED, HIGH), given by the FLASHCUR keyword. The FLSHFILE is then multiplied by the flash duration in seconds (FLASHDUR) and is subtracted from the science image. Finally, the mean value of the scaled Post-Flash image is written to the output SCI extension header as the keyword MEANFLSH.

### Final Output

Upon completion of **ACSCCD**, the overscan regions will be trimmed from the image when it is written out, but only if **doBlev** is performed successfully. Otherwise, the full image array will be written out.

## 3.4.2 ACSREJ

- Header Switch: CRCORR
- Header Keywords Updated: TEXPTIME, SKYSUM, EXPEND, REJ\_RATE, EXPTIME, NCOMBINE, ROOTNAME
- Header Keywords added as ‘HISTORY’ Comments: INITGUES, SKYSUB, CRSIGMAS, MEANEXP, CRRADIUS, CRTHRESH, SCALENSE, CRMASK, NEXTEND
- Reference File: CRREJTAB (\*\_crr.fits)

**ACSREJ**, the cosmic-ray rejection task in **CALACS**, combines CR-SPLIT exposures into a single image, first detecting and then replacing flagged pixels. The task uses the same statistical detection algorithm developed for STIS data (**OCRREJ**) and WFPC2 data (**CRREJ**), providing a well-tested and robust procedure.

First, **ACSREJ** will compute the sky background using the mode of each image. Sky subtraction is performed before any statistical checks are made for cosmic rays. Next, **ACSREJ** constructs an initial comparison image from each input exposure. The comparison image can either be a median- or minimum-value sky-subtracted image constructed from all the input images and represents the ‘first guess’ of a cosmic-ray free image. The comparison image serves as the basis for determining the statistical deviation of each pixel from the input image.

A detection threshold is then calculated for each pixel based on the comparison image. This threshold is equal to a constant times sigma squared, given in the equation below:

$$\tau_n = \sigma^2 \times (\text{noise} + \text{value}(x, y)/\text{gain} + \text{scale}(\text{value}(x, y) - \text{sky}_n)^2)/T_n^2$$

where:

- $\sigma$  is the sigma value used as the detection limit,
- *noise* is the readnoise squared (in DN) and *gain* is the CCD gain (in e<sup>-</sup>/DN) for the amp used to read the pixel,
- *scale* is the scale factor for the noise model,
- $T_n$  is the exposure time (in seconds) for the input image, and
- *value* is the pixel value (in DN) from the median or minimum combined comparison image.

The actual cosmic-ray detection criteria at each pixel is determined as:

$$\Delta = ((pix_n(x, y) - sky_n) / T_n - median(x, y))^2$$

where:

- $pix_n(x, y)$  is the pixel value (in DN) from input image  $n$ ,
- $sky_n$  is the sky background (in DN) of image  $n$ , and
- $median_n(x, y)$  is the median or minimum pixel value (in DN/sec) from the comparison image.

If  $\Delta > \tau_n$ , the pixel is flagged as a cosmic-ray in the input image's DQ array and is ignored when images are summed together. Surrounding pixels within a given expansion radius are marked as 'SPILL' pixels and are given less stringent detection thresholds.

When all input images have been processed, the values of the acceptable pixels are summed over all input images. Each pixel in the summed output array is then scaled by the total exposure time:

$$pixout(x, y) = T \cdot \frac{\sum_n (pix_n(x, y) - sky_n) m_n(x, y)}{\sum_n T_n m_n(x, y)} + \sum_n sky_n$$

where:

- $T_n$  is the exposure time for image  $n$ ,
- $m_n(x, y)$  is the mask value (0 for cr-rejected pixels, 1 for good data) for the  $n$ 'th image at pixel  $(x, y)$ ,
- $T$  is the total exposure time (regardless of whether all input images were used for that particular pixel). This corresponds to the header keywords TEXPTIME, EXPTIME.

The following keywords are derived from the variables in this computation:

- TEXPTIME = EXPTIME = T
- SKYSUM =  $\sum_n sky_n$
- REJ\_RATE =  $(\sum_n T_n m_n(x, y) / T)$  averaged over all pixels
- NCOMBINE =  $n$

The remaining keywords EXPSTART, EXPEND are updated based on the input image headers.

In summary, the cosmic ray rejection task sums all accepted pixel values, computes the true exposure time for that pixel, and scales the sum to correspond to the total exposure time. The final scaled, cleaned pixel is written to the comparison image to be used for the next iteration. This

process is then repeated with successively less stringent detection thresholds, as specified by `CRSIGMAS`. Further processing by `CALACS` will scale the `pixout(x,y)` array by the gain, resulting in the summed, cosmic-ray eliminated, but not sky-subtracted product (`*_crj.fits`) in units of *electrons*.

### Cosmic-ray Rejection Table

`ACSREJ` uses the Cosmic-ray Rejection Parameter Table (`CRREJTAB`) to determine the number of iterations for cosmic-ray rejection, the sigma levels to use for each iteration, and the spill radius to use during detection. This allows the rejection process to be tuned to each detector, with suitable defaults being applied during pipeline processing. Observers may fine-tune the cosmic-ray rejection parameters when manually reprocessing data with `ACSREJ` by editing the `CRREJTAB`.

The `CRREJTAB` reference file contains the basic parameters necessary for performing cosmic-ray rejection. The column names and default values for the `CRREJTAB` are given in Table 3.5. The appropriate row is selected based on the chip being processed (`CCDCHIP`), the number of images into which the exposure was split (`CR-SPLIT`), and the exposure time of each `CR-SPLIT` image (`MEANEXP`). The sky fitting algorithm is controlled by the parameter `SKYSUB` which can have values of ‘mode’ or ‘none’. The ‘first guess’ CR-combined image is then created using the median or minimum value of the input exposures, as specified by the column `INITGUES`.

Table 3.5: Columns in Cosmic-Ray Rejection Parameters Table

Column Name	Default Value	Contents
<code>CRSPLIT</code>		Number of exposures into which observation was split
<code>MEANEXP</code>	<code>INDEF</code>	Average exposure time (sec) for each image
<code>SCALENSE</code>	30.0	Multiplicative term (in percent) for the noise model
<code>INITGUES</code>	minimum	Method for computing initial-guess image (minimum, median)
<code>SKYSUB</code>	mode	Sky fitting algorithm (mode, none)
<code>CRSIGMAS</code>	6.5, 5.5, 4.5	Rejection thresholds (sigma) for consecutive iterations
<code>CRRADIUS</code>	2.1	Radius (in pixels) for propagating cosmic ray
<code>CRTHRESH</code>	0.5555	Propagation factor
<code>BADINPDQ</code>	39	Data quality file bits to reject
<code>CRMASK</code>	yes	Flag CR-rejected pixels in input files?
<code>CCDCHIP</code>		Chip to which this conversion applies

Cosmic-ray detection requires the specification of a threshold above which a pixel value is considered a cosmic-ray. This threshold is defined above as  $\tau_n = \sigma^2 \times constant$  and uses the sigma rejection thresholds  $\sigma$ . These sigmas correspond to the column `CRSIGMAS` in the `CRREJTAB` reference file. `SCALENSE` is a multiplicative term (in percent) for the noise model and is given as *scale* in the threshold equation. This term can

be useful when the pointing of the telescope has changed by a small fraction of a pixel between images. Under such circumstances, the undersampling of the image by the CCD will cause stars to be rejected as cosmic rays if a scale noise term is not included. This is a crude but effective step taken to satisfy the maxim of “first do no harm”. However, for cases in which there have been no frame-to-frame offsets or the image is locally well-sampled, this will unduly bias *against* rejecting cosmic rays.

Pixels within a given radius, CRRADIUS, of a cosmic-ray will also be treated as cosmic-rays. A less stringent rejection threshold, CRTHRESH, can be used for detecting pixels adjacent to a cosmic-ray. As for CRSIGMAS, CRTHRESH is also given as a sigma value. If CRTHRESH is exceeded, pixels within a defined radius of the cosmic ray will also be flagged. All pixels determined to be affected by a cosmic-ray will have their DQ values set to 8192, as described in Table 3.4.

A much more detailed discussion of cosmic ray elimination in repeated ACS exposures may be found in [ACS ISR 2002-08](#), Section 5.1. Of particular note is the appropriate value of SCALENSE to use; the pipeline adopts a conservative value to avoid doing harm. In recalibrating several frames for a new cosmic ray elimination, it would be advisable to determine the full range of relative x,y offsets. An appropriate value of SCALENSE is 100\*(maximum offset in pixels), thus if the full offset range was 0.1 pixels an appropriate SCALENSE is 10.0. To alter this value, one may use **tedit** on the CRREJTAB file (calibration file with the extension ‘crr.fits’). The number of exposures obtained in a repeated observation set can be larger than the maximum CR-SPLIT=8 allowed in Phase II proposals. For example, for program 9662 used in Examples 3 and 4 in Section 3.5.2, there were 14 individual 1.0s HRC exposures all at nominally the same pointing. A check of relative offsets shows that a shift of about 0.2 pixels occurred between the first and last exposures. To obtain a crj combined image of all 14 inputs at 1.0s and with better sensitivity to cosmic ray elimination than provided by the conservative default of SCALENSE = 30.0, the following should be done:

1. Create a new asn.fits table with one EXP-CRJ entry for each of the 14 raw 1.0s images, and an appropriately named PROD-CRJ file line.
2. Use **tedit** on the crr.fits table adding a line with a CR-SPLIT value of 14, and a SCALENSE value of 20.0.
3. Given such a large number of inputs it would also make sense here to change to ‘median’ as the INITGUES value. Then rerun **CALACS** on the new association table with 14 entries to obtain a CRJ extension image based on the full stack of 1.0s images.

For a detailed discussion on manually recalibrating ACS data, refer to Section 3.5.

### 3.4.3 ACS2D

Every observation, whether taken with the MAMA or CCD detectors, will be processed by **ACS2D**. The **ACS2D** primary functions are listed in Table 3.6 and include the dark current subtraction, flat fielding, and photometric keyword calculations. **ACS2D** contains the same data quality and error array initialization functions used in **ACSCCD**, but **ACS2D** will check to ensure that the array initialization is not performed twice on CCD data. Calibration switches in the image header control the performance of the remaining calibration functions, with MAMA-specific functions being initiated only when the relevant calibration switches are set.

Table 3.6: The functions performed in **ACS2D** (in operational order)

<b>doNoise</b>	Apply a simple noise model (if not done in ACSCCD)
<b>doDQI</b>	Initialize data quality array (if not done in ACSCCD)
<b>doNonLin</b>	Correct and flag non-linear data ( <b>MAMA only</b> )
<b>doDark</b>	Subtract dark image
<b>doFlat</b>	Divide by flat field and multiply by gain
<b>doShad</b>	Perform CCD shutter shading correction (currently skipped)
<b>doPhot</b>	Compute photometric keyword values for header
<b>doStat</b>	Compute image statistics

#### **doNoise - Error Array Initialization**

- Header Switch: None
- Header Keywords Updated: None
- Reference File: None

**ACS2D** will first check that the image error array has not been expanded, indicating that no previous processing has been performed. In this case, the value of all pixels in the ERR array will have a value of zero. **ACS2D** will then perform the same initialization as described in “doNoise - Error Array Initialization” for **ACSCCD**. If, however, the input image has already been processed, no changes to the ERR array will be made.

#### **doDQI - Bad Pixel Determination**

- Header Switch: DQICORR
- Header Keywords Updated: None
- Reference File: BPIXTAB (\*\_bpx.fits)

If the DQICORR header keyword switch is set to COMPLETE (e.g. CCD data), this step will be skipped. Otherwise, the same initialization will be performed as described in “doDQI - Bad Pixel Determination” for **ACSCCD**.



### doNonLin - Linearity Correction for MAMA Data

- Header Switch: LFLGCORR, GLINCORR
- Header Keywords Updated: GLOBLIM
- Reference File: MLINTAB (\*\_lin.fits)

This routine is capable of flagging global and local nonlinearity in ACS MAMA observations, where the term global refers to the entire ACS detector and local refers to an individual detector pixel. The MAMA Linearity Table, MLINTAB, provides the basic parameters for determining linearity. The global limit (GLOBAL\_LIMIT) column from this table refers to the total count rate at which the data are affected by greater than 10% non-linearity across the detector.

CALACS will attempt to correct for non-linearity up to the global limit using the non-linearity time constant in the column TAU. The global linearity correction is computed for every pixel below the global linearity limit specified by iteratively solving the equation  $n = Ne^{(-\tau N)}$  to get the true count rate N.

The LOCAL\_LIMIT can actually be much higher than the global limit and is difficult to correct using a simple algorithm. Each pixel found to exceed this limit will simply be marked as non-linear in the DQ file. This DQ flag will be extended by a fixed radius from the original pixel, given in the EXPAND column and is currently set to 2 pixels.

If the LFLGCORR switch is set to PERFORM, ACS2D will *flag* excessive global and local nonlinearity in the DQ array. If GLINCORR is set to PERFORM, it will *correct* excessive global nonlinearity in the SCI array, if it is not too large. If the global linearity limit is exceeded, the keyword GLOBLIM in the SCI extension header will be set to “EXCEEDED”. Otherwise, it will have the value “NOT-EXCEEDED”.

### doDark - Dark Image Subtraction

- Header Switch: DARKCORR
- Header Keywords Updated: MEANDARK
- Reference File: DARKFILE (\*\_drk.fits)

This task is responsible for subtracting the dark image from the input image. For CCD data, the dark image (in *electron s<sup>-1</sup>*) is multiplied by the exposure time and then divided by the gain before subtracting. (MAMA data do not require a gain correction.) The dark reference file, DARKFILE, is read in line-by-line and subtracted from the input image in memory. The mean dark value is then computed from the scaled dark image and used to update the MEANDARK keyword in the SCI image header. The “dark time” is simply the exposure time; it does NOT include the idle time since the last flushing of the chip or the readout time. Any dark accumulation during readout time or post-flash idle will be included automatically into the BIASFILE.

A unique dark reference file is created (approximately) daily using four 1000 sec frames for both the WFC and HRC. The four darks are combined

(with cosmic ray rejection) and bias-corrected to form a “daydark”. Every two weeks, a high signal-to-noise “basedark” is created from all the frames (~56) in that period. It does not contain the newest hot pixels present in the daydarks since they are rejected with the cosmic rays during image combination. A copy of the basedark is made for each day in the two-week period, and daily hot pixels are skimmed from the respective daydarks and added to the basedark copies. Only the hot pixels above 0.08 e<sup>-</sup>/sec are identified with flag 16 in the data quality (DQ) array of WFC and HRC reference darks, which propagates to the DQ array of the calibrated science data. The flagged hot pixels are typically excluded in subsequent processing steps, as they are likely too noisy to be correctable. But the many “warm” pixels below this threshold are assumed to be adequately corrected by the dark calibration. This produces a reference file with high signal-to-noise, which accurately reflects (and corrects/flags) the hot pixels present for a given observation date. The “best” dark file is typically not available in the pipeline until 2-3 weeks after the date of observation, because it takes a few weeks to collect enough frames to make a basedark (see [ACS ISR 04-07](#) for more information).

The reference file for dark subtraction, DARKFILE, is selected based on the values of the keywords DETECTOR, CCDAMP, and CCDGAIN in the image header. The dark correction is applied after the overscan regions are trimmed from the input science image. As for the BIASFILE, CALACS assumes that the images have not been binned, so any input image smaller than the full detector size will be interpreted as a sub-array image.

Sub-array science images will use the same reference file as a full-sized image. CALACS simply extracts the appropriate region from the reference file and applies it to the sub-array input image.

### **doFlat - Flat field image(s) Correction**

- Header Switch: FLATCORR
- Header Keywords Updated: None
- Reference File: PFLTFILE (\*\_pfl.fits), LFLTFILE (\*\_lfl.fits), DFLTFILE (\*\_dfl.fits), CFLTFILE (\*\_ctl.fits)

As done for STIS, the ACS **doFlat** routine corrects for pixel-to-pixel and large-scale sensitivity gradients across the detector by dividing the data by the flat field image. This contrasts with WFPC2 and NICMOS who deliver an “inverse” flat to the pipeline and then multiply the data by the flat field. When performing the flat field correction, CALACS multiplies by the gain so that the calibrated data will be in units of electrons.

Because of geometric distortion effects, the area of the sky seen by a given pixel is not constant, and therefore observations of a constant surface brightness object will have count rates per pixel that vary over the detector, even if every pixel has the same sensitivity. In order to produce images that appear uniform for uniform illumination, the flat fields make an implicit correction for the geometric distortion across the field that is equivalent to

dividing each pixel by the optical distortion which is normalized to unity at the center of the field. A consequence of this procedure is that two stars of equal brightness do not have the same total counts after the flat fielding step. Thus, point source photometry extracted from a flat fielded image must be multiplied by the effective pixel area map, as shown in Figure 6.1. This correction is accounted for in pipeline processing by **MultiDrizzle** which uses the geometric distortion solution to correct all pixels to equal areas. Thus, in the drizzled images photometry is correct for both point and extended sources.

The flat field image used to correct the data is created using up to four flat field reference files: the pixel-to-pixel file (PFLTFILE), the low-order flat (LFLTFILE), the delta flat (DFLTFILE), and the coronagraphic spot flat (CFLTFILE). The PFLTFILE is a pixel-to-pixel flat field correction file containing the small scale flat field variations. The LFLTFILE is a low-order flat which will correct for any large-scale flat field variations across each detector. This file is stored as a binned image which is expanded when being applied by **CALACS**. The DFLTFILE is a delta-flat containing any needed changes to the small-scale PFLTFILE. The CFLTFILE is a spot mask which contains the vignetting patterns of the occulting spots and which is applied to coronagraphic observations only.

If the LFLTFILE, DFLTFILE, or CFLTFILE are not specified in the SCI header, only the PFLTFILE will be used for the flat field correction. If all four reference files are specified, they will be read in line-by-line and multiplied together to form a complete flat field correction image. Currently, the LFLTFILE and DFLTFILE flats are not used for ACS data. The PFLTFILE reference flat in the pipeline is actually a combination of the pixel-to-pixel flats taken during the ground calibration and the low-order flat correction derived in-flight. The CFLTFILE will be applied only when the OBSTYPE is equal to CORONAGRAPHIC.

All flat field reference images will be chosen based on the detector, amplifier, and filters used for the observation. Any sub-array science image will use the same reference file as a full-size image. **CALACS** will extract the appropriate region from the reference file and apply it to the sub-array input image.

### **doShad - Shutter Shading File Correction (skipped)**

- Header Switch: SHADCORR
- Header Keywords Updated: None
- Reference File: SHADFILE (\*\_shd.fits)

The SHADCORR calibration switch is currently set to OMIT and is unlikely to be used in future versions of **CALACS**. Calibration data show that a shading correction is not needed for ACS data. For more information, refer to [ACS ISR 03-03](#), “Stability and Accuracy of HRC and WFC Shutters” and to the report “WFC and HRC Shutter Shading and Accuracy” on the ACS Science and Engineering Team web site at:

[http://acs.pha.jhu.edu/instrument/calibration/results/by\\_it\\_em/shutter/shading\\_accuracy\\_feb2001](http://acs.pha.jhu.edu/instrument/calibration/results/by_it_em/shutter/shading_accuracy_feb2001)

The **doShad** routine applies the shutter shading correction image (SHADFILE) to the science data if SHADCORR is set to PERFORM. The input image is corrected for the differential exposure time across the detector caused by the shutter opening. This correction only has a significant effect on images with short exposure times (less than 10 seconds).

Pixels are corrected based on the exposure time using the relation:

$$\text{corrected} = \text{uncorrected} \times EXPTIME / (EXPTIME + SHADFILE).$$

The SHADFILE is selected using the DETECTOR keyword in the input science image. At present, this reference file is an over scanned-trimmed image, binned by a factor of 8 for each dimension, resulting in a 128x128 HRC and a 256x512 WFC SHADFILE.

The shutter shading correction can either be applied during **ACS2D** processing for single or REPEAT-OBS exposures or during cosmic-ray rejection in **ACSREJ** for CRSPLIT exposures.

### doPhot - Photometry Keyword Calculation

- Header Switch: PHOTCORR
- Header Keywords Updated: PHOTMODE, OBSMODE, PHOTFLAM, PHOTZPT, PHOTPLAM, PHOTBW
- Reference Files: GRAPHTAB (\*\_tmg.fits), COMPTAB (\*\_tmc.fits)

Before photometry can be performed on ACS observations, a transformation from electrons to absolute flux units must be performed. **CALACS** follows the WFPC2 methodology for calculating the photometry keywords in the calibration pipeline. The calibration reference files, GRAPHTAB and COMPTAB, point to the SYNPHOT tables containing the latest ACS component tables. These tables contain the throughput as a function of wavelength for the various ACS detector and filter combinations. This reliance on SYNPHOT allows the ACS team to maintain the latest throughput files in SYNPHOT to keep **CALACS** up to date. For further discussion of SYNPHOT, refer to Chapter 3 of the HST Data Handbook Introduction.

The keywords PHOTMODE and OBSMODE are built to reflect the configuration of the instrument during the exposure. **CALACS** then uses the OBSMODE string with SYNPHOT to compute the total throughput array for the observation, based on the aperture and filter throughputs, and the photometry keywords: PHOTFLAM (the inverse sensitivity in units of  $\text{erg s}^{-1} \text{cm}^{-2} \text{A}^{-1}$  for 1 *electron s*<sup>-1</sup>), PHOTZPT (the Space Telescope magnitude zero point), PHOTPLAM (the bandpass pivot wavelength), and PHOTBW (the bandpass RMS width). Users who wish to convert calibrated images (in units of *electrons*) to flux units may simply divide the image by the exposure time and then multiply by the PHOTFLAM keyword. Drizzled DRZ images are already in units of *electrons per second* and may simply be multiplied by the PHOTFLAM value to attain flux units.

**doStat - Image Statistics Determination**

- Header Switch: STATFLAG
- Header Keywords Updated: NGOODPIX, GOODMIN, GOODMAX, GOODMEAN, SNRMIN, SNRMAX, SNRMEAN
- Reference File: None

This routine computes the number of pixels which are flagged as “good” in the data quality array. The minimum, mean, and maximum pixel values are then calculated for data flagged as “good” in both the science and error arrays. Similarly, the minimum, mean, and maximum signal-to-noise of “good” pixels is derived for the science array. These quantities are updated in the image header.

**3.4.4 ACSSUM**

- Header Switch: RPTCORR
- Header Keywords Updated: NCOMBINE, EXPTIME, EXPEND, ROOTNAME
- Reference File: None

**ACSSUM** sums a list of images one line at a time, using the association file to define the input. A straight pixel-to-pixel addition of the science values is applied, and the error calculated as the square root of the sum of the squares of the errors in the individual exposures. Note that for multiple exposures taken via REPEAT-OBS instead of the observationally equivalent CR-SPLIT, the final processed image is *not* cosmic-ray rejected.

The calibration switch RPTCORR is set to COMPLETE upon successful completion of the summation. In addition, the keywords NCOMBINE, EXPTIME, and EXPEND are adjusted to reflect the total of the summed images.

---

## 3.5 Manual Recalibration of ACS Data

**3.5.1 Requirements for Manual Recalibration****Retrieving Software and Input Data Files**

If the observer decides to recalibrate their ACS data, the following must be available on their system:

- **CALACS** software from the STSDAS **hst\_calib.acs** package
- **MultiDrizzle** and **PyDrizzle** from the STSDAS **dither** package
- PyRAF, to run **MultiDrizzle** and **PyDrizzle**, obtained from STScI
- Reference files obtained from STScI Archive, or personal versions
- Uncalibrated data (\*\_raw.fits) from OTFR

- Association table, if applicable.

Uncalibrated data and calibration reference files can be obtained from OTFR via StarView or the web-based archive request form:

<http://archive.stsci.edu/cgi-bin/hst>.

StarView is available for users to download from:

<http://starview.stsci.edu/html>.

The pages include instructions on installing and using StarView and on how to become a registered archive user.

The most recent version of STSDAS, which includes the **CALACS** package required for reprocessing, can be downloaded from:

[http://www.stsci.edu/resources/software\\_hardware/stsdas](http://www.stsci.edu/resources/software_hardware/stsdas)

The most recent versions of PyRAF, **MultiDrizzle**, and **PyDrizzle** can be downloaded from:

[http://www.stsci.edu/resources/software\\_hardware/stsdas/pydrizzle](http://www.stsci.edu/resources/software_hardware/stsdas/pydrizzle)

### Setting up ‘jref’

Before any recalibration may be done, the user’s local directory containing the calibration reference files must be defined. For ACS, this directory is referred to as ‘jref’. The image header already contains the appropriate keywords defining the reference files. The user must simply define the location of the ‘jref’ directory in the Unix environment.

```
setenv jref /mydisk/myjref/
```

Once this path is set, IRAF must be restarted in the same window in which the setup was performed.

### Selecting Calibration Switches

OTFR will use the latest available calibration reference files by default. In order to use non-default reference files, manual recalibration is required. The calibration reference file keywords will need to be updated manually in the uncalibrated data with the non-default filenames before running **CALACS**. The selection criteria in Table 3.7 are used to set the values for the calibration switch header keywords in uncalibrated ACS data.

Table 3.7: Calibration Switch Selection Criteria.

Switch	Description	Criteria
DQICORR	Data Quality Array Initialization	DEFAULT = “PERFORM” If OBSMODE = ACQ then “OMIT”
ATODCORR	Analog to Digital Conversion	DEFAULT = “OMIT”
BLEVCORR	Overscan Region Subtraction	DEFAULT = “PERFORM”
BIASCORR	Bias Subtraction	DEFAULT = “PERFORM”
FLSHCORR	Post Flash Subtraction	DEFAULT = “OMIT”
CRCORR	Cosmic Ray Rejection	If CRSPLIT $\geq$ 2 then “PERFORM” If CRSPLIT $<$ 2 then “OMIT”
EXPSCORR	Calibrate individual exposures in an association	DEFAULT = “PERFORM”
SHADCORR	Shutter Shading Correction	DEFAULT = “OMIT”
DARKCORR	Dark Subtraction	DEFAULT = “PERFORM”
FLATCORR	Flat field Division	DEFAULT = “PERFORM”
PHOTCORR	Photometric Processing	DEFAULT = “PERFORM”
RPTCORR	Repeat Processing	DEFAULT = “OMIT” If NRPTEXP $>$ 1 then “PERFORM”
DRIZCORR	Dither Processing	DEFAULT = “PERFORM”
GLINCORR	Global Non-Linearity Correction	SBC DEFAULT = “PERFORM”
LFLGCORR	Local and Global Non-Linearity Flagging in DQ Array	SBC DEFAULT = “PERFORM”

### Bypassing the PHOTCORR Step

Raw ACS images are in units of *Data Numbers (DN)*, calibrated images are in units of *electrons*, and drizzled images are in units of *electrons/second*. The pipeline calibration tasks do not alter the units of the pixels in the image. Instead they calculate and write the inverse sensitivity conversion factor (PHOTFLAM) and the ST magnitude scale zero point (PHOTZPT) into header keywords in the calibrated data. Refer to the section “doPhot - Photometry Keyword Calculation” in Section 3.4.3 for more information.

When populating the photometric keywords during the PHOTCORR step, **CALACS** uses the STSDAS synthetic photometry package, **SYNPHOT**, which contains the throughput curves of all HST optical components. (For information on retrieving the **SYNPHOT** dataset, see Appendix A.3.2 of the HST Data Handbook Introduction.) The **SYNPHOT** dataset contains numerous files which may be updated on a regular basis, making it cumbersome for the user to set up. A simple alternative is to set the PHOTCORR calibration switch to OMIT in the primary header of the uncalibrated image. The user may simply copy the photometric keywords from the calibrated data into the raw image header and then run **CALACS** with the PHOTCORR switch set to OMIT.

### Speed of Pipeline Processing

Reprocessing HRC or SBC data will not put a burden on most computing systems since the image sizes, both science data and reference files, are relatively small. Processing WFC observations, on the other hand, will require more computing power, including both CPU run time and disk space.

Great care has been taken to minimize the memory requirements of the pipeline software to accommodate most computing configurations. Line-by-line I/O is used during pipeline processing and is particularly useful when more than one image is operated on at a time, for example during flat fielding or co-adding images. This, unfortunately, places an extra burden on the I/O capabilities of the computing system. **CALACS** requires up to 130MB of memory to process a single WFC exposure, while **MultiDrizzle** requires up to 400MB.

An Ultra-10 class workstation (300 MHz, 512MB RAM) using **CALACS** to process WFC data will take ~13 minutes for a CR-SPLIT=2 association or ~4.5 minutes for a single WFC exposure. **MultiDrizzle** requires ~20 minutes to process a single WFC exposure. These times can be scaled by the processor speed of the computing system, and result in much faster run times for newer workstations.

## 3.5.2 CALACS Examples

We present several examples of **CALACS** reprocessing. The steps required for **MultiDrizzle** reprocessing are summarized in Chapter 4.

### Example 1: Reprocessing a Single Exposure

The following example uses HRC data from the flat field calibration program 9019 which observed the stellar cluster 47 Tucanae. The observations are from visit 07, exposure 12 and utilize the F814W filter. The exposures are CR-SPLIT into two exposures of 20 sec each. The association table for this exposure is `j8bt07020_asn.fits`. Typing `'tprint j8bt07020_asn.fits'` reveals the rootnames of the individual exposures: `j8bt070yq` and `j8bt070zq`.

For the purposes of this first example, let us assume that the observations are *not* part of an association. This example will illustrate the steps required to reprocess a single exposure after changing the bias reference file from the default value to a file specified by the user.

1. In the Unix environment, we must specify the location of the 'jref' directory where the calibration reference files reside and then start IRAF. We assume here that the user has requested calibration files as part of the data archive request and stored these in their directory `'/mydisk/myjref/'`, where `'/mydisk/'` specifies the directory containing the pipeline data.



(Note: This setup must be done in the same window in which IRAF will be used. Note also that setting ‘jref’ from within IRAF will not work even though typing ‘show jref’ would suggest it might.)

```
unix> setenv jref /mydisk/myjref/
unix> cl
```

2. To see what bias reference file is currently in use, we use the `hedid` task. Note that the period at the end of the line is required. The lines below beginning with the ‘`iraf>`’ symbol indicate commands typed into IRAF. Lines with no symbol indicate output from IRAF.

```
iraf> hedid j8bt07oyq_raw.fits[0] BIASFILE .
j8bt07oyq_raw.fits[0], BIASFILE = jref$m4r1753rj_bia.fits
```

3. Next, we edit the global image header of the raw image to reflect the name of the new bias file.

```
iraf> hedid j8bt07oyq_raw.fits[0] BIASFILE jref$mybias.fits verify-
j8bt07oyq_raw.fits[0], BIASFILE: jref$m4r1753rj_bia.fits->
jref$mybias.fits
j8bt07oyq_raw.fits[0] updated
```

4. We then set the PHOTCORR processing step to ‘OMIT’ and copy the photometric keywords from the calibrated to the raw image. (Alternately, the user may keep track of these numbers in any other preferred manner. Most users will only require knowledge of the PHOTFLAM keyword for photometric calibration.) These steps allow users to bypass this SYNPHOT-based calibration step, due to the cumbersome requirements for setup. (See “Bypassing the PHOTCORR Step” on page 3-27 for more information.)

```
iraf> hedid j8bt07oyq_raw.fits[0] PHOTCORR omit verify-
j8bt07oyq_raw.fits[0], PHOTCORR: PERFORM -> omit
j8bt07oyq_raw.fits[0] updated
iraf> hedid j8bt07oyqflt.fits[1] phot* .
j8bt07oyqflt.fits[1], PHOTMODE = "ACS HRC F814W"
j8bt07oyqflt.fits[1], PHOTFLAM = 1.3260861E-19
j8bt07oyqflt.fits[1], PHOTZPT = -2.1100000E+01
j8bt07oyqflt.fits[1], PHOTPLAM = 8.1209805E+03
j8bt07oyqflt.fits[1], PHOTBW = 7.0114880E+02
iraf> hedid j8bt07oyq_raw.fits[1] PHOTFLAM 1.3260861E-19 verify-
j8bt07oyq_raw.fits[1], PHOTFLAM: 0.000000E+00 -> 1.3260861E-19
j8bt07oyq_raw.fits[1] updated
```

5. Within the directory containing the pipeline products (“/mydisk/”), we create the subdirectory “recal”, copy the RAW and ASN files to this subdirectory, and ‘cd’ to this directory.
6. Finally, we load the packages `stsdas.hst_calib.acs` and run **CALACS** on the single raw exposure.

(Note that invoking this package will result in the message: “Warning: package ‘acs’ includes Python tasks that require PyRAF”. This applies only for **calacsdriz** which calls the **CALACS** and **MultiDrizzle** tasks in succession.)

```
iraf> stsdas.hst_calib.acs
iraf> calacs j8bt07oyq_raw.fits
```

The product will be a single calibrated image with the FLT extension.

### Example 2: Reprocessing Multiple Exposures within an Association

This example uses the same data from Example 1 and illustrates the steps required to reprocess an ACS association after changing the bias reference file from the default value to a file specified by the user. The steps required are similar to the previous example, with a few modifications. IRAF output comments which are similar to Example 1 have been omitted.

1. First, we look at the contents of the image association.

```
iraf> tprint j8bt07020_asn.fits
# MEMNAME      MEMTYPE      MEMPRSNT
j8bt07oyq      EXP-CRJ      yes
j8bt07ozq      EXP-CRJ      yes
j8bt07021      PROD-CRJ      yes
```

2. To see what bias reference file is currently in use, we use **hedit**.

```
iraf> hedit j8bt07*raw.fits[0] BIASFILE .
```

3. Next, we edit the global image header of all the raw images to reflect the name of the new bias file.

```
iraf> hedit j8bt07*raw.fits[0] BIASFILE jref$mybias.fits verify-
```

4. We then set the PHOTCORR processing step to ‘OMIT’ and copy the photometric keywords from the calibrated to the raw image.

```

iraf> hedit j8bt07*raw.fits[0] PHOTCORR omit verify-
iraf> hedit j8bt07*flt.fits[1] phot* .
iraf> hedit j8bt07*raw.fits[1] PHOTFLAM 1.3260861E-19 verify-

```

5. Within the directory containing the pipeline products (“/mydisk/”), we create the subdirectory “recal”, copy the RAW and ASN files to this subdirectory, and ‘cd’ to this directory.
6. Finally, we run **CALACS** on the image association.

```

iraf> stsdas.hst_calib.acs
iraf> calacs j8bt07020_asn.fits

```

(If executing this command in the same directory in which you have run the previous example, then one of the FLT files will already exist and **CALACS** will not overwrite existing images. To execute in this case, first delete the existing FLT files or move them to a separate directory.)

The product will be two separate calibrated images with the FLT extension (j8bt07oyq\_ft.fits, j8bt07oyq\_ft.fits) and a single cr-combined image with the CRJ extension (j8bt07021\_crj.fits).

### Example 3: Removing Cosmic-rays from Repeated (RPT-OBS) Exposures

The following example uses HRC data from the shutter stability calibration program 9662 which observed the stellar cluster 47 Tucanae. The observations are from visit 01, exposure 20 and utilize the CLEAR filter. The two repeated (RPT-OBS) exposures are 1.0 sec each.

In this example, we illustrate the steps required to remove cosmic-rays from repeated observations which use the RPT-OBS syntax. By definition, the standard calibration product of multiple repeated exposures is a summed image. We can fool the software into rejecting cosmic-rays from the images, but this requires modification of the image association table.

1. First, we look at the contents of the image association.

```

iraf> tprint j8is01020_asn.fits
# MEMNAME      MEMTYPE      MEMPRSNT
j8is01j2q      EXP-RPT      yes
j8is01j3q      EXP-RPT      yes
j8is01021      PROD-RPT     yes

```

- Update calibration switches in the global header using the **hed** task.

```

iraf> hedit *raw.fits[0] CRCORR perform add-
iraf> hedit *raw.fits[0] RPTCORR omit add-

```

- Update association table MEMTYPE column, by changing each instance of RPT to CR. This may be done using the text editor functionality of **ted**.

```

iraf> tedit j8is01020_asn.fits
# MEMNAME      MEMTYPE      MEMPRSNT
j8is01j2q      EXP-CRJ       yes
j8is01j3q      EXP-CRJ       yes
j8is01021      PROD-CRJ      yes

```

- We then set the PHOTCORR processing step to ‘OMIT’ and copy the photometric keywords from the calibrated to the raw image.

```

iraf> hedit j8is01*raw.fits[0] PHOTCORR omit verify-
iraf> hedit j8is01*flt.fits[1] phot* .
iraf> hedit j8is01*raw.fits[1] PHOTFLAM 4.5803514E-20 verify-

```

- Within the directory containing the pipeline products (“/mydisk/”), we create the subdirectory “recal”, copy the RAW and ASN files to this subdirectory, and ‘cd’ to this directory.
- Finally, we run **CALACS** on the image association.

```

iraf> stsdas.hst_calib.acs
iraf> calacs j8is01020_asn.fits

```

The product will be two calibrated images with the FLT extension (j8is01j2qflt.fits, j8is01j3qflt.fits) and a cr-combined image with the CRJ extension (j8is01021\_crj.fits) instead of the usual SFL extension.

#### Example 4: Combining Exposures from Multiple Associations

This example uses the same data from Example 3 plus an additional exposure from the same program: visit 01, exposure 40. These additional data also use the CLEAR filter and contain two repeated 1.0 sec exposures. The association table for this exposure is j8is01040\_asn.fits. In this example, we illustrate the steps required to combine two separate sets of repeated observations.

1. First we merge the two association tables and edit them appropriately (using **tmerge** and **tedit**, respectively).

```

iraf> tmerge j8is01020_asn.fits,j8is01040_asn.fits \
>>>  outtable="merged_asn.fits" option=append
iraf> tprint merged_asn.fits
# MEMNAME      MEMTYPE      MEMPRSNT
j8is01j2q      EXP-RPT      yes
j8is01j3q      EXP-RPT      yes
j8is01021      PROD-RPT     yes      <---remove this line
j8is01j8q      EXP-RPT      yes
j8is01j9q      EXP-RPT      yes
j8is01041      PROD-RPT     yes      <---edit this line
iraf> tedit merged_asn.fits
# MEMNAME      MEMTYPE      MEMPRSNT
j8is01j2q      EXP-RPT      yes
j8is01j3q      EXP-RPT      yes
j8is01j8q      EXP-RPT      yes
j8is01j9q      EXP-RPT      yes
j8is01xx1      PROD-RPT     yes      <---new product name

```

2. We then set the PHOTCORR processing step to ‘OMIT’ and copy the photometric keywords from the calibrated to the raw image using **hedit**.

```

iraf> hedit j8is01*raw.fits[0] PHOTCORR omit verify-
iraf> hedit j8is01*flt.fits[1] phot* .
iraf> hedit j8is01*raw.fits[1] PHOTFLAM 4.5803514E-20 verify-

```

3. Within the directory containing the pipeline products (“/mydisk/”), we create the subdirectory “recal”, copy the RAW and ASN files to this subdirectory, and ‘cd’ to this directory.
4. Finally, we run **CALACS** on the new image association.

```

iraf> stsdas.hst_calib.acs
iraf> calacs merged_asn.fits

```

The product will be 4 calibrated images with the FLT extension and a single summed image with the SFL extension (j8is01xx1\_sfl.fits).

### Example 5: Reprocessing Images taken as part of a Dither Pattern

The following example uses WFC data from the GOODS program 9425. These observations are from visit 54, exposure 219 and target the CDF-South with the F606W filter. The images are part of a 2-point line

dither pattern and are 480 sec each. In this example, we illustrate the steps required to reprocess data which is part of a dither pattern, using a non-default dark reference file. The steps are similar to Example 2, but the format of the association and the data products are unique.

1. First, we look at the contents of the image association.

```

iraf> tprint j8e654010_asn.fits
# MEMNAME      MEMTYPE      MEMPRSNT
j8e654c0q      EXP-DTH      yes
j8e654c4q      EXP-DTH      yes
j8e654011      PROD-DTH     yes

```

2. To see what dark reference file is currently in use, we use **hedit**.

```

iraf> hedit j8e654*raw.fits[0] DARKFILE .

```

3. Next, we edit the global image header of all the raw images to reflect the name of the new dark reference file.

```

iraf> hedit j8e654*raw.fits[0] DARKFILE jref$mydark.fits verify-

```

4. We then set the PHOTCORR processing step to ‘OMIT’ and copy the photometric keywords from the calibrated to the raw image.

```

iraf> hedit j8e654*raw.fits[0] PHOTCORR omit verify-
iraf> hedit j8e654*flt.fits[1] phot* .
iraf> hedit j8e654*raw.fits[1] PHOTFLAM 7.7792272E-20 verify-

```

5. Within the directory containing the pipeline products (“/mydisk/”), we create the subdirectory “recal”, copy the RAW and ASN files to this subdirectory, and ‘cd’ to this directory.

6. Finally, we run **CALACS** on the image association.

```

iraf> stsdas.hst_calib.acs
iraf> calacs j8e654010_asn.fits

```

The product of the DITH-PATTERN will be two separate calibrated images with the FLT extension. In subsequent processing (see Chapter 4 for details), **MultiDrizzle** will combine these FLT files into a single DRZ image (j8e654011\_drz.fits).

# Distortion Correction and Drizzling of ACS Images

In this chapter. . .

4.1 ACS Geometric Distortions / 4-2
4.2 Combination of Dithered Data / 4-13
4.3 PyDrizzle / 4-17
4.4 MultiDrizzle / 4-17
4.5 Post-Pipeline Reprocessing / 4-21
4.6 Refining the Shifts: Manually and with Tweakshifts / 4-30
4.7 MultiDrizzle Details: Example Application to the Tadpole Galaxy / 4-40
4.8 Creating Custom Association Tables / 4-58

This chapter describes the geometric distortion of the ACS and presents the available tools and methods for removing the distortion and combining dithered datasets into clean, undistorted, and photometrically faithful output products.

The first section describes how the distortion has been quantified and how this information is held in reference files which are used by the calibration pipeline. Plots of the distortion field are given for the three ACS detectors.

The remaining sections give an overview of the drizzle method and discuss the higher level **PyDrizzle** and **MultiDrizzle** software tools available for distortion correction and image combination.

## 4.1 ACS Geometric Distortions

ACS produces the largest single images ever taken with HST. The optics were designed with a minimum number of components, resulting in high throughput, but with ACS focal surfaces far from normal to the principal rays. This results in an image of the sky which is distorted in a large, but predictable manner. The distortion consists of two effects, discussed previously in Section 1.1.3. The first is the tilted elongation of the ACS apertures, causing the pixel scale to be smaller along the radial direction of the Optical Telescope Assembly (OTA) field of view than along the tangential direction. The second effect is the variation of pixel area across the detector.

The results presented in the discussion below are derived from multiple observations of dense star fields with the images displaced from each other by amounts comparable with the size of the field of view. The following discussion is based on reports from the HST Calibration Workshop Proceedings: *Calibration of Geometric Distortion in the ACS Detectors* (Meurer et al. 2002) and *Astrometry with the Advanced Camera: PSFs and Distortion in the WFC and HRC* (Anderson 2002) at:

[http://www.stsci.edu/hst/HST\\_overview/documents/calworkshop/workshop2002/CW2002\\_TableOfContents](http://www.stsci.edu/hst/HST_overview/documents/calworkshop/workshop2002/CW2002_TableOfContents)

### 4.1.1 Distortion Model

The heart of the distortion model relates detector pixel position  $(x, y)$  to sky position (see ACS ISR 2000-11) using a polynomial transformation given by:

$$x_c = \sum_{i=0}^k \sum_{j=0}^i a_{i,j} (x - x_r)^j (y - y_r)^{i-j}$$

$$y_c = \sum_{i=0}^k \sum_{j=0}^i b_{i,j} (x - x_r)^j (y - y_r)^{i-j}$$

where  $k$  is the polynomial order of the fit,  $(x_r, y_r)$  is the reference pixel position taken to be the center of each detector or WFC chip, and  $(x_c, y_c)$  is the undistorted position in arcseconds. The coefficients to the fits,  $a_{i,j}$  and  $b_{i,j}$ , are free parameters. A similar form is used for the inverse relation which provides the conversion from units of arcseconds to distorted input pixels.

For the WFC, an offset is applied to put the two CCD chips on the same coordinate system:

$$X' = x_c + \Delta x(chip), \quad Y' = y_c + \Delta y(chip).$$

The offsets  $\Delta x(chip)$ ,  $\Delta y(chip)$  are 0,0 for chip 1 and correspond to the separation between chips 1 and 2 for chip 2. The chip 2 offsets are free parameters in the fit.  $(X', Y')$  correspond to tangential plane positions in



arcseconds which are tied to the HST (V2, V3) coordinate system. Finally, all frames are transformed to the same coordinate grid on the sky:

$$X_{sky} = \Delta X_i + \cos(\Delta\theta_i)X' - \sin(\Delta\theta_i)Y',$$

$$Y_{sky} = \Delta Y_i + \sin(\Delta\theta_i)X' + \cos(\Delta\theta_i)Y',$$

where the free parameters  $\Delta X_i$ ,  $\Delta Y_i$ ,  $\Delta\theta_i$  are the position and rotation offsets of frame  $i$ .

There is one added complication in the scale term of the geometric distortion due to the effect of differential velocity aberration. The apparent position on the sky of any targets is displaced by the effect of velocity aberration. The speed of the earth in its orbit is about 30 km/sec. Figure 4.1 illustrates a target which is viewed at an angle  $\alpha$  with respect to the velocity of the telescope. The apparent position of the target is at angle  $\alpha'$  where:

$$\tan \alpha' = \frac{\sqrt{1 - \beta^2} \cdot \sin \alpha}{\cos \alpha + \beta}$$

and  $\beta$  is the net telescope velocity divided by the speed of light. The change in angle can amount to tens of arcseconds, but the HST flight software continually accounts for this and keeps the apparent position of the target at a fixed aperture reference point. However a secondary differential effect exists, consisting of a small change in the scale, with a magnitude equal to:

$$\frac{\sqrt{1 - \beta^2}}{1 + \beta \cos \alpha}$$

The scale change is typically of order 1 part in  $10^4$ . For targets near the ecliptic, this can cause a misalignment between different exposures of up to 1.4 pixels in the ACS field of view in WFC images taken 6 months apart, due to changes in orbital position of the Earth. Shifts within an HST orbit are  $\sim 0.3$  pix. This scale change, illustrated in Figure 4.2, can complicate the removal of cosmic rays from images and can cause artifacts when constructing mosaics.

The effective scale change in arcsec per pixel is actually the reciprocal of the factor given above, i.e., if the apparent positions appear closer together then a single pixel sees a larger portion of the sky. The ACS science images now include a keyword VFACTOR equal to the approximation  $(1 + \beta \cos \alpha)$ . This keyword is used by the **MultiDrizzle** software when correcting for geometric distortion.

For a further discussion of the effect of velocity aberration, see *The Effect of Velocity Aberration Correction on ACS Image Processing*: HST Calibration Workshop Proceedings (Cox & Gilliland 2002) at:

[http://www.stsci.edu/hst/HST\\_overview/documents/calworkshop/workshop2002/CW2002\\_Papers/CW02\\_cox](http://www.stsci.edu/hst/HST_overview/documents/calworkshop/workshop2002/CW2002_Papers/CW02_cox)

Figure 4.1: Schematic illustration of the angular change due to velocity aberration.

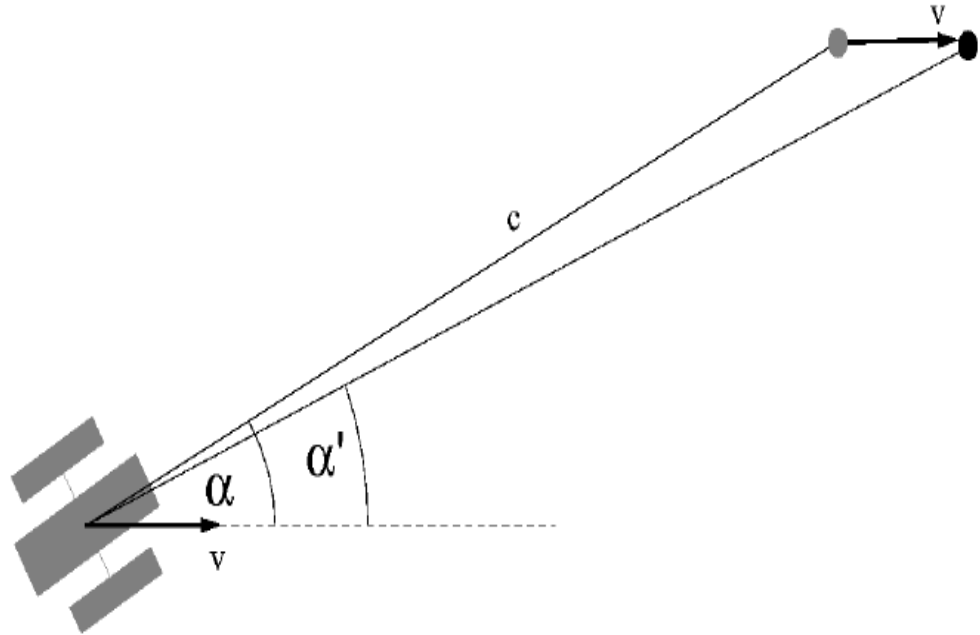
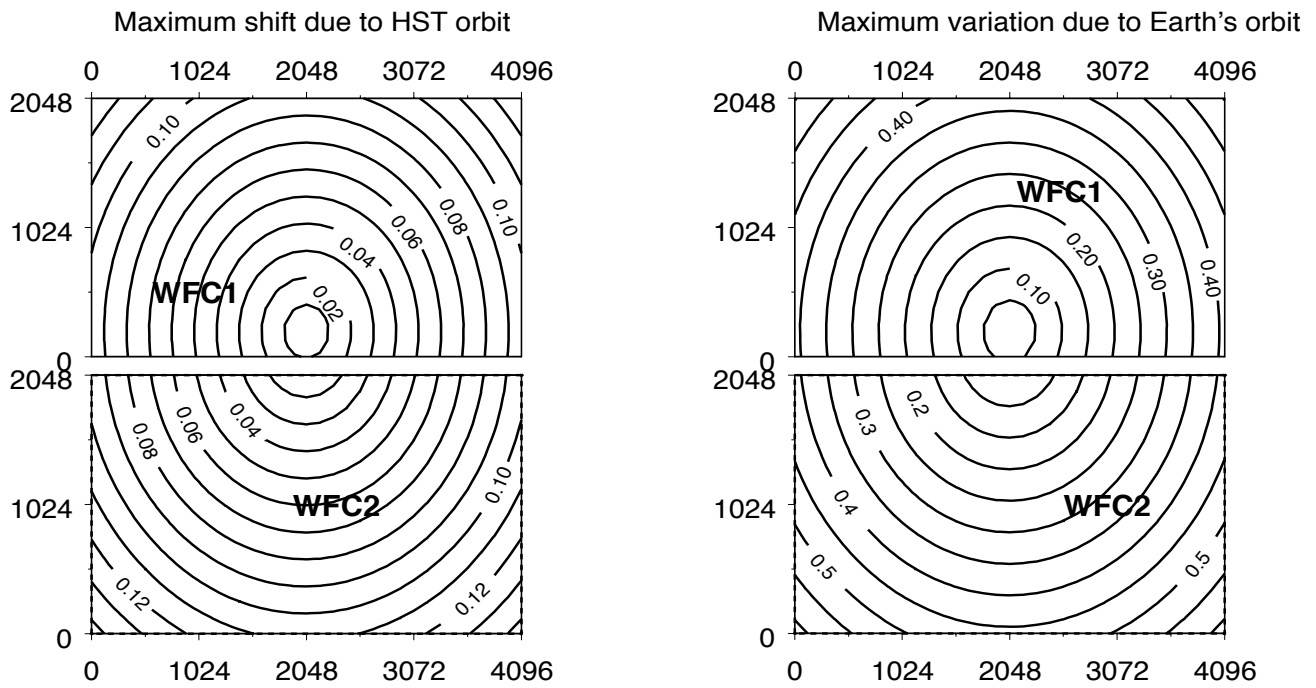


Figure 4.2: Pixel shifts on WFC caused by scale changes from differential velocity aberration.

### PIXEL SHIFTS



### 4.1.2 On-orbit Calibration Programs

The positions of stars observed multiple times in the dithered star fields are used to iteratively solve for the free parameters in the distortion solution: fit coefficients  $a_{i,j}$ ,  $b_{i,j}$ ; chip 2 offsets  $\Delta x$ ,  $\Delta y$  (WFC only); frame offsets  $\Delta X_i$ ,  $\Delta Y_i$ ,  $\Delta \theta_i$ ; and tangential plane position  $X_{sky}$ ,  $Y_{sky}$  of each star used in the fit. These parameters are described in Section 4.1.1.

The original ACS geometric distortion campaign observed the core of 47 Tucanae with the WFC and HRC (program 9028, Meurer). The exposures were designed to detect stars on the main sequence turn-off, allowing a high density of stars with relatively short exposures. The F475W filter (Sloan  $g'$ ) was used to minimize the number of saturated red giant branch stars in the field. For calibrating the distortion in the SBC, exposures of NGC6681 (program 9027, Hartig) were chosen for the relatively high density of UV emitters (hot horizontal branch stars).

Originally, only images taken with a single roll angle were used to define the distortion solutions. The solution using only these data is degenerate in the zeroth (absolute pointing) and linear terms (scale, skewness). Therefore the largest commanded offsets with a given guide star pair were used to set the linear terms.

Comparison of corrected coordinates to astrometric positions showed that residual skewness in the solution remained. Therefore, after November 2002, the results for the WFC and HRC have been based on data from multiple roll angles, incorporating data obtained from the calibration outsourcing program 9443 (Anderson & King, ISR-ACS-04-15). The overall plate scale is set by the largest commanded offset. For the HRC, the linear scale is set by matching HRC and WFC coordinates, since the same field was used in the SMOV observations. The zeroth order terms (position of ACS apertures in the V2,V3 frame) were determined from observations of an astrometric field.

Initially the distortion analysis was performed only with the F475W filter for both WFC and HRC detectors. Further measurements and analysis have provided solutions for 10 HRC filters and 12 WFC filters. Scale variations of a few parts in  $10^4$  are found between regular filters but changes of a percent or more are evident when polarizing filters are included. Separate solutions for the polarizers are specified in the IDCTAB.

### 4.1.3 Results

The most obvious component of the ACS distortion is a marked skew which results in the X/Y detector axes lying at  $\sim 85$  degrees to each other on the sky. In addition, the distortion in all ACS detectors is highly non-linear (see Figure 4.3-4.6). A quartic fit ( $k=4$ , see Section 4.1.1) is adequate for characterizing the distortion to an accuracy better than 0.1-0.2 pixels over the entire field of view.

## WFC

The WFC detector is tilted at 22 degrees giving an elongation of 8% along the diagonal. The non-square projected aperture shape is evident from Figure 1.1 in Chapter 1, where the x axis is approximately in the V2 direction and the y axis is in the -V3 direction.

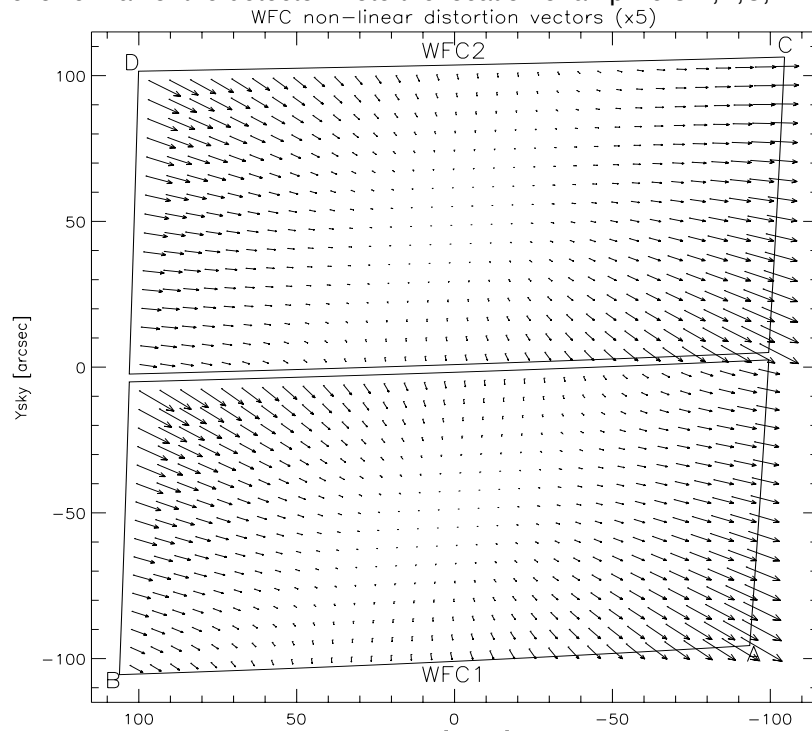
The WFC distortion is also illustrated in Figure 4.3, a vector displacement diagram which shows the contribution of the non-linear part of a quartic fit to the data. The vectors represent the degree of distortion to be expected in the WFC beyond the directional dependence of the plate scale. For display, the vectors are magnified by a factor of 5 compared to the scale of the x and y axes. The largest displacement indicated at the top left corner of the figure is  $\sim 82$  pixels or about 4 arcseconds. While a quartic solution is adequate for most purposes, binned residual maps (Figure 4.6) show that there are significant coherent residuals in the WFC solutions which have amplitudes up to  $\sim 0.1$  pixels due to differences in the distortion with wavelength. These residuals have been incorporated into the pipeline in the form of two-dimensional distortion residual images (Anderson & King 2004, ISR-ACS-04-15, Section 4.1.4), which are contained in the DGEOTILE keywords, extension `_dxy.fits` for each filter. These files, discussed further in Section 4.1.4, allow the characterization of the distortion to better than 0.01 pixel.

The pixel scales and array sizes are summarized in Table 4.1 for each ACS detector. A contour plot of relative pixel area across the WFC is shown in Figure 6.1. The range of area is from 0.89 to 1.08 times the central value.

Table 4.1: Pixel scale (*arcsec/pixel*) and array size (*pixels*) for each ACS detector.

Detector	Pixel Scale at Center $X_{\text{scale}}, Y_{\text{scale}}$	Average Pixel Scale $X_{\text{scale}}, Y_{\text{scale}}$	Array size (pixels)	Array size (arcsec)
WFC1	0.04927, 0.04864	0.04917, 0.04861	4096x2048	201"x100"
WFC2	0.04985, 0.05031	0.04976, 0.05029	4096x2048	204"x103"
HRC	0.02844, 0.02484	0.02843, 0.02484	1024x1024	29"x25"
SBC	0.03374, 0.03009	0.03377, 0.03010	1024x1024	35"x31"

Figure 4.3: Non-linear component of the ACS distortion for the WFC detector using a F475W quadratic fit. Note that this figure is rotated 180 degrees with respect to the default orientation of the drizzled product, where WFC2 would be the lower half of the detector. Note the location of amplifiers A,B,C,D.



When deriving the ACS flat fields, an implicit correction is made for the distortion which is equivalent to dividing each pixel by the relative pixel area. Thus, point source photometry extracted from a flat fielded image must be multiplied by the effective pixel area. This correction is accounted for in pipeline processing by **MultiDrizzle** which uses the distortion solution to correct all pixels to equal areas. When working with FLT files this correction must be applied manually (see Section 6.1.3 for details).

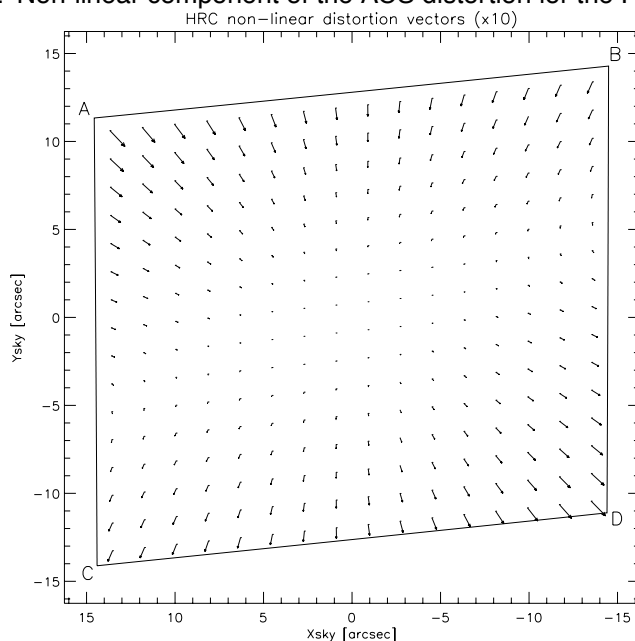
### HRC

The High Resolution Channel has its edges aligned approximately along the V2 and V3 axes (see Figure 1.1). In this case, the center of the aperture lies on a line passing through the V2/V3 origin and making an angle of 22 degrees with the V3 axis. Because the aperture diagonal does not correspond to a radius of the HST field of view, the distortion has no particular symmetry with respect to the detector axes. Because the focal plane, and therefore the detector plane is 25 degrees away from the plane normal to the light path, the scales along the axes differ by  $\sim 14\%$ . However, since the HRC is less than 30 arcsec across, the *total* variation in scale across the detector is much less than for the WFC, being only  $\sim 1\%$ .

A vector plot of the deviation from linearity is given in Figure 4.4 in which the deviations have been magnified by a factor of 10 for illustrative purposes. The largest displacement is 4.9 pixels in the top left corner and corresponds to about 0.1 arcsec. While a quartic solution is adequate for

most purposes, binned residual maps (Figure 4.6) show that there are significant coherent residuals in the HRC solutions which have amplitudes up to  $\sim 0.1$  pixels. These residuals have been incorporated into the pipeline in the form of two-dimensional distortion residual images (Anderson & King 2004, ISR-ACS-04-15) - these DGEFILES (\*\_dxy.fits) are described further in Section 4.1.4.

Figure 4.4: Non-linear component of the ACS distortion for the HRC detector.



The pixel scales and array sizes are summarized in Table 4.1 for the HRC. The variation of pixel area across the detector is shown in Figure 6.1. The maximum deviation from the central value is just over 2%. As explained for WFC, this must be taken into account when doing photometry, either by using **MultiDrizzle** output products (DRZ files) or by manually correcting FLT files with a pixel area map (see Section 6.1.3 for details).

### SBC

The Solar Blind Channel contains the MAMA detector. It is centered at approximately the same place as the HRC in the V2/V3 plane and is slightly larger, about 35 x 30 arcsec, versus 29 x 25 arcsec for the HRC. The average scales in the x and y directions are given in Table 4.1 and are calculated by matching observations of the same sky area by HRC and SBC.

The optical distortions are close to those displayed by the HRC. The only difference in their light paths is the presence of a plane M3 fold mirror which reflects light away from the SBC onto the HRC. Because there is one less mirror in the SBC light path, the distortion corrected image (in sky coordinates) in Figure 4.5 appears flipped with respect to the HRC image in Figure 4.4. The MAMA has a small amount of extra distortion within the

detector itself, arising from irregularities in the multi-channel plate. The largest difference from a square pattern is 2 pixels, or 0.06 arcsec. As explained for WFC, pixel area variations must be taken into account when doing photometry, either by using **MultiDrizzle** output products (DRZ files) or by manually correcting FLT files with a pixel area map (see Section 6.1.3 for details).

Figure 4.5: Non-linear component of the ACS distortion for the SBC detector, derived originally by Meurer from program 9027 consisting of observations of NGC6681 using the F125LP filter. Distortion solutions are 4th order polynomials and assumed to be the same for all filters.

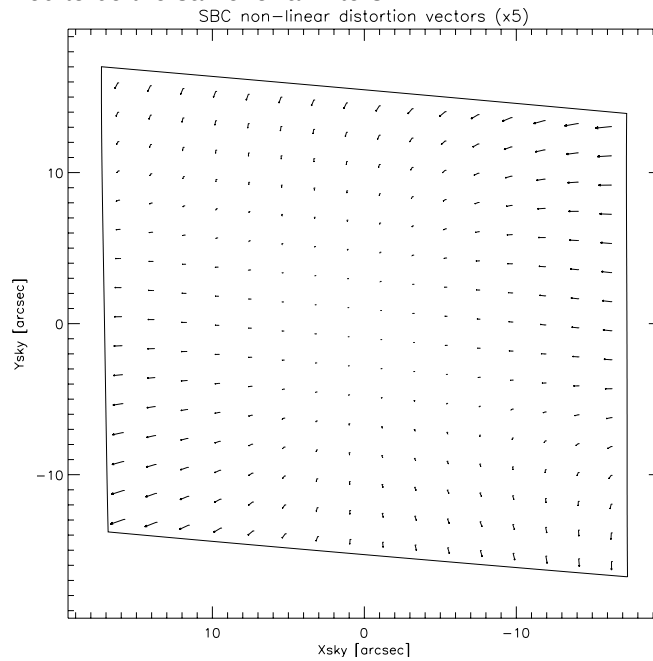
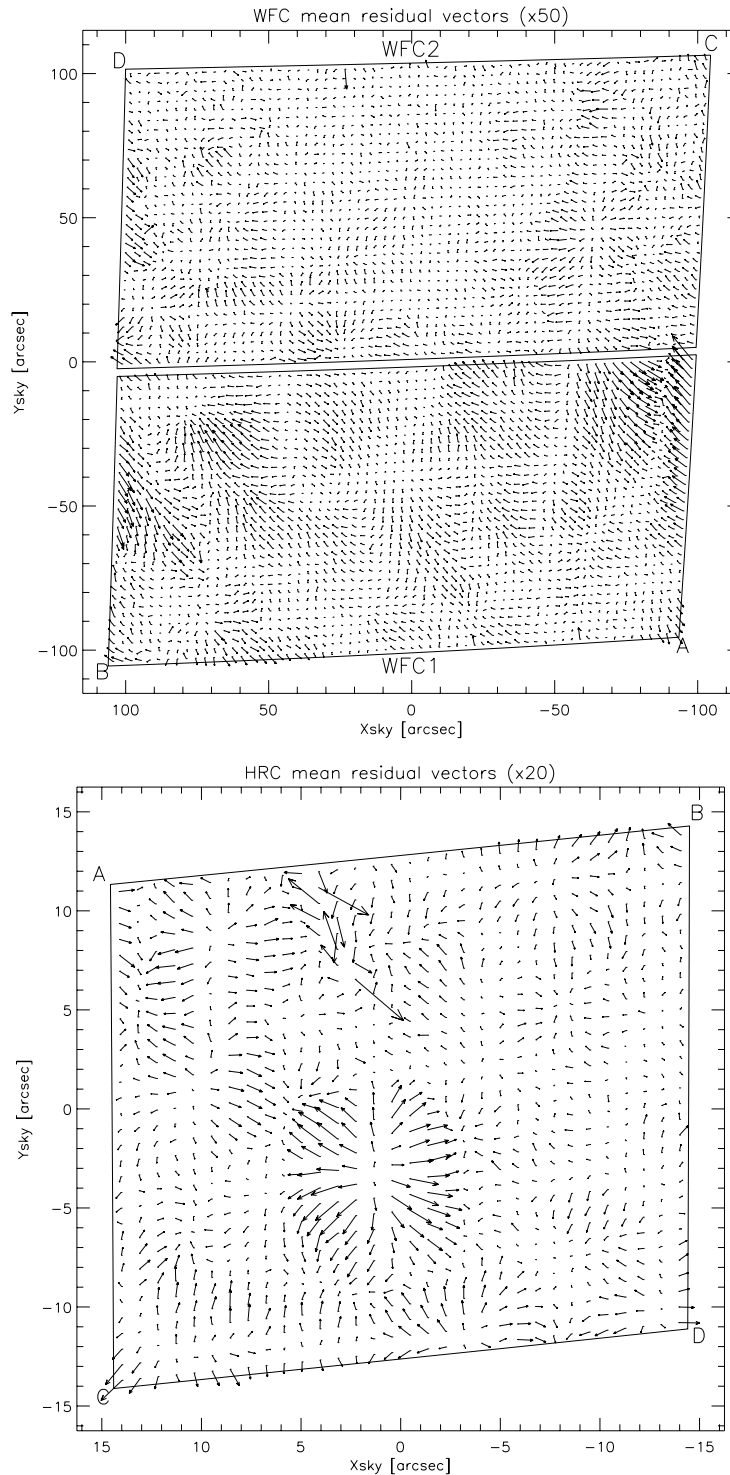


Figure 4.6: Example binned residuals to quartic distortion model fits for the ACS WFC and HRC detectors, for F475W. These residuals depend on the filter used. Note that the WFC figure is rotated 180 degrees with respect to the orientation of the default drizzle product, where WFC2 would have been the lower half of the detector. The large residuals close to the upper edge of the HRC map, left of center, are due to the presence of the Fastie occulting finger. There is insufficient data to make the equivalent plot for the SBC.





#### 4.1.4 Distortion Reference Files (IDCTAB & DGEOFILE)

The Science Instrument Aperture File (SIAF) contains position and scale information for every aperture of each of HST's science instruments. Thus, it supports accurate target acquisitions, image processing, and photometry. The conversion between distorted and undistorted positions in the SIAF is controlled by a polynomial expansion which is derived by the individual instrument teams. A simple, common reference file can therefore be created for each instrument which describes the geometric distortion of each detector. In this section, we describe the format of this common reference file which has been developed to be as general as possible so that it can be used for many different instruments or detectors.

For ACS, the coefficients to the polynomial fit are found in the IDCTAB reference file. The distortion correction is not a part of **CALACS**, but is instead used as input to **MultiDrizzle** (see Section 4.4) where it is used to convert the distorted image into a geometrically corrected image.

##### Application of the Model

The steps performed in the application of the IDCTAB can be summarized in the following steps:

- First, the offset in position of each pixel relative to the reference position is computed.
- These deltas are used to compute the undistorted positions in arcseconds with the coefficients of the polynomial fit given in the IDCTAB reference file. These solutions are computed for each filter as given by Anderson & King (ISR ACS 04-15).
- The undistorted positions are divided by the desired output plate scale, where the default value is taken from the SCALE column in the IDCTAB unless specified by the user. The VAFACOR is also applied to the scale term.
- Finally, both chips (WFC only) are combined into a single mosaiced image by adding the appropriate offset to each pixel to get the final position.

The fit for each chip ensures that the distorted and corrected Y axes for a chip remain at the same angle with respect to the telescope V3 axis. This allows each chip to have a different rotation relative to the other, though this effect has been empirically shown to be less than 0.001 degree.

##### Format of the IDCTAB Reference file

The IDCTAB is stored as a FITS binary table (calibration file with '\_idc.fits' extension), where the primary header contains keywords INSTRUME and DETECTOR which define the model appropriate to a specific instrument and detector. The NORDER keyword gives the order of the polynomial stored in the table. While the original laboratory data provided a cubic solution to the distortion, more accurate in-flight data now supports a fourth-order solution (NORDER=4).

The first extension of the IDCTAB contains the geometric distortion solution, where the table columns are listed in Table 4.2. The table contains distinct rows for each detector chip and filter combination specified by the DETCHIP and FILTER columns. If the DIRECTION column is 'INVERSE' rather than 'FORWARD', the coefficients specify the conversion from undistorted to distorted pixel positions. The SCALE keyword gives the default pixel scale of the drizzled image, where the default output scale for drizzled WFC images is 0.05 arcsec/pixel and for HRC/SBC images is 0.025 arcsec/pixel.

Table 4.2: Columns in the IDCTAB. Note that there is one row for each filter combination, and a different IDCTAB for each detector

Column	Description
<b>DETCHIP</b>	ID of chip/detector used for observation
<b>DIRECTION</b>	Application direction of coefficients (FORWARD,INVERSE)
<b>FILTER1</b>	Name of filter in filter wheel 1
<b>FILTER2</b>	Name of filter in filter wheel 2
<b>XSIZE</b>	Raw image size in X direction (pixels)
<b>YSIZE</b>	Raw image size in Y direction (pixels)
<b>XREF</b>	X position of reference pixel
<b>YREF</b>	Y position of reference pixel
<b>V2REF</b>	V2 position of reference point (arcsec)
<b>V3REF</b>	V3 position of reference point (arcsec)
<b>SCALE</b>	Scale of square corrected pixel (arcsec/pix)
<b>CX10, CX11,...</b>	Distortion Coefficients for X position
<b>CY10, CY11,...</b>	Distortion Coefficients for Y position

The distortion coefficients provide a correction for each pixel relative to the detector chip reference point specified in the XREF and YREF columns. The relationship between each chip must be factored in separately. HST relies on a V2/V3 coordinate system to define each detector's position (in arcseconds) relative to the center of HST's field of view. The V2REF and V3REF columns contain the reference position of each detector in the V2/V3 system. The absolute position is secondary to the relative position of this reference point, because only the offset between V2REF/V3REF positions is used for combining multiple chips into a single output image. The XREF/YREF and V2REF/V3REF positions represent the same point in different coordinate systems.

The columns  $CX_{ij}$  and  $CY_{ij}$  contain the coefficients of the polynomial fit for each chip and convert an input pixel position to an undistorted position. The column names contain the indices for the coefficients from the polynomial fit as discussed in Section 4.1.1, where  $CX_{11}$  and  $CY_{11}$  correspond to the  $a_{11}$  and  $b_{11}$  coefficients. For subarray data, the input pixel position must first be corrected for the subarray offset in order to put it in the coordinate frame of the full chip.

The presently implemented IDC tables include separate rows of coefficients for all the measured filter combinations. Uncalibrated combinations default to the F475W filter solution with scale allowances made in the case of polarizing filters.

### Format of the DGEO File

The solutions described by the IDC tables are correct to about 0.1 pixels. However the distortion can be specified to 0.01 pixels by the inclusion of extra corrections (such as those shown in Figure 4.6) which can not be expressed by the fourth order polynomials. These further corrections are available in the form of two images for each detector for the  $x$  and  $y$  directions. These DGEO correction images have the extension ‘\_dxy.fits’ and have been incorporated into the pipeline processing as of September 2004. For filter combinations for which these images do not exist, the final DGEO image correction step is omitted. However note that for most purposes the polynomial solutions provide adequate precision.

## 4.2 Combination of Dithered Data

### 4.2.1 Introduction to Dithering

Many ACS datasets are dithered - they have shifts between successive images which may be small or large. Dithering is a well established technique for HST imaging and has many advantages. For a general introduction to the concepts behind dithering, please consult the *HST Dither Handbook* (Koekemoer et al. 2002). Dividing observations into multiple exposures allows for the removal of cosmic rays, while dithering can be added for any combination of the following purposes:

- Sub-pixel shifts to improve the sampling of the PSF, since generally the ACS pixels are not quite small enough to fully sample the PSF.
- Shifts of at least a few pixels to enable detection and flagging of detector artifacts such as hot pixels, bad columns, etc.
- Shifts of order a few arcseconds in order to fill in regions not covered by the detector, like the WFC chip gap or the HRC occulting finger.

- Large shifts comparable to the detector size, in order to create mosaics of larger regions of sky.

Because the non-linear component of the ACS optical distortion is large, a given dither offset corresponds to different pixel shifts across the field of view. This must be taken into account when planning observations. For more information on ACS dither patterns, see the [ACS Patterns](#) section of the HST Phase II proposal instructions and also the ACS “dither” webpage: <http://www.stsci.edu/hst/acs/proposing/dither>

## 4.2.2 Introduction to Drizzle

The methods for combining dithered ACS data described in this chapter are all based on the **Drizzle** method (Fruchter & Hook, 2002 *PASP*, 114, 144) and are described in detail in the *HST Dither Handbook* (Koekemoer et al. 2002). Here we give a brief summary of the method and refer the reader to the aforementioned documentation for further details and quantitative information about its properties.

**Drizzle** maps each pixel of the distorted input image onto pixels in a rectified, undistorted output image, taking into account shifts and rotations between images and the optical distortion of the camera. However, in order to avoid re-convolving the image with the large pixel of the camera, the user may shrink each input pixel before it is mapped onto the output image. This shrinking factor is known as the “pixfrac” and is normally between 0.0 (corresponding to interlacing input pixels onto single output ones) and 1.0 (which corresponds to shift-and-add). The degree of sub-sampling (the size of the output pixels relative to that of the original ones) is also a user controllable parameter called “scale” which is typically in the range 1-0.5 for the ACS.

The **Drizzle** algorithm has a number of important features. It preserves both absolute surface and point-source photometry, hence flux can be measured using an aperture whose size is independent of position on the chip, since all pixels in the output image have the same scale. And because the method anticipates that a given output pixel may receive no information from a given input pixel, missing data (due for instance to cosmic rays or detector defects) do not cause a substantial problem, as long as there are enough dithered images to fill in the gaps caused by these zero-weight input pixels. Finally, the linear weighting scheme is statistically optimum when inverse variance maps are used as the input weights.

It should be noted that, while the standard **Drizzle** “kernel” provides near-optimal results for combining multiple sub-pixel dithers, it is less ideal in the limiting case of a single image when both scale and pixfrac are nominally set to unity. This is equivalent to bilinear interpolation and results in strongly correlated noise and varying degrees of pixel sampling across the output image. This can be mitigated by using more optimal

interpolators for the **Drizzle** kernel, for example the “Lanczos3” kernel which is designed to minimize correlated noise and maximize resolution, although it is less robust in dealing with missing pixels that have been flagged as bad. The various kernel options are all available within **Drizzle** which is implemented as an IRAF task within the STSDAS **dither** package, and can be run in stand-alone mode or invoked by **MultiDrizzle**.

### 4.2.3 Overview of Drizzle-Related Software Tools

The tools for the combination of dithered HST images have evolved through the years, starting with those developed for the Hubble Deep Field in late 1995. First came low-level tools which required considerable effort to use. Subsequently higher level wrapper scripts, written in the Python language, have been developed to ease such combination. Some of these capacities are now available within the pipeline. The main three levels applicable to current ACS imaging are as follows:

- The low level tools for mapping pixels from input to output images and support tasks for measuring shifts, detecting cosmic ray events, etc. are available within the dither package of STSDAS. These include **drizzle** itself and **blot** (reverse **drizzle**), as well as **driz\_cr** for finding cosmic rays. Most users will now probably prefer to access these tools via a wrapper script, rather than use them directly.
- **PyDrizzle** and associated Python scripts are layered on these and automate some of the processing. They convert the IDCTAB information into a form suitable for **drizzle**, create appropriate association tables and drizzle images into an appropriate output frame. The user will again probably not use these tools directly. **PyDrizzle** is available within the STSDAS system and requires the PyRAF environment. **PyDrizzle** was used by OTFR until September 2004.
- **MultiDrizzle** is a user-friendly script layered on top of the above tools and is generally recommended for use by observers. In addition to image registration and combination, it also provides automated detection and flagging of cosmic rays. As of 2004, **MultiDrizzle** is implemented in the pipeline with default settings that produce good results for many typical ACS dithered datasets. It provides access to many parameters for users who want to run it directly, and is available within the STSDAS system under the PyRAF environment.

**MultiDrizzle** and **PyDrizzle** are both Python scripts which require the PyRAF environment, as well as the latest version of the STSDAS package. It is recommended that the complete current STSDAS package is installed to avoid potential missing components or mismatched versions. STSDAS and PyRAF are available from:

[http://www.stsci.edu/resources/software\\_hardware](http://www.stsci.edu/resources/software_hardware)

While the software has been well tested and is fairly stable, it is still periodically being improved. We therefore refer readers to the **MultiDrizzle** web site for the most up-to-date software:

<http://stsdas.stsci.edu/multidrizzle>

and to the ACS Drizzling web site for additional documentation:

<http://www.stsci.edu/hst/acs/analysis/drizzle>

The following sections describe in more detail the tasks performed by **MultiDrizzle** and give some example of their use. A help document describing the numerous **MultiDrizzle** parameters can be accessed by typing ‘help multidrizzle’ from within PyRAF. The next version of the HST Dither Handbook is currently also under revision to include documentation for **MultiDrizzle** and several detailed ACS drizzling examples.

#### 4.2.4 Association Table Usage

In order to enable the **Drizzle** task to be used in an automated manner, two issues need to be addressed: calculating the required input parameters automatically, and working with a wide range of input image formats. **MultiDrizzle** relies on several features to address these problems:

- An association table relates multiple input images to a single output product.
- Python “structures” are created in memory for each input image and for the output image field.
- Output field parameters (RA/Dec of center, pixel size, field of view) are specified using a ‘SkyField’ function.

The calibration pipeline uses association tables to define how multiple images, taken at different pointings, relate to a single output image. These association tables are also then used to automatically combine and correct ACS dithered observations or any other related set of observations. Each input/output exposure in the association table contains information about:

- its own world coordinate system,
- the distortion model for its detector,
- the range of output pixels covered by the image, and
- any instrument specific characteristics.

This design provides the flexibility to support multiple instruments simultaneously, and to combine observations from several instruments into a single output field with arbitrary specification. The virtual output image is built using the World Coordinate System (WCS) information from each input image and the distortion model. This provides all the information necessary to calculate the input parameters for **drizzle**. These parameters are then passed to **drizzle** which actually performs the image combination.

---

## 4.3 PyDrizzle

The **PyDrizzle** script provides a PyRAF interface to **Drizzle**, and is specifically designed to automate a number of the user-intensive steps associated with using **Drizzle** to combine dithered data. In particular, this includes:

- determining image shifts from the headers
- calculating shift and rotation parameters to be passed to **Drizzle**
- calculating the output image size to contain the dithered exposures
- ability to include multi-extension FITS files

In addition, **PyDrizzle** translates the IDCTAB geometric distortion files into "coefficient" files that are used by **Drizzle**. As such, **PyDrizzle** provides all the machinery necessary to drizzle a single image, two groups of a single exposure, or a series of associated exposures into geometrically corrected output files.

Until September 2004, **PyDrizzle** was used in the pipeline to produce combined, drizzled image products for ACS data. However, **PyDrizzle** does not perform any cosmic ray rejection, but instead relies upon previous tasks, in particular ACSREJ which is performed as part of the **CALACS** processing step for CR-SPLIT data. If the number of CR-SPLITS is greater than about 3 or 4, then this provides enough individual exposures to enable good cosmic ray rejection by ACSREJ. However, very often observers only obtain a single exposure at each of several dither positions. In this case, each pair of exposures contains thousands of pixels that are affected by cosmic rays in both exposures, and when combined by **PyDrizzle** these cosmic rays propagate through to the final output image.

The solution to this issue is to use all the exposures together to generate cosmic ray masks in a single step. This has required the implementation of a new script, **MultiDrizzle**, described further in Section 4.4, which makes use of **PyDrizzle** to perform image registration but includes additional processing to construct clean intermediate images and create cosmic ray masks, before doing the final drizzling.

---

## 4.4 MultiDrizzle

**MultiDrizzle** (Koekemoer et al. 2002, HST Calibration Workshop 2002, p.337), is a general purpose script for performing automated registration, cosmic ray rejection and drizzle combination of images. It provides a single-step user-friendly interface to **PyDrizzle** and to the other drizzle-related tasks in the STSDAS **dither** package. For a general introduction, refer to the *HST Dither Handbook* (Koekemoer et al. 2002).

### 4.4.1 Steps Performed by MultiDrizzle

For ACS data, **MultiDrizzle** starts with the flat fielded, but still distorted, FLT files created by **CALACS**. While this is the only mandatory input, there are many additional optional inputs including lists of improved user-determined shifts. In default mode, **MultiDrizzle** performs the following steps in order, although the user has full control via the parameter file, of which steps are to be performed or omitted. Each step is described in detail in Section 4.5 and Section 4.7

1. Bad pixel masking, to identify additional bad pixels that may not be present in the image DQ array or BPIXTAB reference file
2. Sky subtraction on each individual input image (optional)
3. Initial image registration (based on world coordinate system information in the header keywords) and drizzling to separate output images
4. Combining the separate drizzled images to create a clean median
5. ‘**Blot**’ transformation of the clean image back to the frame of each input image
6. Creation of a cosmic ray mask for each input image, based on a comparison between the blotted image, its derivative, and the original input image
7. Final drizzle combination, applying the cosmic ray and bad pixel masks

The goal of **MultiDrizzle** is to provide a high-level task that has an extensive suite of user-adjustable parameters with default values that will produce good results for a wide variety of standard dithered datasets with no user intervention. At the same time, the parameters allow the user a large amount of flexibility in controlling the relevant aspects of these steps, in case the default parameters are not sufficient for specific scientific applications. The default MultiDrizzle parameters are listed in the example in Section 4.7.

### 4.4.2 Multidrizzle in the ACS Pipeline

The ACS calibration pipeline currently consists of 2 processing stages, namely **CALACS** followed by **MultiDrizzle**. Standard **CALACS** processing includes bias and dark subtraction, removal of the overscan regions, and flat fielding. It will produce, among other products, a calibrated image with the FLT suffix for each input file. The **CALACS** portion of the pipeline will calibrate and combine CR-SPLIT images. It will not, however, correct for geometric distortion or combine images from multiple dither positions.



Geometric distortion is removed for all images (dithered or not) in the second stage of processing via **MultiDrizzle**. This software makes use of the ACS association tables, allowing the pipeline to combine associated dithered observations for a single visit into a single image. Finally, **MultiDrizzle** converts the data to units of count rate (*electrons/sec*). Regardless of whether observations were taken as a single image or a set of dithered exposures, **MultiDrizzle** produces images which are both astrometrically and photometrically accurate.

Processing comments are recorded in the trailer file for the DRZ image, including which version of **drizzle** was used, what parameters were used, and which images were combined (if dithered). The same default parameters are used for all observations in the pipeline, and are recorded in the MDRIZTAB reference files that are delivered along with the data. These parameters were chosen to avoid introducing any scale changes, shifts, or rotations relative to the original pointing, aside from those corrections incorporated in the distortion model itself. While the pipeline products will be properly corrected for distortion, the combination of dithered observations may not be ideal, and small pointing errors or defects, such as hot pixels or cosmic-rays, may still be present. In this case, we refer readers to Section 4.5 for instructions on post-pipeline reprocessing. For well dithered data, some resolution may be recovered by decreasing *scale/pixfrac*.

The current version of **MultiDrizzle** uses the image header world coordinate system (WCS) to deduce the image-to-image offsets. However, user-supplied offsets may also be applied via a shiftfile during reprocessing. Tasks to ease the determination of such shifts are currently being developed. **MultiDrizzle** processing with default parameters has been part of the standard HST pipeline processing since September 2004.

#### 4.4.3 Data Quality Flags for Bad Pixels: The ‘Bits’ Parameter

The data quality flags which were set during **CALACS** processing can be used as bit masks when drizzling, and the user may specify which bit values should actually be considered ‘good’ and included in image combination. This is done via the parameters ‘*driz\_sep\_bits*’ and ‘*final\_bits*’. Any pixel flagged otherwise will be considered ‘bad’ and will be given zero weight. If a pixel is flagged as bad but has non-zero weight in any other image, the pixel will be replaced with the value from that image during image combination. Otherwise, the pixel will be replaced with the ‘fill value’. The default ‘fill value’ used by **MultiDrizzle** during pipeline processing is ‘INDEF’. If the ‘fill value’ is set to INDEF during reprocessing with **MultiDrizzle**, and if there are no pixels with non-zero weight, the pixel will retain its original value.

The flags for the DQ array were presented in Chapter 3 and are summarized in Table 3.4. The bits value used during pipeline processing is 96 which is the sum of 32 and 64 (two flag values for warm pixels). Note that these pixels were flagged during **CALACS** processing as “bad” or “suspect”, but may have been corrected in later processing steps. The bits parameter indicates which “suspect” pixels to keep. When the total counts in a given pixel have exceeded the full well, for example, the DQ flag is 256. However, testing shows that counts still accumulate in a highly linear manner and that photometry of saturated stars is quite practical if using a gain that samples the full well depth.

The default bits value in the off-line **MultiDrizzle** software available for reprocessing is zero, but can be reset by the user prior to reprocessing. The value chosen for this parameter is completely up to the user and should be selected based on the specific calibration needs. For HRC processing, the user may want to add 8 (masked by aperture) to the value so that pixels which lie behind the occulting finger mask are not given zero weight. (In Figure 4.7 of Section 4.5.1, bit 8 is not included in the bits parameter prior to drizzling. Pixels behind the occulting finger were therefore given zero weight and replaced with the default fill value=zero.) Of course, the photometry in this region will be inaccurate due to improper flat fielding, so this bit would likely only be set for aesthetic reasons.

#### 4.4.4 MultiDrizzle Data Products

The output from **MultiDrizzle** is a single multi-extension FITS file with the suffix ‘\_drz.fits’. The first extension contains the science (SCI) image which is corrected for distortion and which is dither-combined (or mosaiced), if applicable. The drizzled SCI image is in units of *electrons per second*. All pixels have equal area on the sky and equal photometric normalization across the field of view, giving an image which is both photometrically and astrometrically accurate for both point and extended sources. The dimensions of the output image will be computed on-the-fly by **MultiDrizzle** and the default output plate scale will be read from the IDCTAB. These parameters, however, may be chosen by the user during reprocessing to best suit the actual data.

The default pixel scale for the output image is unity, i.e. output pixels have the same scale in arcseconds as the pixels of whichever camera was used to obtain the data (WFC, HRC or SBC). In addition, the value of pixfrac is set to 1 for less than 6 exposures, and is set to 0.8 for 6 or more exposures where dithering provides better sampling of the sub-pixel plane. Finally, the default orientation for images from the pipeline is in the unrotated frame (with amplifiers A and B always at the top, see Figure 1.1). If a different orientation is desired (for example, with North to the top), this

can be easily achieved by re-running **MultiDrizzle** off-line once the data have been retrieved.

The second extension of the output image contains the weight (WHT) image. It gives the relative weight of the output pixels and can be considered an effective exposure time map. The data quality map created by **CALACS** is used by **MultiDrizzle** via the "bits" parameter in creating the weight image (See Section 4.4.3).

The third extension of the **MultiDrizzle** output image contains the context (CTX) image which encodes information about which input image contributes to a specific output pixel. This is done using a bitmask for each output pixel, where 'bit set' means that the image, in the order it was combined, contributed with non-zero weight to that output pixel. The context image starts as a single 32-bit integer image but can be extended with additional 32-bit deep planes, if there are more than 32 input images.

Finally, it should be noted that the calibrated FLT files contain additional bits in the DQ mask that identify pixels flagged as cosmic rays by **MultiDrizzle**. The default value for these bits is 4096, and if **MultiDrizzle** is re-run on the FLT files offline it will be able to use these flags and proceed directly to the final drizzle step without the need to re-do cosmic ray masking, unless that is required. Alternatively, if the cosmic ray rejection needs to be improved, then the pipeline CRs can be ignored/reset by adding 4096 to the "bits" parameter value when running **MultiDrizzle**.

---

## 4.5 Post-Pipeline Reprocessing

The goal of the ACS pipeline is to provide data calibrated to a level suitable for initial evaluation and analysis for all users. Observers frequently require a detailed understanding of the calibrations applied to their data and the ability to repeat, often with improved products, the calibration process at their home institution. There are several occasions when off-line interactive processing with **MultiDrizzle** may be desired:

- Observations which have been manually reprocessed with **CALACS** will still require a correction for geometric distortion.
- Users may wish to modify the default **MultiDrizzle** parameters, specifying an alternate output image orientation, pixel "shrinking factor" `pixfrac`, or pixel scale.
- When images have been taken across multiple visits, the observations are not automatically associated. Creating custom association tables will allow data from multiple visits to be combined. See Section 4.7 for details.

- For optimal image registration and refining the CR rejection, the user may wish to fine-tune the WCS information by supplying additional shifts and/or rotations.
- During pipeline processing, **MultiDrizzle** makes assumptions about which DQ flags should be considered bad. These pixels will be excluded when creating the drizzled product. Users may wish to select which flagged pixels should actually be considered good and included in the drizzled product.
- If cosmic ray rejection parameters need to be fine-tuned for specific datasets, for which the pipeline defaults may not have produced optimal results.

The **MultiDrizzle** software uses the Python language and can only be executed in the PyRAF environment. PyRAF, developed at STScI, allows users to run tasks using the standard IRAF parameter-based interface or by using separate Python programs. The PyRAF interface and the most recent version of **MultiDrizzle** can be downloaded from:

[http://www.stsci.edu/resources/software\\_hardware/stsdas/pydrizzle](http://www.stsci.edu/resources/software_hardware/stsdas/pydrizzle).

**MultiDrizzle** creates many large files and does a considerable amount of processing. It is hence recommended that a modern fast machine with several GBytes of free space be used if possible. In the example to follow, each of the input FLT files is ~168MB and the final combined output product is 310MB. Many large intermediate files are also created but may be cleaned up if required.

The main calibration reference files required by **MultiDrizzle** are the IDCTAB and DGEOFILE files discussed in Section 4.1.4. The IDCTAB file describes the ACS distortion in terms of polynomial coefficients. The appropriate reference file is recorded in the image header keyword IDCTAB. This file should be obtained from the STScI archive (via Starview) and placed in some local directory. Before starting **MultiDrizzle** the environment variable “jref” must be set appropriately to point to this directory (see Section 3.5 for more information). Once the FLT files have been collected and the ‘jref’ environment established, PyRAF should be started and the **stsdas**, **analysis**, and **dither** packages loaded.

The calibrated products from **CALACS** and the corresponding input to **MultiDrizzle** are described for various observing modes in Table 3.1. For example, a single image will produce an FLT file, a RPT-OBS exposure will produce an SFL file, a CR-SPLIT exposure will produce a CRJ file, and a DITH-PATTERN will produce a series of FLT, CRJ, or SFL files at *each* dither position. **MultiDrizzle** may be executed using any of the calibrated data products or the association table itself, and creates a single drizzled image with the DRZ suffix. In the case of dithered observations

which are part of a pattern, the individual FLT files will be combined to create a single DRZ image.




---

*An important variable to set up prior to running MultiDrizzle is the "jref" path, since this specifies the directory where MultiDrizzle searches for the IDCTAB and other distortion-related files. This is described in Section 3.5 and should be set up before starting PyRAF, by typing:*

```
setenv jref /mydisk/jref/
```

---

After defining the "jref" environment and starting PyRAF, the **stdas**, **analysis**, and **dither** packages should be loaded.

```
unix% setenv jref /mydisk/myjref/
unix% pyraf
pyraf> stdas
pyraf> analysis
pyraf> dither
```

To avoid potential problems, it is also recommended that the parameters for both **MultiDrizzle** and **PyDrizzle** be reset to their default values until users are sufficiently familiar with them:

```
pyraf> unlearn pydrizzle
pyraf> unlearn multidrizzle
```

The examples in this section describe the steps required for reprocessing after retrieving pipeline products, and serve as a continuation of the **CALACS** examples described in Section 3.5.2. We advise the reader to work through the **CALACS** examples first to develop a solid understanding of the calibrated data products and their potential limitations.




---

*Note: MultiDrizzle modifies the DQ array of the calibrated images, by adding new bit values for pixels identified as cosmic rays (4096 in the case of ACS), and it also updates the headers with the sky value but doesn't actually subtract the sky from the science array. When reprocessing, we advise retaining a full copy of the original files in a separate directory. A switch can be specified to tell the script to work on copies of the images.*

---

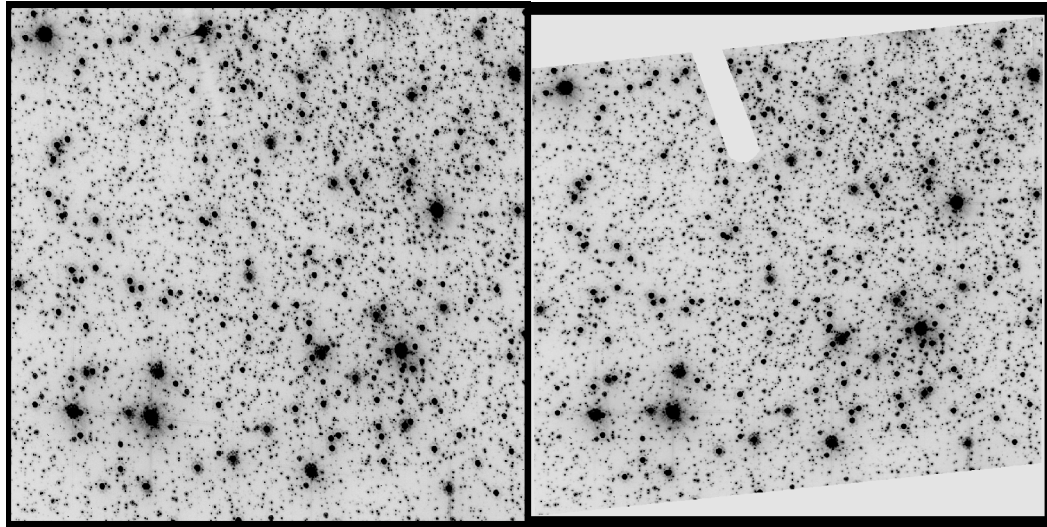
### 4.5.1 Example 1: Running PyDrizzle on a Single Exposure

The following is a continuation of Example 1 from Section 3.5.2 where manual recalibration of a single raw exposure with **CALACS** produced a single image with the FLT suffix. Here, we run **PyDrizzle** on the calibrated FLT image (j8bt07oyq\_flt.fits) to illustrate the geometric distortion. By default, the drizzled output product will be named j8bt07oyq\_drz.fits. To specify an output file which is different than the default, the user may set the 'outfile' parameter to 'myfile\_drz.fits', for example. Section 4.4.3 defined the 'bits' parameter; here we adopt the recommended value of 96. The reader may also wish to add 8 to this value to see the effect of not dropping pixels behind the occulting finger. Prior to running, we recommended clearing any preset values using the 'unlearn' command.

```
pyraf> pydrizzle j8bt07oyq_flt.fits bits=96
```

The distortion corrected HRC science image is shown in Figure 4.7. The image on the left is the flat fielded FLT product from **CALACS** and still contains distortion. The image on the right is the calibrated, distortion-corrected DRZ product.

Figure 4.7: The effect of applying the distortion correction to a single HRC image. The image on the left is the flat-fielded FLT product from **CALACS**. The image on the right is the distortion-corrected DRZ product.



### 4.5.2 Example 2: Running PyDrizzle on an Association file

The following is a continuation of Example 5 from Section 3.5.2 where manual recalibration of a 2-point line dither pattern produced two FLT images (j8e654c0q\_flt.fits, j8e654c4q\_flt.fits).

Using **tprint**, we can view the contents of the image association, including the rootnames of the individual dithered images and the default rootname of the drizzled product.

```
pyraf> tprint j8e654010_asn.fits
# MEMNAME      MEMTYPE      MEMPRSNT
j8e654c0q      EXP-DTH      yes
j8e654c4q      EXP-DTH      yes
j8e654011      PROD-DTH     yes
```

Next we run **PyDrizzle** on the image association. The two FLT images are combined to create a single DRZ image called 'j8e654011\_drz.fits'.

```
pyraf> pydrizzle j8e654010_asn.fits bits=96
```

Note that **PyDrizzle** is not designed to remove cosmic rays from these images.

### 4.5.3 Example 3: Running MultiDrizzle with Different Output Image Options

The simple examples in the preceding Section 4.5.1 and Section 4.5.2 demonstrate the use of **PyDrizzle** as an easy interface to the **Drizzle** program. However, in general we recommend the use of **MultiDrizzle** which includes more functionality, for example cosmic ray rejection, while at the same time combining an easy user interface together with substantial flexibility through access to a wide range of parameters.

The default **MultiDrizzle** parameters within the pipeline produce output images with a scale equal to unity, i.e. with output pixels equal to the pixel scale of whichever camera was used to obtain the images (e.g., ACS/WFC, HRC or SBC). In addition, the `pixfrac` parameter is set to 1.0 for associations with less than 6 images, and 0.8 for 6 or more images. Finally, the images are generally oriented with North to the top, except for polarizer images which are left unrotated for easier ingest by polarization analysis software. An estimate of the sky background will be determined by the software and written to the keyword `MDRIZSKY`.

While these parameters are satisfactory for a wide range of scientific applications, there may be occasions where the user wishes to re-run **MultiDrizzle** offline to repeat the final drizzle combination step using a different output image size or scale, `pixfrac` or orientation. This firstly involves turning off the intermediate steps for **MultiDrizzle** (except for sky subtraction), which can be done either within the `epar` interface:

```
pyraf> epar multidrizzle
```

or on the PyRAF command line:

```
pyraf> iraf.multidrizzle.static = no
pyraf> iraf.multidrizzle.skysub = yes
pyraf> iraf.multidrizzle.driz_separate = no
pyraf> iraf.multidrizzle.median = no
pyraf> iraf.multidrizzle.blot = no
pyraf> iraf.multidrizzle.driz_cr = no
pyraf> iraf.multidrizzle.driz_combine = yes
```

In this particular example, most of the steps are turned off since the cosmic ray rejection and other steps were already performed in the pipeline and are not being re-done, only the final drizzle step.

Note that we recommend sky subtraction to be turned on for broad-band data or other data with significant amounts of sky. This is because the sky background is retained in the science data in the FLT files; the pipeline **MultiDrizzle** calculates a sky background value and subtracts it on-the-fly before creating the pipeline drizzled product, but does not modify the science pixel values in the original FLT files. Therefore, turning on this step when running **MultiDrizzle** offline will ensure that the sky background keywords are read from the header and are applied before drizzling the data.

Next, the final output parameters can be specified. In this example, by way of illustration we wish to re-drizzle with a smaller scale (0.015 arcsec/pixel, instead of the HRC default of 0.025 arcsec/pixel), an orientation placing the y-axis at a position angle of 20 degrees, a different pixfrac and a specific central RA, Dec position, as well as a specific output image size. Since the FLT files already have cosmic ray flag values set in their DQ extensions, these will be applied by **MultiDrizzle** to produce a clean image.

Note that the original Drizzle program expresses the output scale from 0 to 1, as a fraction of the default scale, while **MultiDrizzle** expresses the output scale in arcsec/pixel.

The output settings can be specified as separate parameters, before running **MultiDrizzle**:

```
pyraf> iraf.multidrizzle.ra = 6.0272
pyraf> iraf.multidrizzle.dec = -72.0835
pyraf> iraf.multidrizzle.final_scale = 0.015
pyraf> iraf.multidrizzle.final_pixfrac = 0.9
pyraf> iraf.multidrizzle.final_rot = -20.
pyraf> iraf.multidrizzle.final_outnx = 2500
pyraf> iraf.multidrizzle.final_outny = 2500
pyraf> multidrizzle j8bt07*flt.fits output=test1
```



or on the command line when running **MultiDrizzle**:

```
pyraf> multidrizzle j8bt07*flt.fits output=example3 ra=6.0272
dec=-72.0835 final_scale=0.015 final_pixfrac=0.9 final_rot=20
final_outnx=2500 final_outny=2500 static- skysub+ driz_separate-
median- blot- driz_cr- driz_combine+
```

or in the epar interface, prior to running **MultiDrizzle**:

```
pyraf> epar multidrizzle
```

#### 4.5.4 Example 4: Re-Running MultiDrizzle to Improve Sky Subtraction

The default behavior of **MultiDrizzle** in the pipeline is to estimate the sky by means of the statistical distribution of pixels in the image, and subtract that from copies of the FLT files that are used to create the final drizzled image. The FLT files that are delivered to the user from the archive are not modified, ie they are not sky subtracted, but the sky values calculated by **MultiDrizzle** are contained in the header keyword MDRIZSKY.

For cameras with multiple detectors (such as ACS/WFC, or WFPC2), the sky values in each exposure are first measured separately for the different detectors. Then these different values are compared, and the lowest measured sky value is used as the estimate for all the detectors for that exposure. This is based on the premise that for targets consisting of large extended or bright sources, the pixel intensity distribution in one or more of the detectors may be significantly skewed toward the bright end by the target itself, thereby overestimating the sky on that detector. If the other detector is less affected by such a target, then its sky value will be lower, and can therefore also be substituted as the sky value for the detector with the bright source.

The default behavior for **MultiDrizzle** in the pipeline is to perform iterative sigma-clipping, starting with the full range of pixel intensity values and calculating the standard deviation, then rejecting pixels with values deviating from the mean by more than 4 sigma either way, repeating this for a total of 5 iterations, and then using the median value of the final distribution as the sky value. This gives good results for a wide range of datasets, but occasionally the sky is still slightly overestimated and can be improved by post-pipeline processing.

The example in the preceding section (taken from Section 3.5.2) is of a bright globular cluster where the counts in the calibrated image extend beyond 100,000 electrons per pixel. The sky values calculated by **MultiDrizzle** in the pipeline are about 97 electrons, and inspection of the

pipeline DRZ image product reveals that this is apparently an overestimate, since the background in the DRZ image clearly has a net negative offset

Therefore, **MultiDrizzle** can be run off-line, in this case to limit the range of initial pixel intensity values used in computing the sky, and also to tighten up the sigma-clipping iterations. First, the 'imhist' command is used to examine the distribution of pixel intensity values on the FLT file (see Figure 4.8), and an upper limit of 500 electrons is chosen - high enough to be well above the sky value, but much lower than the counts in the stars. Next, **MultiDrizzle** is re-run:

```
pyraf> multidrizzle j8bt07*flt.fits output=example4a skystat=mode
skylower=-100 skyupper=500 skyclip=5 skylsigma=3 skyusigma=3
static- skysub+ driz_separate- median- blot- driz_cr-
driz_combine+
```

This produces sky values of the order of 60-70 counts, thus the background in the final drizzled image is less negative than before, but it is still negative indicating that the sky is still being somewhat overestimated. At this point, the best solution is for the user to measure the sky independently, and provide this as a value to **MultiDrizzle**. Displaying the image (Figure 4.9) shows that scattered light from the bright stars is very strong across the entire image.

Figure 4.8: Histogram of pixel intensity values in the calibrated science data of j8bt07oyq\_flt.fits, which is dominated by scattered light from bright stars, introducing a significant bright skew to the distribution of pixel intensities near the background, thereby strongly affecting any automated estimate of the background.

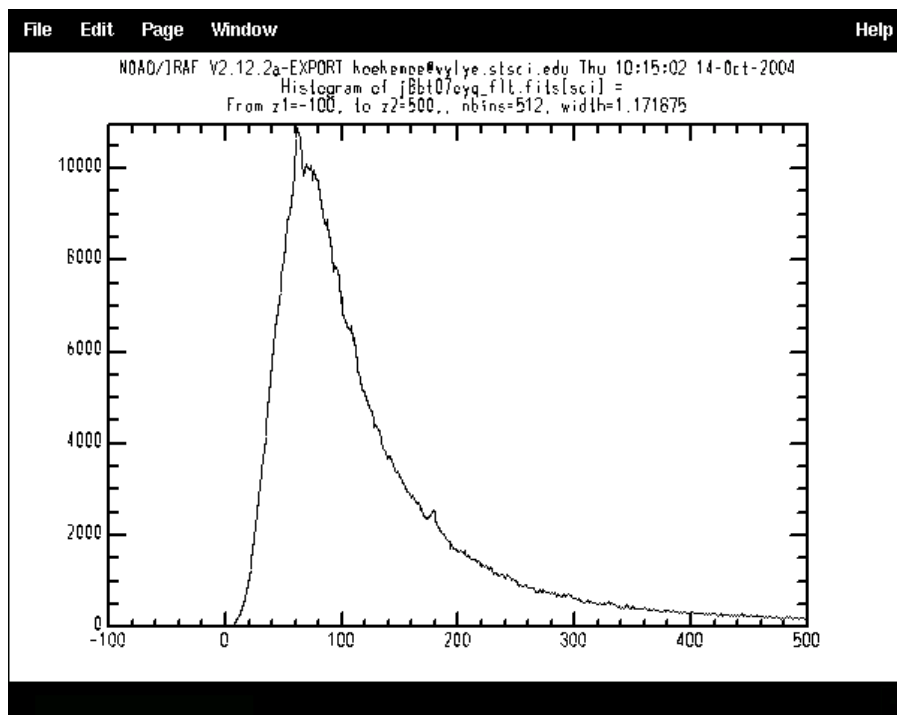
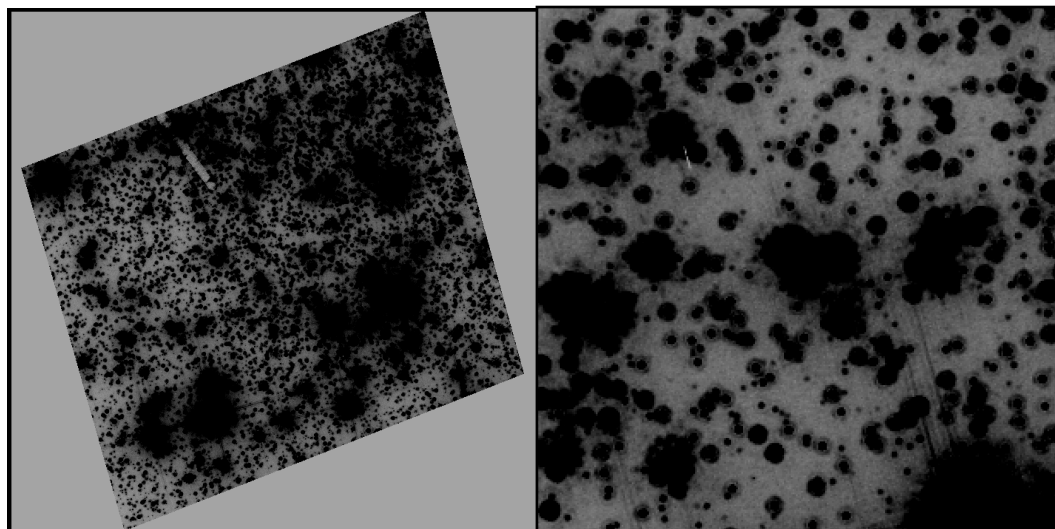


Figure 4.9: Demonstration of the impact of scattered light from bright sources in a crowded field on the accuracy of background determination. In this example, all pixels in the image are affected to some measurable degree by scattered light, so the least affected regions need to be selected manually after visual inspection.



Therefore, we use `imstat` to measure the background values in a few manually selected regions that are less affected:

```
pyraf> imstat j8bt07oyq_flt.fits[sci][45:60,795:810]
pyraf> imstat j8bt07oyq_flt.fits[sci][300:315,700:720]
pyraf> imstat j8bt07oyq_flt.fits[sci][675:700,50:65]
pyraf> imstat j8bt07ozq_flt.fits[sci][45:60,795:810]
pyraf> imstat j8bt07ozq_flt.fits[sci][300:315,700:720]
pyraf> imstat j8bt07ozq_flt.fits[sci][675:700,50:65]
```

In this particular case, we find average values of 31.11 for `j8bt07oyq_flt.fits` and 31.77 for `j8bt07ozq_flt.fits`, based on these manually selected regions. Therefore, we add these to the headers as new keywords (arbitrary called 'NEWSKY'), and then re-run **MultiDrizzle**. Note that the new keywords for the sky background must go into the **image primary header [0]**, not the individual science exposure headers.

```
pyraf> hedit j8bt07oyq_flt.fits[0] 'NEWSKY' 31.11 update+ ver-
pyraf> hedit j8bt07ozq_flt.fits[0] 'NEWSKY' 31.77 update+ ver-
pyraf> multidrizzle j8bt07*flt.fits output=example4b
skyuser='NEWSKY' static- skysub+ driz_separate- median- blot-
driz_cr- driz_combine+
```

Indeed, this finally yields a drizzled image where the background pixels no longer appear to have a net negative offset. Of course, it should be kept in mind that if the background of a field is this strongly affected by the

bright sources within it, then the purpose of the background measurement is primarily to ensure that there are no more varying offset levels in all the exposures prior to combination, due to sky variations from one exposure to the next; the true background may be difficult or impossible to determine in such cases.

This is also why background subtraction is turned off by default when running **MultiDrizzle** in the pipeline on narrow-band data and UV observations that are "dark" (i.e., have no geocoronal emission in the filter bandpass), since: 1) the sky background through such filters is much lower than through an optical broad-band filter, and (2) such observations are often of extended diffuse emission-line targets whose flux is much higher than the background, thus any automated attempt to measure the background may introduce errors that are larger than the background itself. However, if the user is able to determine an accurate background level in such cases, then the above mechanism may be used to propagate those values directly to **MultiDrizzle**.

Sky subtraction is generally recommended for optimal flagging and removal of CR's, when the sky background is more than a few electrons. However, some science applications may require the sky to not be removed. Thus, the final drizzle step can be performed with no sky subtraction.

---

## 4.6 Refining the Shifts: Manually and with Tweakshifts

The ability of **MultiDrizzle** to properly align dithered observations relies on the accuracy of the header WCS information. Unfortunately, there are times when those WCS values may be slightly inaccurate, resulting in a mis-alignment of the final drizzled product. For example, one might wish to combine observations taken in different visits. If the visits were separated by a substantial time interval, then the telescope probably used different guide stars. Due to limitations in the intrinsic accuracy of the Guide Star Catalog, this can lead to WCS coordinates that differ by up to 1-2" between visits, and up to 1" between visits when using Guide Star Catalog 2. Also when all exposures that one wishes to combine were taken in a single visit, it might still be important to correct for relative shifts between images. Even in two-star fine-guiding mode, thermal effects on the telescope can cause slow drifts that can build up to ~50 mas over a few orbits (or in rarer occasions within a single orbit). This corresponds approximately to 1 WFC pixel or 2 HRC pixels. Such shifts between exposures can degrade image quality and corrupt cosmic-ray rejection when left uncorrected.

By deriving shifts based on the position of objects in the data, the user may refine the shifts computed from the WCS header information to create a precisely-aligned drizzled product. Many observers have developed their

own methods of comparing images and computing offsets. We are also developing an automated script, **Tweakshifts**, to perform these tasks, which is available as a prototype and is summarized in Section 4.6.5. The conventions described here should support the majority of users, making it a simple matter to incorporate shift computations into **MultiDrizzle**.

### 4.6.1 Delta Shifts

A *delta shift* is defined as the residual shift required to align sources, *after* applying the offsets implied by the header WCS. Delta shifts may be determined by separately drizzling images onto a common WCS frame with the same central RA/Dec. This is performed in the ‘*driz\_separate*’ step of **MultiDrizzle** or by setting the **PyDrizzle** parameter ‘single=yes’. Object lists derived for each drizzled image may then be matched and fit to derive a single delta shift for each image.

Delta shifts are defined to be in the ‘input’ frame of reference when the distortion-corrected, drizzled image has the same orientation and scale as the distorted image. Shifts will be in the ‘output’ frame of reference if any rotation or scaling was applied while drizzling. When the shifts are given in the ‘output’ frame of reference, **MultiDrizzle** requires the specification of the reference image to properly account for any orientation and scale changes.

### 4.6.2 Absolute Shifts

An *absolute shift*, on the other hand, is the total shift between two images and includes offsets implied by the header WCS. Absolute shifts may be determined by separately drizzling images to their own unique WCS frame. **MultiDrizzle** will use the header information to optimally place the drizzled image in the frame.

To derive absolute shifts in the ‘input’ frame of reference, each distorted image is drizzled separately, and **MultiDrizzle** uses the unique WCS information from each frame to choose the central RA/Dec, the image orientation and final image size. No additional rotation or scaling is applied while drizzling. (Alternately, the user may catalogue sources in each distorted image and then apply the distortion model to the X/Y positions. The new task TRAN has been developed for the STSDAS DITHER package and will perform coordinate transformations back forth between distorted and undistorted space.

Absolute shifts in the ‘output’ frame of reference may be computed by separately drizzling each distorted image, with the same rotation and scaling, onto a unique WCS frame. Target lists in each drizzled image may then be matched to derive the absolute shifts.

Figure 4.10: Delta Shifts in the 'input' and 'output' frame of reference.

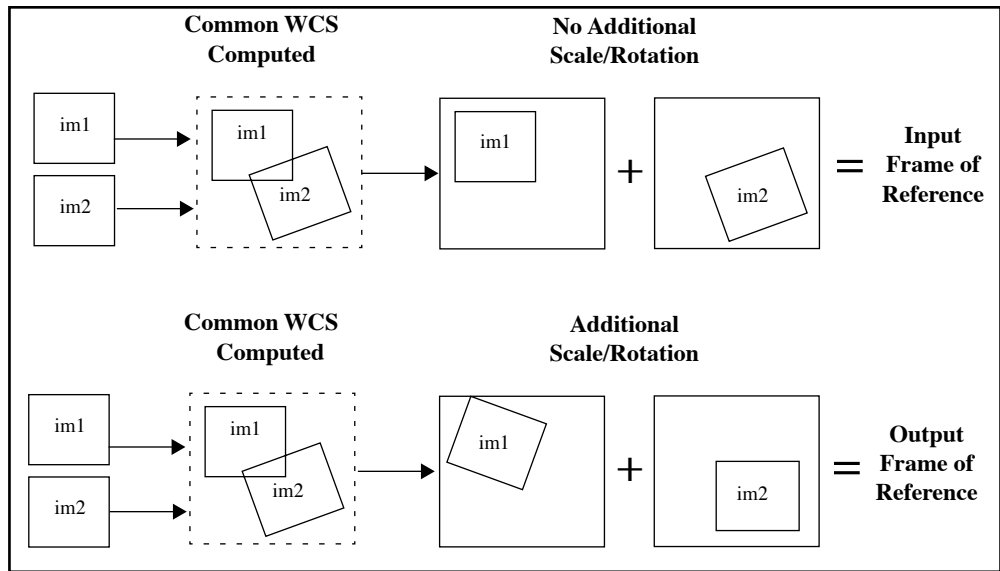
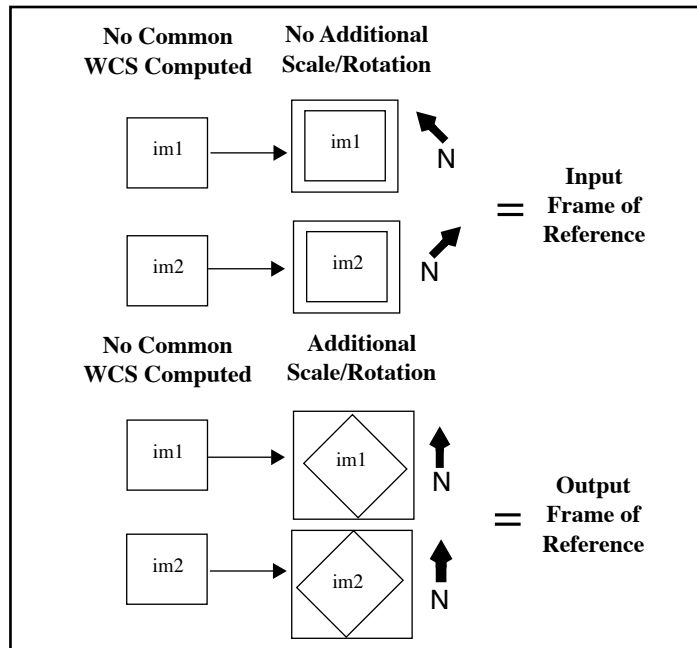


Figure 4.11: Absolute Shifts in the 'input' and 'output' frame of reference. The direction of north is indicated by the bold arrows.



### 4.6.3 Constructing the 'shiffile'

**MultiDrizzle** is capable of interpreting shifts in units of *pixels* or *arcseconds*. A *pixel shift* is the difference in the X/Y pixel position of a source in a given image compared to the reference image. The shifts are interpreted with respect to each image's X/Y pixel reference position and require the specification of 'input' or 'output' frame of reference.

An *arcsecond shift* is the difference in the RA/Dec coordinates of a source in a given image compared to the reference image. Object coordinates must be derived *after* correcting for distortion. These shifts are *not* angular offsets on the sky, rather they are changes in the RA/Dec of the reference pixel and do not require any ‘cos(Dec)’ adjustment. Arcsecond shifts are a natural result of using the RA/Dec coordinates of image sources. They eliminate any ambiguity with the chosen reference frame since RA/Dec coordinates are fixed on the sky. Arcsecond shifts are interpreted as offsets in the direction of increasing RA and Dec.

### Sign Conventions

The shifts are defined in terms of how the targets in the image need to move, rather than on how the telescope would need to move, to allow precise registration. **PyDrizzle** assumes that the shifts were computed as ‘image - reference’. For example, when using **geomap** to cross-correlate two source lists, the reference image coordinates will be in the first two columns and the input image coordinates will be in the last two columns.

### Use of Shifts in Association Tables

The *shift file* is an ASCII file containing the user-computed shifts for a set of images and is used for updating the offsets in the association table. Observers may use either the ASN table delivered by the pipeline or create/modify their own table as described in Section 4.8. **MultiDrizzle** uses the **buildasn** task to incorporate information from the shift file into the association table. The *shift file* uses the following format:

# units: pixels	Values: pixels (default), arcseconds
# frame: input	Values: input (default), output
# form: absolute	Values: absolute (default), delta
# reference: <filename>	Only required when ‘frame = output’
filename1 xshift1 yshift1 [rotation1]	
filename2 xshift2 yshift2 [rotation2]	

The first three lines specify the units, the frame of reference, and the form of the shifts, and only those lines with non-default values are necessary. While the ‘#’ symbol is required, the ‘Values:’ comments are not. When shifts are given in the ‘output’ frame of reference, it is necessary to specify the name of the reference image used.

The following is an example of a shift file in units of pixels, measured in the ‘input’ frame of reference, with the form specified as ‘delta’ shifts. An

x and y shift and a rotation (in degrees) is specified for each dataset. If only a simple shift is required, then the rotation column need not be specified.

```
#units: pixels
#frame: input
#form: delta
j8c0b1skq_flt -2.4 -1.2 -0.002
j8c0b1smq_flt -4.3 -2.3 0.001
j8c0b1sqq_flt -6.9 -3.5 0.003
```

Using this shiftfile as input, the **buildasn** task will update the ASN table as indicated in Table 4.3.

Table 4.3: Association table updated with user-defined shifts.

MEMNAME	MEMTYPE	XOFF- SET	YOFF- SET	XDELTA	YDELTA	ROTATION
j8c0b1skq	EXP-DTH	0	0	-2.4	-1.2	-0.002
j8c0b1smq	EXP-DTH	0	0	-4.3	-2.3	0.001
j8c0b1sqq	EXP-DTH	0	0	-6.9	-3.5	0.003

The shift file can contain shifts for files other than those contained in the ASN table. In that case, only those entries found in the ASN table will be used to update the table. Thus, a single shift file can be generated for a whole set of observations which are represented by multiple association tables.

Association (ASN) tables can support either delta shifts or absolute shifts in units of pixels or arcseconds. Absolute shifts are stored in columns ‘XOFFSET’ and ‘YOFFSET’, while delta shifts are stored in columns ‘XDELTA’ and ‘YDELTA’. The ‘ROTATION’ column is also available if a simple shift does not produce ideal registration and indicates how much should be added to the image’s ORIENTAT to get proper alignment.

If *absolute offsets* are provided in the shift file, **PyDrizzle** will populate the OFFSET columns in the association and fill the DELTA values with zeroes. Similarly, if *delta shifts* are provided, those values will be used to populate the DELTA columns and the OFFSET columns will be zero. If shifts are given in both the OFFSET and DELTA columns, the OFFSET column will be applied and the DELTA columns will be ignored. This convention used by **buildasn** eliminates any ambiguity as to which values are applied to the data. Editing the ASN table directly will then allow the user to further update the offsets using either *delta* or *absolute* shifts.



#### 4.6.4 Example 5: Improving the Image Registration for Different Visits

##### ‘Delta Shifts’ in the ‘Input Frame’

For observations with large dithers or for images which were taken at nominally the same pointing but during different visits, users may wish to fine-tune the image registration, improving on the world coordinate system in the image header. In this case, the images must be separately drizzled and the position of stars cross-correlated. The derived shifts may then be used to update the image association prior to drizzling the final product. More generally, if the drizzle combined product of multiple exposures have PSFs that are not round or as sharp as expected, a likely culprit is the need for improved shifts.

The following example uses WFC observations from separate visits in program 9018: visit 61, exposure 02 (j8c061020\_asn.fits) on 19April 2002 and visit C1, exposure 01 (j8c0c1010\_asn.fits) on 09May2002. Each observation is CR-SPLIT with an exposure time of 45 seconds in F606W. The images are at the same pointing, use the same guide stars, and are at the same ORIENT. We describe the steps required to register the calibrated CRJ products from separate visits. However, the individual FLT files could be alternatively used if improved registration of each CRJ image is desired.

1. First, we use the CRJ images from visits 61 and c1 to create a new association table with the suffix ‘v61c1’. We advise using the **tprint** task to verify the contents of the association.

```
pyraf> import buildasn
pyraf> buildasn f606w_v61c1 suffix='crj.fits'
pyraf> tprint f606w_v61c1_asn.fits
```

#	MEMNAME	MEMTYPE	MEMPRSNT	XOFF	YOFF	XDELTA	YDELTA	ROTATION
j8c061021	EXP-DTH	EXP-DTH	yes	0.	0.	0.	0.	0.
j8c0c1011	EXP-DTH	EXP-DTH	yes	0.	0.	0.	0.	0.
f606w_v61c1	PROD-DTH	PROD-DTH	no	0.	0.	0.	0.	0.

2. Next, we separately drizzle the images onto a common output WCS. This is achieved by setting the **MultiDrizzle** parameter ‘driz\_separate’=yes. Any differences in the aperture RA and Dec, any POS-TARG offsets, or any orientation differences will be automatically accounted for by **MultiDrizzle** which uses the header WCS to transform the images. The drizzled CRJ products are appended with the suffix ‘\_single\_sci.fits’.

```
pyraf> multidrizzle f606w_v61c1_asn.fits static- skysub+
driz_separate=yes driz_sep_bits=96 median- blot- driz_cr-
driz_combine-
```

- Using point sources in each image, we create and cross correlate coordinate lists from each visit. For example, we used **daofind** to create star lists for each DRZ product separately. Then we used **xyxy-match** to match the coordinate lists within a user specified tolerance. Finally, we use **geomap** with the matched coordinate list to compute the transformation required to map the reference coordinate system to the input coordinate system, allowing for a shift and/or rotation. We create the following “shiftfile”, a simple ascii table called ‘shift.txt’, using the derived offsets. The shifts were derived in units of *pixels* and are in the ‘input’ frame of reference since no additional rotation or scale terms were introduced while drizzling. The derived shifts using the above methods are *delta* shifts because the images were drizzled onto a common WCS.

```
#units: pixels
#frame: input
#form: delta
j8c061021_crj    0.00    0.00  0.000
j8c0c1011_crj   24.46   -56.54  0.001
```

- Next, we delete and rebuild the previous association table, this time specifying the derived offsets via the shiftfile. To verify that the association has been correctly populated, we use the **tprint** command. Note that the *delta* shifts appear in the DELTA columns in the association table.

```
pyraf> delete f606w_v61c1_asn.fits
pyraf> buildasn f606w_v61c1 suffix='crj.fits'
shiftfile='shift.txt'
pyraf> tprint f606w_v61c1_asn.fits
# MEMNAME    MEMTYPE    MEMPRSNT    XOFF  YOFF  XDELTA  YDELTA  ROTATION
j8c061021    EXP-DTH    yes         0.    0.    0.      0.      0.
j8c0c1011    EXP-DTH    yes         0.    0.    24.46   -56.54   0.001
f606w_v61c1  PROD-DTH   no          0.    0.    0.      0.      0.
```

- Finally we run **MultiDrizzle** on the new image association. The two CRJ images are combined to create a single DRZ image called ‘f606w\_v61c1\_drz.fits’.

```
pyraf> multidrizzle f606w_v61c1_asn.fits final_bits=96
```

**‘Absolute Shifts’ in the ‘Output Frame’**

As a continuation of the previous example, we illustrate how to specify *absolute* shifts in the ‘output’ frame of reference. For example, this is the case when drizzling an observation to an output orientation of North up.

1. First, the CRJ images from each visit are drizzled to separate output images. Absolute shifts are determined by separately drizzling images onto their own unique WCS frame. In this example, an additional rotation is applied to the drizzled images so that north is oriented up.

```
pyraf> pydrizzle j8c061021_crj.fits output=j8c06102X_drz.fits
bits=96 rotate+ orient=0
pyraf> pydrizzle j8c0c1011_crj.fits output=j8c0c101X_drz.fits
bits=96 rotate+ orient=0
```

2. As in the previous example, we create and cross correlate coordinates lists from each visit using point sources in each image. We create the following “shiftfile”, a simple ascii table called ‘shift1.txt’, using the derived offsets. Note that because we are using absolute shifts, we must specify the name of the reference image.

```
#units: pixels
#frame: output
#form: absolute
#reference: j8c06102X_drz.fits
j8c061021_crj    0.00    0.00    0.000
j8c0c1011_crj  -41.64   45.51    0.001
```

3. Next, we build a new image association using the two CRJ files and the derived shift file.

```
pyraf> import buildasn
pyraf> buildasn f606w_v61c1rot suffix='crj.fits'
shiftfile='shift1.txt'
```

- To verify that the association has been correctly populated, we use the **tprint** command. Notice that the *absolute* shifts have been correctly added to the **OFFSET** columns, not the **DELTA** columns.

```
pyraf> tprint f606w_v61c1rot_asn.fits
# MEMNAME      MEMTYPE  MEMPRSNT  XOFF  YOFF  XDELTA  YDELTA  ROTATION
j8c061021      EXP-DTH   yes       0.    0.    0.    0.    0.
j8c0c1011      EXP-DTH   yes     -41.64 45.51  0.    0.    0.001
f606w_v61c1rot PROD-DTH  no        0.    0.    0.    0.    0.
```

- Finally we run **MultiDrizzle** on the new image association, specifying a rotation such that north is up. The two CRJ images are combined using the updated shift information to create a single DRZ image called 'f606w\_v61c1rot\_drz.fits'.

```
pyraf> multidrizzle f606w_v61c1rot_asn.fits final_bits=96 rotate+
orient=0
```

#### 4.6.5 Tweakshifts

While manually deriving the shifts provides the greatest degree of control and flexibility, the extensive amount of book-keeping required can also make this relatively time-consuming. We are therefore developing a new task, **Tweakshifts**, which is available as a prototype release within Pyraf/STSDAS V3.4 or later (as of November 2005). Not all functional modes of this task are available yet, but it has been tested for basic scenarios, such as the example described here.

**Tweakshifts** can be given several different types of files as input, specified in the same way as for **MultiDrizzle**. In this example we provide it with an association table containing a set of FLT files, although it could also have been a list of FLT files, or an ASCII file containing the names of the FLT files, specified in the same way as for **MultiDrizzle**.

**Tweakshifts** then needs to be told what method to use in determining the shifts, using the **findmode** parameter. It can use essentially two methods: (1) cross-correlation, which would be appropriate for large diffuse targets, very crowded fields, or planetary targets; or (2) cataloging, which is appropriate for less crowded fields, either stellar or extragalactic. Cross-correlation is currently made available on an experimental basis only and will be described more fully in a future update. Cataloging is more generally used, and either SExtractor or DAOfind can be used, the former being more appropriate for extragalactic fields containing mostly extended sources, while the latter is better suited to stellar fields. The parameters to DAOfind are directly accessible from the **Tweakshifts** parameter list, while those for SExtractor are available as the **sextractpars** pset. The

default values for these parameters are chosen to provide useful results in most types of images (more than at least 20 - 30 sources per exposure, preferably 100 or more, and not too many saturated sources). If desired, the cataloging parameters can be adjusted to suit different types of datasets. In this simple example, **Tweakshifts** can be invoked as follows:

```
pyraf> tweakshifts f606w_v61clrot_asn.fits output='shifts.txt'
findmode='catalog' gencatalog='sextractor' fitgeometry='rotate'
```

In this case, the type of shift determination is constrained to measuring x,y shifts and a rotation (fitgeometry='rotate'). Other commonly-used options would consist of 'shift' (measuring only the x,y shifts) and 'rscale' (solving for x,y shifts, rotation, and a uniform scale change in x and y). The behavior of this parameter is the same as in the IRAF task 'geomap'. The shifts that are measured by **Tweakshifts** are stored in two different places:

1. in the association table itself, where the shift and rotation columns are updated to reflect the cumulative shift and rotation if **Tweakshifts** is run multiple times
2. in the output file ('shifts.txt'), which has the same format as described in Section 4.6.3, and contains only the shift values determined in the current run of **Tweakshifts**.

It is almost always desirable to run **Tweakshifts** at least twice, iterating on the shifts. This is simply because, on the second pass, more objects will likely be matched (since the shifts from the first run are being applied), so the resulting shifts will be more accurate, hence different, to those obtained on the first pass. It is worth checking that the shifts on the second pass are generally smaller than those obtained on the first pass, to ensure that more objects are being matched. **Tweakshifts** also produces catalogs of the objects when running in catalog mode, which should be examined and overplotted on the images to ensure that the correct objects are being cross-identified and used to determine the shifts.

When the input files are specified as FLT files, **Tweakshifts** will generate catalogs on the FLT files (in the distorted frame), then remove the distortion using the same algorithms as drizzle when calculating the shifts. It is also possible to provide **Tweakshifts** with an input reference catalog and request that all the images be registered to this catalog. **Tweakshifts** can also be asked to measure shifts for images that are already drizzled, which is often useful when comparing clean combined images of the same target obtained in different orbits or visits.

Since the task is currently available as a prototype, any feedback on its use would be welcomed, by sending email to [help@stsci.edu](mailto:help@stsci.edu). Future improvements will include the ability to directly modify the WCS of the input files (thereby eliminating the need for shiftfiles or ASN table modifications), as well as more generally robust ways to determine shifts.

---

## 4.7 MultiDrizzle Details: Example Application to the Tadpole Galaxy

By default, **MultiDrizzle** uses the world coordinate system (WCS) information in the image headers to align the images. While dithers applied to a target within a single visit of HST are usually accurately reflected by the WCS, this is not the case for multiple visits which normally require guide star re-acquisitions and may utilize different guide stars. Even for nominally back-to-back exposures that are part of a CR-SPLIT association, offsets large enough to degrade final combinations do sometimes occur. As a result, it is essential to accurately determine image-to-image shifts, and possibly rotations, before running **MultiDrizzle**.

These (delta) shifts may be determined by separately drizzling each image onto a common WCS frame. This is performed by the ‘driz\_separate’ task in step 3. Object lists derived for each drizzled image may then be matched and fit to derive a single shift for each image. More details on this topic and a description of the shift file formats are given in Section 4.6.

Once the shifts have been determined, **MultiDrizzle** must be rerun from the beginning with the shift file specified in the ‘shiftfile’ parameter. **MultiDrizzle** will update the association table to reflect these ‘delta’ offsets and will now use both the header WCS information plus the shift file to appropriately align images.

This example describes the combination of six ACS/WFC images of the “Tadpole Galaxy” UGC 10214 which formed part of the ACS Early Release Observations (EROs) from program 8992. These images were acquired in two visits, with a significant shift between visits, as noted by the target RA and Dec, and with small dithers within each visit. The images were taken with the F606W filter and have the exposure times listed in Table 4.4. Prior to attempting this example, we assume that users have worked through the examples in the previous sections and are familiar with using association tables and shift files.

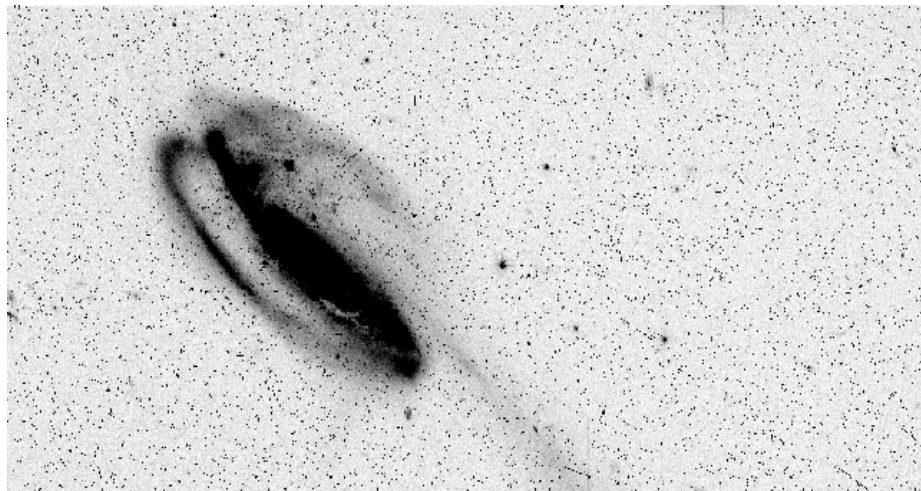
The ERO images are available from the HST archive for anyone wishing to repeat this example. A new capability has been developed in the StarView archive interface, allowing the user to request FLT files only. The FLT files are the output from **CALACS** and have been corrected for bias, dark current and flat fielding. They are not corrected for distortion and still contain numerous cosmic rays. They form the input for **MultiDrizzle**.

Figure 4.12 shows chip 1 for one of these FLT files, j8cw54ovq\_flt[sci,2], which still contains numerous cosmic ray events, hot pixels, and other artifacts. The rectangular, rather than ‘rhombus’ shaped image is a clear indicator that the geometric distortion has not yet been corrected.

Table 4.4: ERO datasets used in the accompanying **MultiDrizzle** example. The two sets of images were taken at different epochs and have a significant shift between epochs. Within a given epoch, small POS-TARG offsets are specified in accordance with the ACS-WFC-DITHER-LINE pattern which spans the WFC interchip gap.

Dataset	Date-Obs	RA (deg), Dec (deg)	POS-TARG1	POS-TARG2	Exposure Time (sec)
j8cw04abq_fit	01 Apr 2002	241.553625,+55.431094	0.000	0.000	150.0
j8cw04c2q_fit	01 Apr 2002		0.248	3.001	580.0
j8cw04c7q_fit	01 Apr 2002		0.248	3.001	840.0
j8cw54oiq_fit	09 Apr 2002	241.537833,+55.427594	0.000	0.000	150.0
j8cw54orq_fit	09 Apr 2002		0.248	3.001	580.0
j8cw54ovq_fit	09 Apr 2002		0.248	3.001	840.0

Figure 4.12: A single, calibrated FLT file, `j8cw54orq_fit.fits[sci,2]`, which still contains numerous cosmic rays, hot pixels, and other artifacts.



First, the appropriate calibrated FLT files and the geometric distortion reference table (IDCTAB) should be placed on the user's local disk. Next the 'jref' directory should be defined, PyRAF started, and the **dither** package loaded. To run **MultiDrizzle**, the parameters may be edited in the standard way using the "epar" facility.

The **MultiDrizzle** software has an extensive set of parameters, but the default values should allow the task to process nearly any set of images for an initial review. The parameters are separated according to the processing step they control, making it easier to interpret them.

In this example, we describe the parameters for each step in succession, though in practice, the user would set all relevant parameters at once. While the majority of relevant parameters are discussed here, a help document

describing all parameters and tasks can be accessed by typing ‘help multidrizzle’ from within PyRAF.

The only required parameter is the rootname for the ‘output’ drizzled product. By default, **MultiDrizzle** will look for all files in the working directory with the FLT extension. The user may modify the ‘suffix’ parameter to include some other extension or may specify a subset of images via the ‘filelist’ parameter. Using the images specified, **MultiDrizzle** calls **PyDrizzle** which uses the ‘**buildAsn**’ task (see Section 4.8) to create an association table named ‘output\_asn.fits’. This association will be used to define the data set. The header WCS information from the entire set is used to define a common WCS output frame, and **MultiDrizzle** sets the **drizzle** parameters appropriately. If user defined shifts are available, these may be specified in the ‘shiftfile’ parameter, and the association table will be updated accordingly. However, a shift file is not usually available until after step 3, separately drizzling the images onto a common WCS, has been performed and objects matched.

### Initial Setup

Parameters	Default	Description
input		List of input files
output		List of input filesRootname for output drizzled products
refimage		Reference image with desired output WCS
runfile	multi.run	File for logging the script commands
restart		Parameter allowing processing to resume at a given step
coeffs	header	Use header-based distortion coefficients? (header, none)
context	no	Create context image during final drizzle?
clean	no	Remove temporary files?
section		Extension or group to be drizzled
driz_sep_bits	0	Integer mask bit values considered good (sep. drizzle)
driz_final_bits		Integer mask bit values considered good (final drizzle)
ra		right ascension output frame center
dec		declination output frame center
build	yes	Create multi-extension output file?
shiftfile		Shift file for improving WCS registration

A reference image which has the desired output WCS may be specified, and the input images will be drizzled to match the WCS of this image. Alternately, the central RA and Dec (ra, dec) of the reference pixel and the dimensions of the output frame (outnx, outny) may be specified, if desired,



though reasonable values will be automatically determined from the images' WCS if these parameters are left blank. While the central RA and Dec are specified in the initial setup parameters listed above, the output image dimensions are specified in both the 'driz\_separate' and 'driz\_combine' parameters in steps 3 and 7, respectively.

The 'bits' parameter is defined as the integer sum of all bit values from the input images' DQ array that should be considered 'good' when building the weighting mask. Because **MultiDrizzle** was designed for use with multiple instruments, the default value is set to zero. For ACS data, the recommended default value is 8578. (For more information on selecting the appropriate bits for your data, refer to Section 4.4.3.) Information from the DQ array for each chip is used in combination with the 'bits' parameter to create temporary mask files called '\*\_inmask?.fits'. Pixels which were flagged in the DQ array *and* which were not specified as good via the bits parameter are assigned the value 0. All other pixels are set to 1 in the mask.

The distortion reference file is read from the image header via the IDCTAB keyword which specifies the name and location of the appropriate file. The distortion coefficients for each chip are written to temporary ascii files named '\*\_coeffs?.dat'. If the user wishes to retain these files, the parameter 'clean' should be set to 'no'.

In general, the default **MultiDrizzle** parameters will work well for most data. When setting up the Tadpole images, for example, we have specified *only* the following non-default parameters: output='example', 'bits=8578', 'combine\_nhigh=2', and 'driz\_cr\_snr=4.0 3.0'. The choice of these last two parameters is explained in the sections that follow. In default mode, **MultiDrizzle** performs each of its 7 steps in order. In this example, however, we perform some of the steps and examine the intermediate products before final drizzle combination is performed. Approximately 5GB of free disk space is required for this example when intermediate products are not removed. An outline of the entire process is described below:

1. Run only steps 1 through 3 to create sky-subtracted, separately drizzled images which are based on a common WCS.

```
pyraf> multidrizzle *_flt.fits output='example'
driz_sep_bits=8578 static+ skysub+ driz_separate+ median- blot-
driz_cr- driz_comb-
```

2. Measure the positions of stars in the separately drizzled images and derive a shift file which defines the residual offsets.

- Rerun step 3 using the derived ‘shiftfile’ to create new separately drizzled images. Also turn on step 4 to create a well-aligned median image.

```
pyraf> multidrizzle *_flt.fits output='example'
driz_sep_bits=8578 shiftfile='shifts' static- skysub-
driz_separate+ median+ combine_nhigh=2 blot- driz_cr- driz_comb-
```

- Examine the median image to ensure that the PSF is ‘round’ and ‘narrow’ and that cosmic-rays and other artifacts are appropriately rejected.
- Run steps 5 through 7 to transform the median image back to the reference frame of each of the original input images and to derive cosmic ray masks. Using these new masks, perform the final drizzle combination.

```
pyraf> multidrizzle *_flt.fits output='example'
driz_sep_bits=8578 final_bits=8578 shiftfile='shifts' static-
skysub- driz_sep- median- blot+ driz_cr+ driz_cr_snr='4.0 3.0'
driz_comb+
```

Once the optimal set of parameters and the optional shift file is derived, as described in the outline above, **MultiDrizzle** may be executed in a single pass by turning all steps on and by specifying any desired non-default parameters:

```
pyraf> multidrizzle output='example' driz_sep_bits=8578
final_bits=8578 shiftfile='shifts' static+ skysub+ driz_sep+
median+ combine_nhigh=2 blot+ driz_cr+ driz_cr_snr='4.0 3.0'
driz_comb+
```

While **MultiDrizzle** may be executed from the command line, as shown in the above examples, it may also be run from the ‘epar’ facility which allows the user to see all parameters at once and to turn particular steps on and off. We recommend that beginners use the ‘epar facility’ to become familiar with all steps and parameters before running **MultiDrizzle** from the command line.

## 1. Creating the ‘Static’ Bad-Pixel Mask

Parameters	Default	Description
static	yes	Create static bad-pixel mask from data?
staticfile		Name of (optional) input static bad-pixel mask
static_sig	4.0	Sigma*rms below mode to clip for static mask
<b>Output Files</b>	Modified DQ arrays in the original input files	

When ‘static=yes’, this step goes through each of the input images, calculates the rms value for each chip, and identifies pixels that are below the median value by more than ‘static\_sig’ times the rms. It is aimed at identifying pixels that may have high values in the dark frame, which is subtracted during calibration, but may not necessarily have high values in the images, and thus subtraction gives them strongly negative values. Such pixels are not always flagged in the DQ file, and this step allows them to be identified. Sometimes such pixels fall on bright objects so instead of being negative, they would be positive but lower than surrounding pixels. If the images are dithered, then they should land on blank sky at least some of the time, in which case they will appear negative and will be flagged.

For the Tadpole Example, we have left the ‘StaticMask’ parameters to their default values. After this step is performed, the image DQ arrays are updated with the static mask, and new flagged pixels are set with bit 4096. The ‘\*\_inmask?.fits’ files are subsequently updated during further processing.

## 2. Performing Sky Subtraction

Parameters	Default	Description
skysub	yes	Perform sky subtraction?
skywidth	0.1	Bin width for sampling sky statistics (in sigma)
skystat	“median”	Sky correction statistics parameter (median, mode, mean)
skylower	INDEF	Lower limit of usable data for sky (always in electrons)
skyupper	INDEF	Upper limit of usable data for sky (always in electrons)
skyclip	5	Number of clipping iterations
skylsigma	4.0	Lower side clipping factor (in sigma)
skysigma	4.0	Upper side clipping factor (in sigma)
skyuser		KEYWORD for sky subtraction value if done by user

When ‘skysub=yes’, this task will subtract the sky from each input exposure. Two important parameters to consider are the upper and lower values for data that will be used to estimate the sky value. These should be set to include most pixels in the sky (so substantially more than the FWHM of the sky distribution) but not so large as to include a substantial amount of power from objects or cosmic rays.

The ‘SkySub’ task will update the header keyword defined by the parameter ‘skyname’ with the derived sky value for each chip and will subtract the sky from the original exposures prior to the final drizzle combination. Note that the FLT images themselves are not modified when **MultiDrizzle** completes, although the sky value is stored in the images headers as the MDRIZSKY keyword. Sky subtraction is recommended for effective cosmic-ray flagging and removal, but only if sufficient blank sky is available to perform an accurate determination.

Great care must be taken when choosing to implement sky subtraction, because if sufficiently blank sky is not available, sky subtraction will produce erroneous results. In the case of the Tadpole images, adequate blank sky is available for each WFC chip to allow an accurate sky determination. The sky is calculated independently for the two chips, and the lowest value is taken to represent the sky on both detectors. Since the bright emission from the Tadpole generally only dominates one of the chips, the sky value from the other chip is used for both, with satisfactory results.

### 3. Drizzling to Separate Output Images

Parameters	Default	Description
driz_separate	yes	Drizzle to separate output images?
driz_sep_outnx		Size of x-axis for separate output frame
driz_sep_outny		Size of y-axis for separate output frame
driz_sep_kernel	“turbo”	Shape of kernel function (square, point, gaussian, turbo, tophat, lanczos3)
driz_sep_wt_scl	exptime	Weighting factor for input data image
driz_sep_scale	INDEF	Linear size of output pixels (relative to input)
driz_sep_pixfrac	1.0	Linear size of drop in input pixels
driz_sep_rot	INDEF	Rotation of input image to be applied (degrees anti-clockwise)
driz_sep_fillval	INDEF	Value assigned to undefined output pixels
driz_sep_bits	0	DQ mask bit values that are to be considered good
<b>Output Files</b>	Images= ‘*_single_sci.fits’, ‘*_single_wht.fits’	

When ‘driz\_separate=yes’, the input images are corrected for geometric distortion and drizzled onto separate output frames which have a common WCS. Any shifts, rotations, or scale changes are calculated from the image headers. The output image dimensions are calculated on-the-fly and the pixel scale is taken from the column ‘scale’ from the IDCTAB, where the default values are  $0.05 \text{ arcsec/pix}$  for the WFC and  $0.025 \text{ arcsec/pix}$  for the HRC. The drizzled images are in units of *electrons/sec*.

By default, this step uses the ‘turbo’ drizzle kernel, ‘pixfrac=1’, and an output scale equal to the input scale. For more information on setting these parameters, refer to the [HST Dither Handbook](#) (Koekemoer et al. 2002). These parameters can be changed; for example, masks can be substantially improved by specifying a smaller value of scale (e.g., 0.5 or 0.66), with the primary trade-off being much larger images (their size increases as the inverse square of the value of ‘scale’) and increased computation time.

In the Tadpole example, we have left the ‘driz\_separate’ parameters to their default values. While the final drizzled image would contain 3 extensions in a single file (the science, weight, and context images), the ‘driz\_separate’ products are separate science and weight images named ‘\*\_single\_sci.fits’ and ‘\*\_single\_wht.fits’. No context image is created.

One of the singly drizzled FLT images, ‘j8cw54ovq\_ft\_single\_sci.fits’, is shown in Figure 4.13. This image still contains numerous cosmic ray events, hot pixels, and other artifacts. The ‘rhombus’ shape is a result of correcting the geometric distortion. The corresponding weight image,

‘j8cw54ovqflt\_single\_wht.fits’, is shown in Figure 4.14, where white indicates pixels with zero weight. Due to the effects of distortion and varying pixel area in the FLT images, the weight image changes gradually across the detector. Because the association table was used to define a common WCS for all images, the drizzled image is ‘padded’ with zeros outside the boundary of the original array. The weight image is set to zero in these regions, allowing these pixels to be rejected during median combination.

The separately drizzled science images may be used to improve the image registration prior to final drizzle combination. In this example, the images form two groups of three. While the WCS information for images within a single group (visit) are adequate to align them, there is a small residual offset between visits. Shifts which are determined from separately drizzling images onto a common WCS are by definition ‘delta’ shifts (see Section 4.6 for details), and will be applied in addition to any offsets from the WCS when a ‘shiftfile’ is provided. Because no additional scale or rotation was applied to the singly drizzled images, the shifts are in the ‘input’ frame of reference.

In this example, unsaturated stars in the short exposures (j8cw04abq and j8cw54oiq) were used to derive the offsets between the two groups of images. Shifts were measured to the nearest 0.1 pixel and are listed below in the form of a shift file. Refined shifts within a given visit may also be determined, but these are typically less than a tenth of a pixel, and accuracy at this level is not as critical for extended sources as it may be for point sources.

```
#units: pixels
#frame: input
#form: delta
j8cw04abqflt 0.0 0.0
j8cw04c2qflt 0.0 0.0
j8cw04c7qflt 0.0 0.0
j8cw54oiqflt -5.6 -0.3
j8cw54orqflt -5.6 -0.3
j8cw54ovqflt -5.6 -0.3
```

When the ‘driz\_separate’ step is run for the second time, but with a ‘shiftfile’ specified, the association table for the data set will be automatically updated. To confirm that the new separately drizzled images are appropriately registered, the position of stars should again be examined. It is also useful to create a median image and examine the width and shape of the PSF over the entire FOV to look for any effects of mis-registration. Median combination is performed in Step 4 of **MultiDrizzle**.

Figure 4.13: The singly drizzled FLT image 'j8cw54ovq\_fit\_single\_sci.fits' from the **MultiDrizzle** example.

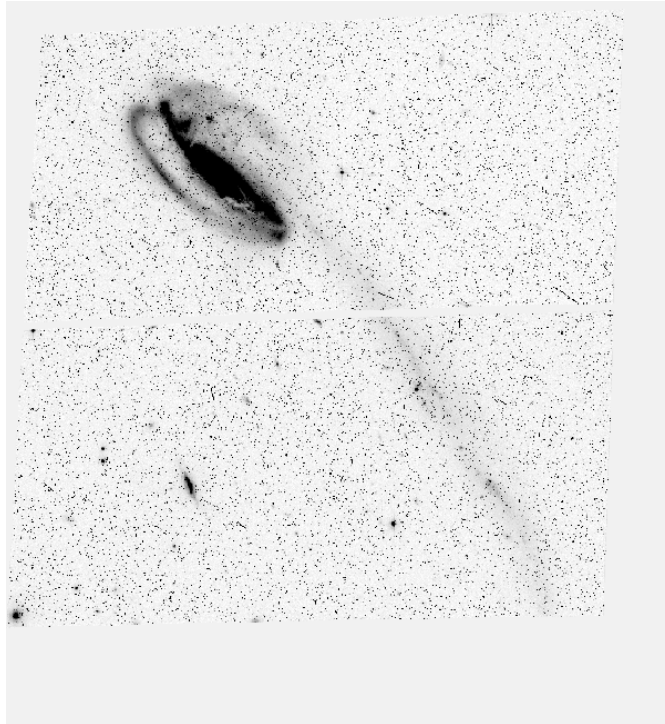
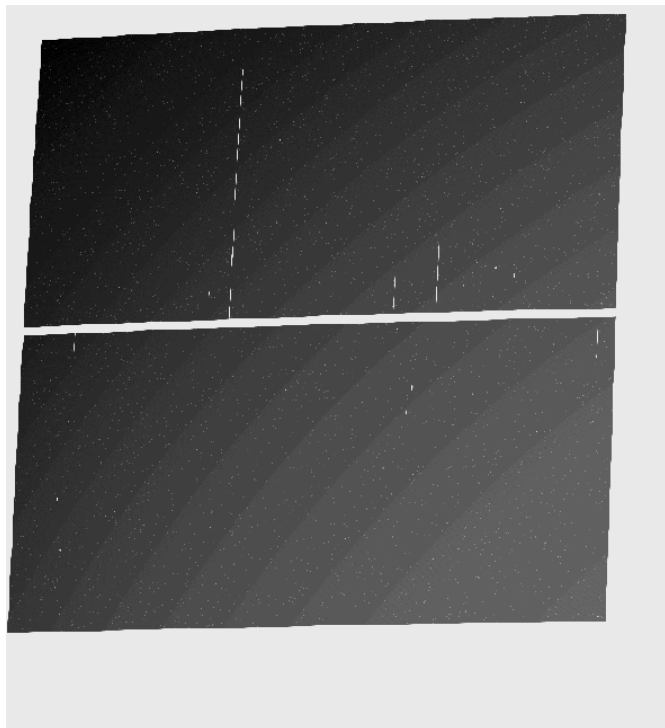


Figure 4.14: The weight image 'j8cw54ovq\_fit\_single\_wht.fits' corresponding to the singly drizzled image in Figure 4.13 where white indicates zero weight.



## 4. Creating the Median Image

Parameters	Default	Description
median	yes	Create median image?
median_newmasks	yes	Create new masks when doing the median?
combine_type	“minmed”	Type of combine operation (average, median, sum, minmed)
combine_nsigma	4 3	Significance for accepting min instead of median
combine_nlow	0	minmax: Number of low pixels to reject
combine_nhigh	1	minmax: Number of high pixels to reject
combine_lthresh	INDEF	Lower threshold for clipping input pixels
combine_hthresh	INDEF	Upper threshold for clipping input pixels
combine_grow	1.0	Radius (pixels) for neighbor rejection
<b>Output Files</b>	Images= ‘output_med.fits’	

When ‘median=yes’, this step creates a median image from the separate drizzled input images, allowing a variety of combination and rejection schemes. If ‘combine\_type’ is set to ‘median’ or ‘average’, then the routine carries out a similar calculation to the standard IRAF task **imcombine**, with equivalent behavior for the parameters ‘combine\_nlow’ and ‘combine\_nhigh’ (the number of low and high pixels to reject), and ‘combine\_grow’ (the amount by which flagged pixels can grow). All **imcombine** parameters other than those specified above are reset to their default values.

If ‘combine\_type=minmed’, a more sophisticated algorithm is used to combine images. The basic concept is that each pixel in the output combined image will be either the median or the minimum of the input pixel values, depending on whether the median is above the minimum by more than  $n$  times sigma. An estimate of the “true” counts is obtained from the median image (after rejecting the highest-valued pixel), while the minimum is actually the minimum unmasked (“good”) pixel. This algorithm is designed to perform optimally in the case of combining only a few images (3 or 4), where triple-incidence cosmic rays often pose a serious problem for more simplified median combination strategies. The ‘minmed’ algorithm performs the following steps:

1. Create median image, rejecting the highest pixel and applying masks.
2. Use this median to estimate the true counts, and thus derive an rms.
3. If the median is above the lowest pixel value by less than the first value in ‘combine\_nsigma’, then use the median value, otherwise use the lowest value.



4. If 'combine\_grow' > 0, repeat the above 3 steps for all pixels around those that have already been chosen as the minimum, this time using a lower significance threshold specified as the second value in 'combine\_nsigma'.

The last step is very successful at flagging the lower signal-to-noise “halos” around bright cosmic rays which were flagged in the first pass.

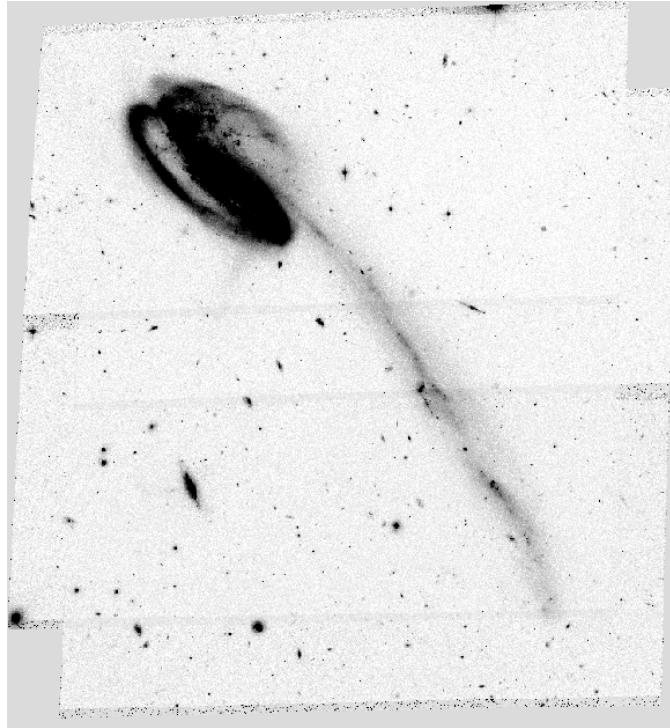
If 'median\_newmasks=yes', then the singly drizzled weight maps (\*\_single\_wht.fits) are used to create pixel masks for each image, based on the pixel flag information originally present in the DQ arrays. These masks will then be used when combining images, in order to prevent bad pixels from adversely affecting the median.

If 'median\_newmasks=no', this task will use whatever masks are specified by the user (and which are created offline) in the 'BPM' header keyword of each image. In general, however, it is recommended that the pixel masks which are generated by default are used instead.

Selecting the best parameters for the median step can be an iterative process and should always involve examination of the clean, combined product to verify that the majority of cosmic-rays and other artifacts are successfully removed. The rejection algorithm which is ultimately chosen depends largely on the number of datasets being combined and the amount of overlap between dithered images.

In this example, we have chosen the default parameters 'combine\_type=median', 'combine\_reject=minmax', 'combine\_nlow=0'. Instead of the default value, we have set 'combine\_nhigh=2' so that hot pixels are rejected in the outer portions of the image, which have only 3 input images contributing to the median calculation, and for which 2 of the 3 images are at the same dither position. Thus, at least 1 valid pixel is retained in the outer portion of the median image. In the central regions of the image, six images have contributed to the median, but two high images are rejected, so up to 4 valid pixels would be retained. The six separately drizzled images are combined using the bad pixel masks and the rejection parameters specified above to create a single clean median image named 'example\_med.fits'. This median image is shown in Figure 4.15.

Figure 4.15: The cleaned median image created using the 6 separately drizzled Tadpole images and their bad pixel masks.



## 5. Blotting Back the Median Image

Parameters	Default	Description
blot	yes	Blot the median back to the input frame?
blot_interp	poly5	Interpolant (nearest,linear,poly3,poly5,sinc)
blot_sinscl	1.0	Scale if sinc kernel is used (ignored otherwise)
<b>Output Files</b>	Images= '*_sci?_bl.fits'	

When 'blot=yes', this task takes the median image and uses the Pyraf **blot** task to apply the geometric distortion and to transform ('reverse drizzle') it back to the reference frame of each of the original individual input images. This involves reversing the shifts and reapplying the geometric distortion that had been removed in step 3. In addition, the median image is resampled to the pixel scale of the original images and is trimmed to match the dimensions of each input image. This step is done in preparation for subsequent cosmic-ray rejection in step 6. The blotted frames are named '\*\_sci?\_bl.fits'.

If desired, the user may wish to display the input images and blink them with their 'blotted' counterparts. The 'blotted' images should align perfectly with their respective input images and should be reasonably

similar in appearance, except for the fact that they should be cleaned of cosmic rays and other defects.

## 6. Creating Cosmic Ray Masks

Parameters	Default	Description
driz_cr	yes	Perform CR rejection with deriv and driz_cr?
driz_cr_corr		Create CR cleaned _cor file and a _crmask file?
driz_cr_snr	"3.5 3.0"	Driz_cr.SNR parameter
driz_cr_grow	1	Pixel width to 'grow' around CRs for 2nd pass
driz_cr_ctegrow	0	Length to convolve in CTE direction for 2nd pass
driz_cr_scale	"1.2 0.7"	Driz_cr.scale parameter
<b>Output Files</b>	Images= '*_sci?_blt_deriv.fits', '*sci?.fits', '*_sci?_crderiv.pl', '*_sci?_cor.fits'	

When 'driz\_cr=yes', this step uses the original input images, the blotted median images, and the derivative of the blotted images (which it creates using the **deriv** task) to create a cosmic ray mask for each input image (using the **driz\_cr** task).

First, the **deriv** task uses the blotted median images ('\*\_sci?\_bl.fits') from step 5 to calculate the absolute value of the difference between each pixel and its four surrounding neighbors. For each pixel, the largest of these four values is saved in an output image, '\*\_sci?\_bl\_deriv.fits', which represents an effective gradient or spatial derivative.

These derivative images are used by the task **driz\_cr** when comparing the original and blotted images. First, the original FLT images for each chip are copied to files named '\*\_sci?.fits' which are the required input for the **driz\_cr** task. These images are compared with the corresponding blotted median image '\*\_sci?\_bl.fits' and its absolute derivative '\*\_sci?\_bl\_deriv.fits' to create a mask of cosmic rays (and other blemishes, like satellite trails). Where the difference is larger than can be explained by noise statistics, or the flattening effect of taking the median, or perhaps an error in the shift (the latter two effects are estimated using the image derivative), the suspect pixel is masked. Cosmic rays are flagged using the following rule:

$$|data\_image - blotted\_image| > scale * deriv\_image + SNR * noise$$

where 'scale' is the user supplied **driz\_cr** parameter listed above and is defined as the multiplication factor applied to the derivative before determining if the difference between the data image and the blotted image is sufficiently great to require masking. 'Noise' is calculated using a combination of the detector read noise and the poisson noise of the blotted median image plus the sky background.

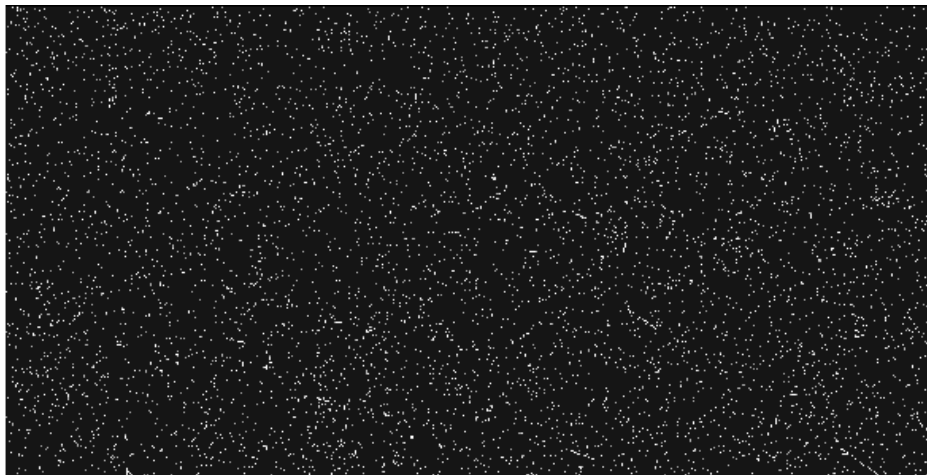
The user must specify a cut-off signal-to-noise (SNR) value for determining whether a pixel should be masked. Actually, two cut-off signal-to-noise ratios are needed, one for detecting the primary cosmic ray, and a second for masking lower-level bad pixels adjacent to those found in the first pass. After the first pass through the image, the procedure is thus repeated on pixels that are adjacent to previously masked pixels using a lower SNR threshold, since cosmic rays often extend across several pixels.

A second-pass CR rejection can be carried out in a larger region ‘grown’ around the CRs initially identified (using the ‘driz\_cr\_grow’ parameter). The second-pass iteration can also be done along the CTE direction by convolving the CR mask with the ‘driz\_cr\_ctegrow’ parameter; 10 - 20 pixels yields good results for removing faint CTE trails from CRs.

The final cosmic ray mask is stored in the DQ array of the original input FLT files, using the value specified for the ‘crbit’ parameter; if this left blank then a default value of 4096 is used. One of the resulting masks for chip 1 is shown in Figure 4.16 and should be blinked with the original image `j8cw54orq_ft[sci,2]` from Figure 4.12 (or the equivalent `j8cw54orq_ft_sci2.fits` file) to visually ascertain that all cosmic rays were flagged. If it appears that the central pixels of some stars were unnecessarily masked, the ‘driz\_cr\_scale’ parameter should be increased. If not enough cosmic rays were masked out, this parameter should be decreased. In this example, the default ‘driz\_cr\_snr’ values “3.0 2.5” were too stringent and resulted in flagging the centers of stars and the core of the Tadpole galaxy. Instead, we have increased the default SNR values to “4.0 3.0” to create ideal cosmic ray masks for this data set.

The **driz\_cr** task can also create a ‘\*\_sci?\_cor.fits’ image, where flagged pixels are replaced with pixels from the blotted median image. The cosmic ray mask files are then multiplied by the bad pixel masks (which are a combination of the image DQ array and the static masks) to create a final CR mask for each input image, stored in the DQ array of the FLT files (default bit 4096), which will be used during final drizzle combination.

Figure 4.16: A single cosmic ray mask ‘j8cw54orq\_ft\_sci2\_crderiv.pl’. This mask should be blinked with the original image ‘j8cw54orq\_ft[sci,2]’ from Figure 4.12 or the equivalent ‘j8cw54orq\_ft\_sci2.fits’ output file to assure that optimal parameters were chosen in the **driz\_cr** task.



## 7. Performing the Final Drizzle Combination

Parameters	Default	Description
driz_combine	yes	Perform final drizzle image combination?
final_wht_type		EXP
final_outnx		Size of FINAL output frame x-axis
final_outny		Size of FINAL output frame y-axis
final_kernel	“square”	Shape of kernel function (square, point, gaussian, turbo, tophat, lanczos3)
final_scale	1.0	Linear size of output pixels (relative to input)
final_pixfrac	1.0	Linear size of drop in input pixels
final_rot	INDEF	Rotation of input image to be applied (degrees anti-clockwise)
final_fillval	INDEF	Value given to undefined output pixels
final_bits	0	DQ mask bit values to be considered good
<b>Output Files</b>	Images= output_drz.fits (multi-extension)	

When ‘driz\_combine=yes’, this step takes the original input images, together with the final cosmic ray masks, and drizzles them all onto a single output image. The standard **drizzle** parameters kernel, scale, pixfrac, and rot can be specified by the user, if desired. By default the scale of the output image is 1.0, but the user is encouraged to experiment with other options (e.g. scale=0.5 and pixfrac=0.7 yields a sharper output PSF).

When the following initial setup parameters are set: ‘build=yes’ (default) and ‘context=yes’ (non-default), the final **MultiDrizzle** output image will be a single multi-extension FITS file named ‘example\_drz.fits’. This file contains the science image in extension 1, the weight image in extension 2, and the context image in extension 3. When ‘build=no’, these files will be written to separate output files. When the default value ‘context=no’ is used, no context image is created.

The first extension of the drizzled product contains the science (SCI) image which is corrected for distortion and which is dither-combined (or mosaiced), if applicable. The drizzled SCI image derived from the Tadpole example is presented in Figure 4.17 and is in units of *electrons/sec*. All pixels have equal area on the sky and equal photometric normalization across the field of view, giving an image which is both photometrically and astrometrically accurate for both point and extended sources. The dimensions of the output image are computed on-the-fly by **MultiDrizzle** and the default output plate scale is read from the ‘scale’ column in the

IDCTAB. These parameters, however, may be chosen by the user to best suit the actual data.

The second extension of the output image contains the weight (WHT) image. This image gives the relative weight of the output pixels and, in standard processing using the **MultiDrizzle** defaults, it can be considered an effective exposure time map, if the default value of 'final\_wht\_type' is set to 'EXP'. The weight image from the example is shown in Figure 4.18, where darker areas have higher weight. The chip edges and gaps are clearly visible, as are column defects and cosmic ray features. The bulk of the image is “dark gray” corresponding to the overlap of all six inputs. In this area the weight value is  $\sim 3140$ , equal to the sum of the exposure times of the six images which contribute. There is also a smooth variation across the image due to the variation of the pixel area on the sky caused by the distortion.

The output weight image can also be specified to be in units of inverse variance, calculated using the error arrays initially present in the FLT file, by setting 'final\_wht\_type' = 'ERR'. This would include all sources of error, including read-noise, dark current, as well as the background sky and all the object photons. Finally, if 'final\_wht\_type' = 'IVM', then **MultiDrizzle** will look for inverse variance files provided by the user (for example, to include all sources of noise except those related to photons from objects in the field). These would be specified by giving all the input FLT files to MultiDrizzle in an ASCII file list, with each line containing just two filenames, namely the name of the FLT file and its corresponding IVM file. the IVM file should have a similar structure as the FLT file, except that the inverse variance values are stored in an extension that is called [IVM]. However, typically we recommend specifying 'final\_wht\_type' = 'ERR' which automatically takes care of calculating all the inverse variance files using the correct noise sources, and requires no additional input files.

The third extension of the **MultiDrizzle** output image contains the context (CTX) image which encodes information about which input image contributes to a specific output pixel. This is done using a bitmask for each output pixel, where 'bit set' means that the image, in the order it was combined, contributed with non-zero weight to that output pixel. The context image starts as a single 32-bit integer image but is extended as a cube with additional 32-bit deep planes as required to handle all the input images. The context image for the Tadpole example is shown in Figure 4.19. As there are six input images, each with two chips which are treated separately, this image has 12 bit planes which may be set. The darkest area shown corresponds to the [sci,2] chip from all six inputs and hence has all the following even bits set:  $2+8+32+128+512+2048=2730$ . Cosmic ray hits or other defective pixels contribute to the appropriate bit plane with zero weight and hence appear as lighter spots.

Figure 4.17: The science (SCI) extension of the drizzled product from the **MultiDrizzle** example. This image has been corrected for distortion and drizzled onto a single mosaic using the six images in the dither pattern.

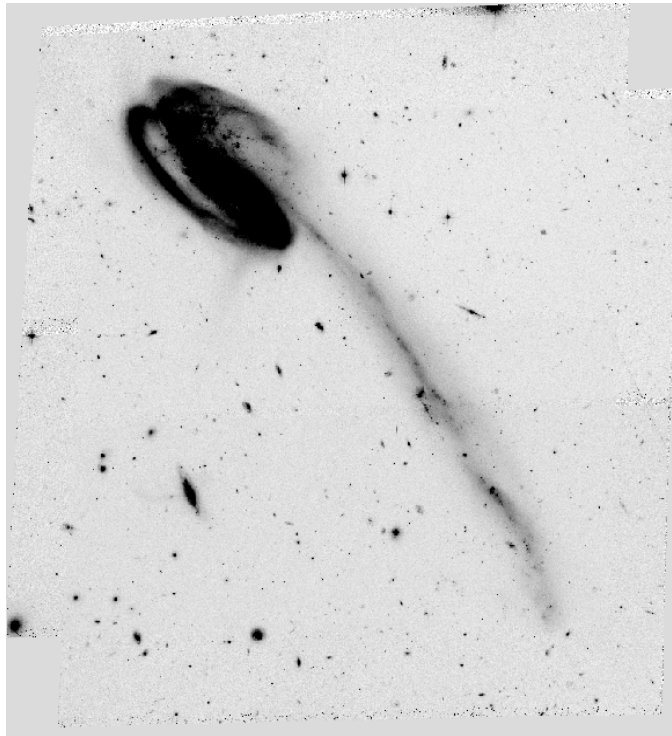


Figure 4.18: The corresponding weight (WHT) extension of the drizzled product from the example.

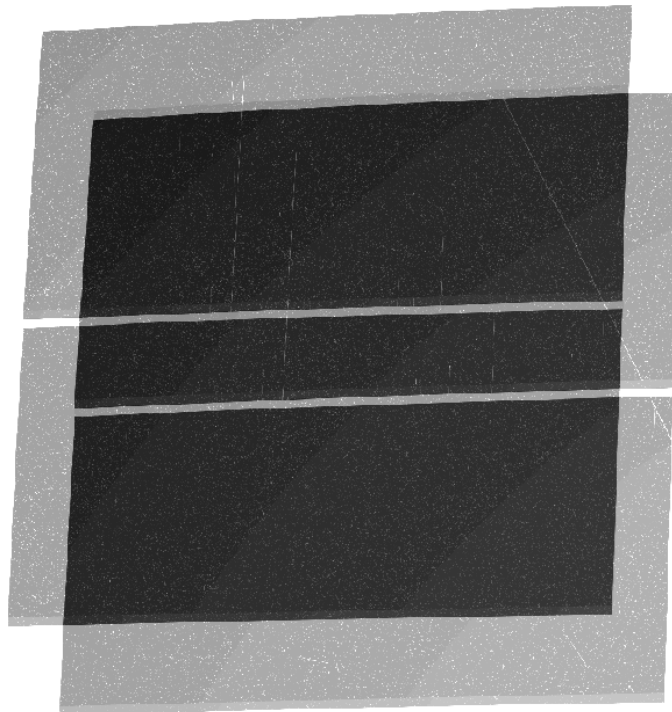
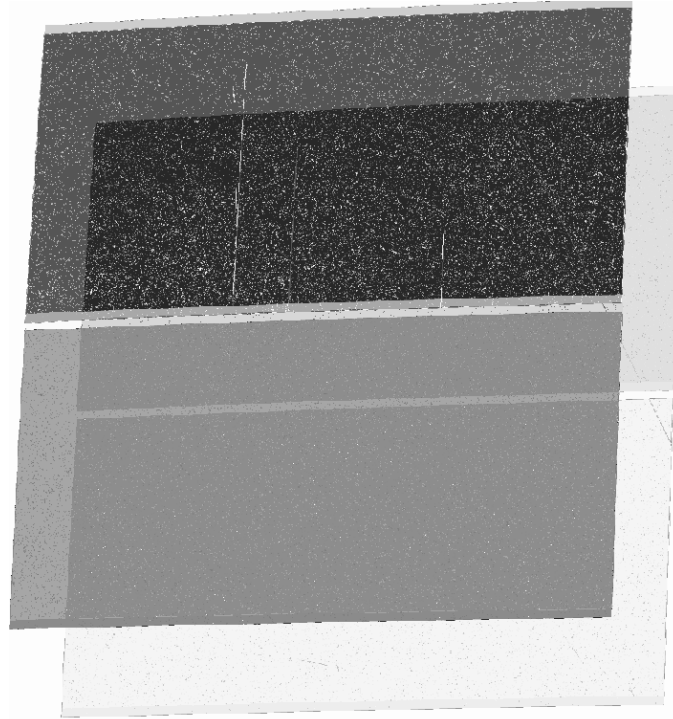


Figure 4.19: The corresponding context (CTX) extension of the drizzled product from the example.



---

## 4.8 Creating Custom Association Tables

Association tables for dithered, REPEAT-OBS, or CR-SPLIT observations are generated by the **CALACS** pipeline. These tables keep track of the input exposure filenames and the output product filenames. Some types of observations, however, will not have association tables. Others will have multiple tables from different visits which need to be combined into one. In the following discussion, we present the methodology for creating custom association tables, either by merging association tables or creating them from scratch. Users also have the capability to manually edit association tables to include any known image offsets. This can be done using the TTOOLS task **tedit** in IRAF, where the user adds the columns XOFFSET, YOFFSET and/or ROTATION to the association table. Alternately, an ascii file with the known image offsets may be specified and the association automatically updated.

### Merging Association Tables

Observing programs which cover a large portion of the sky will generally be made up of multiple pointings. Each of these pointings may be dithered or split for cosmic-ray rejection and will possess their own



association table. In order for **PyDrizzle** to produce a single mosaic product, a composite association table must be built from the separate association tables. Users can easily create this composite by merging the individual tables using the TTOOLS task **tmerge** with “option = append”.

The default product rootname will be taken from the first listed DTH-PROD in the composite association table. This rootname can be modified by the user (with **tedit**) to suit the desired naming convention. Generally, this rootname should match the rootname of the composite association table. A detailed example of merging association tables is given in step 1 of Example 4 from Section 3.5.2.

### Creating Association Tables from Scratch

In some cases, observations of the same target will not have accompanying association tables, for example observations taken in different visits or dithered observations taken using **POS-TARG** offsets. The Python task **buildasn** has been developed for the **DITHER** package to create association tables which may be used for reprocessing with **PyDrizzle** or **MultDrizzle**.

The following illustrates how to use **buildasn** to create an association table from all calibrated files with the FLT suffix in a single directory.

```
pyraf> from pydrizzle import buildasn
pyraf> buildasn.help()
```

The following illustrates how to use **buildAsn** to create an association table from all calibrated input files with the FLT suffix found in a single directory. Within PyRAF and using the IRAF syntax, we type:

```
pyraf> buildasn mymosaic suffix='flt'
```

Alternately, the same result may be obtained using the Python syntax:

```
pyraf> buildasn.buildAsnTable('mymosaic', suffix='flt')
```

The association table will have the name ‘mymosaic\_asn.fits’, the product name will be ‘mymosaic\_drz.fits’, and all files with the FLT suffix found in the working directory will be included in the association. To specify a subset of images within a given directory, the user may specify the ‘suffix’ parameter to be a filelist (‘@filename’), a wild-card list (‘\*8cd\*flt\*’), or any portion of the filename (‘crj’ or ‘f555w’).

If user determined offsets are available, **buildAsn** has the capability of incorporating them into the association table. These offsets (XOFFSET, YOFFSET, and/or ROTATION) are specified by the file listed in the ‘shiftfile’ parameter. MultiDrizzle utilizes the **buildasn** task and creates

association tables automatically when a file suffix (i.e. 'flt.fits') or a file list and/or a shift file is specified in the input parameters.

```
pyraf> buildasn mymosaic suffix='flt' shiftfile='shift.txt'
```

This option allows users to fine-tune the final image combination by providing corrections to the header WCS information, if required.

# ACS Error Sources

## In this chapter. . .

5.1 Readout Noise and A-to-D Conversion / 5-1
5.2 Bias Subtraction / 5-2
5.3 Dark Current, Hot Pixels, and Cosmic Rays / 5-6
5.4 Flat Fields / 5-16
5.5 Image Anomalies / 5-28
5.6 Generic Detector and Camera Properties / 5-38

This chapter describes the sources of uncertainty in ACS data, and provides pointers to resources beyond this manual for the latest descriptions of our evolving understanding of these issues.

---

## 5.1 Readout Noise and A-to-D Conversion

### 5.1.1 Readout Noise

The readout noise is an irreducible contribution to the total error budget. It is linked to the readout process and there are no reduction steps that can minimize or remove it. The effect of the read noise can however be minimized by keeping the number of pixels where signal is measured small and by minimizing the number of CCD readouts (while still allowing for good cosmic ray and hot pixel removal). The read noise is independent of position on the CCD. Table 5.1 lists the read noise (R) expressed in electrons (rms), which is associated with the readout from each amplifier for the main gain settings.

Table 5.1: Readout Noise (R) and Total Noise (Readout+Quantization, TRN) for ACS CCDs

		Gain 1			Gain 2		
Chip	Amp	Gain	R	TRN	Gain	R	TRN
WFC1	A	1.00	4.99	5.00	2.002	5.24	5.27
WFC1	B	0.972	4.89	4.90	1.945	5.08	5.11
WFC2	C	1.011	5.16	5.17	2.028	5.37	5.40
WFC2	D	1.018	4.82	4.83	1.994	5.11	5.14
HRC	C	1.185	4.46	4.47	2.216	4.71	4.78

### 5.1.2 A-to-D Conversion

The analog information (electrons) accumulated in the CCD are converted into data numbers (DN) by the analog-to-digital converter (ADC). Both ACS CCD cameras employ 16-bit ADCs, which can produce a maximum of  $2^{16} = 65,535$  DN. If the gain conversion factor ( $g$ ) is expressed in ( $e^-/DN$ ) the largest number of electrons representable by these ADCs is given by  $g \cdot 2^{16}$ . Any charge packet containing more than  $g \cdot 2^{16}$  electrons will reach the digital saturation limit (see Section 5.6.4). The analog-to-digital converter produces only discrete output levels. This means that a range of analog inputs can produce the same digital output. This round-off error is called quantization noise. It can be shown (Janesick J.R., 2001, Scientific Charge-Coupled Devices, SPIE Press.) that the quantization noise QN is constant for a given gain setting when expressed in DN:  $QN(DN) = 12^{-1/2}$ . The quantizing noise can be converted into noise electrons as:  $QN(e^-) = 0.288675 \cdot g$ . The total noise (TRN) associated with CCD readout noise (R) and quantizing noise is obtained by adding the two figures in quadrature (see Table 5.1),  $TRN = (R^2 + (0.288675 \cdot g)^2)^{1/2}$ .

---

## 5.2 Bias Subtraction

### 5.2.1 Bias Calibration Issues

Bias reference frames are acquired daily for scientific calibration purposes and for monitoring the detector performance. Every week multiple bias frames are combined together into a reference superbias image. The combination removes the cosmic rays accumulated during the readout time and enhances the signal-to-noise ratio of the fixed pattern noise.

CALACS performs the bias correction in two steps (see Section 3.4.1): **doBlev** subtracts the bias level from the overscan region and **doBias** subtracts a reference bias image.

Each quadrant of the WFC focal plane (A&B for WFC1 and C&D for WFC2) has two overscan regions: a 24-pixel-wide leading physical overscan at columns 1-24 and a 20-row-wide virtual overscan at rows 2049-2068 obtained by overclocking after the readout of the last CCD row.

All four WFC amplifiers produce a horizontal ramp in the leading overscan which extends up to 18 columns toward the active area (see Sirianni, M., Martel, A.R., & Hartig, G.F., 2001, JHU-ACS internal report, available on-line at:

[http://acs.pha.jhu.edu/instrument/calibration/results/by\\_instrument/detector/wfc/build4/overscan/](http://acs.pha.jhu.edu/instrument/calibration/results/by_instrument/detector/wfc/build4/overscan/)).

The amplitude of the ramp is different for each amplifier, but it is generally larger in the A&D quadrants than in the B&C quadrants. The perturbation associated with the ramp fades gradually and disappears within approximately 15 columns. The bias level from the physical overscan can be safely measured using the last six columns adjacent to the active area [columns 19-24 for A&D and columns 4121-4126 for B&C].

The virtual overscan is not used to estimate the bias level. This region shows large scale structure which is quadrant and gain dependent. This structure, due to the bias fixed pattern noise, makes using the virtual overscan in an automatic routine problematic. Moreover, this region can be contaminated by deferred charge due to degradation in the parallel charge transfer efficiency.

Analysis of the active area in the bias frames shows small differences in the bias level between the leading physical overscan and the active area (Sirianni, et al., 2002, "HST Calibration Workshop" STScI, page 82). This offset varies from amplifier to amplifier and it can be as large as 3.5 DN. Ideally, no offset would be seen. In principle, if the residual offset between the imaging area and the overscan region were always of the same amplitude, a full frame bias subtraction (**doBias**) would remove any residual differences. Unfortunately, the offset is not constant but shows random variations on the order of few tenths of a DN. These variations are likely due to interference between the WFC integrated electronics module and the telescope and/or other science instruments. The accuracy of the bias level subtraction in a single quadrant is limited by this random effect.

HRC images are read out using only one amplifier. Each image has three overscan regions: the 19-pixel-wide leading and trailing physical overscans at columns 1-19 and 1044-1062, respectively, and the 20-row-wide virtual overscan at rows 1025-1044. The readout amplifier produces a horizontal ramp in the leading overscan which extends up to 10 columns toward the active area. As in the case of WFC images, the bias level is therefore measured in the last six columns of the leading physical overscan. There is not a significant difference between the bias level in the overscan area and in the active area.

Even after the subtraction of the overscan bias level, some structure remains in the bias frames. This structure includes real bias pattern noise

and also some dark current accumulated during the time required to read out the detector. To remove this structure a superbias is subtracted from each science image.

In principle, a perfect bias subtraction would give an image, that once flat fielded and converted to electrons should not present any discontinuity at the boundaries between quadrants.

However, in the case of WFC images the amplitude of the residual offset level varies between each quadrant. This results from the bias level being measured in the leading physical overscan and then subtracted from the active area of each quadrant, causing the center of the resulting image to show a jump between the two adjacent quadrants, A&B or C&D (Sirianni, et al., 2002, “HST Calibration Workshop” STScI, page 82). This jump is not removed by the superbias subtraction. Indeed, since this offset (usually with a maximum amplitude of 0.3 DN) is present in all calibration and scientific frames, the final product of **CALACS**, after bias and dark subtraction, may show a quadrant-to-quadrant jump as large as few DNs (Figure 5.1).

Figure 5.1: Calibrated WFC1 image showing the quadrant-to-quadrant jump



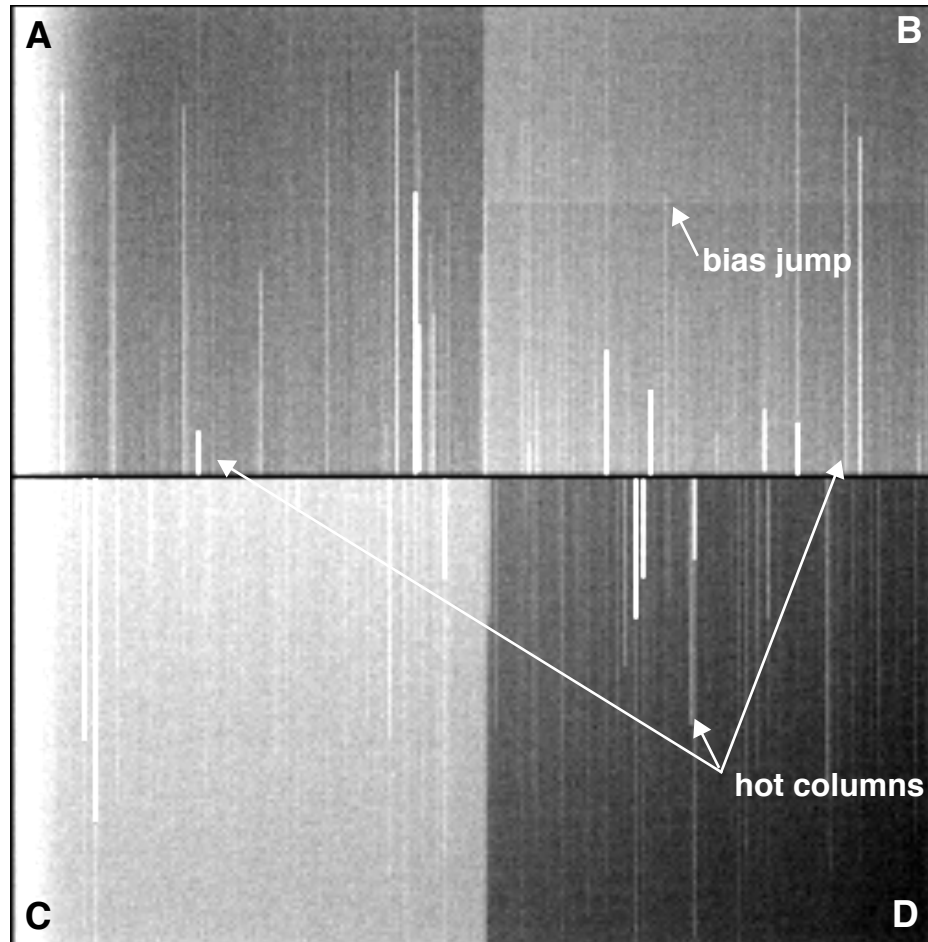
For point source photometry, the local background in an annular region is typically subtracted so that the residual offset has essentially no impact on the integrated magnitudes. However, if the object falls across the quadrant jump the photometry should be considered suspect. Similarly, extended objects may spread over two or more quadrants, so their surface brightness profile will suffer from the residual offset. More studies are in progress to better characterize this problem and to develop a correction that can be applied directly to the calibrated images. At the moment we suggest fitting the sky level in each quadrant separately.

A detailed study of the on-orbit characteristics of bias frames, the overscan regions and superbias used in the pipeline will be published in a future ISR.

## 5.2.2 Bias Jump

There is some evidence for intermittent variations at the sub-DN level in the WFC bias level during the readout. On a few occasions some frames show horizontal bias jumps in one or more quadrants that can run for several hundreds of rows (Figure 5.2). These effects occur at a few tenths of a DN level and they might appear in one or more quadrants simultaneously. The probable source is interference from other activities on the spacecraft and/or scientific instruments with the electronics. At the moment there is no automatic detection of bias jumps within the calibration pipeline. Though bias jumps at the sub-DN level are not important for most applications, users should be cautioned that they might exist in processed data and we recommended a careful inspection of the data for their presence.

Figure 5.2: Bias Jump in the WFC1 Quadrant B only. The vertical stripes in the data are hot columns and are unrelated to bias.



### 5.2.3 Bias Subarrays for the WFC and HRC

When science data are obtained with use of subarrays, dark and flat field images will be extracted from full-frame images. Bias images will also be extracted from full-frame images, if the subarray is contained in a single quadrant. Tests have shown that this does not degrade the quality of the dark, flat field or bias corrections as compared to full-frame data. It is strongly advised that subarrays not be defined such that they span amplifier quadrants. In the case that the subarray extends into the adjacent amplifier quadrant, users must obtain their own subarray bias images (with one-amp readout), otherwise the bias level difference between adjacent amplifier quadrants would be applied inappropriately.

---

## 5.3 Dark Current, Hot Pixels, and Cosmic Rays

### 5.3.1 Dark Current

The procedure for creating ACS dark reference files and applying dark subtraction to ACS science data is described in detail in Section 3.4.3. Because it takes a few weeks to collect enough frames to create the dark reference file, the “best” darkfile is typically not available in the pipeline until 2-3 weeks after the date of observation. Users may verify whether the darkfile most appropriate to their observations has been installed for pipeline use by checking the ACS reference file web pages:

[http://www.stsci.edu/hst/acs/analysis/reference\\_files/dark\\_images.html](http://www.stsci.edu/hst/acs/analysis/reference_files/dark_images.html).

Using an old reference file will produce a poor dark correction: either leaving too many hot pixels uncorrected and unflagged, or creating many negative “holes” caused by the correction of hot pixels which were not actually hot in the science data (i.e., if the detectors were annealed in the interim).

#### WFC/HRC

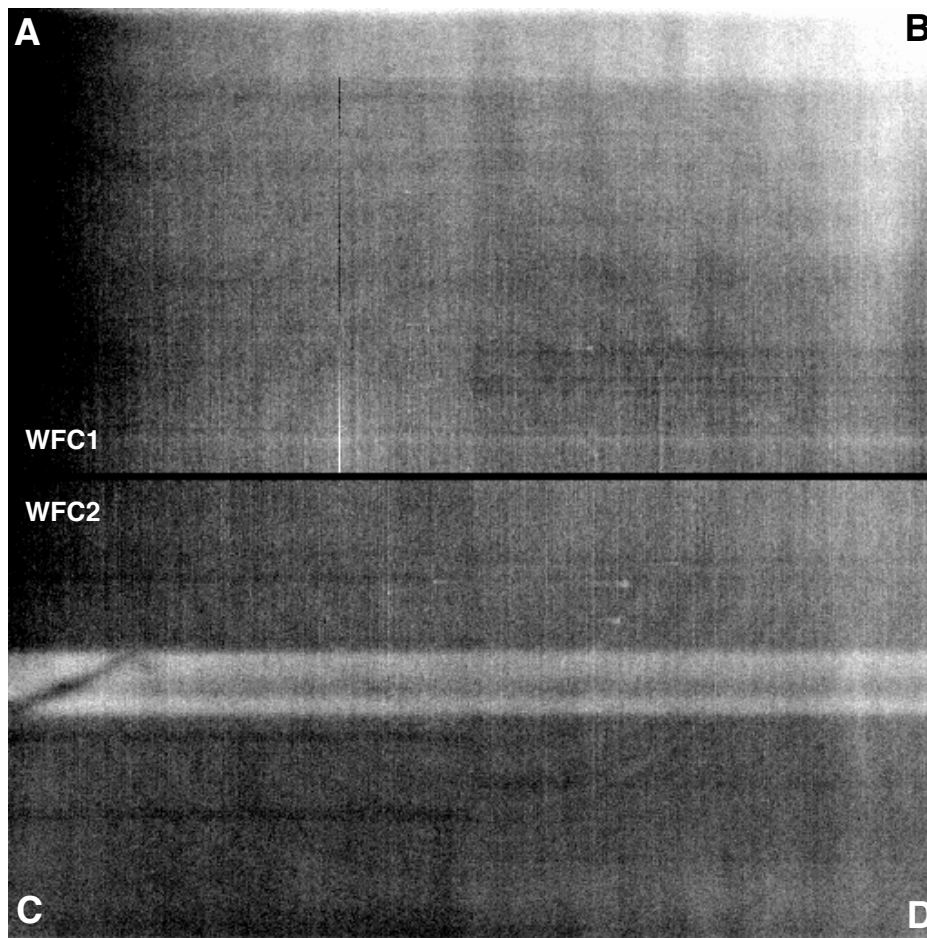
The dark current is not constant across the CCDs. Figure 5.3 shows the dark current features in the WFC1 (above) and WFC2 (below) chips. These features were observed in pre-flight tests, and have generally remained stable in orbit.

There is a gradient, most noticeable on the WFC1 chip, going from a dark edge in the amplifier A quadrant (upper left) to a bright corner in the amplifier B quadrant (upper right). There are two horizontal bright bands of elevated dark current in the center of the WFC2 chip. Many faint rings are also visible: all concentric with the center of both chips. These features are



likely intrinsic to the chips themselves: artifacts embedded in (or on) the silicon during various stages of the CCD manufacturing process.

Figure 5.3: High S/N combination of WFC dark frames illustrating dark current structure



The WFC1 and HRC histograms in Figure 5.4 and Figure 5.5 show the growth of hot pixels (for more information, refer to Section 5.3.2). A less obvious result is that the peak of the normal pixel (Poisson) distribution (i.e., the mean dark current, excluding the hot pixels) has also increased.

The increase in the mean dark current for WFC has been from 6.8  $e^-/\text{pixel}/\text{hr}$  at launch to 11.1  $e^-/\text{pixel}/\text{hr}$  (an average of 11.4 for WFC1 and 10.8 for WFC2) in April 2004. For HRC the change in dark current has been from 9.3  $e^-/\text{pixel}/\text{hr}$  at launch to 13.4  $e^-/\text{pixel}/\text{hr}$  in April 2004. The dark calibration tracks the mean dark current very closely at 2 week intervals (see Section 3.4.3).

Figure 5.4: WFC dark current histogram for chip 1. Statistics for chip 2 are nearly identical. The figures illustrate the growth of hot pixels over time.

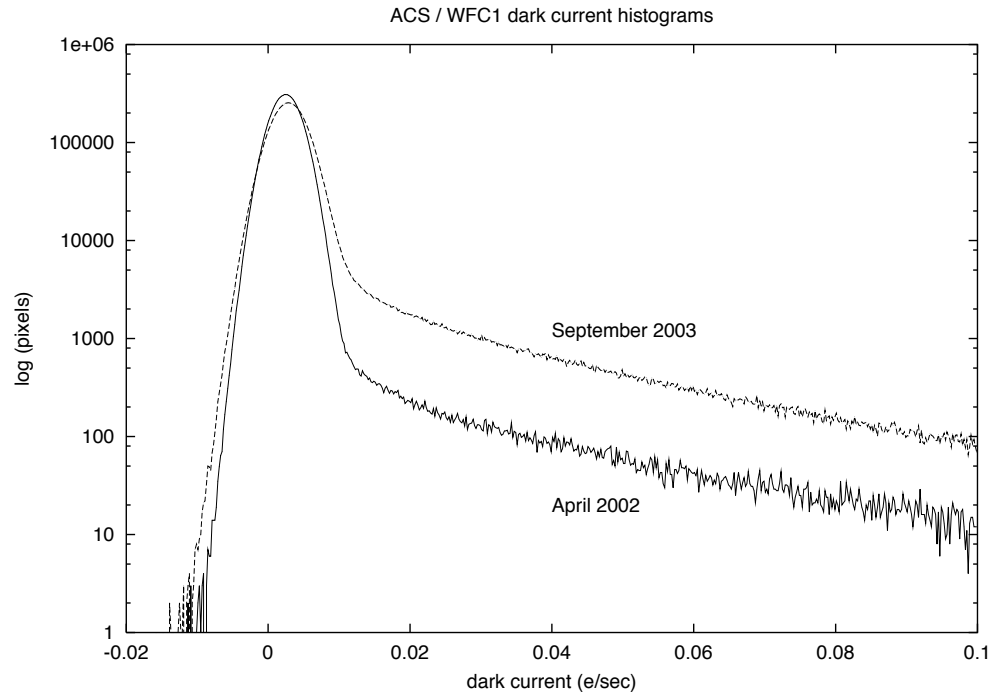
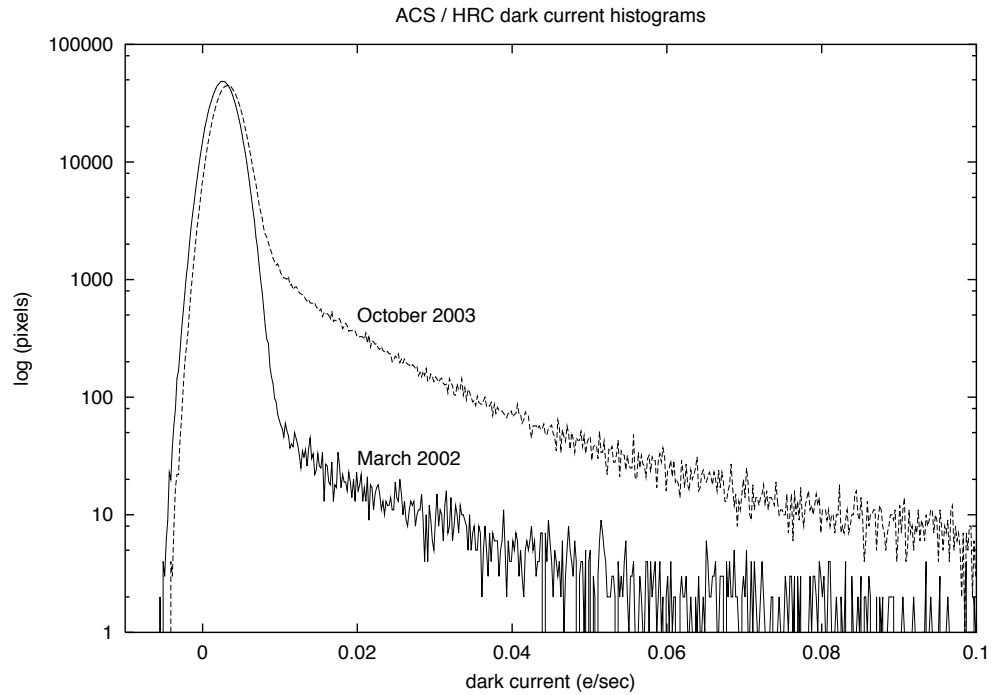


Figure 5.5: HRC dark current histogram



### SBC

The SBC, or ACS MAMA detector, intrinsically has no readout noise and very low detector noise levels which normally will be negligible compared to statistical fluctuations. A dark current image was compiled during ground tests with a total exposure time of 14,400 seconds and remains as the calibration dark image. This has a mean dark count of  $3.8 \times 10^{-5}$  counts/pixel/second. Approximately once per month since ACS was installed, 1800 second SBC darks have been accumulated. The dark rate for these is typically  $2.0 \times 10^{-5}$  counts/pixel/second. The principal reason for taking these images is to provide a measure of the health of the SBC. No major fluctuation has been noted. An in-flight super-dark will be constructed from the in-flight measurements.

### 5.3.2 Hot Pixels

A “hot pixel” is a state of radiation damage affecting the dark current production of an individual pixel. Such pixels likely result from the close interaction of an incident heavy nucleon with Si nuclei in a pixel, creating new Si-SiO<sub>2</sub> interface states. Once produced, such pixels almost always remain hot before the next anneal producing a continuum of excess dark current rates more than 1 to 4 orders of magnitude greater than the mean value. Although such pixels have temporarily lost their ability to yield precise measurements of faint photon flux, the majority of such pixels are “healed” in monthly anneals when the CCD temperature is raised by ~100 degrees over operating temperature for ~16 hours.

As seen in Figure 5.4 and Figure 5.5, the dark current distribution is well described by a Gaussian. As expected from experience with earlier HST cameras, very significant tails (all pixels with dark current above the 5 sigma limit [ $\sim 0.02$  e<sup>-</sup>/sec]) are seen in these distributions. These tails consist of the pixels that have suffered radiation damage. The pixels with values between 0.02 and 0.08 e<sup>-</sup>/sec are referred to as “warm” pixels and those above 0.08 e<sup>-</sup>/sec as hot pixels. Figure 5.6 and Figure 5.7 show these tails for WFC and HRC for two different dates. As shown, many thousands (HRC) or tens of thousands (WFC) of pixels have greatly elevated dark current with the number markedly increasing with time.

Figure 5.6: Dark Current Distribution Tails in WFC for March 15, 2002 and March 28, 2002. All pixels with dark current above the 5 sigma limit ( $\sim 0.02$  e<sup>-</sup>/sec) are due to so-called “warm” and “hot” pixels which have suffered radiation damage. The number of these pixels can be seen to increase rapidly with time.

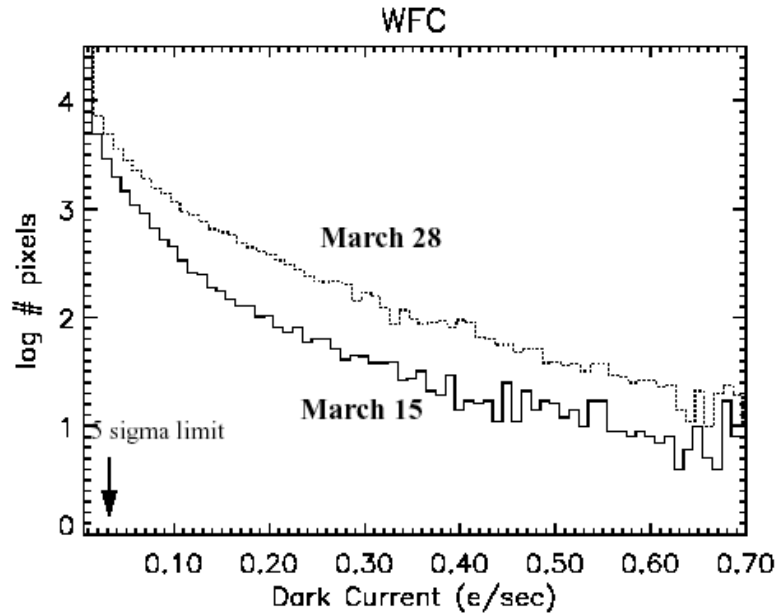
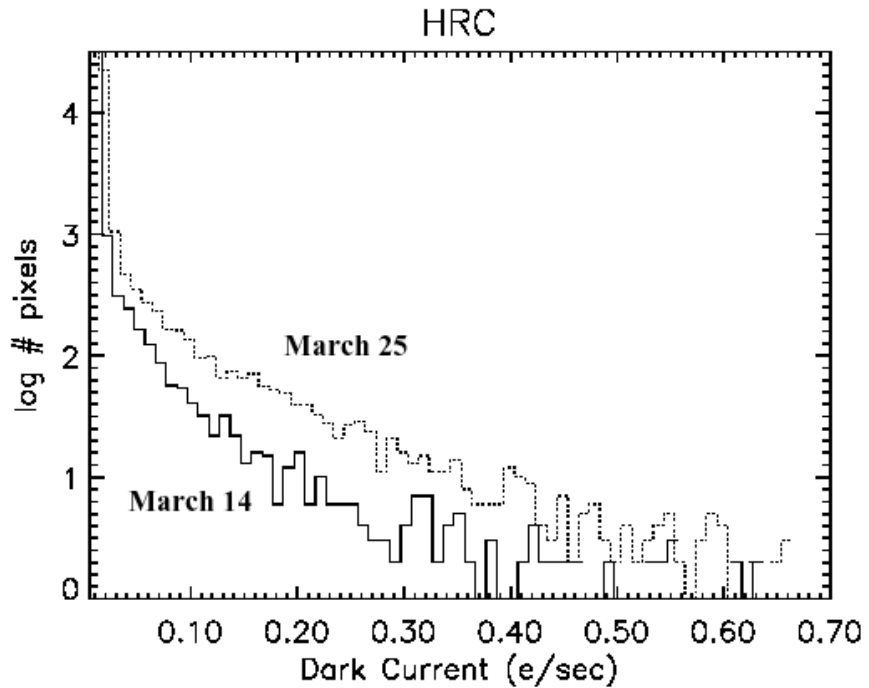


Figure 5.7: Dark Current Distribution Tails in HRC for March 15, 2002 and March 28, 2002.



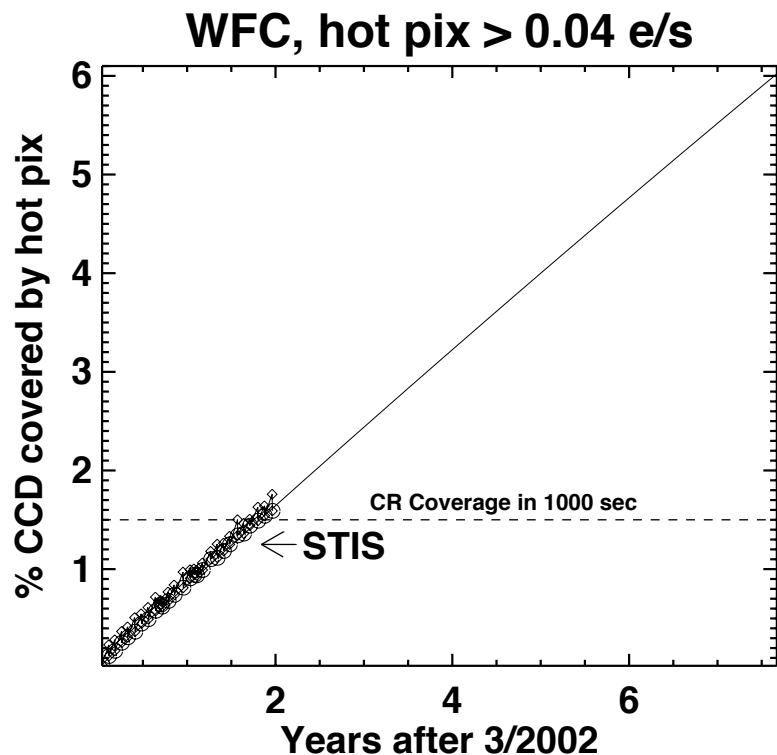
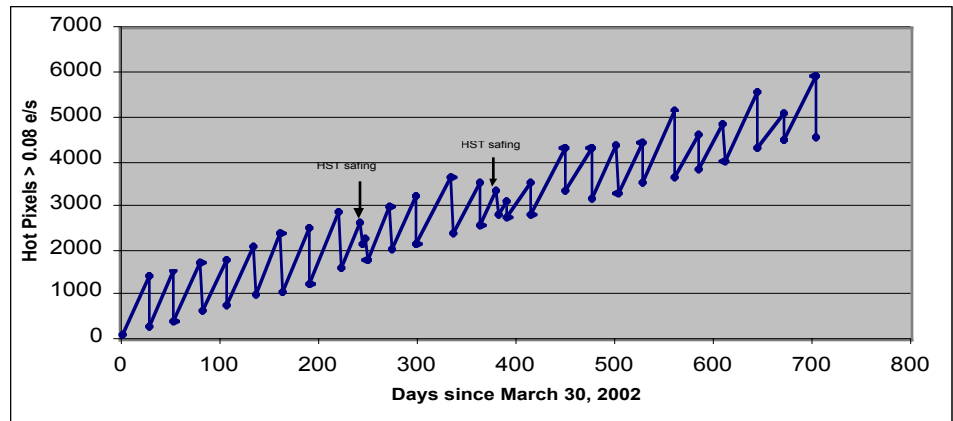
## Trending

Even with 16 million pixels, the WFC would not be expected to have any pixels with dark current more than 6 standard deviations beyond the mean (i.e., with dark current greater than  $0.02 \text{ e}^-/\text{sec}$ ) were it not for the effects of radiation damage. To analyze hot pixel trending, we have chosen a conservative limit of twice that, or  $0.04 \text{ e}^-/\text{sec}$  for WFC and  $0.08 \text{ e}^-/\text{sec}$  for HRC as a threshold above which we consider a pixel to be “hot” and not part of the normal distribution of pixel dark current. Note that even though trending is analyzed at these limits, only pixels above  $0.08 \text{ e}^-/\text{sec}$  are flagged in the DQ array.

For WFC we find a growth rate of approximately 1200 new hot pixels per day with dark current greater than  $0.04 \text{ e}^-/\text{sec}$ . For HRC the number of new hot pixels per day above the threshold is approximately 90. Because the distribution of dark current in hot pixels is strongly concentrated near the threshold, the specific number of such pixels is necessarily a strong function of the chosen threshold.

Subtraction of a superdark frame from a science image can remove the dark current from hot pixels just as it does for normal pixels. However, hot pixels are often orders of magnitude noisier than normal pixels, which in many cases limits their ability to provide useful measurements of flux. For the hottest pixels, the observed noise exceeds even the Poisson noise by an order of magnitude. Observations which do not employ contemporaneous superdarks will suffer from uncorrected and unflagged hot pixels, a particular concern to programs whose aim is to search for astrophysical transients or broad-band drop-outs. The problems associated with hot pixels can be mitigated by using the best reference files (usually necessitating recalibration with OTFR several weeks after the data were obtained), flagging and discarding data from hot pixels, and dithering observations to provide additional sampling of pixel positions on the sky and allow rejection of hot pixels.

Figure 5.8: Hot pixel growth rate for HRC (top) and WFC (bottom).



The anneal rate of new hot pixels (dark current > 0.04 e<sup>-</sup>/sec) on the ACS WFC has been disappointingly low: ~60% in the first eight monthly anneal cycles of the instrument. This rate is significantly lower than the observed and characteristic value for other HST CCDs: 80-85% for WFPC2, STIS, and ACS HRC. The anneal rate is significantly less than 60% for pixels which are much hotter than 0.04 e<sup>-</sup>/sec. The consequence of poor annealing is a greater fractional coverage of the camera by pixels with elevated dark current than was the experience of other HST CCDs. Figure 5.8 shows the observed growth of hot pixels on both HRC and WFC. The saw-tooth appearance is due to regular anneals. For WFC hot pixel coverage is more than cosmic ray coverage in a typical exposure. By the

end of the decade one in every 16 pixels is predicted to be hot on WFC. For more details see [ACS ISR 02-09](#).

### 5.3.3 Cosmic Rays

Like all HST cameras before it, the ACS HRC and WFC fields of view are heavily peppered by cosmic rays in even the shortest of exposures. For full orbit integrations, approximately 5% of the pixels receive significant charge from cosmic rays via direct deposition or from diffusion from nearby pixels. Great care must be taken in planning and analyzing HST ACS observations to minimize the impact of cosmic rays on science images.

#### Fractional Coverage

For most users of the HRC and WFC, the most important characteristic of cosmic rays is simply the fraction of pixels they impact. This number provides the basis for assessing the risk that the target(s) in any set of exposures will be compromised. For ACS the observed rate of cosmic ray impacts on an individual frame varies by a factor of two depending on the proximity of the spacecraft to the confluence of the Earth's magnetic field lines (e.g., the South Atlantic Anomaly). For a 1000 second exposure the fraction of pixels affected by cosmic rays (in non-SAA passages) varies between 1.5% and 3%. This fraction is the same for the WFC and HRC despite their factor of two difference in pixel areas, because the census of affected pixels is dominated by charge diffusion, not direct impacts. This fraction is also consistent with what is observed for WFPC2. For most science observations, a single CR-split (i.e., two exposures) is sufficient to insure that measurements of the targets are not compromised by cosmic rays.

More consideration is required for survey-type observations with WFC, a bonafide survey instrument. Observers seeking rare or serendipitous objects as well as transients may require that every single WFC pixel in at least one exposure among a set of exposures is free from cosmic ray impacts. For the cosmic ray fractions of 1.5% to 3% in 1000 sec, a single ~2400 second orbit must be broken into 4 exposures (4 CR-splits of 500 to 600 sec each) to reduce the number of uncleanable pixels to 1 or less. (It is also recommended that users dither these exposures to remove hot pixels as well.)

#### Cosmic Ray Events

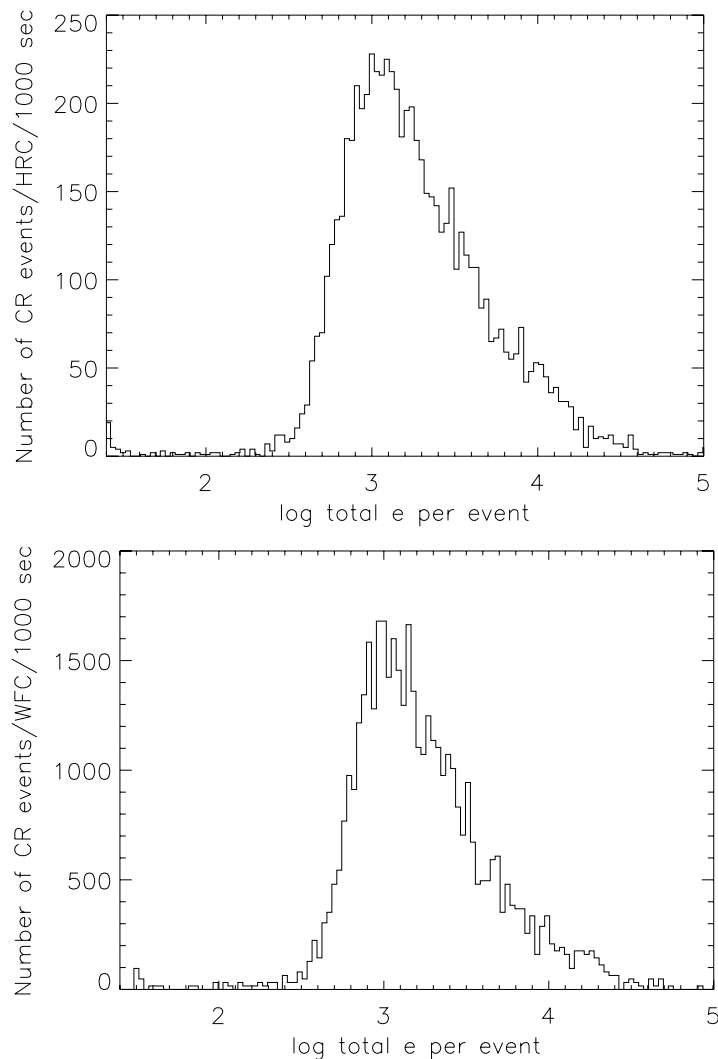
Many science observations require a careful consideration of individual cosmic rays events. To either remove cosmic rays events or distinguish them from astrophysical sources users might consider the distributions of observed cosmic ray fluxes, sizes, anisotropies, and the number of attached pixels per event.

### Electron Deposition

The flux deposited on the CCD from an individual cosmic ray does not depend on the energy of the cosmic ray but rather the length it travels in the silicon substrate. As a result the deposition distribution has a well-defined minimum with few events of less than 500 electrons (where such low-electron events correspond to cosmic rays which pass through the CCD at a normal angle of incidence). As seen in Figure 5.9, the median charge deposited for WFC and HRC is about 1000 electrons, the same as for WFPC2.

A useful characteristic of the deposition distribution is its well-defined minimum; e.g., multi-pixel events which have an apparent magnitude of 25th or fainter, in a 500 second broad-band exposure, are unlikely to be caused by cosmic rays. Such information can help with the removal of false positives from searches for faint transients (e.g., high-redshift SNe).

Figure 5.9: Electron deposition by cosmic rays on HRC (top) and WFC (bottom). A minimum deposition of  $\sim 500$  e is seen corresponding to CR's with normal incidence. The median deposition is  $\sim 1000$  e.

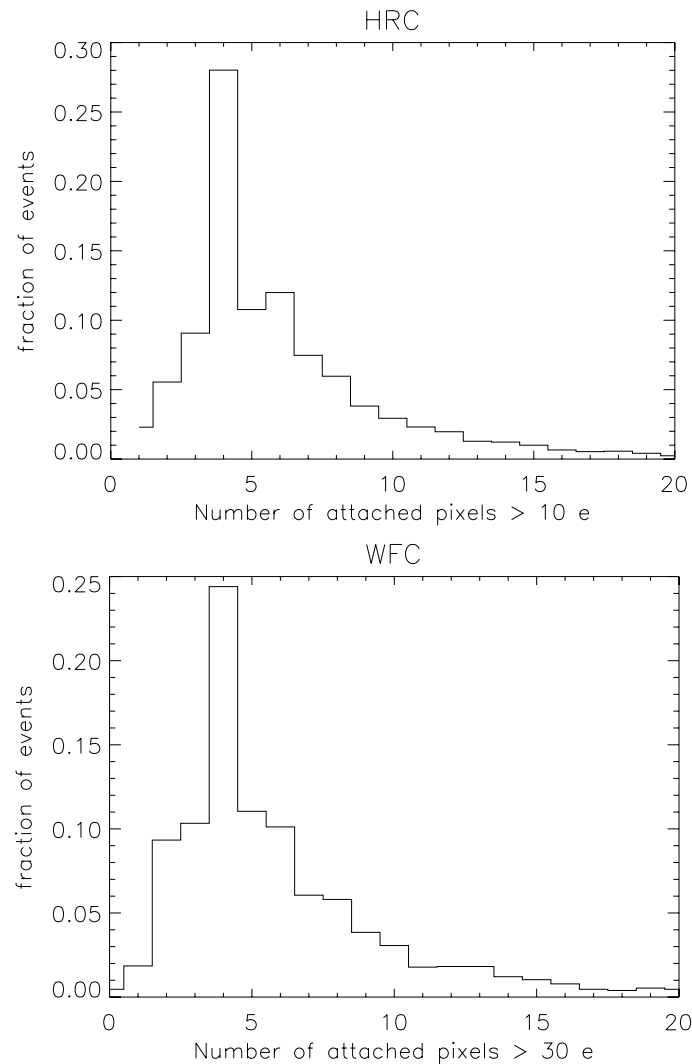




### Attached Pixels

As seen in Figure 5.10 for HRC and WFC the salient features of electron deposition are a strong peak in the distribution function at 4 to 5 pixels. On the smaller side there is a sharp decline in events. Although a few events are seen which encompass only one pixel, examination of these events indicate that at least some and maybe all of these sources are actually transient hot pixels or unstable pixels which can appear hot in one exposure (with no charge diffusion) and normal in the next. Such pixels are very rare but do exist. There is a long tail in the direction towards increasing numbers of attached pixels. Some of these are likely due to two individual events associated by their chance superposition, but more are from oblique incidence cosmic rays which skim the surface of the CCD leaving a long trail (which is wider near the surface). Unfortunately the number of attached pixels is not a very useful characteristic to distinguish cosmic rays from unresolved astrophysical sources.

Figure 5.10: Distribution of the number of pixels associated with a single CR event for the HRC (top) and WFC (bottom). Some bias exists for events >6 pixels which may be composed of two events with chance superposition.



---

## 5.4 Flat Fields

The flat field reference files currently in use by the ACS calibration pipeline were derived via different methods, depending on the detector and the filter used. These LP-flats are a combination of two files, a P-flat which accounts for the pixel-to-pixel variations in sensitivity, and an L-flat which models the low-frequency variations in sensitivity over the detector field of view. The CCD P-flats were created in the laboratory using an external illumination source, while the P-flats for the SBC were taken inflight using the internal lamps. The L-flats were derived inflight from dithered stellar observations of 47Tuc for the CCDs and NGC6681 for the SBC MAMA. The two files were then multiplied to make the LP-flats used for calibration.

### 5.4.1 Ground Flats (P-flats)

#### CCDs

In early 2001, flat field images for the ACS were produced in the laboratory (see [ACS ISR 2001-11](#)) using the Refractive Aberrated Simulator/Hubble Opto- Mechanical Simulator (RAS/HOMS). The RAS/HOMS is an HST simulator capable of delivering OTA-like, external, monochromatic point-source and broad-band, full field illumination above its refractive cutoff wavelength of  $\sim 3500 \text{ \AA}$ .

Because the RAS/HOMS optics are opaque below  $3500 \text{ \AA}$ , flats for the UV filters F330W and F344N (see [ACS ISR 03-02](#) and [ACS ISR 05-12](#)) were created using inflight observations of the bright Earth (see Section 5.4.4). Unfortunately, red leaks in F220W and F250W are so large that the out-of-band light dominates, and the lab flats made with the deuterium lamp illumination are superior to the Earth flats for these two filters.

A total signal of about 100,000 electrons per pixel is required for each flat field to avoid degrading the intrinsic pixel-to-pixel rms response of  $<1\%$  for the ACS CCD detectors. The flats are normalized by dividing by the average number of counts in the central 1% of the frame. In the case of full WFC frames, the chip 2 images are divided by the chip 1 central value, in order to preserve the overall sensitivity difference between the two CCD chips across the  $\sim 50$  pixel gap that separates the two independent pieces of the WFC detector. For small filters that cover just part of one quadrant of the WFC (i.e., F892N, polarizers), flats were masked to unity below 90% of the central value of the data, so that no flat field correction is done on the scattered light outside the physical edge of the filter.

More information on the HRC and WFC ground flats may be obtained from [ACS ISR 01-11](#) for the standard filters, polarizers, and coronagraph,

from [ACS ISR 02-01](#) for the ramp filters, and from [ACS ISR 02-04](#) for the prism and grism.

### **MAMA**

Flat fields for the full set of SBC filters were also taken in the laboratory ([ACS ISR 1999-02](#)), but were later replaced with inflight observations using the internal deuterium lamp ([ACS ISR 2005-04](#)). In total integration time of 20.5 hours through the F125LP filter, a flat field with a total signal of 12,000 counts per pixel was produced. Analysis of original laboratory flats indicates that the P-flat response is independent of wavelength, so the F125LP lamp flat was used for all filters. The internal lamp illumination does not simulate the OTA optics and, therefore, is useful only for correcting the pixel-to-pixel detector response. In order to accurately model the low-frequency variations in sensitivity, which may depend on wavelength, dithered starfield observations were required. (See Section 5.4.2 for a discussion of the SBC L-flats.)

## **5.4.2 L-flats**

### **CCDs**

The large scale uniformity of the WFC and HRC detector response, as provided by the CCD laboratory flats, has been improved inflight by using multiple dithered pointings of stars in 47 Tucanae. By placing the same stars over different portions of the detector and measuring relative changes in brightness, low frequency spatial variations in the response of each detector have been measured. Photometric errors of  $\pm 3\%$  to  $\pm 9\%$  corner-to-corner have been found in the original WFC and HRC laboratory flat fields (see [ACS ISR 02-08](#)). The derived L-flats are based on a 4th-order polynomial fit and are shown in Figure 5.11 and Figure 5.12 for WFC and HRC, where white indicates that the photometry produced using the laboratory flats is too faint with respect to the true stellar magnitude, and black indicates that the photometry is too bright. There is a continuous gradient in the L-flat correction along the diagonal of the detector which corresponds to the axis of maximum geometric distortion.

L-flats were determined from inflight observations using filters F435W, F555W, F606W, F775W, F814W, and F850LP for both the WFC and HRC. The HRC study included two additional filters: F475W and F625W. The L-flat correction for the remaining filters was derived by using linear interpolation as a function of wavelength. The pivot wavelength of each filter was used for the interpolation, where the resulting L-flat is equal to the weighted average of the L-flat for the two filters nearest in wavelength. Due to red leaks in the F220W and F250W HRC filters, no L-flat correction has been applied, and errors in the flats of  $\pm 2$  to 4% corner-to-corner are expected for these filters. For a detailed discussion of

ACS L-flat corrections, refer to [ACS ISR 02-08](#). For a discussion of the mathematical algorithm used to derive the L-flats, refer to [ACS ISR 03-10](#).

To verify the interpolated L-flat corrections, additional observations of the same stellar field have been acquired and are undergoing analysis. The L-flat calibration program revisits the same target several times per year; therefore, observations are obtained for a range of orientations due to the roll of the telescope. Differential photometry of stars falling on different portions of the detector as the telescope rolls will provide a verification of the L-flats for the interpolated filters and will also provide an independent test of the absolute sensitivity dependence with time for the full suite of ACS filters. Initial testing indicates that the photometric response for a given star is now the same to  $\sim 1\%$  for any position in the field of view for filters which were observed during the inflight L-flat campaign. For the interpolated L-flats, the expected accuracy is  $\sim 2\%$ . Once the analysis for the additional stellar observations is complete, new flat fields will be delivered to the pipeline and the errors are expected to be reduced to  $< 1\%$ .

### **MAMA**

As was done for the CCDs, the SBC L-flats were derived using dithered starfield observations. Instead of 47Tuc, however, the UV-bright globular cluster NGC6681, which is rich in blue horizontal branch stars, was selected. This work is summarized in [ACS ISR 2005-13](#). The required corrections to the inflight lamp flats are given in Figure 5.13 and range from  $\pm 8\%$  to  $\pm 20\%$ , depending on wavelength. Since insufficient observations with the F122M filter exist, this L-flat is simply a copy of the F115LP filter correction. Six new flat fields have been delivered for use in the calibration pipeline, and the resulting photometric accuracy is now  $\pm 1\%$  for F115LP, F122M, and F140LP and  $\pm 2\%$  for F150LP and F165LP.

Figure 5.11: WFC low frequency (L-flat) flat-field corrections required for the laboratory data. While the pixel-to-pixel (P-flat) structure of the laboratory flats is robust, a low frequency correction is required to achieve uniform detector response. This correction ranges from  $\pm 5\%$  for the F555W filter to  $\pm 9\%$  for the F850LP filter.

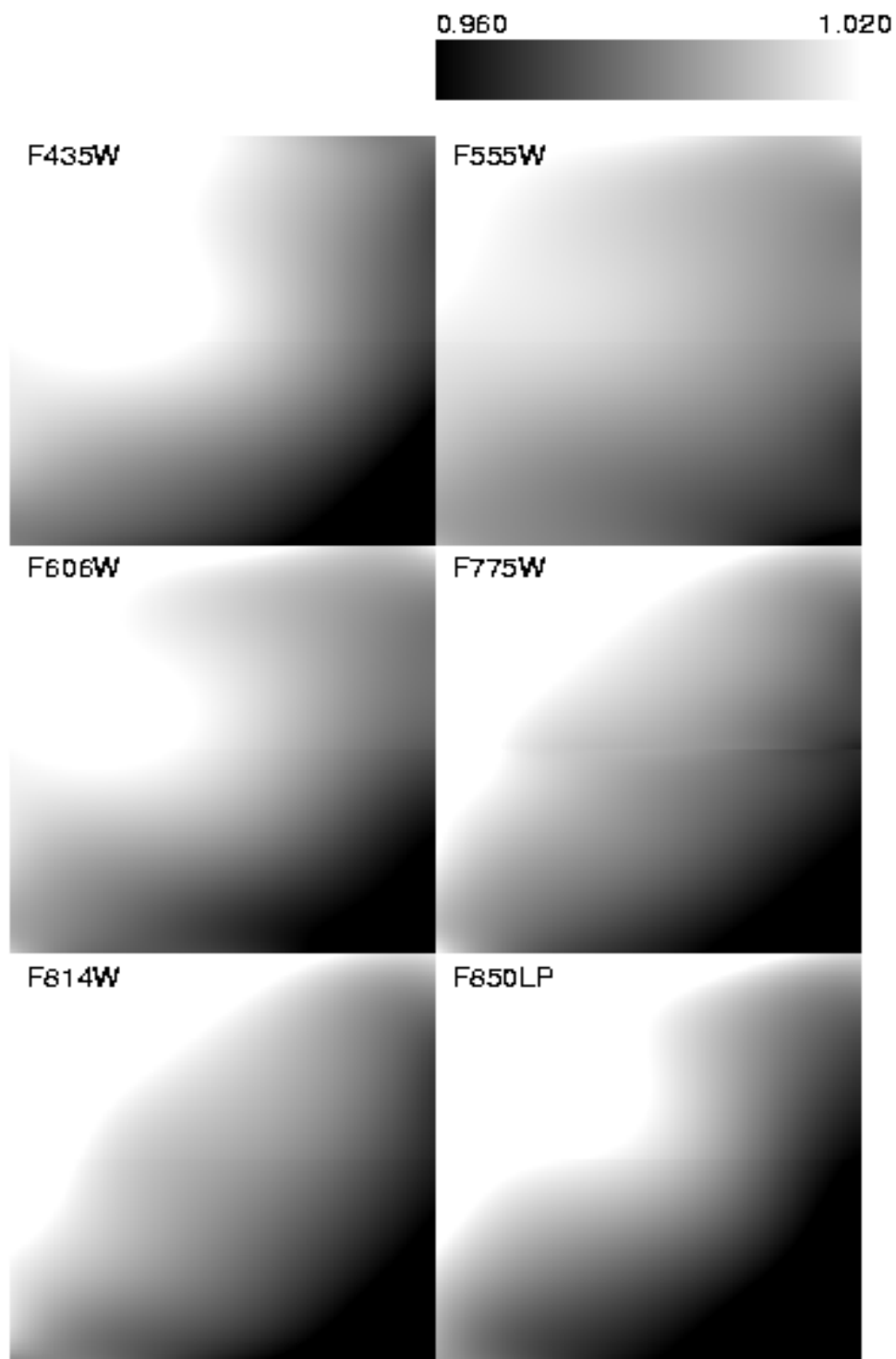


Figure 5.12: HRC low frequency (L-flat) flat-field corrections required for the laboratory flats. This correction ranges from +/- 3% for the F555W filter to +/- 6% for the F850LP filter.

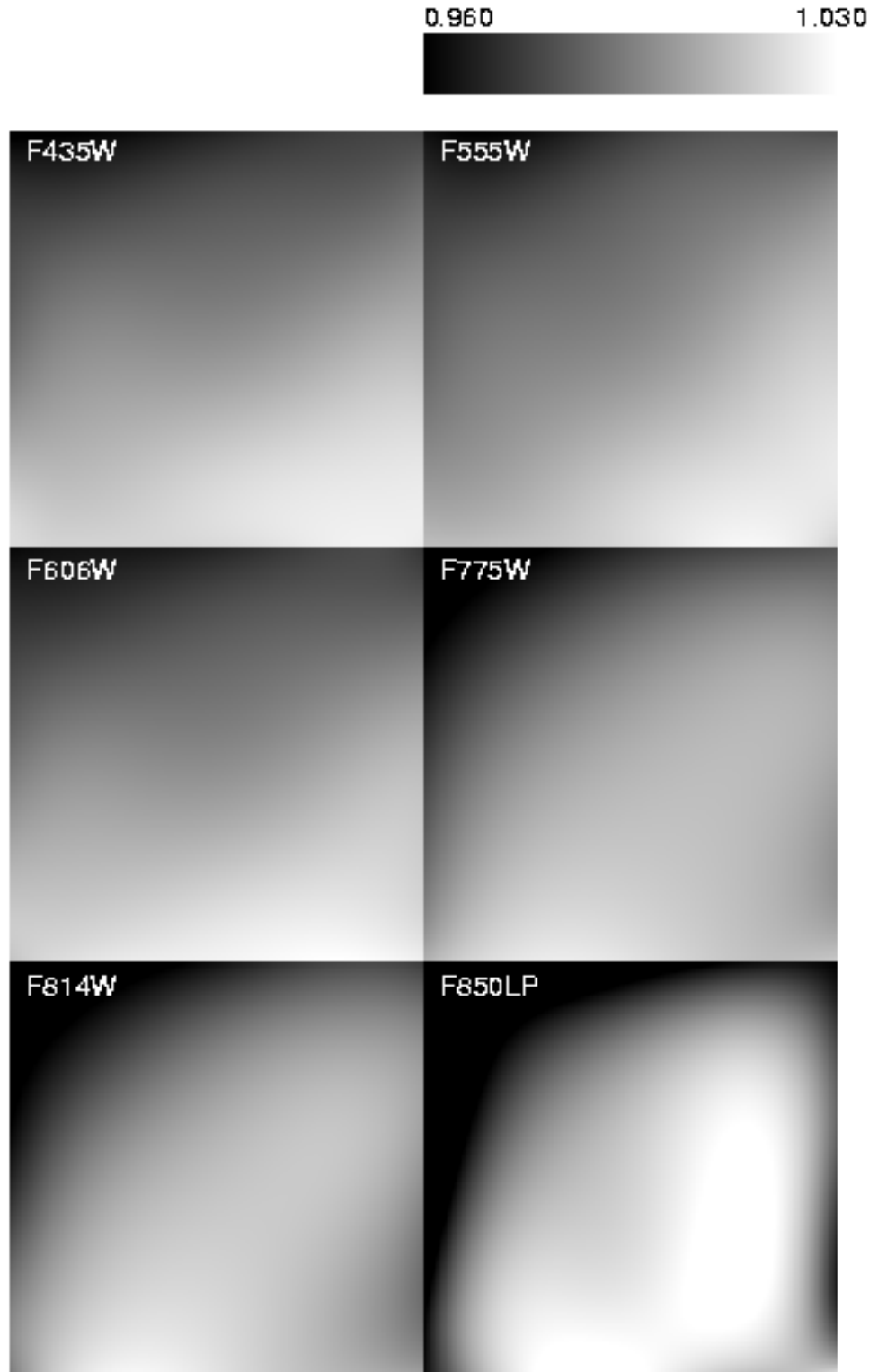
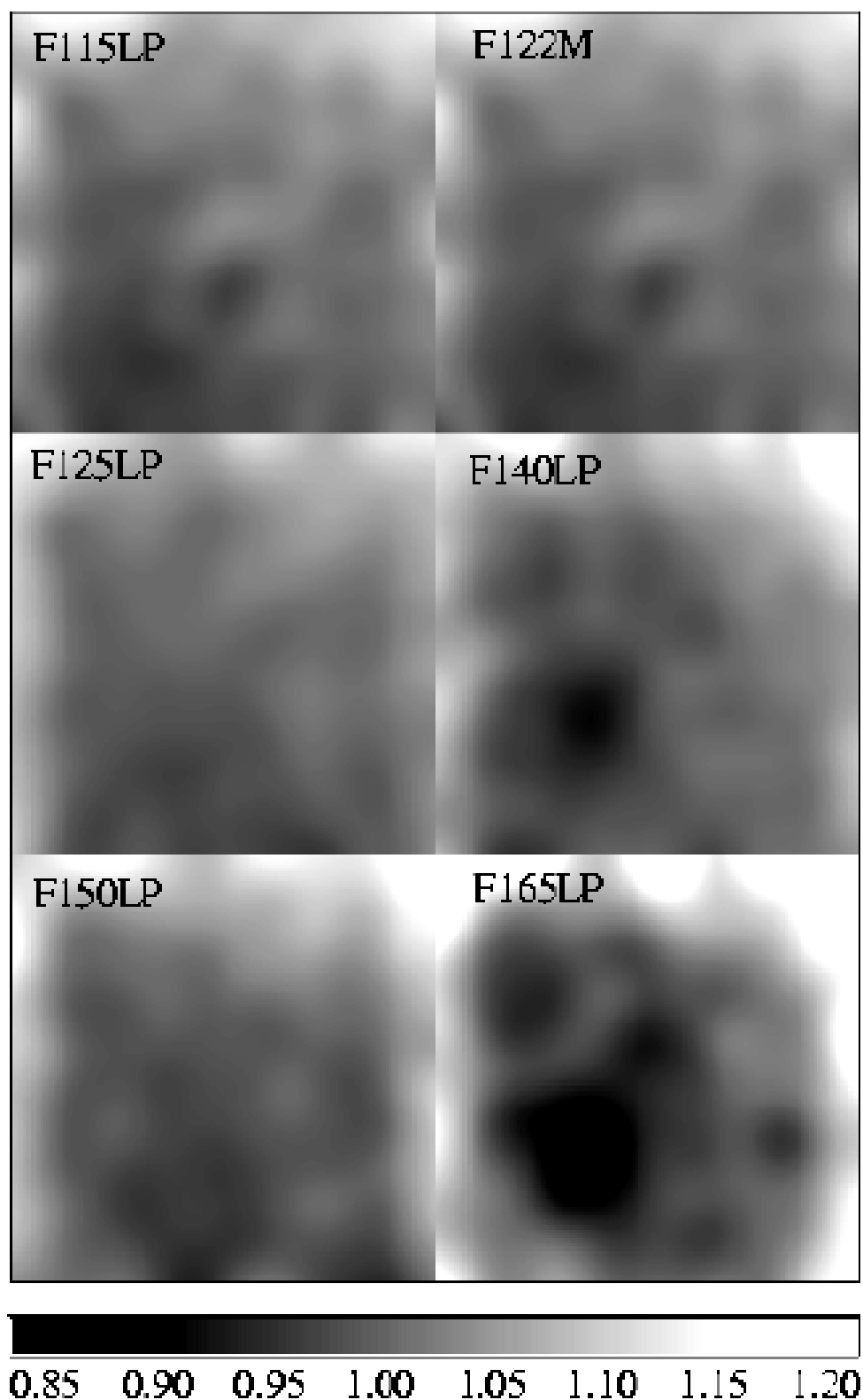


Figure 5.13: SBC low frequency (L-flat) flat-field corrections required for the inflight deuterium lamp data. This correction ranges from +/-8% for the F115LP filter to +/-20% for the F165LP filter.



### 5.4.3 Pipeline Flats

The inferred L-flat corrections were multiplied by the corresponding P-flats, and the resulting flat fields have been in use in the calibration pipeline. Observers are encouraged to check the ACS web site for the most recent flat fields available for recalibration at

[http://www.stsci.edu/hst/acs/analysis/reference\\_files/flats.html](http://www.stsci.edu/hst/acs/analysis/reference_files/flats.html)

Figure 5.15 shows the corrected WFC laboratory flats for several broadband filters. Note that on the sky a gap of  $\sim 50$  pixels exists between the top and bottom halves that is not shown here. The central donut-like structure is due to variations in chip thickness (see ACS ISR 03-06) and is dependent on wavelength. Pixels in the central region, for example, are less sensitive than surrounding pixels in the blue F435W filter and more sensitive in the red F850LP filter.

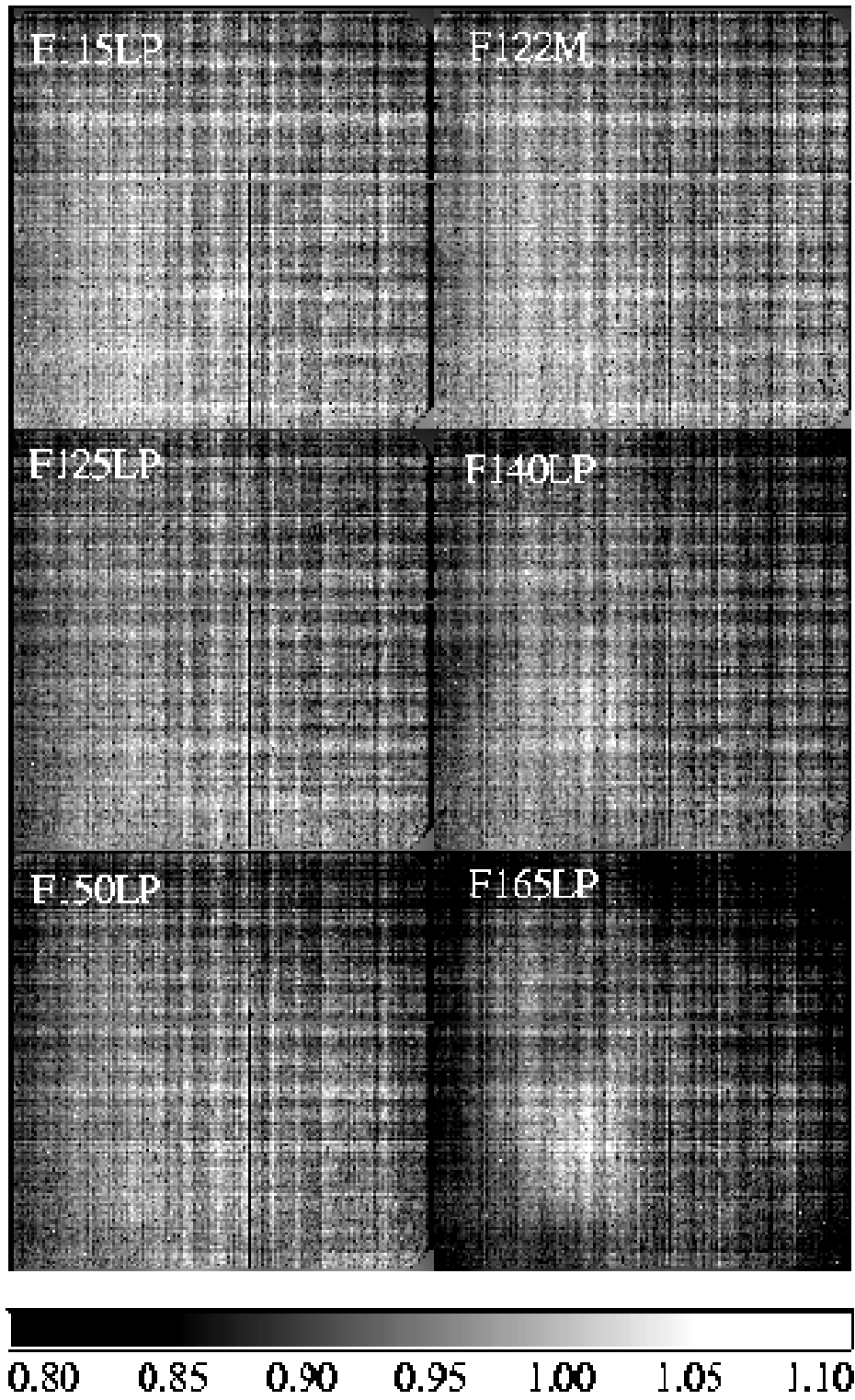
The HRC corrected laboratory flats for the same broadband filters are shown in Figure 5.16. The donut-like structure seen in the WFC response is not found in the HRC flats. The small dark rings are shadows of dust on the CCD window (see Section 5.5.1). The large dust mote seen in the WFC F606W flat is due to dust on the F606W filter. That portion of the filter is not “seen” by the HRC detector.

The SBC pipeline flats, a combination of the inflight deuterium lamp flat and the stellar L-flats, are presented in Figure 5.14.

Because of geometric distortion effects, the area of the sky seen by a given pixel is not constant; therefore, observations of a constant surface brightness object will have count rates per pixel that vary over the detector, even if every pixel has the same sensitivity. In order to produce images that appear uniform for uniform illumination, the observed flat fields include the effect of the variable pixel area across the field. A consequence of dividing by these flat fields is that two stars of equal brightness do not have the same total counts after the flat fielding step. Thus, point source photometry extracted from a flat fielded image must be multiplied by the effective pixel area map (see Section 6.1.3). This correction is accounted for in pipeline processing by **MultiDrizzle** (see Chapter 4), which uses the geometric distortion solution to correct all pixels to equal areas. In the drizzled images, photometry is correct for both point and extended sources.



Figure 5.14: SBC Flat Fields



The accuracy of pipeline flats can be verified using a variety of complementary methods. In Section 5.4.2, we discussed how follow-up observations of the same stellar field can be used to verify the derived L-flat corrections. Alternately, observations of the bright Earth can provide a uniform flat field source for the complete OTA optical complement and incorporate both the low frequency L-flat and the high frequency pixel-to-pixel P-flat response. Earth flats are described in Section 5.4.4. For most filters, the flats agree to within  $\sim 1\%$ , except for the interpolated L-flat filters which usually agree to within  $\sim 2\%$ .

The third method for verifying the ACS pipeline flats is with sky flats. These can be made by filtering and summing many observations of a sparse field. Sky flats have been created for a few of the most frequently used broadband WFC filters and are discussed in detail in Section 5.4.5. The sky flats are generally similar to the corrected ground flats at the 1% level, in accordance with the results of the previous two methods. While the WFC can show residuals in the central donut-region which are as large as 2%, these are most likely due to differences in the color of the spectrum of the sky from that of the bright globular cluster stars used for the L-flat determination.

To summarize, the pipeline flats were created by correcting the pixel-to-pixel flats by low-frequency corrections derived from dithered stellar observations. For the most used modes, the flats are accurate to better than 1% across the detector. For a few filters, improved L-flats will be derived from additional stellar observations to improve the flat field errors to  $<1\%$  for all modes. Additional verification of the pipeline flats will be provided by both earth flats and sky flats, thus confirming the derived L-flats and setting limits to their dependence on the color of the source spectrum.

Figure 5.15: WFC Flat Fields

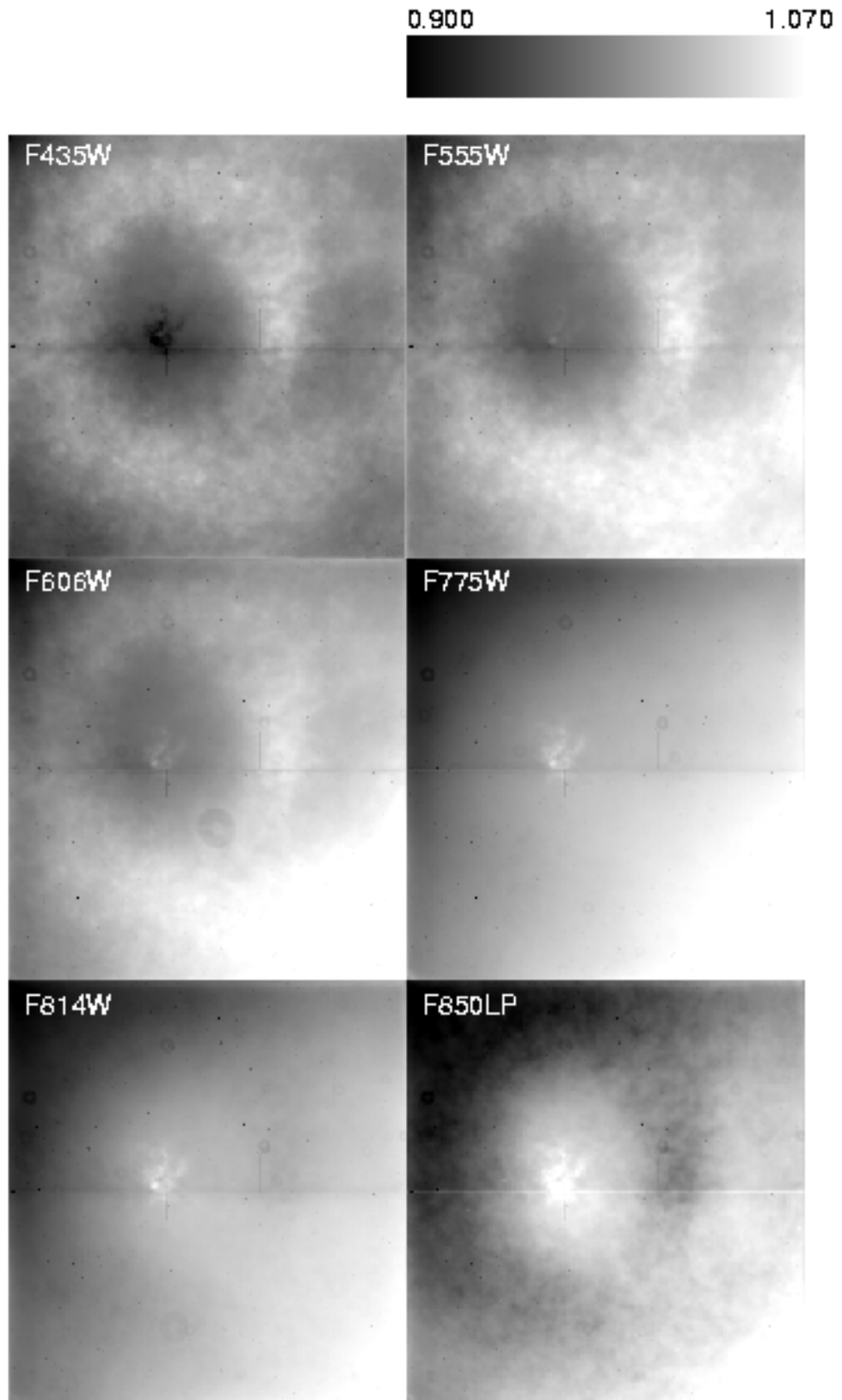
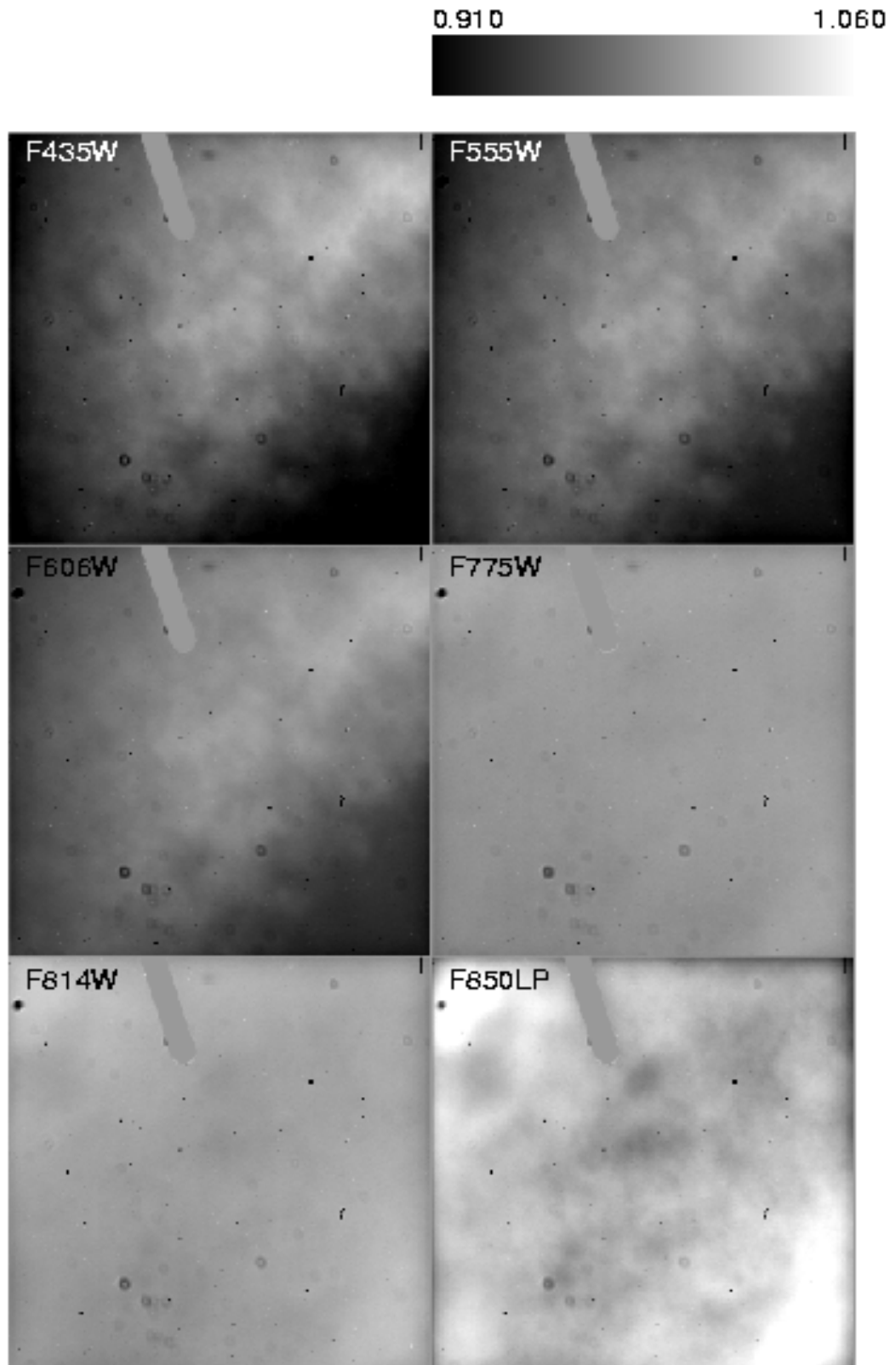


Figure 5.16: HRC Flat Fields



#### 5.4.4 Earth Flat Verification

Because the RAS/HOMS optics are opaque below 3500 Å (see Section 5.4.1), flat fields for the HRC UV filters were created using inflight observations of the bright Earth. The Earth is a poor flat field source at optical wavelengths because structure in the cloud cover can cause streaking in the flat. However, HRC modes that utilize the F220W, F250W, F330W, and F344N are immune to streaks because of the large optical depth down to the tropospheric cloud layers. The bright Earth then provides a uniform flat field source for the complete OTA+HRC optical complement. The required calibration flat, which incorporates both the low frequency L-flat and the high frequency pixel-to-pixel P-flat response, can be easily produced from these observations. Unfortunately, the red leaks in F220W and F250W are so large that the out of band light dominates, and the lab flats made with the deuterium lamp illumination (see [ACS ISR 01-11](#) for details) are superior to the observed earth flats for the modes that include these two filters. Because no L-flat correction has been applied, errors in the flats of +/- 2 to 4% corner-to-corner are expected for these filters. The HRC F330W and F344N pipeline flats, on the other hand, are defined entirely by the Earth flat data (see [ACS ISR 2003-02](#) and [ACS ISR 2005-12](#)). With ~20-30 observations each over the course of 3 years, these flats have very high signal-to-noise and show repeatability to much better than the required 1% accuracy.

The HRC Earth flats at wavelengths longward of 4000 Å often show streaking and non-uniformities from clouds or the terminator. However, a number of the images are free from these defects and provide an independent verification of the stellar L-flat correction technique at visible wavelengths. Unfortunately, the WFC Earth flats suffer from a shutter light leak, and the Earth limb is too bright for SBC observations, so the HRC is the best detector for comparison.

Several hundred observations of the bright Earth during occultation were obtained using the full set of HRC standard filters ([ACS ISR 2005-12](#)). In general, the flat fields are confirmed to a precision of ~1%, validating the stellar L-flat corrections. While the 'interpolated' L-flats were expected to have larger uncertainties (see Section 5.4.2), they do not appear to be significantly worse than the L-flats derived from direct observations. One exception is the F550M filter which shows a total deviation of more than 2%. Other exceptions are the four longest wavelength HRC filters which show large systematic differences with the pipeline flats. These differences appear to be caused by stray light originating from the detector surface, where most of the long wavelength photons are reflected and then scattered back from nearby focal plane structures. Any filter transmitting at these long wavelengths will see the extra pattern from this light, though the strength of the additional stray light will be proportional to the total flux of the source. Thus, for large diffuse objects that fully illuminate the detector, these Earth flats are more

appropriate for calibration than the existing pipeline flats, which are appropriate for point sources.

### 5.4.5 Sky Flats

The ACS sky flat program takes advantage of the many survey programs that have executed on ACS, such as the GOODS program, to build high signal-to-noise flats. These non-proprietary data consist mostly of sparsely populated images with relatively uniform sky that can be stacked to further quantify the pixel-to-pixel variation of the instrumental response.

The GOODS program consists of either 15 or 16 unique pointings over 5 epochs for both the Chandra Deep Field South (CDFs) and the Hubble Deep Field North (HDFN) using the most commonly used F606W, F775W and F850LP filters in the WFC. In total between 50-70 images were stacked in each filter.

The sky flats were created by median combining the pipeline reduced FLT files after removing cosmic rays and masking all of the sources. Because the GOODS data contained 2-4 dithers at each pointing, depending on the filter, masking was necessary to eliminate the high values at each pixel. In addition before combining, each image was corrected for the pedestal bias signature and inspected for scattered light.

The combined sky flat in each filter was box medianed down to a 32x32 image, in order to directly compare it to the corrected ground flat. Since the sky flats were created starting from the pipeline calibrated FLT files, it will show any flat field signatures that were not accounted for by the pipeline. The resulting sky flats show variations across the field of view of <2% for each of the 3 filters. The CDFs and HDFN fields were analyzed separately and compared. The two fields showed excellent agreement (<1%) for all 3 filters. The inferred sky flats will be made available on the ACS web site and a future ISR will describe the sky flats in more detail. Please check the ACS web site for updates on this issue.

---

## 5.5 Image Anomalies

### 5.5.1 Dust Motes

Several circular patterns, consisting of a dark ring with a bright center, are visible in the ACS flat fields, with typical diameters of ~30 pixels on HRC and ~100 pixels on WFC. These artifacts are shadows of dust on the CCD windows and are weaker on the f/25 WFC than on the f/68 HRC. These motes can be seen in the WFC and HRC flats in Figure 5.15 and Figure 5.16. Since the shapes and depths of these motes are almost

independent of wavelength, their effects will be removed by the flats to  $\ll 1\%$ , unless any of these particulate contaminants move to different positions on the CCD windows. In case of particulate migrations, the internal lamp flats have a lower f-ratio with a wider angular distribution and cannot be used to patch the flat fields, because they wash out the mote shadows. To correct for new motes, patches to the pipeline flats must be made using the original laboratory flats, corrected for the low-frequency flats derived inflight or, for short wavelengths, using observations of the bright earth.

Larger motes are sometimes present due to dust and blemishes on several ACS filters, including F606W, POL0V, and POL60V. Because the filters are located farther from the detector windows in a converging light beam, imperfections on the filters produce an out of focus image at the detector, where typical mote diameters are  $\sim 350$ - $400$  pixels on the WFC and  $\sim 250$ - $300$  pixels on the HRC. One of these large motes can be seen on chip 2 of the WFC F606W flat in Figure 5.15.

Until April 2004, the positioning accuracy of the filter wheels has been within  $\pm$  one motor step of the nominal position. This delta corresponds to a distance on the detectors of  $\sim 18$  HRC pixels and  $\sim 20$  WFC pixels. Features with sharp transmission gradients at the filter wheels cause a corresponding flat field instability, where errors are 1-3% for a few pixels near the blemishes. If the filter wheel lands in a different place the dust mote will move. Blemish misregistration is an error in the pixel-to-pixel high frequency component of the flat fields and is not related to the low-frequency L-flat correction, which has been applied for all standard and polarizing filters. For details on the L-flat correction, see Section 5.4.2.

This problem was recognized and addressed before launch by a laboratory calibration campaign to obtain flat fields at the nominal position and at plus and minus one step for the F606W+CLEAR on the WFC and for the two POLV filters in combination with the highest priority F475W, F606W, and F775W filters on both HRC and WFC. Since the resolver position uniquely determines the filter wheel step, the ACS pipeline data processing has been enhanced to automatically apply the proper flat for the wheel step position. The keyword FWOFFSET has been added to the ACS image headers to indicate the position of the filter wheel. In April 2004 an update was made to the ACS flight software and the filter wheel is now always positioned at its nominal position. For more information on flat fields for filter wheel offset positions, refer to [ACS ISR 03-11](#).

### 5.5.2 Optical Ghosts and Scattered Light

The ACS was designed with a requirement that no single straylight feature may contain more than 0.1% of the detected energy in the object producing it. This goal has generally been met, but during the extensive ground and SMOV test programs a few exceptions have been identified

(Hartig et al. 2002, Proc SPIE 4854) such as the WFC elliptical haloes and the F660N ghosts. While these ghosts exceed the specified intensity, their origin and characteristics are well defined and they should have minimal impact on the ACS science program. We describe below in more detail some of the optical ghosts relevant for ACS.

- WFC elliptical haloes: These ghosts are caused by reflection from the CCD surface (which lies at an  $\sim 20$  degree angle to the chief ray) up to the detector windows and back to the CCD. They show up as pairs of elliptical annuli, aligned along the negative diagonal of the FOV (see Figure 5.17), and are observed when bright sources are placed on the lower right (D amplifier) quadrant of the WFC detector. The surface brightness of the annuli increases and size decreases with proximity to the corner. Two pairs of ghosts are seen, produced by reflection from the four window surfaces. The total energy fraction in each ghost may exceed 0.2% of the target signal.
- F660N ghosts: The F660N narrow band filter produces pairs of relatively bright circular annuli stationed near to (but radially outward from) the target image (see Figure 5.18). This is due to reflection from the two surfaces of the second "blocker" substrate back to the many-layer dielectric stack on the first substrate, which in turn reflects at high efficiency at the filter wavelength range. These haloes contain  $\sim 2\%$  of the detected target energy and are always  $\sim 10$  and  $20$  pixels in diameter.
- Annular ghosts: Large annular ghosts near their parent images are caused by reflection from the detector windows, back to the filters, then returning to the CCD. The fringes arise from interference between the HeNe laser light reflections from the two surfaces of the windows (Figure 5.17). Another type of annular ghost arises from reflections between the inner and outer window surfaces; these are much smaller in diameter, relatively low in intensity (well within the specification) and are displaced radially from the parent image by a small amount.

In general, little can be done about ghosts and blooming in the post-observation data processing phase. Instead, some judicious planning of the actual observations, particularly if bright sources are expected in the field of view, is recommended. For instance, the impact of diffraction spikes (which for ACS lie along X and Y axes) and of CCD blooming (which occurs along the Y direction) due to a bright star, can be reduced by choosing an ORIENT which prevents the source of interest from being connected to the bright star along either of these axes. Alternatively, a suitable ORIENT could move the bright star(s) into the interchip gap or off the field of view altogether. Similarly, the impact of WFC elliptical haloes can be minimized by avoiding a bright star in the quadrant associated with amplifier D.



Figure 5.17: Optical ghosts, diffraction spikes, and blooming. This image was obtained during ground calibration at Ball Aerospace using a HeNe laser (633nm) through F625W. It is a factor of  $\sim 50,000$  saturated with 9 highly saturated point sources in and just off of the field of view. Note the diffraction spikes along the X and Y axes of the WFC, and the severe blooming of the charge along the Y axis. Several optical ghosts with different origins and intensities (see text for details) are visible: (a) WFC elliptical haloes show up in the lower left as pairs of elliptical annuli aligned along the negative diagonal of the FOV; (b) Large annular ghosts are seen near their parent images; (c) To the lower right, there exist smaller fainter annular ghosts which tend to be displaced radially from the parent image by a small amount.

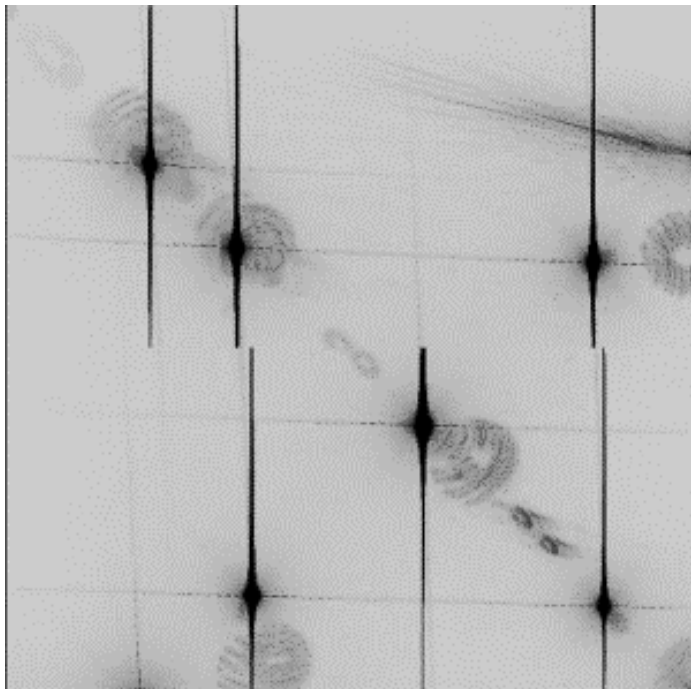
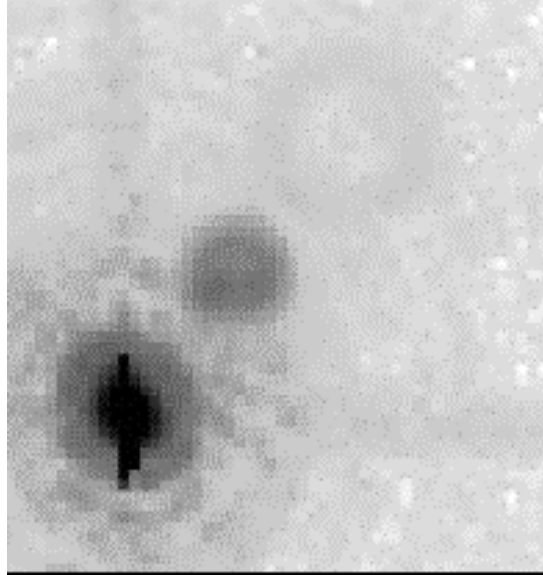


Figure 5.18: F660N optical ghosts. This 700 s F660N exposure illustrates the F660N ghosts, namely pairs of relatively bright circular annuli stationed near to (but radially outward from) the target image. These haloes contain  $\sim 2\%$  of the detected target energy and are always  $\sim 10$  and  $20$  px in diameter.



### 5.5.3 Cross Talk

Images obtained with the WFC are affected by a small amount of electronic cross talk between the four CCD quadrants that correspond to the four amplifiers of the two detectors. The effect produces electronic "ghost" (i.e., negative) images in a given quadrant that mirror real images recorded on other quadrants. Figure 5.19 shows an example of the cross talk in one of the images obtained during the Great Observatories Origins Deep Survey (GOODS) program, a pointing in the GOODS-S field taken through the F850LP passband. Source images a, b, c and d, which are recorded on quadrant C, produce negative ghost images a', b', c', d', a'', b'', c'', d'', and a''', b''', c''' and d''' in quadrants A, B and D, respectively.

Inspection of images affected by cross talk reveals a number of interesting characteristics of this effect. The cross talk ghosts have a surface brightness that is a few electron lower than those of the average background and there does not appear to be a simple proportionality between the light profile of the sources and the ghosts. Rather, as Figure 5.20 shows, the strength of the cross talk, measured as the average surface brightness of ghosts, seems to be roughly proportional to the logarithm of the sources.

The intensity of the cross talk ghost also appears to vary depending on which quadrant hosts the source and which hosts a ghost. For example, sources in quadrant D of Figure 5.19 produce clearly visible ghosts in quadrant C, but much fainter ghosts (if any at all) in quadrant A and B.

Also, sources in quadrant A and B do not seem to produce any obvious ghosts in the other quadrants.

Figure 5.19: Cross Talk in the WFC Detectors. Due to the cross talk, galaxies a, b, c and d recorded in quadrant C have mirror ghost images in quadrants A, B, and D. Note the effect appears stronger in quadrants C and B than in quadrant A, and that sources in quadrant D produce ghosts that follow a similar trend. However, sources in quadrants A and B do not seem as effective in producing ghost images.

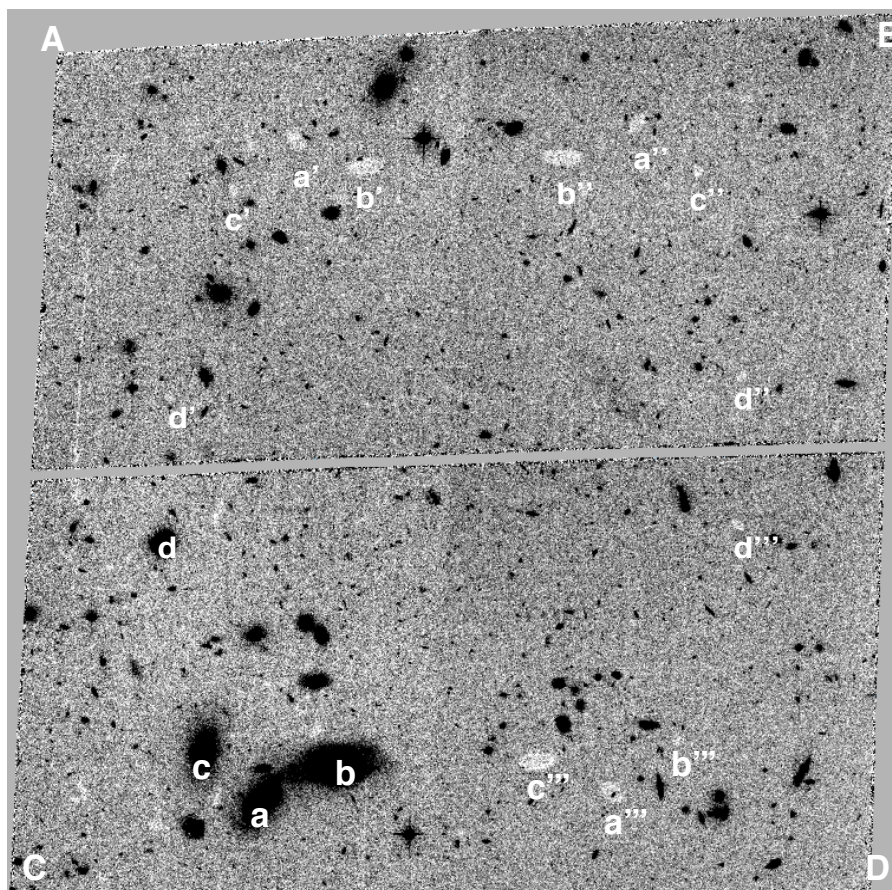
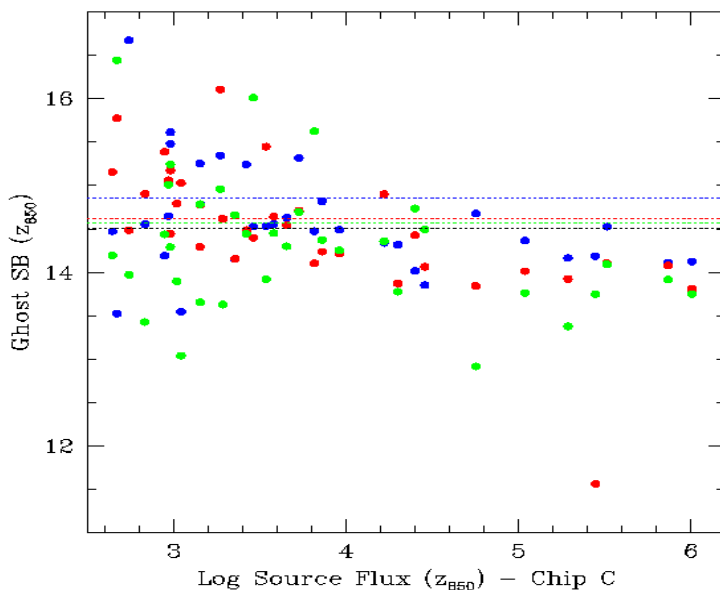


Figure 5.20: The average surface brightness of ghost images plotted as a function of the flux of the sources. All sources are in quadrant C. There is a correlation between the surface brightness of the ghosts and the flux of the sources.



The magnitude of the cross talk depends on the background of the victim quadrant, the sense of the correlation being that the cross talk is stronger when the background is lower. Figure 5.21 shows that in images with low background the cross talk creates ghosts whose surface brightness is  $\sim 40\%$  lower than the average background. In images with high background the ghost surface brightness is only  $\sim 3\%$  lower.

Tests on existing images show that the cross talk has minimal impact on flux measurements of sources superimposed on ghost images and thus mostly presents a cosmetic issue. The bottom panel of Figure 5.22 shows six growth curves of the same star derived from six individual frames, all with identical exposure time and filter. In three of the frames, due to the adopted dithering strategy, the star is located within a major ghost image (the annulus around the photometric aperture is also within the ghost image), while in the remaining three frames the star is outside the ghost image. The observed photometric scatter is typical for a star with this brightness of post-pipeline processed data (FLT files) with no correction for geometrical distortions and no cosmic ray removal. As a comparison, the upper panel shows the growth curves of a star of comparable apparent magnitude in the same frames but located in an region unaffected by cross talk. The photometry of the latter star has the same amount of scatter as the former one, showing in particular that the cross talk acts as an additive effect and not as a multiplicative one.

Figure 5.21: The dependence of the cross talk, measured as the difference of the sky background in affected and non affected areas, as a function of the sky background. The strength of the cross talk diminishes as the background increases.

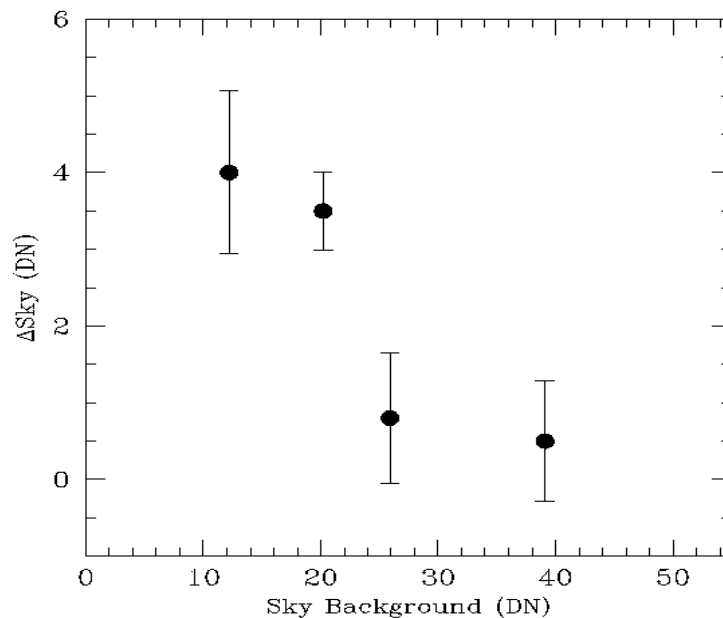
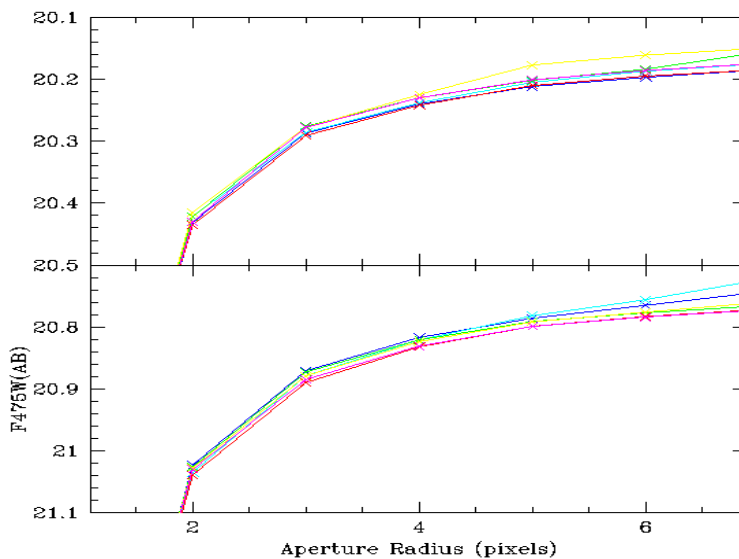


Figure 5.22: BOTTOM - Six growth curves of the same star derived from six individual frames, all with identical exposure time and filter. In three of the frames, due to the adopted dithering strategy for the observations, the star is located within a major ghost image (the annulus around the photometric aperture is also within the ghost image), while in the remaining three frames the star is outside the ghost image. The observed photometric scatter is typical, for a star with this brightness, of post-pipeline processed data (FLT files) with no correction for geometrical distortions and no CR removal. TOP - As above but for a star of comparable apparent magnitude and in the same frame that is located in a region unaffected by cross talk. The photometric scatter of the two stars is very similar.





There is evidence that the strength of the cross talk is significantly weaker in images acquired with GAIN=2, than in images taken with GAIN=1. Figure 5.23 shows two exposures through the same filter and with the same exposure time, the former acquired with GAIN=1 (upper panel), the second with GAIN=2 (lower panel). Cross talk ghosts are clearly observed in the former image, but not in the latter one. A more quantitative comparison supports the visual inspection. Figure 5.24 shows the median value of pixels in ghost images as a function of the source pixel flux, i.e., of pixels located in mirror symmetric locations relative to the pixels in the source quadrant.

Observers who do not need to sample the readout noise of the CCD with the accuracy afforded by the GAIN=1 setting, might want to consider to use GAIN=2 in order to minimize the cross talk.

At this time we have not yet determined a robust way to predict the size of a cross talk residual and the exposure parameters on which it depends. Efforts are ongoing to identify algorithms to remove the effect of cross talk from the WFC images and we encourage GO's to look for updates on the [ACS STScI web page](#).

Figure 5.23: Two exposures through the same filter (F814W) and with the same exposure time (22.5 sec), the former acquired with GAIN=1 (TOP), the second with GAIN=2 (BOTTOM). Cross talk ghost images are observed in the former image, but not in the latter one.

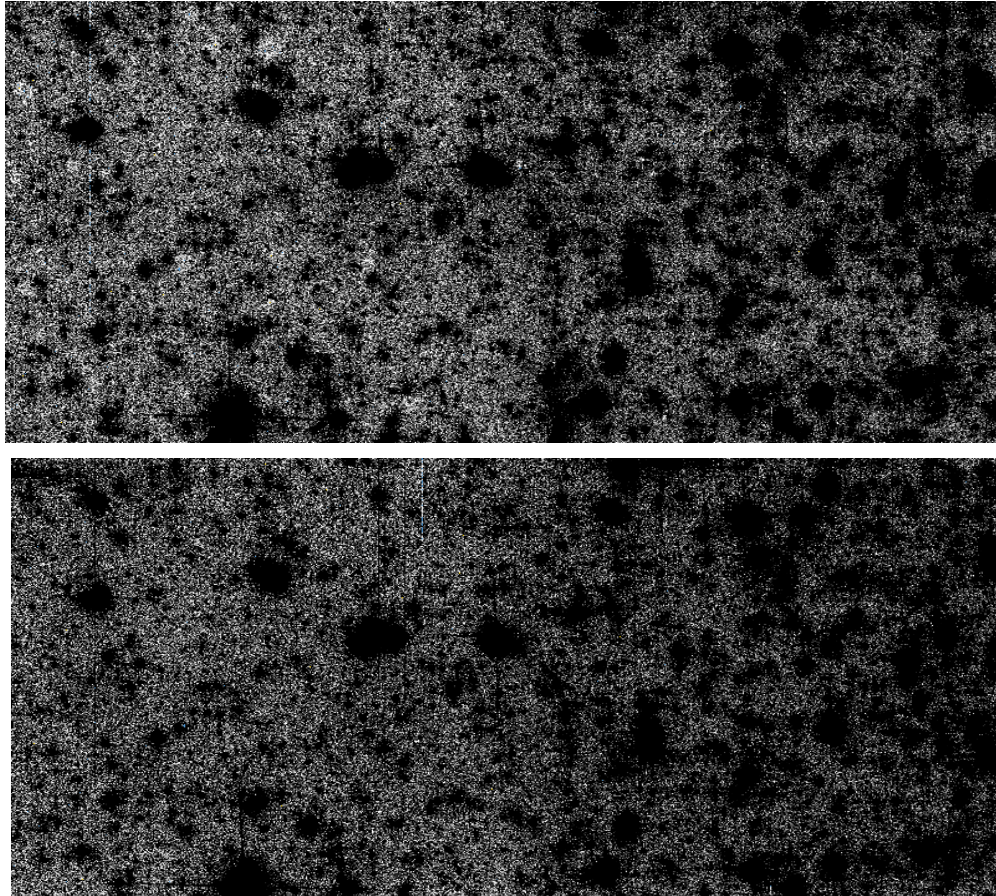
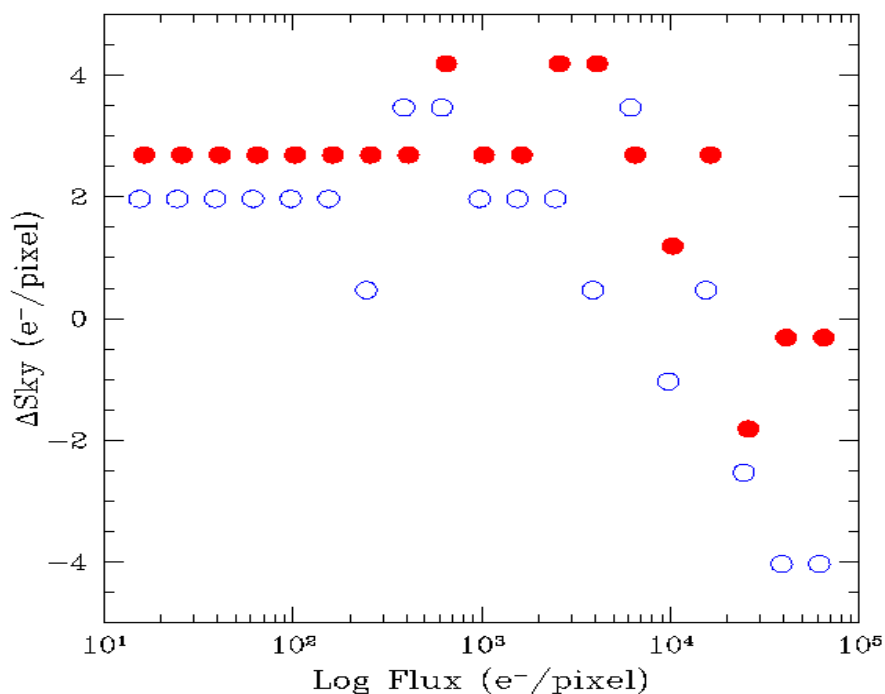


Figure 5.24: The median value of pixels in ghost images as a function of the source pixel flux, i.e. of pixels located in mirror symmetric locations relative to the pixels in the source quadrant, derived from the CCD frames shown in Figure 5.17. The images are sky subtracted. Source pixel flux is binned in logarithmic bins 0.2 in size. Using the median ensures that mostly background pixels, as opposed to pixels affected by sources, are being considered in the analysis. Filled symbols are for GAIN=2, hollow one for GAIN=1. The pixels in the image with GAIN=1 have systematically lower values than those of the image with GAIN=2, an indication that the cross talk is stronger in this case. Their values also decrease as a function of the source pixel value more steeply than in the GAIN=2 case.



### 5.5.4 Scattered Earth Light

Most observers will not experience significant issues with scattered Earth light in their observations. Normally observations are scheduled only when the bright Earth limb is more than 20 degrees from the HST pointing direction. This is sufficient to eliminate serious impacts from scattered Earth light -- the most severe impact will be for observers with targets in the CVZ who may notice the sky background increased by a factor of 2 or 3.

It is possible to make arrangements for observations at smaller bright Earth limb angles, and these images have a potential for serious impacts from scattered light. There are two types of impact: elevated background and non-uniformity in the background. For example, at a bright Earth

avoidance angle of 14 degrees it is possible for the sky level to be increased by a factor of 100 compared to normal pointings away from the Earth; this will of course have a serious impact on the background noise and detection of faint targets. Also, non-uniformity can arise since the scattered light is taking an increasingly non-standard path through the HST optics, and hence the flat fielding becomes corrupted. At this same angle of 14 degrees, it is possible to have both large scale gradients across the field of view (up to ~20% amplitude in the WFC) and small scale features in the background (up to ~12% in WFC and ~30% in the HRC). See [ACS ISR 2003-05](#) for more details.

---

## 5.6 Generic Detector and Camera Properties

### 5.6.1 Gain Calibration

The ACS CCDs have default gain values of approximately 2 e-/DN for both the WFC and HRC (prior to Cycle 14 the WFC default was 1e-/DN). The relative values of gains 1 and 2 for the WFC are determined to an accuracy of about 1 part in 10,000. Although the original default settings were used to establish adjustments to basic quantum efficiency curves, current gains have consistent values. Minor errors in the default gain values would therefore be absorbed into revisions of the QE curves. There is no compelling reason to seek refinement in the quantitative values of the default used for primary calibrations and the bulk of the science program.

The default gain for the WFC does sample the full well depth of the CCDs, the HRC default falls short by 22%. Use of the next higher gain value of approximately 4 e-/DN for the HRC does provide full sampling of the 165,000 e- full well depth. Since the readout noise is only marginally higher than with the default gain, and the readout noise for the HRC is nearly critically sampled even at the higher value (much more so than any WFPC2 data ever taken), many science and calibration programs may logically choose this gain.

ACS gain values in use between on-orbit installation and January 2004 can be traced to ground test results. The primary tool for measuring gain values is the photon-transfer method which is described in the Appendix at

[http://acs.pha.jhu.edu/instrument/calibration/results/by\\_instrument/detector/wfc/build4/gain/](http://acs.pha.jhu.edu/instrument/calibration/results/by_instrument/detector/wfc/build4/gain/)

This technique relies on analysis of pairs of identical exposure flat fields taken at a range of intensity levels. Over an ensemble of pixels at a given exposure level, the relation between differences of intensity values (noise) and the direct signal level depends on the readout noise and the gain. This relation can be fit at a range of intensity levels to uniquely determine these two quantities. This technique can also provide limited information on linearity (which depends on the constancy of the lamp source, or experimental techniques to control for drifts) and the saturation count level



(which may be different for a uniform illumination pattern than for point sources) by determining where the photon-transfer curve departs from linearity at high signal levels. Errors of about 0.6% in the gain values are quoted for the WFC determinations, and similar values hold for the HRC as given at

[http://acs.pha.jhu.edu/instrument/calibration/results/by\\_instrument/detector/hrc/build1/gain/](http://acs.pha.jhu.edu/instrument/calibration/results/by_instrument/detector/hrc/build1/gain/)

On the WFC, with two CCDs and the default use of two readout amplifiers per CCD, errors of 0.6% in the normalization of gains quadrant-to-quadrant would leave easily visible steps in observations of spatially flat sources. A redetermination of the WFC gains (ACS ISR 02-03), maintaining the same mean over all amplifiers at a given gain setting but using a continuity constraint across quadrant boundaries, provided an improvement in amplifier-to-amplifier gains at better than 0.1% for the default gains. Any steps of intensity seen in data across quadrant boundaries are likely to reflect minor errors in bias and overscan values (see section 5.2), rather than errors in relative gains.

In ACS ISR 04-01 on-orbit data was used to redetermine the mean absolute gain values relative to the standard adopted for the default gains on each camera, e.g., WFC GAIN=1 and HRC GAIN=2 values were retained and other gains adjusted relative to these. Through analysis of observations of the same stellar field, in the same filter and at the two gain settings it is possible to obtain accurate adjustments of these gain values relative to the default gain levels. The results discussed here supply these to better than 0.1%, removing errors that averaged about 1% for the two cameras prior to updates made in January 2004.

Absolute errors of about 0.6% could remain in the default gain values, but these are of no real consequence since redetermination of the CCD quantum efficiency would compensate for this, since the QE adjustments were based on data acquired with the default gains. Basic photometric calibrations apply with equal accuracy to data acquired at all supported gains (assuming for the non-default gains that reprocessing was done after January 6, 2004 to include the revised values).

### High Resolution Camera

The prelaunch GAIN = 4 value using the default AMP C is 4.289. The revised value based on on-orbit calibrations is 4.235. For GAIN = 1 (less important since this is available-but-unsupported), the prelaunch value of 1.185 has been revised to 1.163.

### Wide Field Camera

Revisions of WFC GAIN = 2 values based on on-orbit testing are for prelaunch (new): AMP A 2.018 (2.002), AMP B 1.960 (1.945), AMP C 2.044 (2.028), and AMP D 2.010 (1.994). And for the available-but-unsupported GAIN = 4 the prelaunch (new) values are: AMP A 4.005 (4.011), AMP B 3.897 (3.902), AMP C 4.068 (4.074), and AMP D 3.990 (3.996).

## 5.6.2 Full Well Depth

Conceptually, full well depths can be derived by analyzing images of a rich star field taken at two significantly different exposure times, identifying bright but still unsaturated stars in the short exposure image, calculating which stars will saturate in the longer exposure and then simply recording the peak value reached for each star in electrons (using a gain that samples the full well depth, of course). In practice, as discussed in [ACS ISR 04-01](#), it is also necessary to correct for a ~10% "piling up" effect of higher values being reached at extreme levels of over-saturation relative to the value at which saturation and bleeding to neighboring pixels in the column begins.

Since the full well depth may vary over the CCDs, it is desired to have a rich star field observed at a gain that samples the full well depth, and for which a large number of stars saturate. Calibration programs have serendipitously supplied the requisite data of rich fields observed at two different exposure times.

### High Resolution Camera

The HRC shows large scale variation of about 20% over the CCD. The smallest full well depth values are at about 155,000 e- and the largest at about 185,000 e-, with 165,000 representing a rough estimate at an area weighted average value. See Figure 3 of [ACS ISR 04-01](#) for details.

### Wide Field Camera

As with the HRC there is a real and significant large scale variation of the full well depth on the WFC CCDs. The variation over the WFC CCDs is from about 80,000 e- to 88,000 e- with a typical value of about 84,000 e-. There is a significant offset between the two CCDs. The spatial variation may be seen as Figure 4 in Gilliland [ACS ISR 04-01](#).

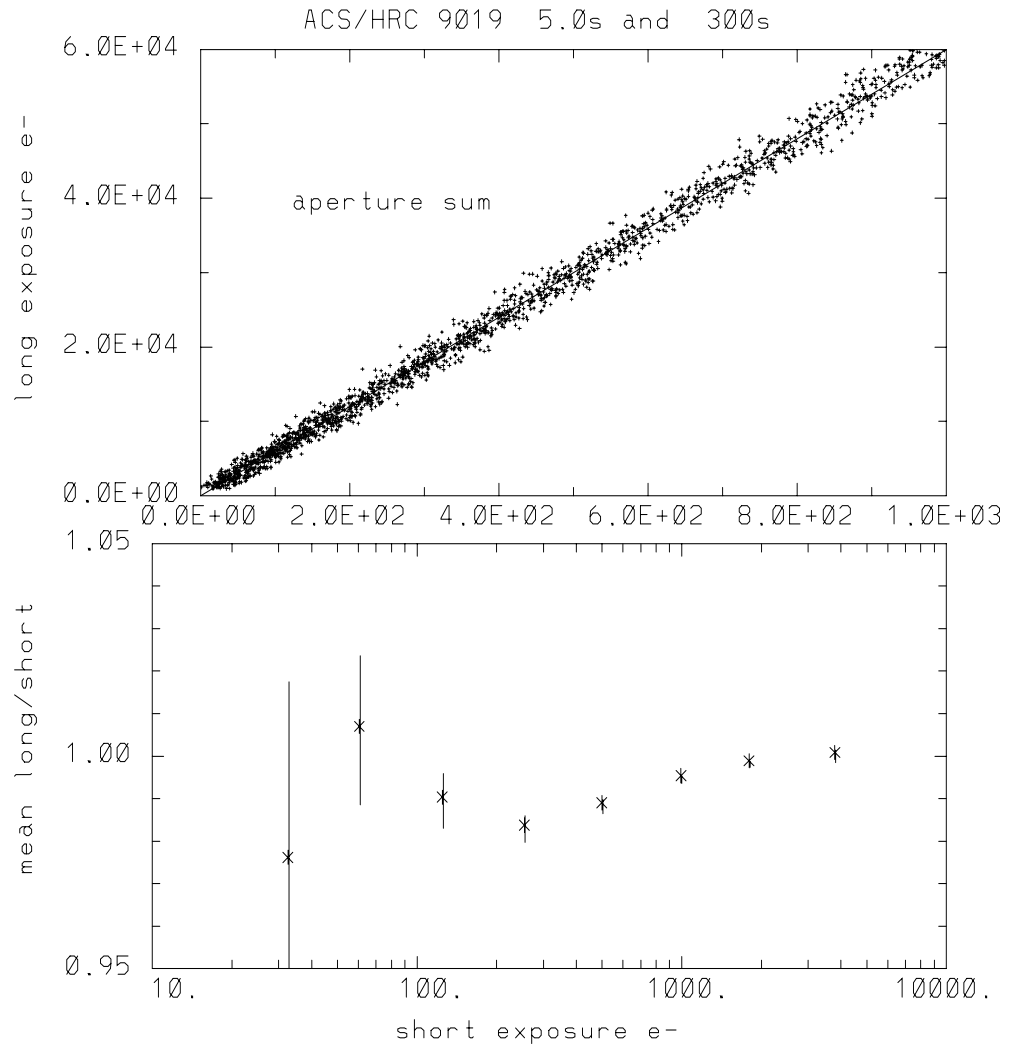
## 5.6.3 Linearity at Low to Moderate Intensity

### High Resolution Camera

Rich star fields observed at quite different exposure times provide a simple, direct test for linearity. In Figure 5.25 the results of such tests are shown in two ways. The first is a simple plot of aperture sum values in the long exposures versus the same stars on the same pixels in the short exposure -- no deviations from linearity are evident. For a more sensitive test the bottom plot shows the results of summing counts over all stars within a defined magnitude range in the short and long cases separately, before then taking the ratio and normalizing to the relative exposure times.

The linearity of the HRC at low and moderate intensity levels, as evidenced by comparing stars observed with exposures differing by a factor of 60, appears to be excellent.

Figure 5.25: The upper panel shows aperture sums over 9 pixels for all stars used over a range emphasizing results at low to moderate count levels. The plotted line has a slope set by the relative exposure time. In the lower panel the ratio of counts in ensembles of stars divided into factor of two intensity bins, and further normalized by the relative exposure time are shown. One sigma error bars are derived based on the ensemble signal to noise of the short exposure case. The lowest bin has 81 stars, with typical values of 400 stars per bin above this.

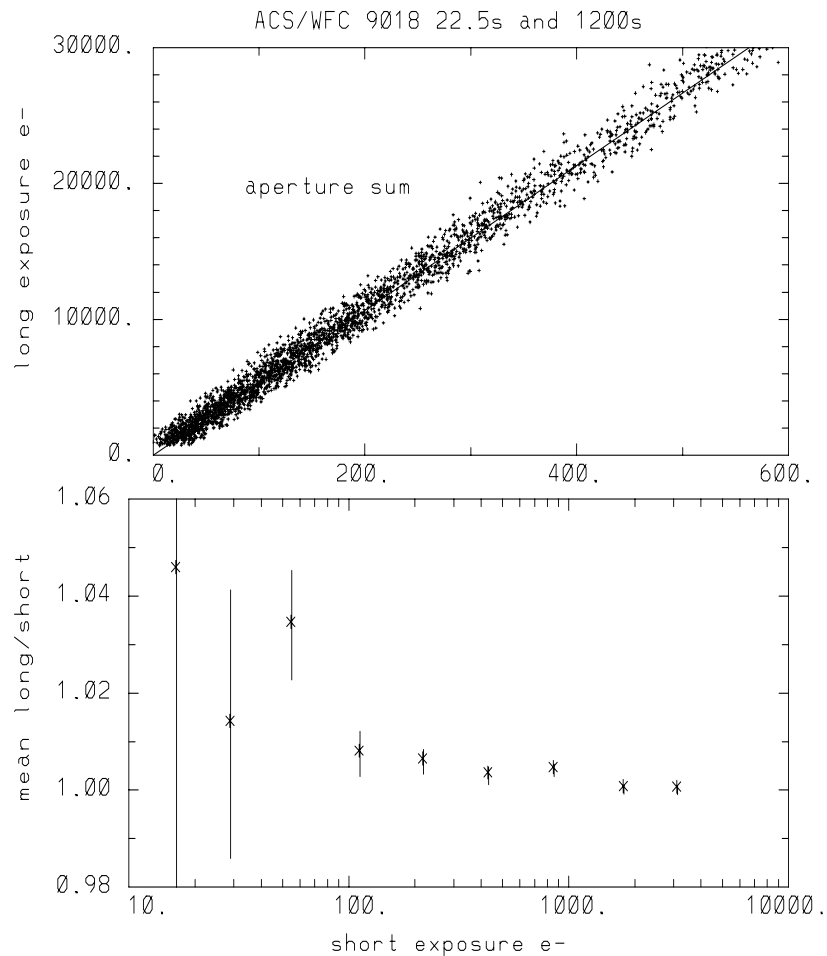


### Wide Field Camera

As shown in Figure 5.26 counts within small apertures suggest excellent linearity down to quite low exposure levels of about 5 e- in the central pixel for stellar sources, i.e., down to a level where individual stars cannot be recognized in single exposures. The data used for this test were taken in April, 2002, only one month after on-orbit installation of ACS. CTE effects are of course a source of low-intensity non-linearity (that correlates with y-positioned detector) and should have been very small at this early date (tests verified this). By contrast, for the approximately one year after launch observations used in ISR 2003-09 (quantifying CTE more

generally), the CTE impact (at middle of CCDs) at the three lowest intensity levels in Figure 5.27 are at 24, 16, and 10.3% respectively. Thus, any intrinsic non-linearities that may exist at low intensity levels are small compared to the normal losses expected from CTE growth after ACS had been on orbit for only a few months. Within the mutual error bars results for the GAIN = 2 comparisons are entirely consistent -- the low-level linearity of the WFC channel is obviously excellent.

Figure 5.26: The upper panel shows simple aperture sums for the long and short exposures for all stars of low-to-moderate intensity, the line has a slope set by the relative exposure times. The lower panel shows ratio of counts summed over all stars within intensity bins (in factor of two steps) for the 1200 second to mean 22.5 second exposures after normalization to the relative exposure time. To account for minor encircled energy differences for the very small 9 pixel (total, not radius) apertures used all points have been normalized by 1.006, the initial value for the brightest bin. The error bars show plus/minus one sigma deviations based on the total signal to noise of the short exposure sums. The number of stars per bin is typically about 400, although the lowest bin contains only 33 stars.



### 5.6.4 Linearity Beyond Saturation

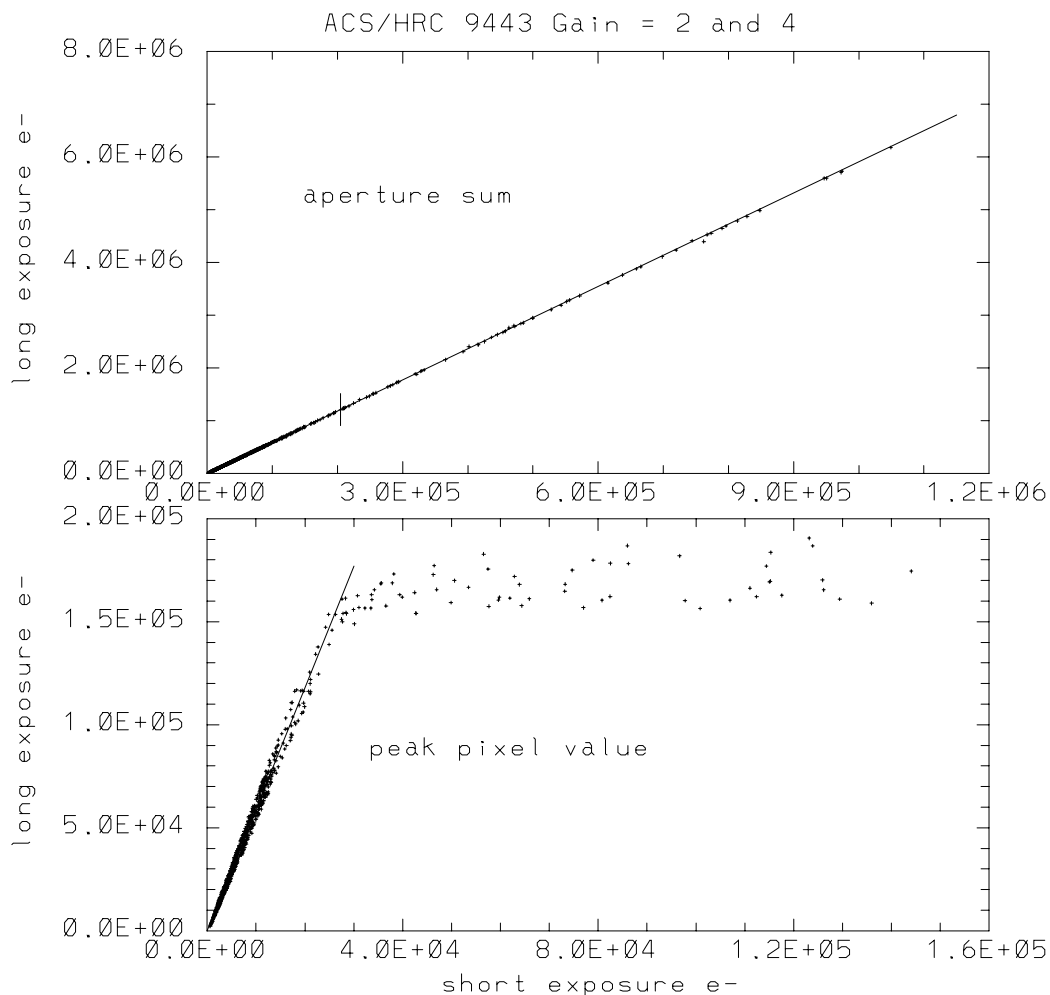
The response of the ACS CCDs remains linear not only up to, but well beyond, the point of saturation when using a GAIN value that samples the full well depth. [ISR 04-01](#) shows the well behaved response of the ACS: electrons are clearly conserved after saturation. This result is similar to that of the STIS CCD (Gilliland et al., 1999, PASP, 111 1009-1020) and the WFPC2 camera (Gilliland, R.L. 1994, ApJ, 435, L63-66). It is possible to easily perform photometry on point sources that remain isolated simply by summing over all of the pixels bled into with a GAIN value that samples the full well depth. Given the extra dynamic range afforded before saturation at GAIN=2 (WFC) and GAIN=4 (HRC), and the only modestly increased readout noise coupled with the potentially beneficial aspect of being able to recover photometry on saturated objects, more frequent use of these GAIN values may be appropriate.

Here the extent to which accurate photometry can be extracted for point sources in which one or more pixels have exceeded the physical full well depth is explored. Only the cases of GAIN = 4 for the HRC and GAIN = 2 for the WFC are considered, which provide direct sampling of the count levels independent of whether saturation has occurred. Ideal data for these tests consist of multiple exposures taken back-to-back on a moderate-to-rich star field with a broad range of exposure times resulting in both unsaturated and saturated data for many stars.

#### High Resolution Camera

Figure 5.27 illustrates linearity beyond saturation. In the lower panel peak values in the long exposure are plotted against peak values from the short exposure. Over the expected linear domain, points fall within a narrow cone centered on a line that has a slope equal to the exposure time ratio while above this the values in the long exposure saturate as expected. Deviations from lying perfectly along the line here result primarily from a 0.1 pixel offset between the images used for this test leading to different relative fractions of light falling on the central pixel. The upper panel of Figure 5.27 shows the same stars but now using identical extraction apertures in the two exposures, the vertical tick mark near 205,000 e<sup>-</sup> on the x-axis flags stars below which the central pixel remained unsaturated, above which the central pixel experienced saturation. In the aperture sum data there is no difference in the long exposure photometric quality between stars that saturate, even up to a factor of 5, and those that do not. Within the domain sampled here the accuracy of saturated star photometry is much better than 1%.

Figure 5.27: The lower panel shows peak pixel values for many stars observed for 350 seconds (long) and 60 seconds (short) with the HRC; over the range for which stars are unsaturated in both exposures there is a linear relation with slope equal to exposure time ratio. Brighter stars in the long exposure saturate at values near the full well depth. The upper panel shows the same stars using photometry sums from identical apertures in both exposures, stars above the vertical mark near 205,000 on the x-axis separates stars that are saturated in the long exposure. The photometric response when summing over saturated pixels that have been bled into remains perfectly linear far beyond saturation of the central pixel at GAIN=4.

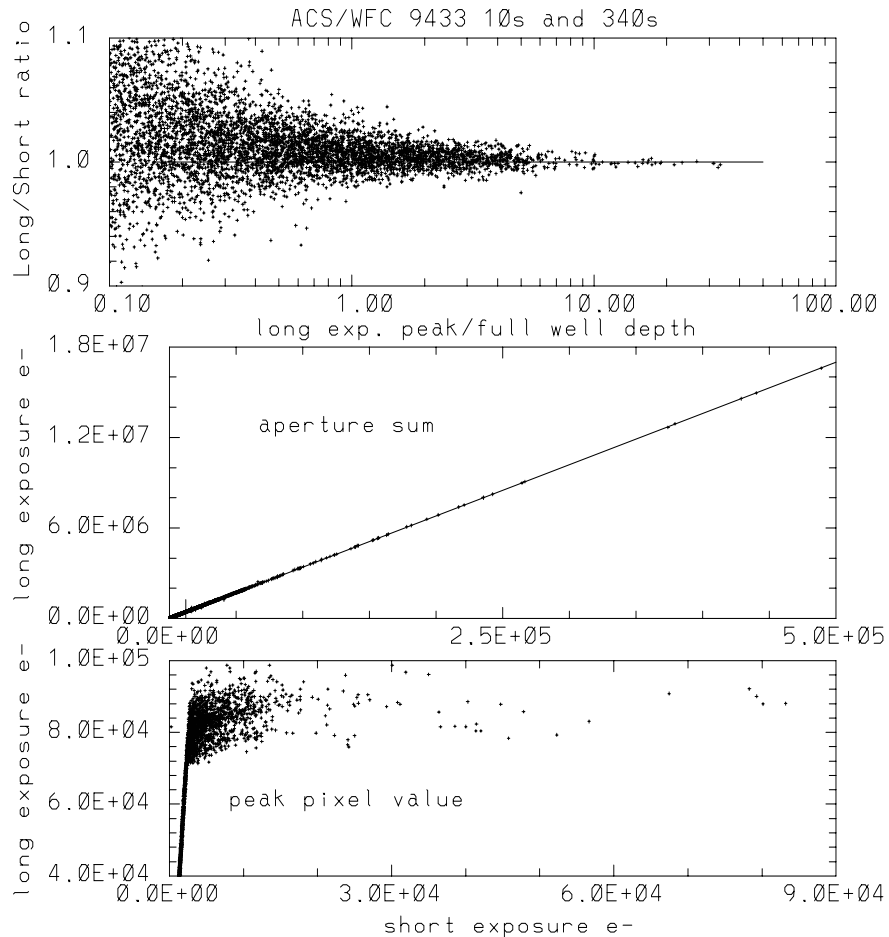


### Wide Field Camera

Figure 5.28 shows results for the WFC. Over a range of nearly 4 magnitudes beyond saturation, photometry remains linear to < 1%.

All of the above linearity results are based upon comparisons of FLT images. The conservation of flux property of drizzle leads to equally good results for linearity beyond saturation comparing long and short DRZ images. An analysis of the drizzled data sets corresponding to Figure 5.28 show equally impressive results.

Figure 5.28: The lower panel shows peak pixel values for many stars observed for 340 seconds (long) and 10 seconds (short) with the WFC; over the range for which stars are unsaturated in both exposures there is a linear relation with slope equal to the exposure time ratio. Brighter stars in the long exposure saturate at values near the full well depth. The middle panel shows the same stars using photometry sums from identical apertures in both exposures, stars above the vertical mark near 12,350 on the x-axis separates stars that are saturated in the long exposure. The upper panel shows the ratio of long to short aperture sums normalized by the relative exposure time plotted against the degree of over-saturation in the central pixel of the long exposure. The plotted line in each panel represents perfect linearity, rather than fits to the data. The photometric response when summing over saturated pixels that have been bled into remains perfectly linear far beyond saturation of the central pixel at GAIN=2.



### 5.6.5 Shutter Stability

The shutter mechanism operation varies for different commanded exposure times. For example, the WFC shutter management varies for the shortest exposures, e.g., at 0.5 sec for WFC it is a continuous motion, 0.6 sec is not allowed and 0.7 sec begins the standard mode of operation. Similar differences exist for the shortest HRC options. Ground-based

testing is discussed in Martel, Hartig and Sirianni (2001c) and should be referred to for background on operation of the shutters.

For short exposure times, field dependent timing (shutter shading), A versus B blade shutter control dependence, stability, and timing accuracy were assessed for the HRC and WFC during ground based testing and through utilizing on-orbit data. The ground results using time variable flat-field sources were suggestive of deviations in actual versus nominal exposure times up to, but no larger than  $\sim 1\%$  for short exposures of less than 1.0 sec.

For a full discussion of on-orbit data used to assess shutter stability see [ACS ISR 03-03](#) (Gilliland and Hartig 2003).

Even at the shortest exposures, shutter shading measures did not exceed  $\sim 0.5\%$  center-to-edge for either camera. This supports a previous decision to not actively invoke a shading correction in **CALACS**.

No systematic biases in timing reach the  $0.5\%$  level for any average over multiple pairs at any exposure time when switching between A and B shutter control. This supports not actively utilizing a record of which shutter was used.

Stability of shutter timing is a bit more problematic. For the HRC stability appears excellent, measured as rms across several exposures, the errors remain well under  $0.5\%$ . At exposure times of 1.0 sec peak-to-peak fluctuations on the HRC are at only the  $0.1\%$  level. Only at 0.1 sec do the HRC exposures exhibit peak-to-peak fluctuations up to  $\sim 1.0\%$  (and part of this may be measurement error). The WFC shutter timing stability is not as good, but was also more difficult to quantify given a higher level of systematic errors. Again measured as an rms across several exposures, errors are well under  $0.5\%$ . However, out of 7 pairs of back-to-back 1.0 sec exposures, two of the pairs have individual components differing by  $> 1.3\%$ . Where such differences exist on WFC, it is always the case that shutter timing under A control is shorter than the following B exposure. At 0.5 sec on WFC (where shutter operation is one continuous rotation) the greatest discrepancy A to B remains  $< 0.3\%$ . These results suggest that if generally short WFC exposures are required (where short is taken to be  $< 2$  sec), then 0.5 sec exposures seem stable and likely to support  $1\%$  accuracy, but exposures over the range 0.7 to  $< 2.0$  sec may experience timing fluctuations that could compromise such accuracy. This conclusion regarding WFC exposures is not regarded as robust, but is offered as that most consistent with a simple and conservative interpretation of the test data.

Adopting a threshold of  $0.5\%$  in absolute timing, only 4 exposure times over HRC and WFC required revisions from pre-launch values. The 0.1 sec HRC exposure is actually larger than this by  $4.1\%$  WFC exposures at 0.5 sec, 0.7 sec and 0.8 sec in reality differ by  $+1.6\%$ ,  $-1.0\%$  and  $-0.6\%$  respectively. For these 4 exposures, using revised times in **CALACS** is recommended in order to support accurate photometry; retrievals made after March 11, 2004 will have invoked use of these corrected values.



# ACS Data Analysis

## In this chapter. . .

6.1 Photometry / 6-1
6.2 Astrometry / 6-24
6.3 Polarimetry / 6-28
6.4 Coronagraphy / 6-34
6.5 Ramp Filters / 6-37
6.6 Spectroscopy with the ACS Grisms and Prisms / 6-39

This chapter describes the data reduction applications available to work with ACS data, and the specific analyses you may want to apply to your imaging, spectroscopy, polarimetry and coronagraphy data.

---

## 6.1 Photometry

### 6.1.1 Photometric Systems, Units, and Zeropoints

We strongly recommend that, whenever practical, ACS photometric results be referred to a system based on its own filters. Transformation to other photometric systems is possible (see Sirianni et al., 2004, PASP submitted) but such transformations have limited precision and strongly depend on the color range, surface gravity and metallicity of the stars considered.

Three magnitude systems, based on ACS filters are commonly used, VEGAMAG, STMAG and ABMAG. They are all based on the knowledge of the throughput of the entire system (OTA + ACS CAMERA + FILTER + DETECTOR). These synthetic systems are tied to the observed standard

stars. VEGAMAG is a standard-based system and therefore is subject to systematic errors tied to the calibration of the standard star. In the last decades it has become more and more common to use photometric systems such as ABMAG (Oke, J.B. 1964, ApJ 140,689) or STMAG (Koorneef, J. et. al. 1986, in Highlights of Astronomy (IAU), Vol.7, ed. J.-P. Swings, 833) which are directly related to physical units, and they are therefore much simpler and cleaner. The choice between standard-based and flux-based systems is mostly a matter of personal preference. Any new determination of the absolute efficiency of the instrument results in revised magnitudes for all three systems.

### VEGAMAG

The VEGAMAG system uses Vega ( $\alpha$  Lyr) as the standard star. The spectrum of Vega used to define this system is a composite spectrum constructed by assembling empirical and synthetic spectra together (Bohlin & Gilliland, 2004, AJ, in press). The Vega magnitude of a star with flux  $F$ :

$$VEGAMAG = -2.5 \log_{10} \left( \frac{F}{F_{vega}} \right)$$

where  $F_{vega}$  is the calibrated spectrum of Vega in SYNPHOT. In the VEGAMAG system, by definition, Vega has zero magnitude at all wavelengths.

### STMAG and ABMAG

These two similar photometric systems are flux-based. The conversion is chosen so that the magnitude in V corresponds roughly to that in the Johnson system.

In the STMAG system, the flux density is expressed per unit wavelength, while in the ABMAG system, the flux density is expressed per unit frequency. The magnitude definitions are:

- STMAG = -2.5 Log  $F_{\lambda}$  - 21.10
- ABMAG = -2.5 Log  $F_{\nu}$  - 48.60

where  $F_{\nu}$  is expressed in  $\text{erg cm}^{-2}\text{sec}^{-1}\text{Hz}^{-1}$ , and  $F_{\lambda}$  in  $\text{erg cm}^{-2}\text{sec}^{-1}\text{\AA}^{-1}$ . Another way to express these zeropoints is to say that an object with a constant  $F_{\nu} = 3.63 \times 10^{-20} \text{ erg cm}^{-2}\text{sec}^{-1}\text{Hz}^{-1}$  will have magnitude AB=0 in every filter, and an object with  $F_{\lambda} = 3.63 \times 10^{-9} \text{ erg cm}^{-2}\text{sec}^{-1}\text{\AA}^{-1}$  will have magnitude ST=0 in every filter.

### Zeropoints

By definition the zeropoint of an instrument is the magnitude of an object that produces one count per second. Each zeropoint refers to a count rate measured in a specific aperture. Since for point source photometry it is not practical to measure counts in a very large aperture, counts are instead measured in a small aperture and an aperture correction is applied to transform the result to an "infinite" aperture. For ACS all zeropoints refer to

a nominal "infinite" aperture of radius 5.5 arcsec. Independently from the different definitions, the magnitude in the passband P in any of the ACS systems is given by:

$$\text{ACSmag}(P) = -2.5 \log(\text{total electrons/sec}) + \text{zeropoint}.$$

The choice of the zeropoint determines the magnitude system of ACSmag(P). There are several ways to determine the zeropoints:

- Using SYNPHOT you can renormalize a spectrum to 1 count/sec in the appropriate ACS passband and output the zeropoint in the selected magnitude system (provided that the most updated throughput tables are included in your SYNPHOT distribution). This example renormalizes a 10,000 K blackbody:

```
iraf> calcphot obsmode "rn(bb(10000),band(obsmode),1,counts)" form
```

where `obsmode` is the passband, for example "acs,hrc,f555w", and `form` is the output magnitude system: ABMAG, VEGAMAG or STMAG.

- Using the header keywords. The simplest way to calculate the most updated STMAG and ABMAG zeropoints for your data is to use the photometric keywords in the SCI extension of ACS images:
  - PHOTFLAM is the inverse sensitivity ( $\text{erg cm}^{-2}\text{sec}^{-1}\text{\AA}^{-1}$ ); it represents the flux of a source with constant  $F_\lambda$  which produces a count rate of 1 electron per second.
  - PHOTPLAM is the pivot wavelength.

The header keywords PHOTFLAM and PHOTPLAM relate to the STMAG and ABMAG zeropoints through the formulae:

$$\text{STMAG\_ZPT} = -2.5 \text{ Log} (\text{PHOTFLAM}) - \text{PHOTZPT} = -2.5 \text{ Log} (\text{PHOTFLAM}) - 21.10$$

$$\text{ABMAG\_ZPT} = -2.5 \text{ Log} (\text{PHOTFLAM}) - 21.10 - 5 \text{ Log} (\text{PHOTPLAM}) + 18.6921$$

- Using a list of published zeropoints such as those published on the ACS web page:

<http://www.stsci.edu/hst/acs/analysis/zeropoints>

This web page will be maintained with the most current zeropoints. More information about the zeropoint determinations can be found in Sirianni et al. (2004, PASP submitted) and [ACS ISR 04-08](#).

## 6.1.2 Aperture and Color Corrections

In order to reduce errors due to the residual flat fielding error and background variations and to increase the signal-to-noise ratio, both of the

most popular photometric techniques, aperture photometry and PSF-fitting photometry, are usually performed by measuring the flux within a small radius around the center of the source. (For a discussion on the optimal aperture size, see Sirianni et al. 2004 PASP submitted). As a consequence, this measurement must be tied to the total count rate by applying an aperture correction.

For historic consistency, ACS zeropoints refer to the total flux in a nominal "infinite" aperture and are ready to use for surface photometry. When performing point source photometry, users should convert their count rates within any given aperture to the count rates in the infinite aperture. In order to facilitate this conversion Sirianni et al. (2004, PASP submitted) provides the correction derived from the encircled energy profiles of an intermediate aperture (0.5" radius) to an infinite aperture. This correction is filter dependent and varies between  $\sim 0.09$  and  $\sim 0.12$  for WFC and between  $\sim 0.09$  and  $\sim 0.31$  for the HRC.

Users should determine the offset between their own photometry and aperture photometry with a 0.5" radius aperture. This is usually done by measuring a few bright stars in an uncrowded region of the field of view and applying the offset to all photometric measurements. If such stars are not available, encircled energies have been tabulated (Sirianni et al. 2004, PASP submitted). However users should be reminded that accurate aperture corrections are a function of time and location on the chip and also depend on the kernel used in Drizzle. They should avoid the blind application of tabulated encircled energies especially at small radii.

The aperture correction for the near-IR filters presents further complications. All ACS CCD detectors suffer from scattered light at long wavelengths. These thinned backside illuminated devices are relatively transparent to near-IR photons. The transmitted long wavelength light illuminates and scatters in the CCD header, a soda glass substrate. It is then reflected back from the header's metallized rear surface and re-illuminates the CCDs front-side photosensitive surface (Sirianni et al. 1998, proc SPIE vol. 3555, 608, ed. S. D'Odorico). The fraction of the integrated light in the scattered light halo increases as a function of wavelength. As a consequence the PSF becomes increasingly broader at increasing wavelengths. WFC CCDs incorporate a special anti-halation aluminum layer between the frontside of the CCD and its glass substrate (Sirianni et al. 1998, proc SPIE vol.3355, 608, ed. S. D'Odorico). While this layer is effective at reducing the IR halo, it appears to give rise to a relatively strong scatter along one of the four diffraction spikes at wavelength  $> 9000 \text{ \AA}$  (Hartig et al. 2003, proc SPIE vol.4854, 532, ed. J.C. Blades, H.W. Siegmund), see Section 6.1.4 for more details.

The same mechanism responsible for the variation of the intensity and extension of the halo as a function of the wavelength is also responsible for the variation of the shape of the PSF as a function of color of the source. As a consequence, in the same near-IR filter the PSF for a red star is broader

than the PSF of a blue star. Gilliland et al. (2002, proc SPIE vol.4854, 532, ed. J.C. Blades, H.W. Siegmund.) and Sirianni et al. (2004, PASP submitted) provide assessments of the scientific impact of these PSF artifacts in the red. The presence of the halo has the obvious effect of reducing the signal-to-noise and the limiting magnitude of the camera in the red. It also impacts the photometry in very crowded fields. The effects of the long wavelength halo should also be taken into account when performing morphological studies and performing surface photometry of extended objects (see Sirianni et al., 2004, PASP submitted, for more details).

The aperture correction for red objects should be determined using an isolated same-color star in the field of view, or using the effective wavelength versus aperture correction relation (Sirianni et al. 2004, PASP submitted). If the object's SED is available an estimate of the aperture correction is also possible with SYNPHOT. In fact, a new keyword "aper" has been implemented to call the encircled energy tables in the OBSMODE for ACS. A typical OBSMODE for an aperture of 0.5" would read like "acs,wfc,f850lp,aper\$0.5". A comparison with the infinite aperture magnitude using the standard OBSMODE "acs,wfc,f850lp" would give the estimate of the aperture correction to apply. See the [SYNPHOT](#) handbook for more details.

### Color Correction

In some cases it may be necessary to compare ACS photometric results with existing datasets in different photometric systems (e.g., WFPC2, SDSS or ground Johnson-Cousins). Since the ACS filters do not have exact counterparts in any other "standard" filter set, the accuracy of these transformations is limited. Moreover if the transformations are applied to objects whose spectral type (e.g., color, metallicity, surface gravity) do not match the spectral type of the calibration observation, serious systematic effects could be introduced. The transformations can be determined by using SYNPHOT, or by using the published transformation coefficients (Sirianni et al., 2004, PASP submitted). In any case users should not expect to preserve the 1-2% accuracy of ACS photometry on the transformed data.

### 6.1.3 Pixel Area Maps

When ACS images are flat fielded by the CALACS pipeline the resultant FLT files are flat if the original sky intensity was also flat. However, there is still very significant geometric distortion remaining in these images and the pixel area on the sky will vary around the field. Consequently, the relative photometry in the FLT images must be corrected.

One option is to drizzle the data to remove the geometric distortion and allow the sky to remain flat. Therefore both surface and point-source relative photometry are correct in the resulting DRZ files and the

photometric zeropoint in the header will allow conversion from electrons/s to absolute flux units.

Unfortunately users who wish to perform photometry directly on the distorted FLT files, rather than the drizzled (DRZ) data products, will require a field-dependent correction to match their photometry with the DRZ zeropoint.

The correction to the FLT images may be made by multiplying the measured flux on the FLT image by the pixel area at the corresponding position using a pixel area map (PAM), and then dividing by the exposure time (DRZ images have units of electrons/s). The pixel area must be expressed in units of the reference scale (50mas/pixel for WFC and 25mas/pix for HRC). Once this correction has been applied the same zeropoint as applied to the drizzled data products may be used to convert to absolute flux units.

$$\text{DRZ\_flux} = \text{FLT\_flux} * \text{PAM} / \text{exposure time.}$$

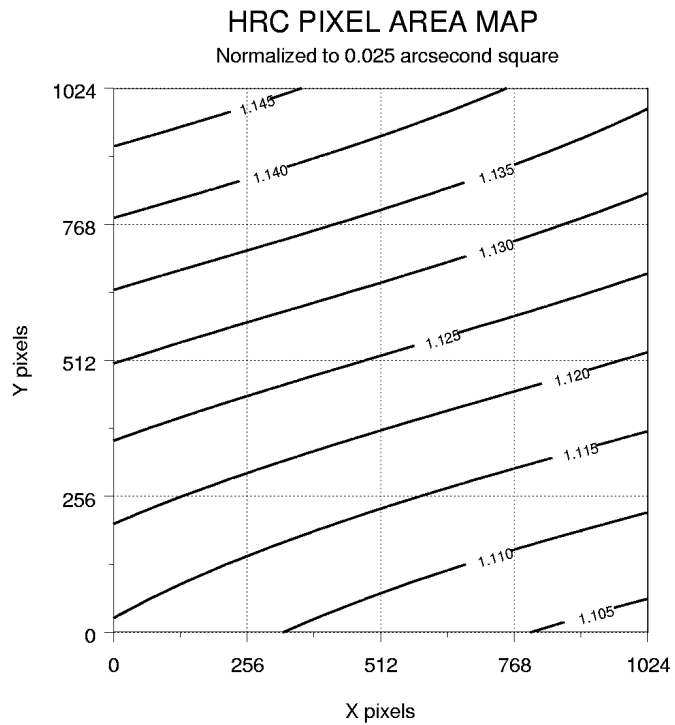
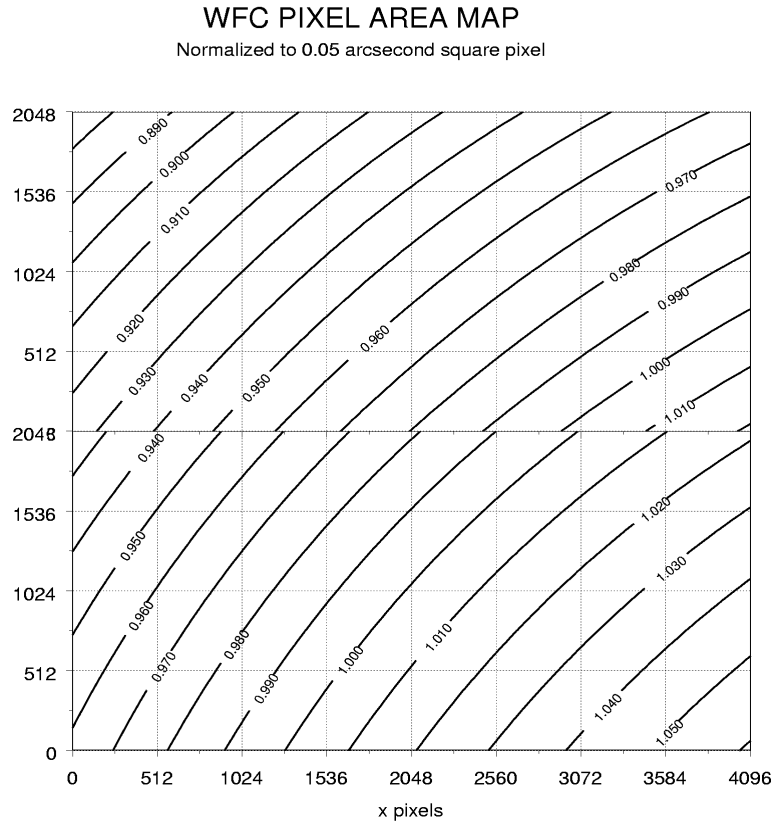
The PAM for the WFC is approximately unity at the center of the WFC2 chip, ~0.95 near the center of the WFC1 chip and ~ 1.12 near the center of the HRC.

Users may construct PAM images for themselves by downloading the script example files as well as the coefficients files which are needed from the web page:

<http://www.stsci.edu/hst/acs/analysis/PAMS>

and executing the scripts in IRAF or PyRAF. Alternatively PAM images may be downloaded directly from the same page, but they are very large.

Figure 6.1: Variation of the WFC and HRC effective pixel area with position in detector coordinates.



**PAM Concept Illustration**

To illustrate the concepts of extended source and point source photometry on FLT and DRZ images we consider a simple idealized example of a 3x3 pixel section of the detector. We assume that the bias and dark corrections are zero and that the quantum efficiency is unity everywhere.

**Example #1 Constant Surface Brightness Object**

Let's suppose we are observing an extended object with a surface brightness of  $2 \text{ e}^-/\text{pixel}$  in the undistorted case. With no geometric distortion the image is:

Actual scene on the sky:	2	2	2
	2	2	2
	2	2	2

In reality ACS suffers from geometric distortion and as a consequence pixels are not square and the pixel area varies across the detector:

Detector pixel layout on the sky:			

Let's suppose the pixel area map (PAM) is:

PAM:	1.4	1.2	1.0
	1.2	1.0	0.9
	1.0	0.9	0.8



As a result in the raw data there is an apparent variation in surface brightness.

RAW image:

2.8	2.4	2.0
2.4	2.0	1.8
2.0	1.8	1.6

The geometrical area of each pixel is imprinted in the flat field as well as the photometric sensitivity. In this example, since we assumed that the quantum efficiency is unity everywhere, the flat field is just the equivalent of the PAM:

Flat field:

1.4	1.2	1.0
1.2	1.0	0.9
1.0	0.9	0.8

ACS flat fields are designed to level out a uniformly illuminated source and not to conserve total integrated counts, so after the flat field correction the FLT image has the correct surface brightness and can be used to perform surface photometry. However the image morphology is distorted.

FLT image:

2.0	2.0	2.0
2.0	2.0	2.0
2.0	2.0	2.0

**MultiDrizzle** can be run on the FLT image. The result is that each pixel is free of geometric distortion and is photometrically accurate.

DRZ image:	2.0	2.0	2.0
	2.0	2.0	2.0
	2.0	2.0	2.0

**Example #2 Integrated photometry of a point source**

Now let's suppose we are observing a point source and that all the flux is included in the 3x3 grid. Let the counts distribution be:

Actual scene on the sky:	2.0	10.5	2.0
	10.5	50	10.5
	2.0	10.5	2.0

The total counts are 100. Due to the geometric distortion, the PSF as seen in the raw image is distorted. The total counts are conserved, but they are redistributed on the CCD.

RAW image:	1.9	10	1.9
	10.1	50	10.1
	2.5	11	2.5

After the flat field correction, however, the total counts are no longer conserved:

FLT image:	1.36	8.33	1.9
	8.42	50	11.22
	2.5	12.22	3.13

In this example the counts now add up to 99.08, instead of 100.

In order to perform integrated photometry the pixel area variation need to be taken into account. this can be done by multiplying the FLT image by the PAM or by running **MultiDrizzle**.

FLTx- PAM	1.9	10	1.9	DRZ im- age	2.0	10.5	2.0
	10.1	50	10.1		10.5	50	10.5
	2.5	11	2.5		2.0	10.5	2.0

Only by running **MultiDrizzle** can the geometric distortion be removed, but both approaches correctly recover the count total as 100. Users should be cautioned that this is just an idealized example. In reality the PSF of the star extends to a much bigger radius. If the user decides to work on the flat fielded image after correcting by the pixel area map, they need to calculate a new aperture correction to the total flux of the star. The aperture corrections discussed in Section 6.1.2 are only for **MultiDrizzle** output images. In most cases the aperture correction for distorted images will be quite different from the same star measured in the DRZ image. This is particularly true for small radius apertures.

## 6.1.4 PSF

### PSF Field Dependence

The point spread functions in the ACS cameras are more stable over the field of view than in any other HST camera, especially when compared to WFPC2. The PSF does vary slightly in both shape and width across the field to a degree that may affect photometric measurements. This effect is described in detail in [ACS ISR 03-06](#). The variations in the HRC are very small and probably negligible when using apertures greater than  $r=1.5$  pixels or using PSF fitting. However, the WFC PSF varies enough in shape and width that significant photometric errors may be introduced when using small apertures or fixed-width PSF fitting.

The WFC PSF width variation is mostly due to changes in CCD charge diffusion. Charge diffusion, and thus the resulting image blur, is greater in thicker regions of the detector (the WFC CCD thickness ranges from 12.6 to 17.1 microns, see Figure 6.2). At 500 nm, the PSF FWHM varies by 25% across the field. Because charge diffusion in backside-illuminated devices like the ACS CCDs decreases with wavelength, the blurring and variations in PSF width will increase towards shorter wavelengths. At 500 nm, photometric errors of as much as 15% may result when using small ( $r < 1.5$  pixel) apertures. At  $r=4$  pixels, the errors are reduced to  $<1\%$ .

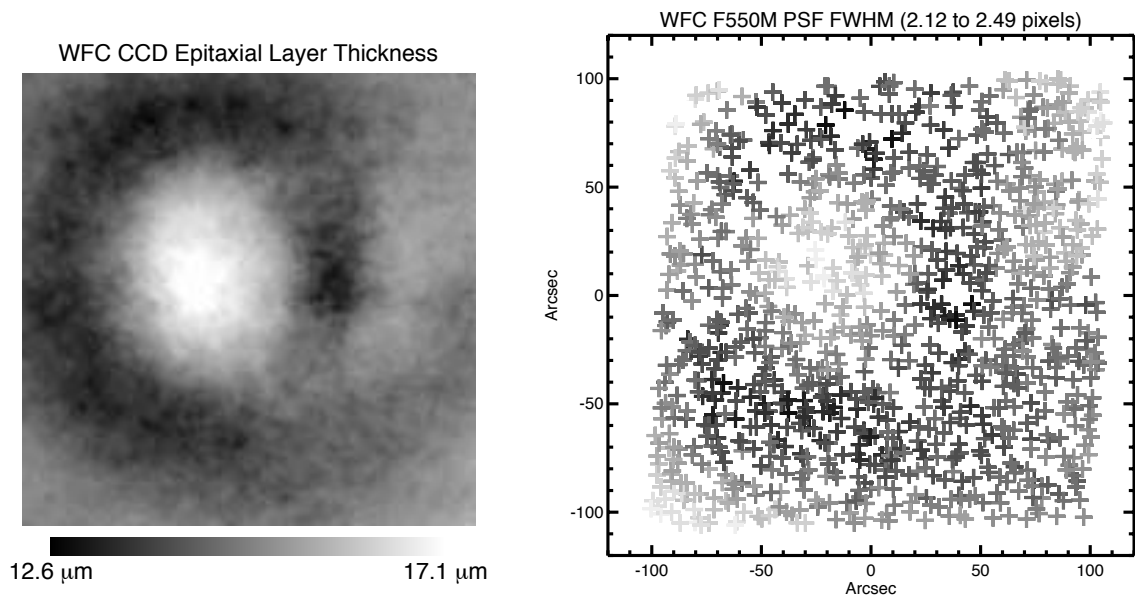
Significant errors may also be introduced when using fixed-width PSF fitting (see [ACS ISR 03-06](#)).

The shape of the PSF also changes over the WFC field due to the combined effects of aberrations like astigmatism, coma, and defocus. Astigmatism noticeably elongates the PSF cores along the edges and in the corners of the field. This may potentially alter ellipticity measurements of the bright, compact cores of small galaxies at the field edges. Coma is largely stable over most of the field and is only significant in the upper left corner, and centroid errors of  $\sim 0.15$  pixels may be expected there.

Observers may use **TinyTim** to predict the variations in the PSF over the field of view for their particular observation. **TinyTim** accounts for wavelength and field-dependent charge diffusion and aberrations, and can be found at:

<http://www.stsci.edu/software/tinytim/>

Figure 6.2: WFC chip thickness (left) and PSF FWHM (right).



### PSF Long-Wavelength Artifacts

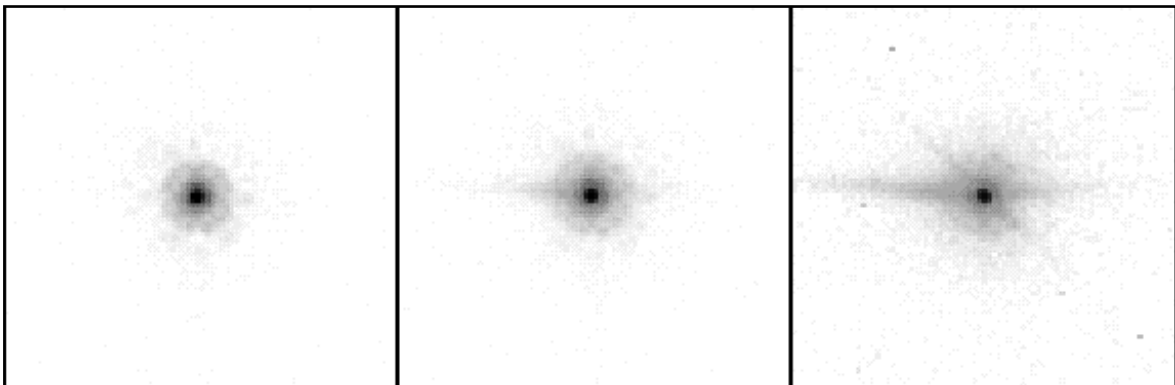
Long wavelength ( $\lambda > 700$  nm) photons can pass entirely through a CCD without being detected and enter the substrate on which the detector is mounted. In the case of the ACS CCDs, the photons can be scattered to large distances (many arcseconds) within the soda glass substrate before reentering the CCD and being detected. This creates a large, diffuse halo of light surrounding an object, called the “red halo.” This problem was largely solved in the WFC by applying a metal coating between the CCD and the mounting substrate that reflects photons back into the detector. Except at wavelengths longer than 900 nm (where the metal layer becomes

transparent), the WFC PSF is unaffected by the red halo. The HRC CCD, however, does not have this fix and is significantly impacted by the effect.

The red halo begins to appear in the HRC at around 700 nm. It exponentially decreases in intensity with increasing radius from the source. The halo is featureless but slightly asymmetrical, with more light scattered towards the lower half of the image. By 1000 nm, it accounts for nearly 30% of the light from the source and dominates the wings of the PSF, washing out the diffraction structure. Because of its wavelength dependence, the red halo can result in different PSF light distributions within the same filter for red and blue objects. The red halo complicates photometry in red filters. In broadband filters like F814W and especially F850LP (in the WFC as well as the HRC), aperture corrections will depend on the color of the star, see Section 6.1.2. for more discussion of this. Also, in high-contrast imaging where the PSF of one star is subtracted from another (including coronagraphic imaging), color differences between the objects may lead to a significant residual over-or-under-subtracted halo.

In addition to the halo, two diffraction-spike-like streaks can be seen in both HRC and WFC data beyond 1000 nm (including F850LP). In the WFC, one streak is aligned over the left diffraction spike (right spike in the HRC) while the other is seen above the right spike (below the left spike in the HRC). These seem to be due to scattering by the electrodes on the back sides of the detectors. They are about five times brighter than the diffraction spikes and result in a fractional decrease in encircled energy. They may also produce artifacts in sharp-edged extended sources.

Figure 6.3: CCD scatter at red wavelengths. WFC images of the standard star GD71 through filters F775W (9s, left), F850LP (24s, middle), and FR1016N at 996 nm (600s, right). The CCD scatter, undetected below  $\sim 800$  nm, grows rapidly with longer wavelength. In addition to the asymmetrical, horizontal feature, a weaker diagonal streak also becomes apparent near 1 micron.



### HRC and SBC UV PSFs

Below  $3500\text{\AA}$  the low and mid-spatial-frequency aberrations in HST result in highly asymmetric PSF cores surrounded by a considerable halo of scattered light extending 1-2 arcseconds from the star. The asymmetries may adversely affect PSF fitting photometry if idealized PSF profiles are

assumed. Also, charge scattering within the SBC MAMA detector creates a prominent halo of light extending about 1" from the star that contains roughly 20% of the light. This washes out most of the diffraction structure in the SBC PSF wings.

### 6.1.5 CTE

To date, all CCDs flown in the harsh radiation environment of HST suffer degradation of their charge transfer efficiency (CTE). The effect of CTE degradation is to reduce the apparent brightness of sources, requiring the application of photometric corrections to restore measured integrated counts to their "true" value.

The principle of correcting for CTE losses to achieve unbiased measurements is straightforward, but in practice it can be quite difficult to utilize. The charge loss due to imperfect CTE depends on combinations of scene characteristics such as the total counts and physical extent of a source on the detector, its background rate (global and local), the number of parallel and serial transfers, and elapsed time in the life of the detector. It is difficult to quantify and calibrate the degree to which each of these factors affects the measurements of a source over time. The general solution has been to use repeated observations of cluster fields to quantify the impact of CTE on point sources, to use internal measures of CTE degradation to track changes in between costly, external calibrations and, in the future, to do additional studies of the impact to more complicated sources (e.g., extended sources) when the CTE losses become large.

ACS has two CCDs, WFC and HRC, which clock charge and are therefore subject to CTE losses. Here we describe the external calibration of their photometric losses due to imperfect CTE. All CTE calibrations were derived from matched sets of observations of 47 Tucanae using a wide range of position, filter, and exposure time. All CTE measurements were performed by comparing the brightness of individual stars as a function of pixel transfers. The present discussion summarizes the results presented in [ACS ISR 03-09](#) and [ACS ISR 04-06](#).

Figure 6.4 gives a clear and consistent snapshot of the impact of imperfect CTE on photometry in early 2003 for WFC. The statistics are sufficient to detect non-trivial CTE losses from individual bins (~a few hundred stars) at the ~5-10 sigma confidence level for faint stars.

Figure 6.4: An example of the linear relationship determined for WFC for one filter and exposure time (F606W for 30 sec providing a sky level of  $\langle s \rangle = 3.6$  electrons) at one brightness range (stars with an average of  $\langle f \rangle \sim 400$  electrons and a full range of  $\pm 1$  mag) contained within a  $r=3$  pixel aperture. The upper panel shows a parallel transfer relation, the lower panel illustrates the serial transfer dependence.

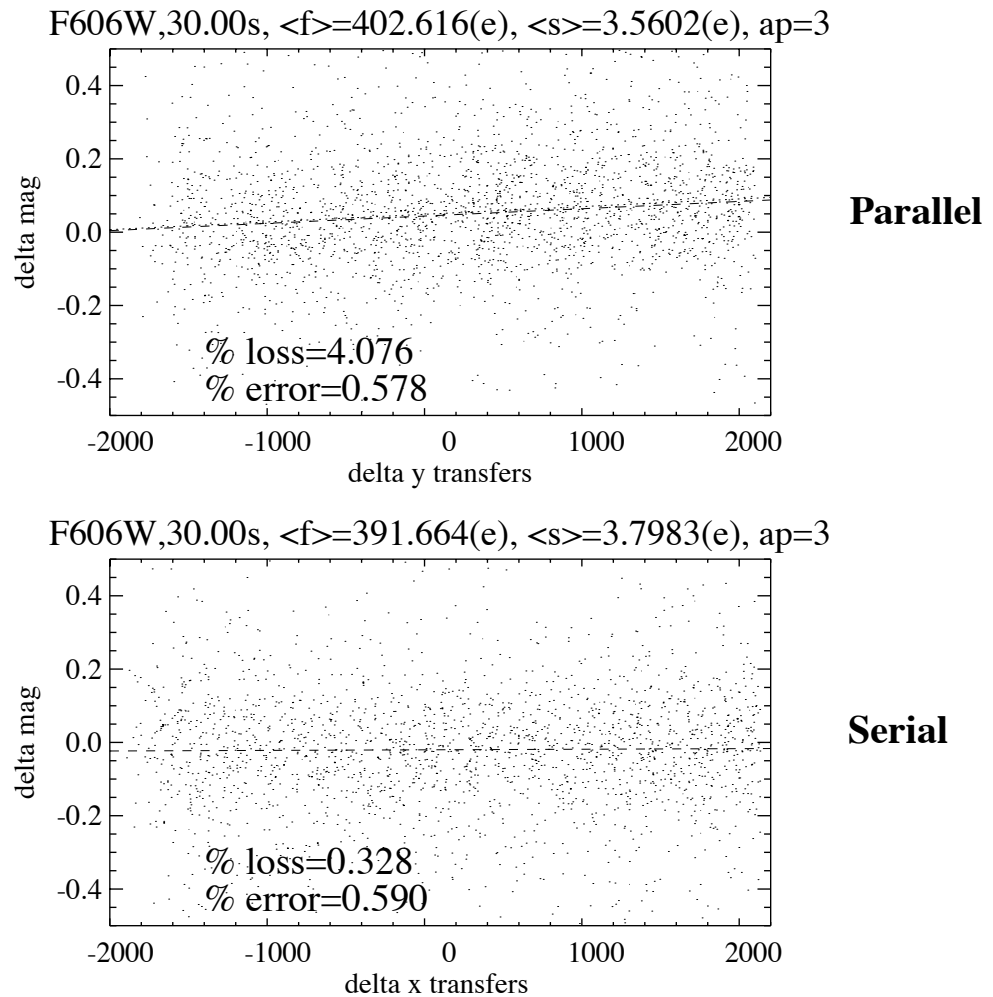
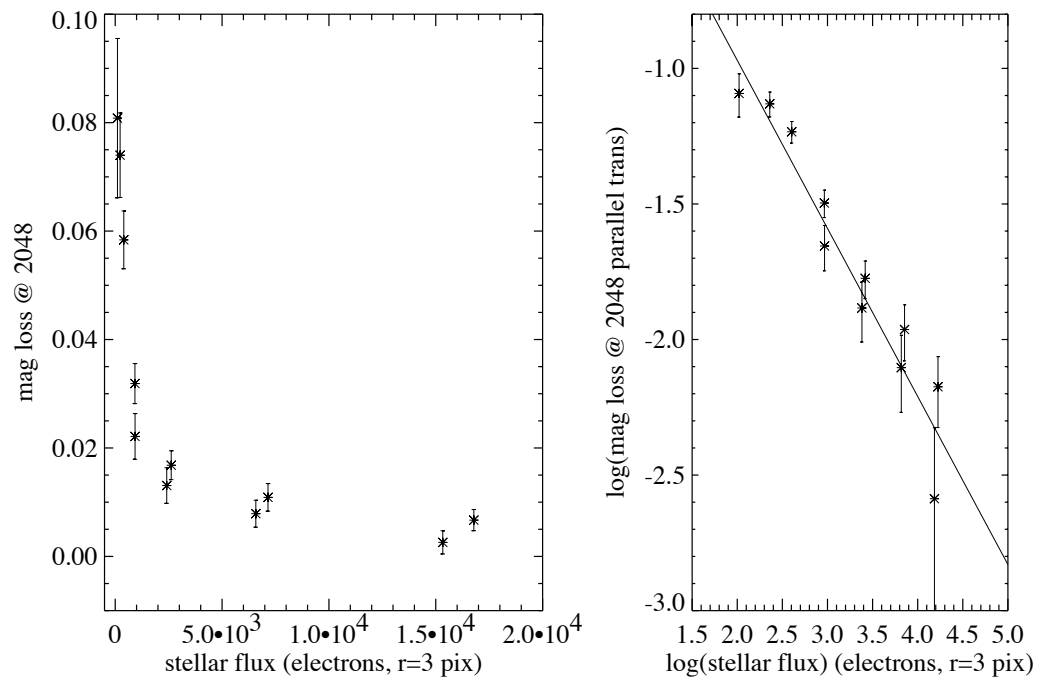


Figure 6.5: The dependence of parallel transfer CTE loss for WFC (over 2048 transfers) versus stellar flux contained within an  $r=3$  pixel aperture (all images at low sky level and taken in March 2003). As shown, the relation is strong and suggests a power-law relation which was utilized in the correction formulae. The panel on the right shows the same in log-log space.

#### Low Background (2-4 e) Parallel CTE



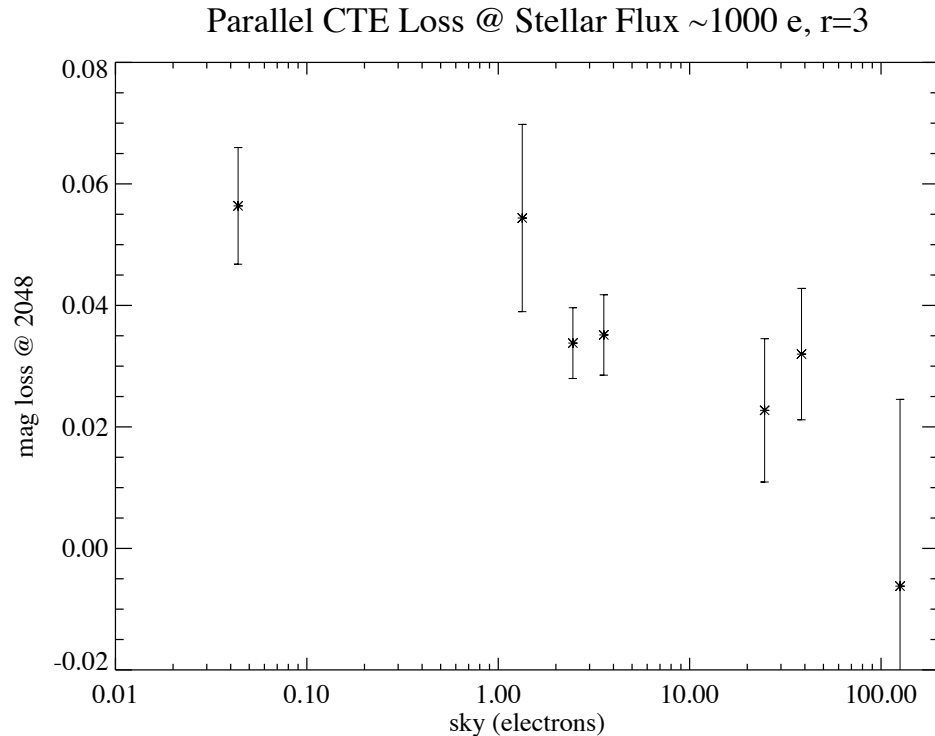
#### WFC Parallel and Serial CTE

As seen in Figure 6.5, the parallel WFC CTE loss appears to be a strong function of the stellar flux. This is not surprising given similar experience with WFPC2 and STIS. Charge traps may be present at varying depths of the silicon substrate of WFC. Larger charge packets (from brighter stars) may be subject to greater absolute flux losses by accessing deeper traps, but smaller charge packets (from fainter stars) appear to lose a larger fraction of their flux. As seen in Figure 6.5, the data suggests a power-law relationship between CTE loss and stellar flux which we have utilized in the following correction formula.

In Figure 6.6 we show the relationship between CTE loss and background. Increased background can mitigate the CTE losses (presumably by filling traps in advance of the arrival of the stellar charge packet during read-out), and this phenomenon has been seen for WFPC2 and STIS. For the dependence on background we also use a power-law in our correction formula.



Figure 6.6: The relationship between parallel transfer CTE loss and sky background for WFC in March 2003. As seen, the correlation is weak (and is insignificant for apertures of  $r=5$  and 7) and in the sense of reduced loss with higher background. The measurement was made for stars with a flux of  $\sim 1000$  electrons to remove the dependence on stellar flux.



Our CTE parameterization is:

$$YCTE = 10^A \times SKY^B \times FLUX^C \times \frac{Y}{2048} \times \frac{(MJD - 52333)}{365}$$

The term,  $(Y/2048)$  reflects the linear relationship of the CTE loss with pixel transfer as seen in Figure 6.4. The last term involves the modified Julian date (MJD) from the header and reflects a linear degradation with time. The full range of sky values (SKY) sampled extended from  $\sim 0.1$   $e^-$  (F502N for 30 sec) to 125  $e^-$  (F606W for 1100 sec). The full range of aperture flux values (FLUX) sampled ranged from  $\sim 100$   $e^-$  to 300,000  $e^-$ .

Table 6.1 contains the best fit values of the parameters A, B, and C and their uncertainties for the equation given above, for 3 different aperture sizes. The parameters were determined by simultaneously fitting data obtained in March 2003, August 2003 and February 2004. The fit to the data is shown in Figure 6.7. To determine the CTE correction (YCTE) expressed in magnitudes for a particular image observers should:

- select the appropriate aperture size,

- measure the flux in the aperture and the sky value (if working with drizzled data in  $e^-/\text{sec}$  one must multiply by the exposure time),
- determine the number of parallel transfers,  $Y$  ( $Y=y$  coordinate for  $1 < y < 2048$ ,  $Y=4096-y$  for  $y > 2048$ ),
- determine the MJD,
- and evaluate the correction.

The correction must be derived for the individual exposures, not for a “stack”. Figure 6.7 shows the corrections derived from the formula for different observing parameters.

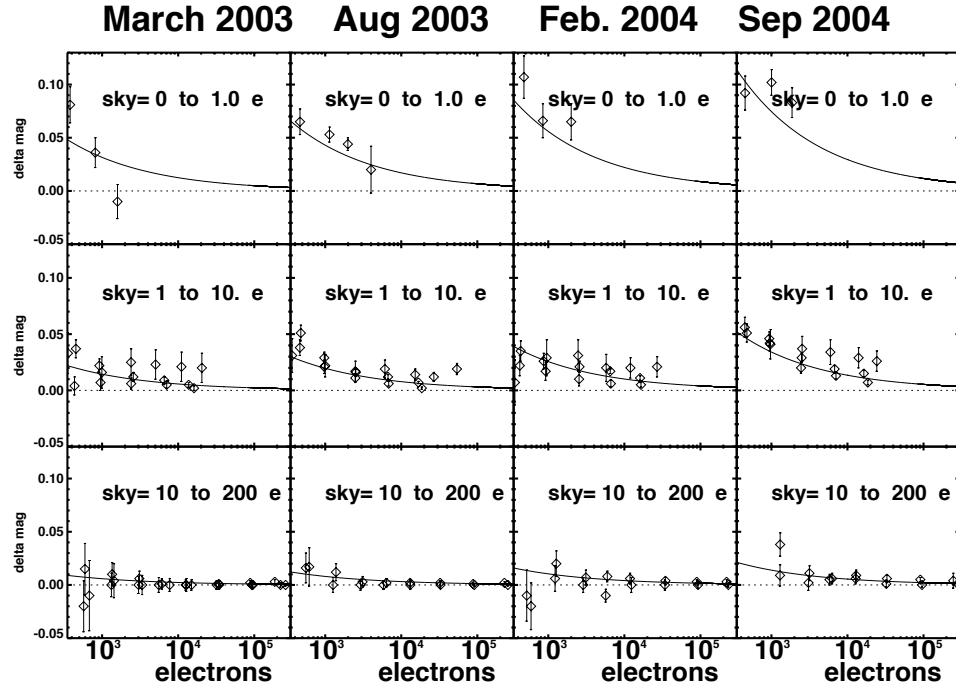
Table 6.1: CTE Correction Coefficients and Uncertainties for WFC Parallel Transfer.

aperture radius (pixels)	$A(\sigma)$	$B(\sigma)$	$C(\sigma)$
3	0.14(0.14)	-0.31(0.02)	-0.64(0.05)
5	-0.55(0.15)	-0.32(0.03)	-0.40(0.04)
7	-0.70(0.24)	-0.34(0.04)	-0.36(0.07)

In principle, first fitting the CTE trends in bins of stellar flux (and individual sky levels), followed by the step of constraining the multi-parameter fitting formula could result in information loss. However, the combination of contaminants (cosmic rays) and the large range of photon statistics (requiring different sigmas for sigma-clipping) dictated the adopted approach.

As of 2004 we have seen no evidence of photometric losses due to imperfect serial CTE on the WFC.

Figure 6.7: Parallel CTE trends. The rows and columns show the photometric losses (at  $y=2048$ ) for different sky levels and dates, respectively for aperture radii of 3 pixels. The fitted line uses the global, time-dependent correction formula in “WFC Parallel and Serial CTE” with the appropriate stellar flux and sky levels.



### HRC Parallel and Serial CTE

The same procedure described above for WFC was utilized to analyze HRC data and to quantify the photometric losses due to imperfect CTE. By utilizing all 4 read-out amplifiers, we obtained 2 independent measures of the CTE loss trend for all combinations of filter and exposure time and stellar flux.

Overall, the quantification of photometric losses due to imperfect CTE on HRC is of much lower accuracy than for WFC due to the small field of view of HRC (45 times less area) and the resulting paucity of stars. The adopted parallel CTE correction parameterization in magnitudes is:

$$Y_{CTE} = 10^A \times SKY^B \times FLUX^C \times \frac{Y}{1024} \times \frac{(MJD - 52333)}{(52714 - 52333)}$$

The terms in the equation are the same as for the WFC equation except for the modified Julian date (MJD) term, which characterizes the time evolution of the degradation of CTE away from the calibration date (MJD=52714). Table 6.2 contains the best fit values of the parameters A, B and C and their uncertainties for the YCTE equation for HRC. At present, our calibration of CTE on HRC is based on a single epoch (March 2003).

The method to correct HRC data is the same as for WFC. Observers should:

- select the appropriate aperture size,
- measure the flux in the aperture and the sky value (if working with drizzled data in electrons/sec one must multiply by the exposure time),
- determine the number of parallel transfers,  $Y$  ( $Y=y$  coordinate for read-outs with amps C or D,  $Y=1024-y$  for read-outs with amps A or B),
- determine the MJD,
- and solve for the correction.

For most observations the default amplifier, C, is used but users can determine which amplifier was used by consulting the header keyword CCDAMP. Similar to the case for WFC, at present we see no significant photometric loss in HRC due to serial transfers.

Table 6.2: CTE Correction Coefficients and Uncertainties for HRC Parallel Transfer.

aperture (pixels)	A( $\sigma$ )	B( $\sigma$ )	C( $\sigma$ )
3	-0.89(0.26)	-0.24(0.13)	-0.21(0.07)
5	-0.87(0.36)	-0.27(0.17)	-0.21(0.09)
7	-2.22(1.10)	-0.58(0.46)	0.12(0.28)

Similar to the case for WFC, at present we see no significant photometric loss in HRC due to serial transfers.

### CTE Trending and Evolution

The YCTE correction formulae include a linear time-dependence term which is bounded by the condition that the photometric losses due to imperfect CTE were zero at launch (MJD=52333). While future data will help refine the time-dependence, we believe the linear time-dependence is well motivated by other, on-orbit data such as internal CTE measurements (see “Internal CTE”) and measurements of cosmic ray charge deferred tails.

### The Relationship between field-dependent Charge Diffusion and CTE

The CCDs in HRC and WFC are both thinned and the thinning process inevitably results in large-scale variations in the CCD thickness. Because the charge diffusion of the CCD depends on thickness (thicker regions suffer greater diffusion), the breadth of the PSF and aperture corrections can also exhibit a field-dependence (see Section 6.1.4.). [ACS](#)

ISR 03-06 has characterized the spatial variation of charge diffusion as well as its impact on fixed-aperture photometry. For intermediate and large apertures ( $r > 4$  pixels), the spatial variation of photometry is very small (less than 1%), but becomes significant for small apertures ( $r < 3$  pixels).

It may be of interest to decouple the impact of imperfect CTE and charge diffusion on the field dependence of photometry but it is not necessary for observers to consider these two effects separately. The correction formulae given in Section 6.1.5 include both effects and hence corrects photometry for both effects. This is true as long as the user seeks to correct photometry to a perfect CTE and fiducial PSF width standard. An aperture correction from the fiducial aperture to a nominal "infinite" aperture is still necessary (see Section 6.1.2).

### Internal CTE

Internal CTE measurements have been obtained since before launch for both the WFC and HRC. Extended Pixel Edge Response (EPER) and First Pixel Response (FPR) data is routinely collected to monitor the relative degradation of the CTE over time. These data indicate a linear degradation but are otherwise not directly useful for the scientific calibration of ACS data. These results will be published in an ISR that is presently in preparation and will be posted on the web site:

<http://www.stsci.edu/hst/acs/documents/isrs/>.

## 6.1.6 Red Leak

### HRC

When designing a UV filter, a high suppression of off-band transmission, particularly in the red, has to be traded with overall in-band transmission. The very high blue quantum efficiency of the HRC compared to WFPC2 makes it possible to obtain an overall red leak suppression comparable to that of the WFPC2 while using much higher transmission filters. The ratio of in-band versus total flux, determined with SYNPHOT, is given in Table 6.3 for the UV and blue HRC filters, where the cutoff point between in-band and out-of-band flux is defined as the filter's 1% transmission points. The same ratio is also listed for the equivalent filters in WFPC2. Clearly, red leaks are not a problem for F330W, F435W, and F475W and are more important for F250W and F220W. In particular, accurate UV photometry of objects with the spectrum of an M star will require correction for the red leak in F250W and will be essentially impossible in F220W. For the latter filter a red leak correction will also be necessary for K and G types.

Table 6.3: In-band Flux as a Percentage of the Total Flux.

Stellar Type	WFPC2 F218W	HRC F220W	WFPC2 F255W	HRC F250W	WFPC2 F300W	HRC F330W	WFPC2 F439W	HRC F435W	WFPC2 F450W	HRC F475W
O5V	99.8	99.8	99.6	99.7	99.9	99.9	99.9	99.9	99.9	99.9
B1V	99.7	99.7	99.6	99.7	99.9	99.9	99.9	99.9	99.9	99.9
A1V	99.4	99.1	99.2	99.3	99.2	99.9	99.9	99.9	99.9	99.9
F0V	98.5	97.8	98.8	99.0	98.8	99.9	99.9	99.9	99.9	99.9
G2V	92.5	90.2	97.4	98.4	97.4	99.9	99.9	99.9	99.8	99.9
K0V	71.7	69.6	95.0	97.3	95.0	99.9	99.9	99.9	99.8	99.9
M2V	0.03	2.5	45.5	71.9	45.4	99.9	99.9	99.9	99.6	99.9

### SBC

The visible light rejection of the SBC is excellent, but users should be aware that stars of solar type or later will have a significant fraction of the detected flux coming from outside the nominal bandpass of the detector. Details are given below in Table 6.4.

Table 6.4: Visible-Light Rejection of the SBC F115LP Imaging Mode.

Stellar Type	Percentage of all Detected Photons which have $\lambda < 1800\text{\AA}$	Percentage of all Detected Photons which have $\lambda < 3000\text{\AA}$
O5V	99.5	100
B1V	99.4	100
A0V	98.1	100
G0V	72.7	99.8
K0V	35.1	94.4

### 6.1.7 UV Contamination

In an ongoing calibration effort, the star cluster NGC6681 has been observed since the launch of ACS to monitor the UV performance of the HRC and SBC detectors. Preliminary results for the HRC detector for the first year following launch were published in [ACS ISR 04-05](#). For the three filters, F220W, F250W, and F330W, 8 standard stars in the field were routinely measured, indicating a sensitivity loss of not more than ~1 to 2% per year. New data obtained in the 3 years since this analysis was performed are currently being studied and will be used to confirm this result and to characterize any dependence of loss with wavelength for the HRC.

New results for the SBC detector have been obtained using repeated measurements of ~50 stars in the same cluster to provide an estimate of the UV contamination in addition to the accuracy of the existing flat fields (see

ISR ACS 2005-13). The uniformity of the detector response must be corrected prior to investigating any temporal loss in sensitivity. (See Section 5.4.2 for a discussion of the SBC L-flat corrections.)

The absolute UV sensitivity just after launch appears to decline linearly for the first ~1.6 years in orbit and then to level off. Following the methodology for applying the STIS time-dependent sensitivity corrections (STIS ISR 2004-04), these data have been fit using line segments. Because the sensitivity losses moderate after ~1.6 years in all five SBC filters, this was chosen as the break point for the two line segments. The slope of the first line segment gives the sensitivity loss and is summarized in Table 6.5 (in percent per year). A decline in UV sensitivity of ~2-4% per year is found for the SBC detector during this time. This result agrees with the sensitivity loss derived for the STIS FUV-MAMA with the G140L filter for the first 5 years in orbit, where a 2-3% loss was observed. In the last two years of life, the rate of the STIS sensitivity loss slowed significantly compared to the previous 5 years. Similarly, after 1.6 years the ACS SBC loss rate is consistent with zero, though more follow-up data is required to confirm this result.

Table 6.5: UV sensitivity loss for the SBC detector for the first 1.6 years in orbit. The UV sensitivity decreases linearly with time during this period and then levels off after 1.6 years, indicating no further loss.

Filter	Pivot Wavelength (Å)	Loss (%/year)
F115LP	1406	2.1+/-0.4
F125LP	1438	3.1+/-0.4
F140LP	1527	2.7+/-0.5
F150LP	1611	3.9+/-0.4
F165LP	1758	3.3+/-0.5

The UV sensitivity monitoring program for the HRC and SBC will be continued at a frequency of twice per year to monitor any temporal changes in response. Further development to the ACS pipeline software is required before the new sensitivity corrections can be applied within the HST on-the-fly-reprocessing (OTFR) pipeline. Until that time, the losses given in Table 6.5 must be applied manually.

Over time both the HRC and the SBC have a constant sensitivity within 1% (except the SBC filter F165LP which is within 2%). The three HRC filters F220W, F250W and F330W, do not change sensitivity by more than 1%. Presently, for the SBC the only conclusion is that any change in sensitivity is less than 2% because the precision of the current analysis is limited by the lack of an accurate L-flat field for the SBC.

---

## 6.2 Astrometry

### 6.2.1 Coordinate Transformations

There are three coordinate systems applicable to ACS images. First, there is the position of a pixel on the geometrically distorted raw image (RAW) or, identically, the position on the flat fielded images (FLT) after pipeline processing through **CALACS**. Second, there is the pixel position on the drizzled images (DRZ) created by **MultiDrizzle** which corresponds to an undistorted pixel position on a tangent plane projection of the sky. Third, there is the corresponding position (RA, Dec) on the sky.

A position measured on a drizzled output image (DRZ) from **MultiDrizzle** may be transformed to a position on the celestial sphere using the utility **xy2rd** in the **stsdas.toolbox.imgtools** package within STSDAS. There is also a corresponding **rd2xy** task to go from the sky to the pixel position on a drizzled frame. These tools cannot be used for RAW/FLT files as they do not include the very large effects of geometric distortion.

The transformation between the pixel position on a distorted (RAW or FLT) and drizzled (DRZ) image may be performed using utilities in the **dither** package in STSDAS. The tasks **traxy** and **tranback** implement the same geometric mapping as **drizzle** and **blot** except applied to X,Y pixel positions rather than images. For more details on how to use these the IRAF help files should be consulted. As a more convenient high-level wrapper, the **tran** task, which was released as part of the late-2004 version of STSDAS, allows the mapping of X,Y positions between FLT and DRZ images. This task uses information in the image headers to define the necessary geometrical transformation and requires that the drizzle-style "coeff" geometric distortion coefficients files are also available. These files are not provided by the STSDAS archive and must be recreated by running **MultiDrizzle** on the FLT file on the local machine. Please note that to run **MultiDrizzle** you also need the IDCTAB distortion file, along with the DGEO files appropriate for the particular filter used in the observations. If DGEO files were used when the drizzled products were produced, then these files are also needed when **tran** is run. They are standard calibration reference files available from the archive (see Section 4.1.4). A new version of the **tran** task that is to be released in 2005 will not require the coefficients file from MultiDrizzle, but only the IDCTAB.



For example, if an object was found to be at (123,234) on an FLT image (testflt.fits[sci,1]) the position on the drizzled DRZ product (testdrz.fits) can be found as follows:

```
pyraf> tran testflt.fits[sci,1] testdrz.fits[1] forward 123 234
Running Tran Version 0.11 (May 2004)
-Reading drizzle keywords from header...
-Image testflt.fits[sci,1] was # 1
-to be drizzled onto output testdrz.fits[1]
-Transforming position...
Xin,Yin: 123.00000 234.00000 Xout,Yout: 128.20980 239.63962
PAM: 0.96218
```

The last number refers to the pixel-area map value at this point (see Section 6.1.3).

The reverse operation, DRZ to FLT, can be applied as follows:

```
pyraf> tran testflt.fits[sci,1] testdrz.fits[1] backward
128.20980 239.63962
Running Tran Version 0.11 (May 2004)
-Reading drizzle keywords from header...
-Image testflt.fits[sci,1] was # 1
-to be drizzled onto output testdrz.fits[1]
-Transforming position...
Xin,Yin: 123.00000 234.00000 Xout,Yout: 128.20980
239.63962
```

Finally the **xytosky** task, which forms part of the current dither package, will convert a pixel position on a distorted FLT file directly to a sky position, by applying the distortion correction from the IDCTAB and using the world coordinate information from the header. It may be used as follows:

```
pyraf> xytosky testflt.fits[sci,1] x=123 y=234 linear=no
- IDCTAB: Distortion model from row 22 for chip 2 : CLEAR and F814W
RA (deg.) = 5.53751673945 , Dec (deg.) = -72.0652050903
```

This task doesn't require the coefficient files but, like **MultiDrizzle**, requires a copy of the IDCTAB to be available. Both **tran** and **xytosky** have options for lists of positions to be supplied as text files to allow multiple positions to be efficiently transformed. The task **xytosky** does not currently support DGEO files. If accuracy at a level better than 0.1 pixels is needed, then we recommend either of the following: (a) run **tran** to get the corresponding X, Y pixel position on the drizzled (DRZ) image, followed by **xy2rd**; or (b) use other tasks in the dither package, such as **wtraxy**.

## 6.2.2 Absolute and Relative Astrometry

The astrometric information in the header of an ACS image comes indirectly from the positions of the guide stars used. As a result the absolute astrometry attainable by using the image header world coordinate system directly is limited by two sources of error. First, the positions of guide stars are not known to better than about 1 arcsecond. Second, the mapping from the guide star to the instrument aperture introduces a smaller, but significant error.

Although absolute astrometry cannot be done to high accuracy without additional knowledge, relative astrometry with ACS is possible to a much higher accuracy. In this case the limitations are primarily the accuracy with which the geometric distortion of the camera has been characterized. This is discussed in detail in Section 4.1. Typical accuracy of the distortion correction in the pipeline with fourth order polynomial solutions is 0.1-0.2 pixels (5-10mas for the WFC). The application of the work of Anderson and King allows even better distortion correction by the inclusion of additional small corrections held in image files (e.g., Figure 4.6) which contain effects not included in the polynomial solutions. These "distortion residual images" have been included in the pipeline since September 2004.

## 6.2.3 Impact of Guide Star Failure

The guiding performance and pointing stability of HST are described in the HST Primer. The normal guiding mode uses two guide stars that are tracked by two of HST's Fine Guidance Sensors (FGSs). However, sometimes two suitable guide stars are not available and single-star guiding is used instead with the telescope roll controlled by the gyros. These observations will suffer from small drift rates. To determine the quality of tracking during these observations please review Appendix C of the Introduction to the HST Data Handbook.

The gyros have a typical drift rate of 1.0 mas/sec, although on rare occasions it can be as large as 1.5 mas/sec. This causes a rotation of the target around the single guide star, which in turn introduces a small translational drift of the target on the detector. The exact size of the drift depends on the exact roll drift rate and distance from the single guide star to the target in the HST field of view. For ACS with single-star guiding, the typical and maximum drift rate of the target on the detector are in Table 6.6.

We are currently developing the **Tweakshifts** script which will be able to measure and correct for such shifts between successive exposures. A prototype version is currently available for testing, and a full release will take place in a future update of Pyraf/STSDAS.

Table 6.6: Drift Rates for single-star guiding with ACS

<b>TYPICAL</b>	<b>per 1000 sec exposure</b>	<b>per orbit(96 min)</b>
WFC	0.0041 arcsec (0.08pix)	0.024 arcsec (0.47 pix)
HRC	0.0048 arcsec (0.19 pix)	0.028 arcsec (1.11 pix)
<b>MAXIMUM</b>	<b>per 1000 sec exposure</b>	<b>per orbit (96 min)</b>
WFC	0.0080 arcsec (0.16 pix)	0.046 arcsec (0.92 pix)
HRC	0.0092 arcsec (0.37 pix)	0.053 arcsec (2.12 pix)

The drift over an orbital visibility period can be calculated from these numbers; the typical visibility period in an orbit (outside the Continuous Viewing Zone [CVZ]) is in the range 52-60 minutes, depending on target declination (see Section 6.3 of the [Cycle 14 HST Primer](#)). The drifts inherent to single-star guiding are **not** represented in the image header astrometric information, and have two important consequences:

- There will be a slight drift of the target on the detector within a given exposure. For the majority of observations and scientific applications this will not degrade the data (especially if the exposures are not very long). The drift is smaller than the FWHM of the point spread function (PSF). Also, the typical jitter of the telescope during an HST observation is 0.003-0.005 arcsec, even when two guide stars are used.
- There will be small shifts between consecutive exposures. These shifts can build up between orbits in the same visit. This will affect the **MultiDrizzle** products from the pipeline, since these rely on the header astrometry, hence the structure of sources in the image will be degraded during the cosmic ray rejection routine. This can however be addressed during post-processing if the user first measures the shifts and then runs **MultiDrizzle** off-line, using the measured shifts.

Also, even when two guide stars are used, there is often a slow drift of the telescope up to 0.01 arcsec/orbit due to thermal effects. So, it is generally advisable to check the image shifts, and if necessary measure them to improve the alignment of exposures before running **MultiDrizzle** off-line to perform the cosmic ray rejection and image combination.

In summary, for most scientific applications single-star guiding will not degrade the usefulness of ACS data, provided that the shifts are measured post-facto and **MultiDrizzle** is re-run offline using these shifts. However, we do not recommend single-star guiding for the following applications:

- Programs that require very accurate knowledge of the PSF, including coronagraphic programs and astrometric programs.
- Programs that rely critically on achieving a dithering pattern that is accurate on the sub-pixel scale. (However, note that even with two-star guiding this can often not be achieved).

Observers who are particularly concerned about the effect of pointing accuracy on the PSF can obtain quantitative insight using the **TinyTim** software package. While this does not have an option to simulate the effect of a linear drift, it can calculate the effect of jitter of a specified RMS value.

---

## 6.3 Polarimetry

### 6.3.1 Absolute Calibration

ACS contains a set of six filters which are sensitive to linear polarization; there are three visible polarizer filters with their polarization directions set at nominal 60 degree angles to each other, and three UV polarizer filters arrayed in a similar manner. These filters are typically used in combination with a spectral filter which largely defines the spectral bandpass. In most cases observers will obtain images of the target in each of the three filters. The initial calibration steps for polarization data are identical to that for data taken in any other filter -- the data are bias corrected, dark subtracted, and flat fielded in the normal manner. The polarization calibration itself is accomplished by combining the set of images (or the resulting counts measured on the images) in the three filter rotations to produce a set of I, Q, and U images, or equivalently, a set of images giving the total intensity, fractional polarization, and polarization position angle.

### 6.3.2 Instrumental Issues

The design of ACS is far from ideal for polarimetry. Both the HRC and WFC optical chains contain three tilted mirrors and utilize tilted CCD detectors. These tilted components will produce significant polarization effects within the instrument that must be calibrated-out for accurate results. There are two primary effects in the tilted components -- diattenuation and phase retardance. Diattenuation refers to the fact that a tilted component will likely have different reflectivities (or transmissions) for light which is polarized parallel and perpendicular to the plane of the tilt. This can be an important source of instrumental polarization, and can also alter the position angle of the polarization E-vector. The second effect, phase retardance, will tend to convert incident linear polarized light into an elliptically polarized light. These effects will have complex dependencies on position angle of the polarization E-vector, and hence will be difficult to fully calibrate. Additional discussion of these effects can be found in (WFPC2 ISR 97-11) and Biretta, et al., 2004 (ACS ISR 04-10).

The instrumental polarization, defined as the instrument's response to an unpolarized target, provides a simple measure of some of these effects. Figure 6.8 shows the instrumental polarization derived for the HRC through on-orbit observations of unpolarized stars (HST programs 9586 and 9661). The instrumental polarization is approximately 5% at the red end of the spectrum, but rises in the UV to about 14% at the shortest wavelengths. Also shown is a rough model for the effects of the M3 mirror together with a very crude model of the CCD. The mirror is Aluminum with a 606 Å thick overcoat of Magnesium Fluoride and has an incidence angle of 47 degrees. The details of the CCD are proprietary so we have simply modeled it as Silicon at an incidence angle of 31 degrees; no doubt this is a serious over-simplification. Figure 6.9 shows the same plot for the WFC, which has an instrumental polarization around 2%. Here the IM3 mirror is a proprietary Denton enhance Silver Coating with an incidence angle of 49 degrees, and the CCD has an incidence angle of 20 degrees. While the lower instrumental polarization of the WFC seems attractive, we caution that the phase retardance effects are not known for the Denton coating, and have some potential to cause serious problems -- if sufficiently large, the retardance could produce a large component of elliptical polarization which will be difficult to analyze with the linear polarizers downstream.

Figure 6.8: Instrumental Polarization for the HRC

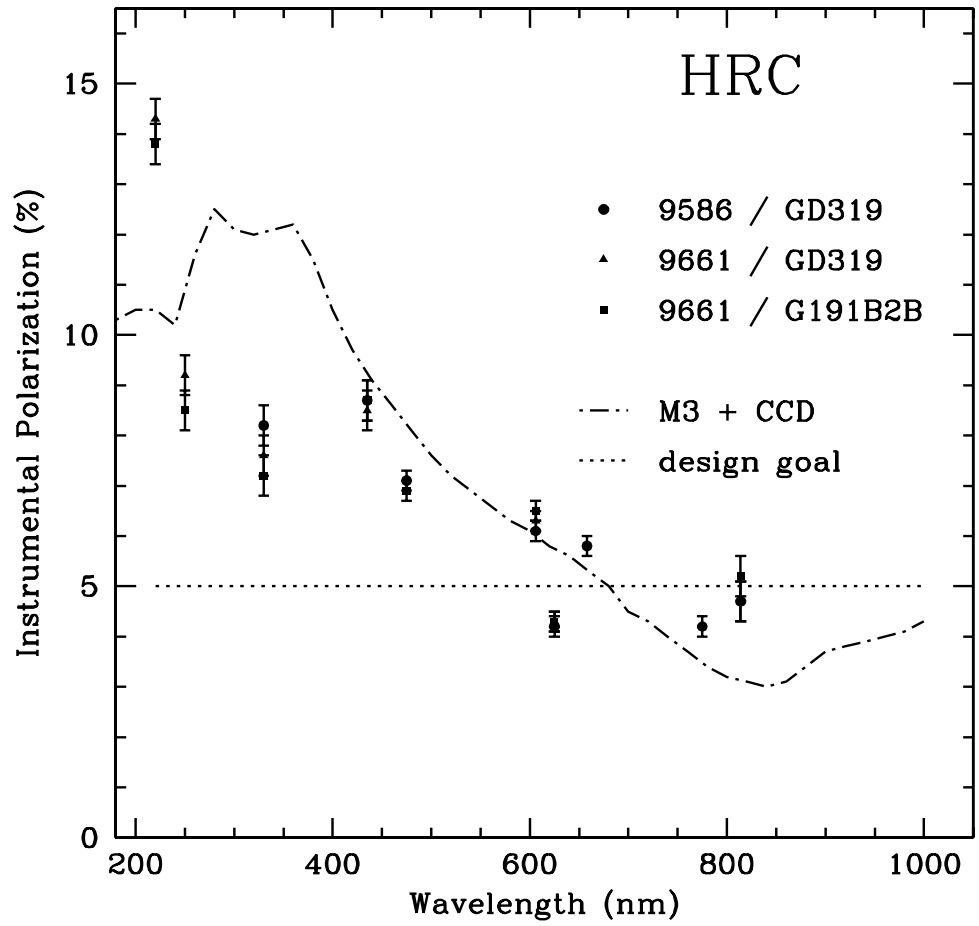
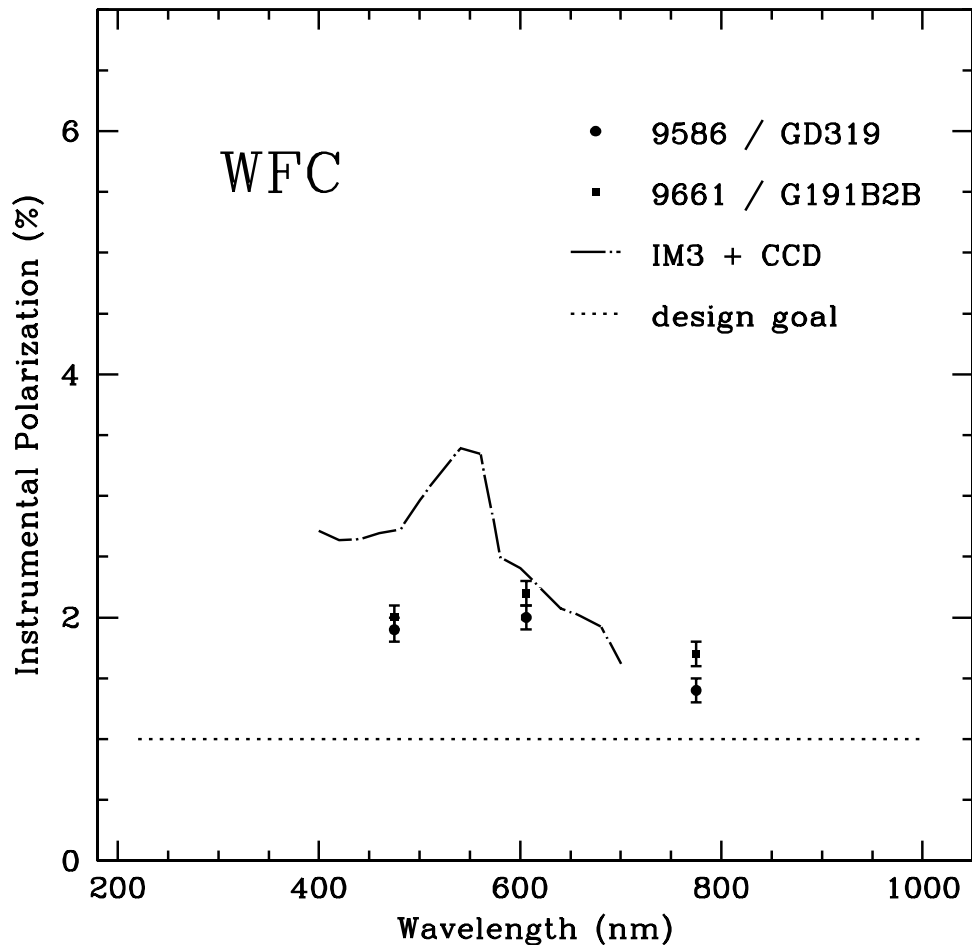


Figure 6.9: instrumental Polarization for the WFC



The ACS polarizer filters were characterized prior to installation in ACS by Leviton and the results as summarized in Figure 5.1 of the ACS Instrument Handbook. The cross-polarized transmissions are essentially zero for the POLV set, but are significant in the UV (5% - 10%) and far-red (20%) for the POLUV set.

One further issue for polarizer data is added geometric distortion. The polarizers contain a weak lens which corrects the optical focus for the presence of two filters in the light path. The lens causes a large-scale distortion which appears to be well-corrected by the drizzle software. There is also, however, a weak ( $\pm 0.3$  pixel) small-scale distortion in the images caused by slight ripples in the polarizing material. There is presently no correction available for this, although we hope to have one soon. There is also the possibility of polametric field dependencies; while there has been study of intensity flats for the polarizers, the polarization field dependencies are not known.

### 6.3.3 Flats

Flat fields for the ACS polarizers were obtained in the laboratory and corrected for low-frequency variations using the in-flight L-flat corrections which were derived for the standard (non-polarizer) filters. The pivot wavelength of the combined optical components is typically within 1% when the standard filters are used in combination with the polarizers instead of with the clear filters. To assess the accuracy of this approximation, we compared in-flight observations of the bright earth using the F435W+POLUV filters and the F475W+POLV filters with the corrected laboratory flats. The HRC earth flats agreed with the corrected lab flats to better than 1%, where the largest deviations occurred near the edges of the detector. Improved polarizer L-flats are currently being derived from stellar observations, and these should bring the flat field uncertainties down to <1%.

### 6.3.4 Polarization Calibration

An extensive series of on-orbit polarization calibration observations were carried out at the end of Cycle 11 (programs 9586 and 9661). These included observations of unpolarized and polarized standard stars, the star cluster 47 Tuc, and an extended reflection nebula. Additional observations of polarized standards are needed over a wide and well-sampled range of HST roll angles; this will help quantify the angular dependences which are expected as the wavefront interacts with the diattenuation and phase retardation in the mirrors and CCD. Some of these observations are included in program 10055, which is underway (May 2004).

We now present a preliminary calibration for use by polarization observers which is based largely on data in programs 9586 and 9661. (Observers are urged to check the ACS web pages for updates) The strategy here is to create a calibration based upon the small amount of data which are available as of this writing. This calibration can be applied to either aperture photometry results, or to the images themselves (i.e., for an extended target). We begin by calibrating the polarization “zeropoint” using corrections which are derived from observations of unpolarized standard stars. Corrections  $C(\text{CCD}, \text{POLnXX}, \text{spectral filter}, n)$  are applied to the observed count rate  $r_{\text{obs}}$  in each of the three polarizers (POLnUV or POLnV, where  $n=0, 60, 120$ ). These corrections are tabulated in Table 6.7, and have been scaled such that Stokes I will approximate the count rate seen with no polarizing filter.

$$r(n) = C(\text{CCD}, \text{POLnXX}, \text{spectral filter}, n) r_{\text{obs}}(n)$$



Next, an “instrumental” Stokes vector is computed for the target. We note our definition of  $U$  is slightly different from that in the ACS Instrument Handbook:

$$I = \left(\frac{2}{3}\right)[r(0) + r(60) + r(120)]$$

$$Q = \left(\frac{2}{3}\right)[2r(0) - r(60) - r(120)]$$

$$U = \left(\frac{2}{\sqrt{3}}\right)[r(60) - r(120)]$$

Next we compute the fractional polarization of the target. We include a factor which corrects for cross-polarization leakage in the polarizing filters. This correction is useful for the POLUV filters, and values of  $T_{\text{par}}$  and  $T_{\text{perp}}$  can be found in Figure 5.4 of the ACS Instrument Handbook:

$$P = \frac{\sqrt{Q^2 + U^2}}{I} \times \left[ \frac{T_{\text{par}} + T_{\text{perp}}}{T_{\text{par}} - T_{\text{perp}}} \right]$$

Finally we compute the position angle on the sky of the polarization E-vector. The parameter PAV3 is the roll angle of the HST spacecraft, and is called PA\_V3 in the data headers. The parameter  $\chi$  contains information about the camera geometry which is derived from the design specifications; for HRC we have  $\chi = -69.4$  degrees, and for the WFC we have  $\chi = -38.2$  degrees. Note that the arc tangent function must be properly defined; here we use a definition where the result is positive in quadrants I and II, and negative in III and IV.

$$PA = \left(\frac{1}{2}\right) \text{Tan}^{-1}\left(\frac{U}{Q}\right) + (PAV3) + \chi$$

For example, a target that gives 65192, 71686, and 66296 counts per second in the HRC with F606W and POL0V, POL60V, and POL120V, respectively, is found to be 5.9% polarized at PA=96.9 degrees.

We have modeled the full instrumental effects and the above calibration together in an effort to determine the impacts of the remaining uncalibrated systematic errors. We believe these will cause the fractional polarizations to be uncertain at the one-part-in-ten level (e.g. a 20% polarization has an uncertainty of 2%) for highly polarized sources; and at about the 1% level for weakly polarized targets. The position angles will have an uncertainty of about 3 degrees. (This is in addition to uncertainties which arise from photon statistics in the observer’s data.) We have checked this calibration against polarized standard stars (~5% polarized) and found it to be reliable within the stated errors. Better accuracy will require improved models for the mirror and detector properties as well as additional on-orbit data. We have not given a calibration for F220W, F250W, or F814W, as we believe

these are too unreliable at this time. There is also some evidence of a polarization pathology in the F625W filter, and observers should be cautious of it until the situation is better understood. In addition, we have seen one incidence of a 5 degree PA error for F775W, suggesting this waveband is not calibrated as well as the others.

Table 6.7: Correction factors C(CCD, POLnXX, specfilt, n) for polarization zeropoint.

CCD	POLnXX	Spectral Filter	n=0	n=60	n=120
HRC	POLnUV	F330W	1.7302	1.5302	1.6451
		F435W	1.6378	1.4113	1.4762
	POLnV	F475W	1.5651	1.4326	1.3943
		F606W	1.4324	1.3067	1.2902
		F625W <sup>1</sup>	1.0443	0.9788	0.9797
		F658N <sup>1</sup>	1.0614	0.9708	0.9730
		F775W	1.0867	1.0106	1.0442
WFC	POLnV	F475W	1.4303	1.4717	1.4269
		F606W	1.3314	1.3607	1.3094
		F775W	0.9965	1.0255	1.0071

1. Not scaled for Stokes I

## 6.4 Coronagraphy

The coronagraphic mode of ACS HRC provides improved imaging of low-contrast features, such as circumstellar disks, compared to what is possible with direct, normal imaging. It does this by preventing saturation of the detector and suppressing the diffraction pattern of the central source. The coronagraphic Lyot stop alters the PSF of the field sources and reduces the overall system throughput, so must be accounted for when performing photo measurements.

While the coronagraphic data appears at first to be similar to normal ACS images, there are some important differences. The calibration steps for both types of data are the same, except that the coronagraphic flat fields are different and for the moment must be manually applied to the images. The coronagraphic Lyot stop reduces throughput and must be accounted for when performing photometric measurements, and the stop also alters the PSF of field sources.

### 6.4.1 Flat Fielding

The coronagraphic flat fields are different from normal HRC flats. The most obvious differences are the shadows of the two occulting spots located at the center and the upper left corner. Because the spots are in the aberrated HST beam, there is vignetting out to 0.5 arcsec past the spot edges, causing them to appear somewhat diffuse. In addition, the Lyot stop alters the large scale flat field variation pattern as well as the diffraction pattern caused by dust specks and filter pinholes. Because the occulting spots wander by several pixels over weekly time scales, their effects must be treated separately from the static features in the flat field. Therefore, there are two separate flats that must be applied to coronagraphic images.

The first is the static pixel-to-pixel flat (PFLTFILE, \*\_pfl.fits) which contains the dust specks, detector response patterns, etc. For the five supported coronagraphic filters, static flats have been created using either coronagraphic ground test flats (F606W, F814W) or earth flats (F330W, F435W, F475W). These have been modified by replacing the occulting spot patterns with corresponding regions from normal flats. These should be accurate to better than 2% over multi-pixel spatial scales, but they may be less accurate for pixel-to-pixel response. For all other filters, normal HRC flat fields are used as the static flat in the pipeline. These may create some visible artifacts where dust spots occur, causing localized errors of up to 10%. Observers should examine the flat fields used to calibrate their data to verify that any features are not caused by these errors.

The second flat applied to coronagraphic data is the spot flat field (CFLTFILE, \*\_cfl.fits) which contains the vignetting patterns of the occulting spots. There is a different spot flat for each fully supported filter (F330W, F435W, F475W, F606W, F814W). These spot flats must be shifted so that the patterns match the positions of the spots at the time a given set of science images was taken. STScI regularly monitors the position of the small occulting spot using earth flats. A table of spot position versus time (SPOTTAB, \*\_csp.fits) is available as part of the calibration reference files. The ACS calibration pipeline uses this table to determine the spot position nearest in time to the observation date. It then shifts the spot flat by the required offset. The two flat field images (PFLTFILE and CFLTFILE) are multiplied together, and the science data is divided by the combined flat.

### 6.4.2 PSF Subtraction

While the coronagraph suppresses the central source's diffracted light, it does not affect the halo of scattered light created by the polishing errors in the telescope's optics. That must be subtracted out by using the image of an isolated star with a color similar to that of the source. Observers should

observe a PSF reference star immediately before or after their science observations.

The reference PSF must be scaled to match the intensity of the central source in the science observation. The normalization constant can be derived from photometry of non-coronagraphic images of the stars (if such were taken), or by iterative adjustment until the subtraction residuals are visually minimized. Experience shows that the by-eye value is typically accurate to within 5% or less.

The reference PSF must also be aligned with the science image for optimal subtraction. Alignment errors of about 0.05 pixels can be seen by eye in the subtracted image. Subpixel registration is required and is best accomplished by iteratively adjusting the shift of the reference PSF until the subtraction residuals are minimized and symmetrical about the source (discounting any potential circumstellar material). To achieve the best results, higher-order interpolation methods should be used for shifting -- due to the high frequency structure in the scattered light halo, bilinear interpolation is insufficient. In IDL, for instance, the INTERPOLATE routine with cubic convolution interpolation will provide good results. In IRAF imshift using sinc interpolation may also suffice. It may be necessary to iteratively interleave shift and normalization adjustments.

### 6.4.3 Photometry

Observers with ACS coronagraphic data must account for the effects of the Lyot stop when making photometric measurements. The stop decreases field source intensity by 52.5% relative to the normal HRC imaging mode. Note that this reduction is included in SYNPHOT when the coron specifier is included in the observing mode (e.g., "acs,hrc,f606w,coron"). The stop also broadens the field PSF and places more light into the diffraction spikes and Airy rings (see Chapter 5 in the [ACS Instrument Handbook](#)).

### 6.4.4 Ghosting

A point-source-like ghost appears about 30 pixels to the lower right of every field star and is about 8 magnitudes fainter than the star. There are no ghosts known to be associated with the occulted central source.

---

## 6.5 Ramp Filters

### 6.5.1 Introduction

Five slots on ACS filter wheel #2 each contain a ramp filter unit that is made up of an inner, an outer, and a middle segment. For the sake of simplicity, we will refer to these three segments as individual inner (IRAMP), outer (ORAMP), and middle (MRAMP) ramp “filters” although strictly speaking, they form part of the same physical ramp filter unit.

All fifteen ramp filters can be used with the WFC over specified regions of the WFC1 and WFC2 chips. IRAMP and ORAMP filters can only be placed on the WFC1 or WFC2 chips, respectively, over regions which define the WFC1-IRAMP and WFC2-ORAMP apertures. The MRAMP filter is by default placed on the WFC1 chip over the WFC1-MRAMP aperture, but it can in principle also be placed on the WFC2 chip over the WFC2-MRAMP aperture. The different ramp apertures and their reference points on the WFC chip are shown in Table 8.1 and Figure 8.3 of the ACS Instrument Handbook. In practice, the observer specifies a ramp filter and a central wavelength, and the filter wheel is appropriately rotated in order to place the central wavelength at the reference point of the relevant aperture. With the HRC, only the five middle ramp filters are available and they cover the region over the HRC chip defined by the HRC aperture (Table 8.2; ACS Instrument Handbook).

The fifteen ramp filters provide a total wavelength coverage of 3700-10,700 Å. Twelve of the filters have a narrow bandpass ( $\Delta\lambda/\lambda$ ) of 2% and three have a medium bandpass of 9% (Table 4.2; ACS Instrument Handbook).

### 6.5.2 Existing Ground Calibrations

For each of the 15 ramp filters and different specified central wavelengths, the transmission was measured as a function of wavelength over the bandpass. For each ramp, analytical fits to these measurements generated eleven transmission profiles spaced by 10% of the wavelength coverage of the ramp (ISR ACS 00-05). Using these delivered profiles, SYNPHOT interpolates the transmission curve for any wavelength within the bandpass of each ramp filter. The interpolation errors are below 1% which is better than the measurement accuracy.

WFC and HRC flat fields have been derived from pre-flight data by illuminating the ramps with continuum and monochromatic light using the Refractive Aberrated Simulator/Hubble Opto-Mechanical Simulator (RAS/HOMS) (ISR ACS 02-01). Each of the five WFC ramp filter units associated with the five wheel #2 slots is made up of three segments (inner,

outer, middle) which cover three different adjacent wavelength ranges. A composite WFC flat was made for each of the five ramp filter units by combining three pieces of full-field broadband surrogate LP-flats (flats that incorporate both low frequency and pixel-to-pixel variations) nearest in central wavelength. For instance, for the ramp filter unit made up of FR505N (middle), FR551N (inner), and FR601N (outer) segments, surrogate broadband LP-flats of F475W, F555W, and F606W were used. HRC ramp flats were made from surrogate HRC flats appropriate for the middle segment. These flats have been delivered to the ACS pipeline. The broadband flats reduce the rms structure in monochromatic P-flats from 1% to 0.2% except at the shortest measured wavelength of 3880 Å.

After flat fielding test ramp images with the relevant composite L-flats, correcting for anamorphic geometric distortion, rotating and median filtering to remove residual noise, the response for FR505N is found to be uniform to below 1% over a 30x80 arcsec field of view for the WFC and 11.5x24 arcsec FOV for the HRC. Out of the five middle ramp filters, the FR388N shows the least uniform response (< 10%) over such regions ([ISR ACS 02-01](#)).

Preliminary values for the dispersion of the middle ramp filters FR388N, FR459M, FR505N, FR656N, and FR914M are, respectively 0.192, 0.0399, 0.146, 0.120, 0.0219 mm/Å at the ramp filters

(<http://acs.pha.jhu.edu/instrument/filters/ramp/coefficients/wavelength/>).

Due to the extra divergence of the beam from the filter to the detector, the dispersion at the WFC and HRC detector is estimated to be a factor of 1.2 and 1.3 lower respectively.

### 6.5.3 Future In-flight Calibrations

While the existing ground-based surrogate broadband L-flats provide some preliminary calibrations, improved monochromatic and continuum ramp L-flats are planned in order to take into account the fact that the transmitted wavelengths and sensitivity varies as a function of position within the ramp aperture. Two calibration sets were obtained in Cycle 12 (listed as 'future' since analysis results are not yet available):

1. A well-calibrated region in the Orion Nebula is being observed with the primary goal of deriving monochromatic L-flats at specified central wavelengths for (a) the WFC (inner+outer ramp) H-alpha (FR716N, FR782N) and [OIII] (FR551N, FR601N) ramp filters, (b) WFC middle ramp filters (FR388N, FR459M, FR505N, FR656N, FR914M), and (c) HRC middle ramp filters (FR388N, FR459M, FR505N, FR656N, FR914M).

2. Two well-calibrated standard star fields in 47 Tucanae are being observed with the primary goal of deriving WFC and HRC continuum L-flats for three middle ramp filters (FR656N, FR388N, and FR505N). These filters are selected as they are frequently used to map the H-alpha 6563 Å, [OII] 3727 Å and [OIII] 5007 Å lines, which are of great astrophysical interest, and they include the filters which seem to be the least (FR388N) and most (FR505N) uniform.

A Cycle 14 program extends the 47 Tuc observations to higher S/N for a select set of ramp filters.

---

## 6.6 Spectroscopy with the ACS Grisms and Prisms

The ACS WFC has a grism (G800L) which provides slitless spectra at a dispersion of  $\sim 40$  Å/pixel in the first order over the whole field of view. The same grism used with the HRC produces higher dispersion spectra ( $\sim 23$  Å in first order). A prism (PR200L) available with the HRC provides slitless spectra from the UV cut-off to  $\sim 3500$  Å. The SBC is fitted with two prisms (PR110L and PR130L) which provide far-UV spectra, the latter blocked below 1230 Å to prevent transmission of Lyman alpha.

All of the ACS spectroscopic modes present the well-known advantages and disadvantages of slitless spectroscopy. The chief advantage is area coverage enabling spectroscopic surveys; among the disadvantages are overlap of spectra, high background from the integrated signal over the passband and modulation of the resolving power by the sizes of dispersed objects. For ACS the low background from space and the narrow PSF make slitless spectra competitively sensitive to ground-based spectra from larger telescopes in the presence of sky background.

The primary aim of reduction of slitless spectra is to provide one-dimensional wavelength and flux calibrated spectra of all the objects with detectable spectra. The reduction presents special problems on account of the dependence of the wavelength zero point on the position of the dispersing object, the blending of spectra in crowded fields and the necessity of flat fields over the whole available wavelength range. For ACS slitless modes, a dedicated package has been developed by the ST-ECF to enable automatic and reliable extraction of large numbers of spectra. This package, called aXe

(<http://www.stecf.org/software/axe>)

is sufficiently general to be used for other slitless spectra applications.

### 6.6.1 What to Expect from ACS Slitless Spectroscopy Data

The default method for taking ACS slitless spectra is to take a pair of images, one direct and one dispersed, in the same orbit (using special requirement `AUTOIMAGE=YES`, see the [STScI Phase II Proposal Instructions](#) for details). Or at the least, to take them with the same set of guide stars and without a shift in between. The filter to be used for the direct image is set by the `AUTOIMAGE=YES` parameter or can be user selected in the range of the spectral sensitivity by setting `AUTOIMAGE=NO`. The direct image provides the reference position for the spectrum and thus sets the pixel coordinates of the wavelength zero point on the dispersed image. The adequacy of the direct image to provide the wavelength zero point can be assessed by checking the WCS of the direct and dispersed images. In general this can be trusted at the level of a pixel or better. Some information on the jitter during an exposure is available in the ACS Quicklook products (see [ACS ISR 99-10](#)). More detailed information about the pointing during an observation can be obtained from the jitter files. In the case of a direct image not being available, such as when the pairing with the direct image was suppressed (`AUTOIMAGE=NO`), then it is possible for G800L grism observations to use the zeroth order to define the wavelength zero point. However the detected flux in the zeroth order is a few percent of that in the first order and it is dispersed by about 5 pixels, so the quality of the wavelength information will be degraded.

As an example, Figure 6.10 shows a WFC2 image (one chip only) taken with F775W and Figure 6.11 shows the companion G800L dispersed image (for one chip). This illustrates well the general characteristics of slitless spectra and the characteristics of ACS spectra in particular.

Figure 6.10: Direct image of WFC chip2 in F775W.

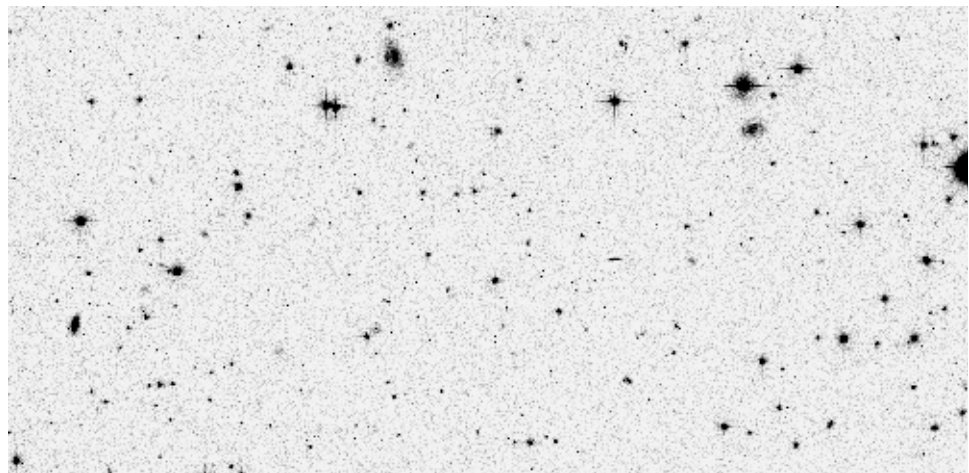
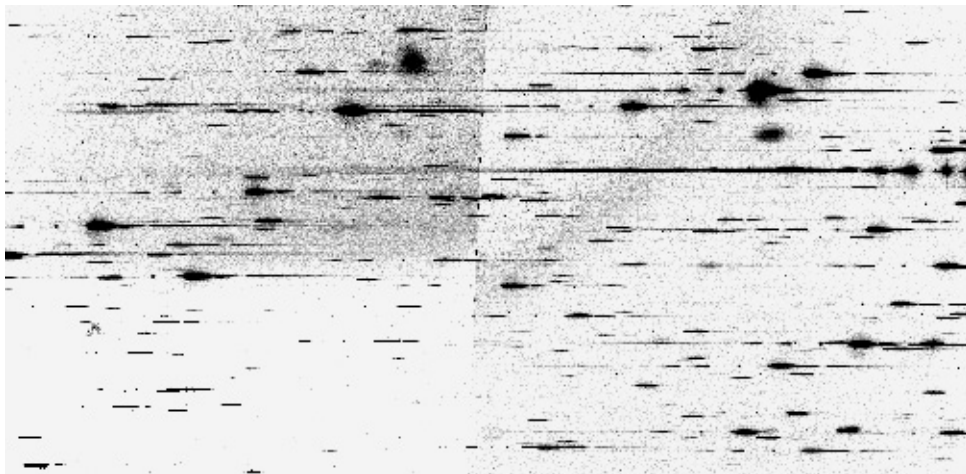




Figure 6.11: WFC G800L slitless image corresponding to the direct image.



### Bright Stars

The brightest objects produce spectra which can extend far across the chip. Although for the G800L grism only about 10% of the flux is in orders other than the first, for bright objects, orders up to +4 and -4 can be detected. These spectra, while in principle can be analyzed (dispersion solutions have been derived for orders -3, -2, -1, 0, 1, 2 and 3 for the WFC G800L for example; see [ACS ISR 03-01](#)), provide a strong source of contamination for fainter spectra. In addition for the grism, the higher order spectra are increasingly out of focus and thus spread in the cross-dispersion direction. In the case of the prisms, the strongly non-linear dispersion can result in heavily saturated spectra to longer wavelengths. An additional effect for bright stars is the spatially extended spectra formed by the wings of the PSF.

### Resolution and Object Size

In slitless spectrometry the object itself provides the "slit". The ACS PSF has a high Strehl ratio for most channels and over most of the accessible wavelength range of the dispersing elements. Therefore, the degradation of point sources beyond the theoretical resolution is minimal. However for an extended object the spectral resolution will be degraded depending on the size and light distribution in the object and spectral features will be diluted (see [ACS ISR 01-02](#)).

### Zeroth Order

The grism zeroth order, only detectable for brighter objects since it contains about 3% of the total flux, can be mistaken for an emission line. The direct image can be used to determine the position of the zeroth order and for brighter sources, distinguish unequivocally between the zeroth order and an emission line.

### Background

The background in a single pixel is the result of the transmission across the whole spectral range of the disperser and can thus be high depending on the spectrum of the sky background. The SBC PR130L prism, for example, provides lower detected background than the PR110L since it excludes the geocoronal Lyman alpha line. Bright objects in the field elevate the local background both in the dispersion direction and in the cross-dispersion direction. This background needs to be carefully removed before extracting the spectra of targets.

### Crowding

Although Figure 6.10 and Figure 6.11 show a relatively uncrowded field, close examination shows many instances where spectra overlap, either in the dispersion direction or between adjacent spectra. It is important to know if a given spectrum is contaminated by that of a neighbor. This can be done by obtaining slitless spectra at a number of different roll angles, which improves the chances of cleanly extracting spectra, which overlap in the dispersion direction.

### Extra-field Objects

There will inevitably be cases of objects outside the field which produce detectable spectra. This is more serious for the HRC and SBC where the fields are small and the spectra are long relative to the size of the detector. In such cases reliable wavelengths cannot be assigned since the zero point of the wavelength scale cannot be determined unless the zeroth order is also present. Brighter sources will be a source of contamination but correct flagging is hampered by the lack of knowledge of the precise image position.

## 6.6.2 Pipeline Calibration

The direct image half of the grism dispersed and direct image pair can be fully reduced by **CALACS** including bias subtraction, dark subtraction, flat fielding and inclusion of photometric zero point in the header (processing by ACS2D, see Section 3.4.3). However on account of the individual wavelength coverage of each object in the dispersed image, the pipeline reduction of slitless images is necessarily more restricted. Only the steps of the ACSCCD routine, involving noise and data quality initialization, bias subtraction and trimming of the overscan are applied. In addition, division by a dummy flat field (unity filled) is also applied in order to correct for the CCD gain, providing an image in electrons. This "flat" image (unity) is supplied as a pixel-to-pixel flat field file. Application of this dummy flat corrects very well the offsets in level between both quadrants of the WFC1 and WFC2 chips which have differing gain values. For the single quadrant detectors (HRC and SBC) this step merely corrects

the ADU values by a single gain value. Table 6.8 shows the calibration switches appropriate for a WFC G800L frame.

Table 6.8: Calibration switch settings for ACS WFC slitless spectrometry frames

Keyword	Switch	Description
STATFLAG	F	calculate statistics? (T/F)
WRTErr	T	write out error array extension? (T/F)
DQICORR	PERFORM	data quality initialization?
ATODCORR	OMIT	correct for A to D conversion errors?
BLEVCORR	PERFORM	subtract bias level computed from overscan image?
BIASCORR	PERFORM	subtract bias image?
FLSHCORR	OMIT	subtract post flash image?
CRCORR	OMIT	combine observations to reject cosmic-rays?
EXPSCORR	PERFORM	process individual observations after cr-reject?
SHADCORR	OMIT	apply shutter shading correction?
DARKCORR	PERFORM	subtract dark image?
FLATCORR	PERFORM	apply flat field correction?
PHOTCORR	OMIT	populate photometric header keywords?
RPTCORR	OMIT	add individual repeat observations?
DRIZCORR	PERFORM	process dithered images?

No unique photometric keywords can be attached to all the spectra in a slitless image, so the photometric header keywords are left as default - see Table 6.9.

Table 6.9: ACS Slitless spectra (grism or prism) photometric keywords

Keyword	Value	Description
PHOTMODE	'ACS WFC2 G800L'	observation con
PHOTFLAM	0.00000E+00	inverse sensitivity, ergs/cm <sup>2</sup> /Ang/electron
PHOTZPT	0.00000	ST magnitude zero point
PHOTPLAM	0.00000	Pivot wavelength (Angstroms)
PHOTBW	0.00000	RMS bandwidth of filter plus detector

In contrast to direct imaging data, no single flat field image can be correctly applied to slitless spectroscopy data, since each pixel cannot be associated with a unique wavelength. Rather, flat fielding is applied during

the extraction of spectra in the aXe task aXe\_PETFF (see Section 6.6.4, “Extracting and Calibrating Slitless Spectra,” on page 45). Each pixel receives a flat field correction dependent on the wavelength falling on that pixel as specified by the position of the direct image and the dispersion solution.

For all subsequent reductions of slitless data, the pipeline product FLT files should be the starting point. The units of the SCI and ERR extensions are electrons.

### 6.6.3 Slitless Spectroscopy Data and Dithering

The common desire to dither ACS imaging data in order to improve the spatial resolution and to facilitate removal of hot pixels, applies equally well to slitless spectroscopy data. Typically for long slitless spectroscopic exposures, and especially for parallel slitless data, the data taking is broken into many sub-orbit dithered exposures.

The **MultiDrizzle** script (see Section 4.5.2) corrects for the large geometrical distortion of the ACS and provides a very convenient tool for combining ACS data sets. However slitless grism data have both a spatial and a spectral dimension, but the correction for the geometrical distortion is only applicable to the cross-dispersion direction. The ACS grism dispersion solutions are computed for non-geometrically corrected images (see [ISR 03-01](#), [03-07](#)). Tracing the light path for slitless data shows that the distortions apply to the position and shape of images as they impinge on the grism, but not from the grism/prism to the detector. Extraction of drizzled and geometrically corrected slitless data for WFC (the ACS channel in which the geometrical distortion is largest) have shown that the correction has the effect of decreasing the resolution (increasing the dispersion in Å/pixel) across the whole field by around 10%. This is clearly disadvantageous, and we do not recommend to extract spectra from the combined slitless data. An additional complexity is that the dispersion solution must match the particular set of drizzle parameters used (such as `pixfrac` and `scale`). However, the **MultiDrizzle** combination of many grism images is useful for visual assessment of the spectra.

Part of the **MultiDrizzle** combination is the flagging of cosmic rays and hot pixels detected in the input data, and the data quality images created by **MultiDrizzle** can be used to update the quality arrays of the FLT images. The **aXe** Spectral Extraction package (see Section 6.6.4) can then be run on these updated FLT images to extract the spectra from each image separately. The individual extracted 1D wavelength, flux spectra, with the bad pixels excluded from the spectrum, can then be converted to individual FITS images and `noao.onedspec.scombine` used, for example, to merge all the spectra of each object to a single deep spectrum.

For data taken with the G800L grism for both WFC and HRC, **aXe** offers, with `aXedrizzle` (see Section 6.6.4), a method to combine the

individual images of the first order slitless spectra in 2D into a pseudo longslit spectrum. aXedrizzle derives for each first order spectrum on each image the transformation coefficients to coadd the pixels to deep drizzled 2D spectra. The final, deep 1D spectra are then extracted from the drizzled 2D spectra.

#### 6.6.4 Extracting and Calibrating Slitless Spectra

The software package aXe provides a streamlined method for extracting spectra from the ACS slitless spectroscopy data. aXe is distributed as part of the STSDAS ([http://www.stsci.edu/resources/software\\_hardware/stsdas](http://www.stsci.edu/resources/software_hardware/stsdas)) software package (under stsdas.hst\_calib.acs.axe). Moreover the latest aXe release, which may include improved capabilities, can be downloaded from the aXe web page: (<http://www.stecf.org/software/aXe>).

There is a detailed aXe manual (<http://www.stecf.org/software/aXe/manual/html/index.html>) and so only a brief outline of its use will be presented here. Also a demonstration package with all necessary data and a script to drive the extraction can be downloaded from the aXe web page:

(<http://www.stecf.org/software/aXe/testdata.html>).

##### Preparing the aXe Reduction

The starting point is always a set of dispersed slitless images and catalogues of the objects on the slitless images. The object catalogues may alternatively refer to a set of direct images which may be displaced from the slitless images. For each slitless mode (e.g., WFC G800L, HRC G800L, HRC PR200L, SBC PR110L and SBC PR130L), a configuration file is required which contains the parameters of the spectra. Information about the location of the spectra relative to the position of the direct image, the tilt of the spectra on the detector, the dispersion solution for various orders, the name of the flat field image and the sensitivity (flux per Å/e-/sec) table, is held in the configuration file and enables the full calibration of extracted spectra. For each instrumental configuration the configuration files and all necessary calibration files for flat fielding and flux calibration can be downloaded following the links given on the aXe web page.

##### aXe Tasks

The aXe software is a PyRAF/IRAF package with several tasks which can be successively used to produce extracted spectra. There exist two classes of aXe tasks. The so called Low Level Tasks work on individual grism images. The High Level Tasks work on data sets with the aim to perform certain processing steps for a set of images. Often the High Level Tasks use Low Level Tasks to perform reduction steps on each frame. The set of four High Level Tasks was designed to cover all steps of the aXe

reduction, therefore working with aXe means, in most cases, to apply High Level Tasks to a set of data.

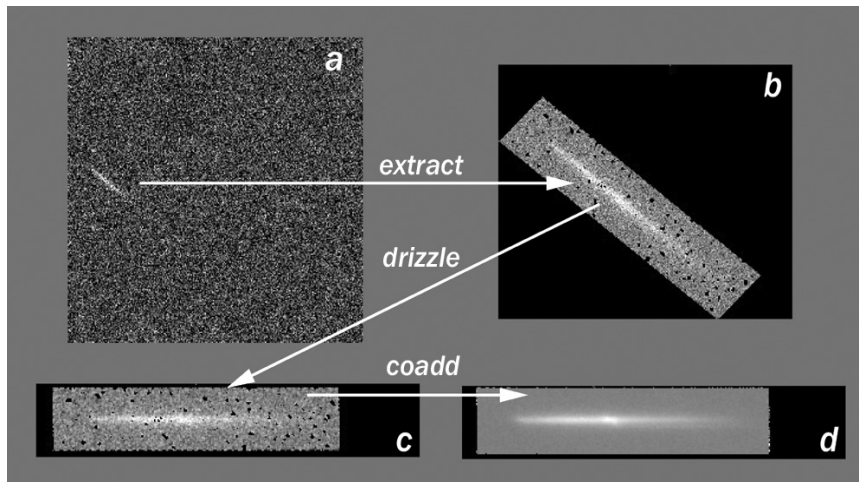
### **aXedrizzle**

The aXe data reduction is based on the individual extraction of object beams on each science image. ACS data sets usually consist of several images, with small position shifts or dithers between them. The aXedrizzle technique offers the possibility to combine the first order beams of each object extracted from a set of dithered G800L slitless images.

The input for aXedrizzle consists of flat fielded and wavelength calibrated pixels extracted for all beams on each science image. For each beam those pixels are stored as stamp images in multi-extension FITS files. aXe computes for each beam transformation coefficients which are required to drizzle the single stamp images of each object onto a single deep, combined 2D spectral image. These transformation coefficients are computed such that the combined drizzle image resembles an ideal long slit spectrum with the dispersion direction parallel to the x-axis and cross-dispersion direction parallel to the y-axis. The wavelength scale and the pixel scale in the cross-dispersion direction can be set by the user with keyword settings in the aXe Configuration File. If the set of slitless images to drizzle has a range of position angles then caution is required in the use of aXedrizzle. Since the shape of the dispersing object acts as the 'slit' for the spectrum then the slit orientation and length may differ for extended objects which are not circular. Naively combining the slitless spectra at different position angles with aXedrizzle will result in an output spectrum which suffers distortions. The resultant 1D extracted spectrum may then be a poor representation of the real spectrum.

To finally extract the 1D spectrum from the deep 2D spectral image aXe uses an (automatically created) adapted configuration file that takes into account the modified spectrum of the drizzled images (i.e. orthogonal wavelength and cross-dispersion and the Angstrom/pixel and arcsec/pixel scales).

Figure 6.12: Illustrates the aXedrizzle process for one object. Panel a shows one individual grism image with an object marked. Panel b displays the stamp image for this object out of the grism image a. Panel c shows the drizzled grism stamp image derived from a, and the final coadded 2D spectrum for this object is given in panel d.



### Background Subtraction

aXe has two different strategies for removal of the sky background from the spectra.

The first strategy is to perform a global subtraction of a scaled "master-sky" frame from each input spectrum image at the beginning of the reduction process. This removes the background signature from the images, so that the remaining signal can be assumed to originate from the sources only and is extracted without further background correction in the aXe reduction. Master-sky frames for the HRC and WFC G800L configurations are available for download from links given on the aXe web page.

The second strategy is to make a local estimate of the sky background for each beam by interpolating between the adjacent pixels on either side of the beam. In this case, an individual sky estimate is made for every beam in each science image. This individual sky estimate is processed (flat fielded, wavelength calibrated) parallel to the original beam. Subtracting the 1D spectrum extracted from the sky estimate from the 1D spectrum derived from the original beam results finally in the pure object spectrum.

### Output Products: Extracted Spectra

The primary output of aXe is the file of extracted spectra (SPC). This is a multi-extension FITS binary table with as many table extensions as there are extracted beams. The beams are designated by an alphabetic postscript; the correspondence with order being defined by the configuration file. For example the G800L WFC 1st order is BEAMA in the configuration file ACS.WFC.CHIP2.Cycle11.4.conf; see:

<http://www.stecf.org/instruments/acs/calib/Cycle11/WFC/ACS.WFC.CHIP1.Cycle11.4.conf>.



The first order spectrum of the object with number 8 in the input SExtractor catalogue for Chip 1 of the slitless image grism.fits, would therefore be accessed as `grism_5.SPC.fits[BEAM_8A]`. The table contains 12 columns listing wavelength, total and extracted and background counts and their errors, the calibrated flux and error, the weight and a contamination flag. The header of the primary extension of the SPC table is a copy of the header of the frame from which the spectrum was extracted.

aXe can also create for each beam a stamp image for the individual inspection of single beams. The stamp images of all beams extracted from a grism image are stored as a multi-extension fits file with each extension containing the image of a single extracted beam. The stamp image of the first order spectrum of object number 8 from the above example would be stored as `grism_5.STP.fits[BEAM_8A]`. It is of course also possible to create stamp images for 2D drizzled grism images.

Other output products such as Pixel Extraction Tables, contamination maps or Object Aperture Files are intermediate data products and their contents are not normally inspected.

### Handling the aXe Output

The output products from aXe consist of ASCII files, FITS images and FITS binary tables. The FITS binary tables can be assessed using the tasks in the `stdas.ttools` package and wavelength flux plots, with error bars, can be plotted using `stdas.graphics.stplot.sgraph` (see Figure 6.13 for an example).

When there are many detected spectra on a single image, such as is usually the case for data taken with the WFC G800L, then a dedicated task `aXe2web` is available (<http://www.stecf.org/software/aXe>). `aXe2web` creates html pages consisting of direct image cut-outs, stamp images and 1D spectra (see Figure 6.14) for each extracted beam. This enables convenient browsing of large numbers of spectra or the publishing of aXe spectra on the web with minimal interaction.

### Open Problems

Two facets of the reduction of ACS slitless data are not yet handled. First, fringing occurs in the WFC and HRC detectors arising from multiple reflections within the CCD layers, with an amplitude highest in the wavelength range 8000-9500Å (see ACS ISR 03-12). Fringing modulates the signal of the slitless spectra and should be corrected for the highest fidelity applications. Second, for optimal extraction of faint spectra, weights proportional to the cross-dispersion profile of the objects should be applied to the data points during the extraction process. While the PET files have a column for weight, the current aXe version (aXe-1.4) uses these weights only in `aXedrizzle` to correct within a spectral resolution element for the different exposure times of the individual pixels. A task to reset the weights based on the cross-dispersion profile shape is being developed.



### Tuning the Extraction Process

All aXe tasks have several parameters which may be tuned in various ways to alter or improve the extraction. See the aXe manual for further details.

Figure 6.13: Example WFC G800L extracted spectrum.

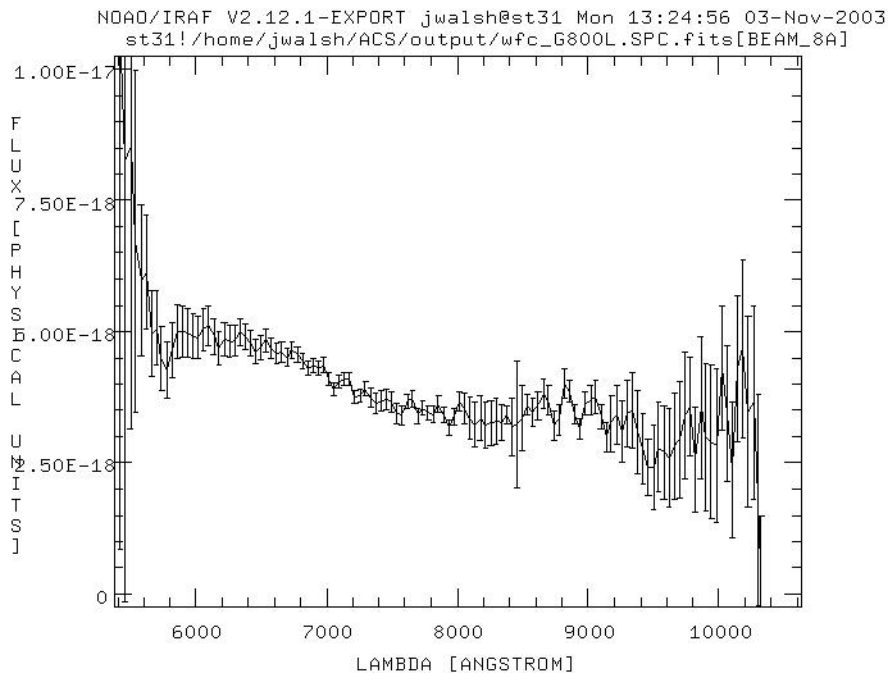


Figure 6.14: Web page produced by axe2Web for browsing extracted spectra.

Object number	Magnitude	Image-coordinates	Direct image	Grism stamp	Raw Spectrum	Calibrated Spectrum
65	22.922	x = 2318.15 y = 3450.95 ra: 1:30:11.1 dec: -16:05:19.4				
61	22.935	x = 311.67 y = 3500.96 ra: 1:30:07.8 dec: -16:03:50.8				

## 6.6.5 Accuracy of Slitless Spectra Wavelength and Flux Calibration

### Wavelength Calibration

The dispersion solution was established by observing astronomical sources with known emission lines (e.g., for the WFC G800L and the HRC G800L, Wolf-Rayet stars were observed see [ACS ISR 03-01](#) and [ACS ISR 03-07](#)). The field variation of the dispersion solution was mapped by observing the same star at different positions over the field. The internal accuracy of these dispersion solutions is good (see the ISR's for details) with an rms generally less than 0.2 pixels.

For a given object the accuracy of the assigned wavelengths depends most sensitively on the accuracy of the zero point and the transfer of the zero point from the direct to the slitless spectrum image. Provided that both direct and slitless images were taken with the same set of guide stars, systematic pointing offsets less than 0.2 pixels can be expected. For faint sources the error on the determination of the object centroid for the direct image will also contribute to wavelength error. Realistic zero point errors of up to 0.3 pixels are representative. For the highest wavelength accuracy it is advised to perform a number of pixel offsets of about ten percent of the field size for each of several direct and slitless image pairs and average the extracted spectra.

### Flux Calibration

The sensitivity of the dispersers was established by observing a spectrophotometric standard star at several positions across the field. The sensitivity (aXe uses a sensitivity tabulated in  $\text{ergs/cm/cm/sec/\AA}$  per detected  $\text{\AA}$ ) was derived using data flat fielded by the flat field cube (see Section 6.6.2). In fact the adequacy of the WFC flat field was established by comparing the detected counts in the standard star spectra at several positions across the field. These tests showed that the sensitivity at the peak of the WFC G800L varied by less than 5% across the whole field. However at the lower sensitivity edges of the spectra, to the blue ( $<5,800 \text{ \AA}$ ) and to the red ( $>10,000 \text{ \AA}$ ), the counts in the standards are low, and the errors in flux calibration approach 20%. In addition, small errors in wavelength assignment have a large effect in the blue and red where the sensitivity changes rapidly with wavelength. This often leads to strong upturns at the blue and red end of extracted flux calibrated spectra, whose reality may be considered suspect.

# Index

## A

### ACS2D

- flow diagram ACS:3–10
- task, MAMA calibrations ACS:3–20

### ACSCCD

- flow diagram ACS:3–9
- task, CCD calibrations ACS:3–11

### ACSREJ

- task, cosmic-ray rejection ACS:3–16

### ACSSUM

- task, image combination ACS:3–25

### analog-to-digital conversion ACS:5–2

### Aperture correction ACS:6–3

- encircled energies ACS:6–4
- red objects ACS:6–5
- scattered light halo ACS:6–4

### Apertures

- detectors in V2/V3 frame ACS:1–6

### Association Tables

- applying user-defined shifts ACS:4–33
- creating custom tables ACS:4–58
- creating tables from scratch ACS:4–59
- merging tables ACS:4–58
- structure ACS:2–2
- use with PyDrizzle ACS:4–16

### Astrometry

- Anderson and King correction ACS:6–26
- coordinate transformations ACS:6–24
- guide star failure impact ACS:6–26

## B

### Bad Pixels

- data quality array ACS:3–12, ACS:3–20

pixel flag values ACS:3–13

reference file (BPIXTAB) ACS:3–12

### Bias jump

- between quadrants ACS:5–4
- horizontal ACS:5–5

### Bias subarrays ACS:5–6

### Bias subtraction

- bias image (BIASFILE) ACS:3–15
- overscan subtraction table (OSCNTAB) ACS:3–14
- superbias ACS:5–2

### Blooming ACS:5–30

### Buffer memory ACS:1–8

## C

### CALACS

#### flow diagram

- CCD data ACS:3–9
- general ACS:3–8
- MAMA data ACS:3–10

#### gain correction ACS:3–22

#### individual tasks

- ACS2D ACS:3–20
- ACSCCD ACS:3–11
- ACSREJ ACS:3–16
- ACSSUM ACS:3–25

#### list of calibration steps ACS:3–6

#### memory requirements ACS:3–28

#### overview ACS:3–3

#### processing dithered exposures ACS:3–4

#### processing repeated exposures ACS:3–4

#### processing single exposures ACS:3–3

### Calibration

CCD ACS:3–11

- coronagraphy ACS:6–34
- flat field ACS:5–17
- gain ACS:5–38
- MAMA ACS:3–20
- manual ACS:3–25
- on-the-fly ACS:3–2
- photometry ACS:6–1
- pipeline ACS:3–10
- polarimetry ACS:6–28, ACS:6–32
- processing speed ACS:3–28
- ramp filters ACS:6–37
- shading correction ACS:5–46
- software ACS:3–3
- spectroscopy ACS:6–42
- switch selection criteria ACS:3–27
- Capabilities
  - coronagraphy ACS:1–2
  - imaging ACS:1–1
  - polarimetry ACS:1–2
  - spectroscopy ACS:1–2
- Chip offset
  - WFC ACS:4–2
- Color transformation ACS:6–5
- Context Image ACS:4–21, ACS:4–56
- Coronagraphy
  - flat fields ACS:6–35
  - ghosting ACS:6–36
  - observing considerations ACS:1–7
  - optical path ACS:1–4
  - photometry ACS:6–36
  - PSF ACS:6–35
- Cosmic-ray Rejection
  - ACSREJ task ACS:3–16
  - algorithm ACS:3–16
  - attached pixels ACS:5–15
  - DQ flags ACS:3–13
  - events ACS:5–13
  - fractional coverage ACS:5–13
  - reference file (CRREJTAB) ACS:3–18
- Cross talk
  - dependence on sky ACS:5–34
  - impact on object flux ACS:5–34
  - intensity ACS:5–32
  - quadrant dependence ACS:5–32
  - readout noise ACS:5–36
- CTE ACS:6–14
  - internal ACS:6–21
  - parallel ACS:6–16, ACS:6–19
  - PSF ACS:6–20
  - serial ACS:6–18, ACS:6–20
  - trending ACS:6–19, ACS:6–20
  - YCTE equation ACS:6–17, ACS:6–19
- D**
- Dark Current
  - distribution tails ACS:5–9
  - features ACS:5–6
  - reference file (DARKFILE) ACS:3–21, ACS:5–6
  - subtraction, pipeline calibration ACS:3–21
  - superdark ACS:5–11
- Data
  - array size (arcsec) ACS:4–6
  - array size (pixels) ACS:2–8, ACS:4–6
  - associations ACS:2–2
  - file size (MB) ACS:2–8
  - file suffixes ACS:2–2
  - FITS file structure ACS:2–5
  - storage requirements ACS:2–7
- Data Quality
  - array initialization ACS:3–12, ACS:3–20
  - FITS image extension ACS:2–5
  - flags
    - cosmic-rays ACS:3–13
    - hot pixels ACS:3–13
    - saturation ACS:3–13
  - pixel flag values ACS:3–13
- Data Storage
  - buffer memory ACS:1–8
  - file size (MB) ACS:2–8
  - storage requirements ACS:2–7
- Detectors
  - CCD ACS:1–3
  - MAMA ACS:1–3
- Distortion
  - see "Geometric Distortion"
- Dithered data
  - combining ACS:4–13
- Drizzling
  - ACS software tools ACS:4–15

- applying user-defined shifts ACS:4–30
- introduction ACS:4–14
- kernel ACS:4–14
- MultiDrizzle software ACS:4–17
- pixfrac ACS:4–14
- PyDrizzle ACS:4–19
- scale ACS:4–14

Dust motes ACS:5–28

**E**

Error Array

- FITS image extension ACS:2–5
- initialization ACS:3–11, ACS:3–20

**F**

Filter wheel position accuracy ACS:5–29

FITS file structure ACS:2–5

Flat field

- coronagraphy ACS:6–35
- correction, pipeline calibration ACS:3–22
- earth flat ACS:5–27
- ground flat ACS:5–16
- L-flat correction ACS:5–17
- pipeline flats ACS:5–22
- pixel area map ACS:6–5
- polarimetry ACS:6–32
- ramp filters ACS:6–38
- reference file (PFLTFILE) ACS:3–22
- sky flat ACS:5–28
- spectroscopy ACS:6–42

Full well depth

- HRC ACS:5–40
- WFC ACS:5–40

**G**

Gain calibration

- HRC ACS:5–39
- WFC ACS:5–39

Gain correction ACS:3–22

Generic Conversion

- OPUS processing ACS:3–2

Geometric Distortion

- calibration program ACS:4–5
- detector orientations ACS:1–5

- distortion model ACS:4–2
- HRC ACS:4–7
- overview ACS:1–4, ACS:4–2
- reference file (IDCTAB) ACS:4–11
- SBC ACS:4–8
- velocity aberration correction ACS:4–3
- WFC ACS:4–6

**H**

Header

- extension header keywords ACS:2–14
- primary header keywords ACS:2–9

Hot columns ACS:5–5

Hot pixels ACS:3–3, ACS:5–9

- "Warm" pixels ACS:5–9
- anneal rate ACS:5–12
- DQ flags ACS:3–13
- growth ACS:5–7
- trending ACS:5–11

HRC

- capabilities ACS:1–2
- description ACS:1–2, ACS:1–3
- distortion ACS:1–4, ACS:4–7

**I**

IDCTAB

- distortion table ACS:4–11

**K**

Keywords

- extension header ACS:2–14
- primary header ACS:2–9

**L**

Linearity

- HRC ACS:5–40, ACS:5–43
- WFC ACS:5–41

Linearity Correction

- MAMA ACS:3–21
- reference file (MLINTAB) ACS:3–21

**M**

MultiDrizzle

- data products ACS:4–20, ACS:4–55
- list of tasks performed ACS:4–17
- removing cosmic-rays ACS:3–6
- system requirements ACS:4–22
- use with PyDrizzle ACS:3–6

## O

### Observing Considerations

- coronagraph ACS:1–7
- dithering ACS:1–7
- parallel observing ACS:1–8
- pattern ACS:1–7
- target acquisitions ACS:1–7

### Optical Ghosts ACS:5–29

### Optics

- coronagraph ACS:1–4
- HRC/SBC ACS:1–4
- WFC ACS:1–4

### OTFR

- on-the-fly reprocessing ACS:3–2

### Overscan Region Table

- reference file (OSCNTAB) ACS:3–14

### Overscan subtraction ACS:3–14, ACS:5–3

## P

### Photometry ACS:6–1

- aperture correction ACS:6–3
- bypassing PHOTCORR during recalibration ACS:3–27
- color correction ACS:6–5
- coronagraphy ACS:6–36
- header keywords ACS:3–24
- photometric systems ACS:6–1, ACS:6–2
- pixel area map ACS:6–8
- red leaks ACS:6–21
- reference files (GRAPHTAB, COMPTAB) ACS:3–24
- UV contamination ACS:6–22
- zeropoints ACS:6–2

### Pipeline

- CALACS image calibration ACS:3–3
- generic conversion ACS:3–2
- PyDrizzle dither combining ACS:3–5

### Pixel area map ACS:6–5

- extended sources ACS:6–8
- geometric distortion ACS:6–11
- photometry ACS:6–8
- point sources ACS:6–10

### Pixel Scale

- average scale ACS:4–6
- default drizzled image scale ACS:4–12

### Polarimetry

- calibration ACS:6–28, ACS:6–32
- diattenuation ACS:6–28
- flat fields ACS:6–32
- geometric distortion ACS:6–31
- instrumental ACS:6–29
- phase retardance ACS:6–28
- zeropoint ACS:6–32, ACS:6–34

### Post-Flash Correction

- reference file (FLSHFILE) ACS:3–15

### PSF

- CTE ACS:6–20
- red halo ACS:6–12
- UV ACS:6–13
- variation ACS:6–11

### PyDrizzle

- association tables ACS:4–16
- data products
  - context image ACS:4–21, ACS:4–56
  - science image ACS:4–20, ACS:4–55
  - weight image ACS:4–21, ACS:4–56
- memory requirements ACS:3–28
- overview ACS:4–19
- PyRAF environment ACS:4–22
- use with MultiDrizzle ACS:3–6

## Q

- quantization noise ACS:5–2

## R

### Ramp filters

- apertures ACS:6–37
- flat fields ACS:6–38
- ground calibration ACS:6–37

### Readout noise ACS:5–2

### Recalibration

- bypassing PHOTCORR ACS:3–27

- manual ACS:3–25
  - on-the-fly ACS:3–2
  - removing cosmic rays ACS:3–6
  - requirements ACS:3–25
  - see also "Calibration"
  - setting switches ACS:3–27
- Red leaks
  - HRC ACS:6–21
  - SBC ACS:6–22
- Reference files
  - bad pixel table ACS:3–12
  - bias image ACS:3–15
  - calibration switches ACS:3–27
  - CCD characteristics table ACS:3–11
  - cosmic-ray rejection table ACS:3–18
  - dark image ACS:3–21, ACS:5–6
  - flat field ACS:3–22
  - header keywords ACS:2–11
  - MAMA linearity table ACS:3–21
  - overscan table ACS:3–14
  - post-flash image ACS:3–15
  - shutter shading image ACS:3–23
  - throughput component tables ACS:3–24
- Repeat Observations
  - summing ACS:3–25
- S**
- Saturation
  - DQ flags ACS:3–13
- Saturation limit
  - digital ACS:5–2
- SBC
  - capabilities ACS:1–2
  - description ACS:1–3
  - distortion ACS:1–4, ACS:4–8
- Scale
  - average pixel scale ACS:4–6
  - default drizzled pixel scale ACS:4–12
- Scattered earth light ACS:5–37
- Shading Correction
  - reference file (SHADFILE) ACS:3–23
- Shift file ACS:4–30
- Shutter operation ACS:5–45
- Shutter stability
  - revised exposure times ACS:5–46
- South Atlantic Anomaly ACS:5–13
- Spectroscopy
  - AUTOIMAGE ACS:6–40
  - background ACS:6–42
  - bright stars ACS:6–41
  - calibration ACS:6–42
  - calibration keywords ACS:6–43
  - crowding ACS:6–42
  - dispersion ACS:6–39
  - extra-field objects ACS:6–42
  - flat field ACS:6–42
  - flat fielding ACS:6–43
  - flux calibration ACS:6–50
  - resolution ACS:6–41
  - wavelength calibration ACS:6–50
  - zeroth order ACS:6–41
- Statistics
  - image ACS:3–25
- Suffix
  - pipeline suffixes ACS:2–2, ACS:3–4
- T**
- Target Acquisitions ACS:1–7
- Trailer Files
  - comments from PyDrizzle ACS:4–19
  - creation by CALACS ACS:2–4
- U**
- Units
  - calibrated data ACS:3–27
  - drizzled data ACS:3–27
  - raw data ACS:3–27
- V**
- Velocity Aberration
  - correction to distortion model ACS:4–3
- W**
- Warm pixels ACS:5–9
- Weight Image ACS:4–21, ACS:4–56
- WFC
  - capabilities ACS:1–1
  - chip offsets ACS:4–2

**ACS INDEX: 6 ■ Index**

description ACS:1-2, ACS:1-3

distortion ACS:1-4, ACS:4-6

**Z**

Zeropoint

determining ACS:6-2

photometric ACS:6-3